9-10-1991

Formation of low temperature silicon dioxide films using chemical vapor deposition

Hsiao-Hui Chen

Recommended Citation

Chen, Hsiao-Hui, "Formation of low temperature silicon dioxide films using chemical vapor deposition" (1991). Thesis. Rochester Institute of Technology. Accessed from

Formation of Low Temperature Silicon Dioxide Films Using Chemical Vapor Deposition

by

Hsiao-Hui (Mike) Chen

Formation of Low Temperature Silicon Dioxide Films Using Chemical Vapor Deposition

by

Hsiao-Hui (Mike) Chen

September 10, 1991
Date

Formation of Low Temperature Silicon Dioxide Films Using Chemical Vapor Deposition

by

Hsiao-Hui (Mike) Chen

A Thesis Submitted in Partial Fulfillment
of the Requirements for the Degree of

MASTER OF SCIENCE

in Materials Science and Engineering at

The Rochester Institute of Technology

Approved by:

Dr. Richard Lane, Thesis Advisor
Microelectronic Engineering
Rochester Institute of Technology

Dr. Lynn F. Fuller
Microelectronic Engineering
Rochester Institute of Technology

Dr. Vern Lindberg
Physics Department
Rochester Institute of Technology

TABLE OF CONTENTS

Page

2. CVD Basic Principles and Alternative Processes

3. LPCVD Systems for Low Temperature Oxide Films

4. Experimental Design and Response Surface Methodology

5. Experimental Procedure and Analytical Techniques

Page

6. Results and Interpretation

7. Summary and Recommendations

8. Appendices

LIST OF FIGURES

LIST OF TABLES

ACKNOWLEDGEMENT

During the course of this project, I had the opportunity of meeting many talented and knowledgeable people in their respective fields. Without them, I could not have possibly completed this project.

I would like to thank the following people for their contribution and help: Tony (Glass Fab, Rochester), Bill Hawkins (Xerox Corp.), Cathy Burke (Xerox Corp.), Dan O. Roll (Xerox Corp.), Tom Orlowski (Xerox Corp.), Chris Langdon (Advanced Crystal Sciences), Al Sasaci (Advanced Crystal Sciences), Loretta Fendrock (CVC Inc.), David Casilio (CVC Inc.) and Jamie Oliver (Eastman Kodak). I would like to thank CVC Inc. for allowing access to their ellipsometer PLASMOS SD2000 and Dektak Profilometer.

I would like to give my gratitude to Dr. Richard Lane, Dr. Lynn Fuller, Dr. Vern Lindberg, Dr. Andy Langner and Dr. Joe Voelkel for their advice and contributions. I would like to acknowledge the Microelectronic Engineering and the Materials Science and Engineering departments at RIT for financial support. I would also like to thank Scott Blondell and Gary Runkle, for their help with the equipment, Professor Michael Jackson, Professor Rob Pearson, Dan Loven, HJ Bijker, Rongthep Rochanapruk, Todd Sieger, Michael Bailey and Rich Holscher for their respective contributions to this project.

Special thanks for the financial support and the "other" supports from my parents. Also special thanks to my girlfriend, Becky Williams, for her understanding and companionship.

DEDICATION

I would like to dedicate this project in memory
of my cousin, Shung Tsung Ren.

Abstract

Low Temperature Oxide (LTO) thin films were prepared using a Low Pressure Chemical Vapor Deposition process. The process was characterized by applying traditional statistical studies and response surface technique. The uniformities within wafer and from wafer to wafer were examined by determining the mean and the standard deviation of films thicknesses. Response surface methodology was employed to determine the optimum process conditions. Time, temperature and gas flow ratio were used as the experimental factors. Index of refraction and deposition rate were used as the experimental responses. Additionally, etch rate, density, dielectric constant and infrared (IR) spectra were found for the silicon dioxide films prepared at the determined optimum condition. The IR spectra were obtained by employing Fourier Transform Infrared Spectroscopy (FTIR).

The average deposition rate was found to be 46 Å per minute and the average index of refraction was 1.44. The calculated density, activation energy, etch rate, dielectric constant and dielectric strength agreed with reported values. A double metal test run was performed using LTO oxide. The results indicated that the recommended baseline LTO process is suitable for multilayer metallization processes.

Section 1 : Introduction

Low Temperature (typically 400 °C) Chemical Vapor Deposition of silicon dioxide thin film is used in numerous VLSI manufacturing processes today [27 ,28 ,29]. This type of film is typically used as insulation between polysilicon/metal layers, metal layers in multilevel systems, as diffusion and ion implantation masks, or as final passivation layers. At the Rochester Institute of Technology's Center for Microelectronic and Computer Engineering, low temperature silicon dioxide film will be employed as the insulation film in multilayer metallization processes for CMOS integrated circuits.

Silicon dioxide thin films can be deposited by physical or chemical vapor processes. Physical vapor deposition processes form the silicon dioxide thin film by means of sputtering silicon atoms in an oxygen-rich ambient atmosphere. The silicon atoms bond with oxygen upon adsorption at the substrate surface to form the thin film. Chemical vapor deposition processes involve the formation of the silicon dioxide films by heterogeneous reaction of oxygen gas with a gas containing silicon, such as silane. The basic principles governing the CVD processes are presented in Section 2. Alternative techniques to CVD oxide are described and compared in Section 2.

There are numerous types of deposition tools available commercially today. Sputtering equipment is the most commonly used physical vapor deposition tool used for silicon dioxide film deposition [2]. The chemical vapor deposition equipment for silicon dioxide can be classified into three main categories: Low Pressure (LPCVD) [1, 27], Plasma Enhanced (PECVD) [1, 27] and PHoton Enhanced (PHCVD) [7, 39]. Detailed descriptions of these systems and processes can be found elsewhere. An

LPCVD reactor was chosen for this project. A description of this system and the process parameters are presented in Section 3.

Response Surface Methodology (RSM) was used in this project to characterize the low temperature deposition process. By employing statistically designed experiments, the number of experimental runs required was minimized. A central composite design and a three factorial design were employed. Complete details on the experimental design and analysis of this project can be found in Sections 4 and 6.

The controlling experimental factors were time, temperature and gas concentration. The uncontrolled factors included temperature gradients, and gas flow dynamics in the furnace. The observed responses were deposition rate and index of refraction. Deposition rate provided information on the process itself where as index of refraction provided information on the film. Once the process was characterized and optimized using these two responses, density, dielectric constant, etch rate and IR spectra were determined. The experimental techniques used to determine these properties are described in Section 5.

Silicon dioxide films deposited by LPCVD are generally amorphous in nature and it is difficult to fully describe the morphology and the structure. Therefore, a comparison method is commonly employed to describe the film. The most frequently used reference film is the thermally grown silicon dioxide. Since the properties of thermally grown silicon dioxide are well understood, the comparison method can be used effectively to describe silicon dioxide films created by other processes. Fourier Transform Infrared Spectroscopy was the analytical tool chosen to characterize the silicon dioxide film created by the process developed in this project. Comparisons were made between the FTIR spectra of thermally grown oxide and LPCVD oxide films deposited at different process conditions. The FTIR spectra provide information on the chemical bonding nature and distribution in the film. A description of FTIR spectroscopy and the results found in this project are contained in Sections 5 and 6.

Finally, the results and the process parameter dependences of the Low Temperature Chemical Vapor Deposition of Silicon Dioxide system at RIT are summarized in Section 7. Recommendations and observations made during the course of this project are also presented in this final section.

Section 2 : CVD Basic Principles and Alternative Processes

A Chemical Vapor Deposition (CVD) process occurs when one or more gaseous species react on a solid surface and one of the reaction products becomes a solid phase thin film material. Several steps occur during a CVD reaction [1, 8]:

1. Transport of reacting gaseous species to the substrate.
2. Adsorption of the species on the surface.
3. Heterogeneous reaction on the surface.
4. Desorption of gaseous reaction by-products.
5. Transport of reaction by-products away from the surface.

In the following sections, chemical, thermodynamic, kinetic and transport principles involved in the above steps will be discussed in detail. Additionally, the effects of the basic principles on the final film morphology are presented.

2.1 Chemistry of CVD :

Chemical reactions in CVD systems are governed by the equilibrium principle and the Law of Mass Action. The Law of Mass Action states that the rate at which a reaction proceeds is proportional to the active masses of the reacting substances [1]. The active mass for a mixture of ideal gases is the number density of each reacting species. At equilibrium conditions, the reaction could be described by the following formula:

$$aA + bB \rightleftharpoons cC + dD \qquad (2.1)$$

where A, B, C and D are the reactants and the products and a, b, c and d are the equilibrium coefficients.

The equilibrium constant is defined as:

$$K_c = \{ [C]^c \times [D]^d \} / \{ [A]^a \times [B]^b \} \qquad (2.2)$$

where the concentrations, indicated by square brackets, are expressed as molar concentrations. According to the law of Mass Action, the value of K_c is constant for a particular reaction at a given temperature.

It is also known that the concentration of a gas is proportional to its partial pressure. Therefore, by using the ideal gas law, $PV = nRT$, it can be shown the molar concentration, n/V, of a gas equals its partial pressure, P, divided by RT, where RT is constant at a given temperature. The equilibrium expression in terms of partial pressure is defined exactly like K_c, except that partial pressures are used in place of molar concentrations. In general, K_p can be expressed in terms of K_c as follows:

$$K_p = K_c (RT)^{\Delta n} \qquad (2.3)$$

where Δn is the sum of the equilibrium coefficients of gaseous products minus the sum of the coefficients of gaseous reactants.

Both equilibrium constants, K_p and K_c, provide information on the direction of the reaction, as long as the reaction equation can be written. The equilibrium constant can also be used to determine the composition at equilibrium for any set of starting concentrations. Therefore, equilibrium constant is useful for CVD reactions since it predicts whether deposition or etching reactions will occur given the reactant concentrations.

Two types of equilibrium reactions can occur; homogeneous and heterogeneous. The homogeneous equilibrium reaction is a reaction that involves reactants and products in a single phase. On the other hand, a heterogeneous equilibrium reaction involves reactants and products in more than one phase. An example of a heterogeneous reaction would be the formation of water with hydrogen and oxygen gases. It is obvious from these definitions that the deposition reactions in the gas phase CVD are heterogeneous type reactions. However, both types of reactions co-exist in the reaction chamber in CVD systems. The two processes compete for the reaction species, therefore to maximize deposition rate, homogeneous reactions must be minimized or eliminate. The heterogeneous surface reaction is only one that will form the desired thin film.

2.2 Thermodynamics of CVD :

By means of thermodynamic calculations, the general conditions required by the process can be determined. When accurate values of pressure, temperature and concentration are used, the values of partial pressure of the species and amount of deposition can be predicted. However, these calculations will not provide the deposition rate, since the system is assumed to be time independent [1]. Furthermore, chemical equilibrium conditions required by thermodynamics are not usually met, especially in flow reactors. Therefore, the calculated results can only be used as guidelines rather than absolute solutions.

In order to perform the calculations, the free energy of formation of the species in the reaction must be known. The free energy of any chemical reaction, ΔG_r, can be written as [30]:

$$\Delta G_r = \Sigma (\Delta G_f \text{ products}) - \Sigma (\Delta G_f \text{ reactants}) \qquad (2.4)$$

where ΔG_r is a function of the partial pressure equilibrium constant K_p, and ΔG_f is a function of the standard free energy of formation. Variation of total free energy in a chemical reaction system is proportional to the degree of completion. Figure 1 shows this relationship at two temperatures, where $T_2 > T_1$.

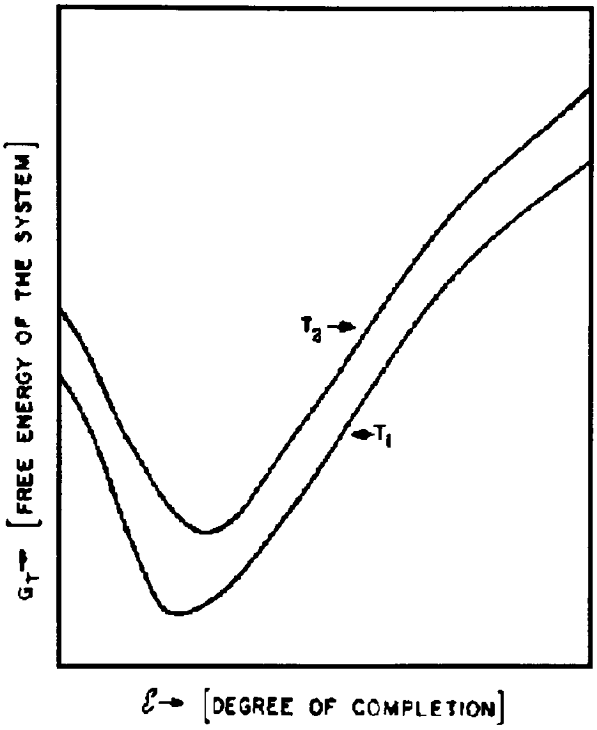

Figure 1. Variation of total free energy of the system with degree of completion at two different temperatures, $T_2 > T_1$ (After John L. Vossen and Werner Kern, "Thin Film Processes" [30]).

The minimum value for free energy in Figure 1, at some degree of completion, is equal to the equilibrium value. At equilibrium, the concentrations of reactants and products are equal. The equation describing the free energy, G, of the entire system can be expressed as follows:

$$G = \Sigma \left(n_{i(g)} \, \Delta \, G_{fi(g)} + RT \ln P + 2T \ln (n_{i(g)}/N) \right) + \Sigma \, n_{i(s)} \, \Delta \, G_{fi(s)} \qquad (2.5)$$

where the first summation term goes from 1 to m, the number of gaseous species, and the second summation term goes from 1 to s, the number of solid phase species. The n_x terms are the number of moles and N is the total number of moles in gaseous phase. To determine the equilibrium concentrations, a set of solutions for n_i must be found. Computer algorithms have been developed to solve this equation [30], by which very large numbers of species can be handled.

As mentioned before, in most cases the system is not at equilibrium conditions. By offsetting the equilibrium condition, it is possible to favor the forward reaction direction over the reverse direction. Several factors can offset the equilibrium, they include pressure, temperature and the reactant and product concentrations.

2.3 Kinetics of CVD :

Two cases of limiting rate reaction are possible for CVD systems. On page 5, the five reaction steps were listed, and they can be separated into two groups: gas-phase processes (steps 1 and 5) or surface processes (steps 2, 3 and 4). The slowest of the steps will be the limiting step and it will dictate the reaction rate, and therefore the deposition rate. In the surface limited reaction case, the amount of reactant species arriving at the substrate surface is greater than the reactions that can take place. This case is commonly known as the reaction rate limited condition. The reaction process is then determined by the reaction rate at the surface. In the diffusion limited case, the reactant species react rapidly as they arrive at the surface because the reaction rate is greater than the species arrival rate. The limiting factor is therefore the diffusion rate of the reactant through gas adjacent to the surface. This case is also called mass transport limited deposition.

Uniform deposition rates throughout a reactor require conditions that maintain a constant reaction rate. In processes that run under reaction rate limited conditions, the temperature of the process is a very important parameter. This implies that a constant temperature must also exist everywhere at the substrate surface. In this case, the rate at which reactant species arrive at the surface is not as important, since their concentration is far in excess of that which would slow the reaction. In processes that are mass transport limited, the temperature control is not nearly as critical. However, the species arrival rate is very important since that will determine the growth rate. In systems where temperature control is difficult to achieve, it is more convenient to operate under mass transport limited conditions. In general, the operating region is chosen according to the equipment setup.

Figure 2 shows the deposition rate versus inverse of the temperature in the system. At higher temperature, the mass transport limited condition applies as the reaction rate at the surface is high compared to diffusion to the surface. On the other hand, the surface rate limited condition is valid at lower temperature region.

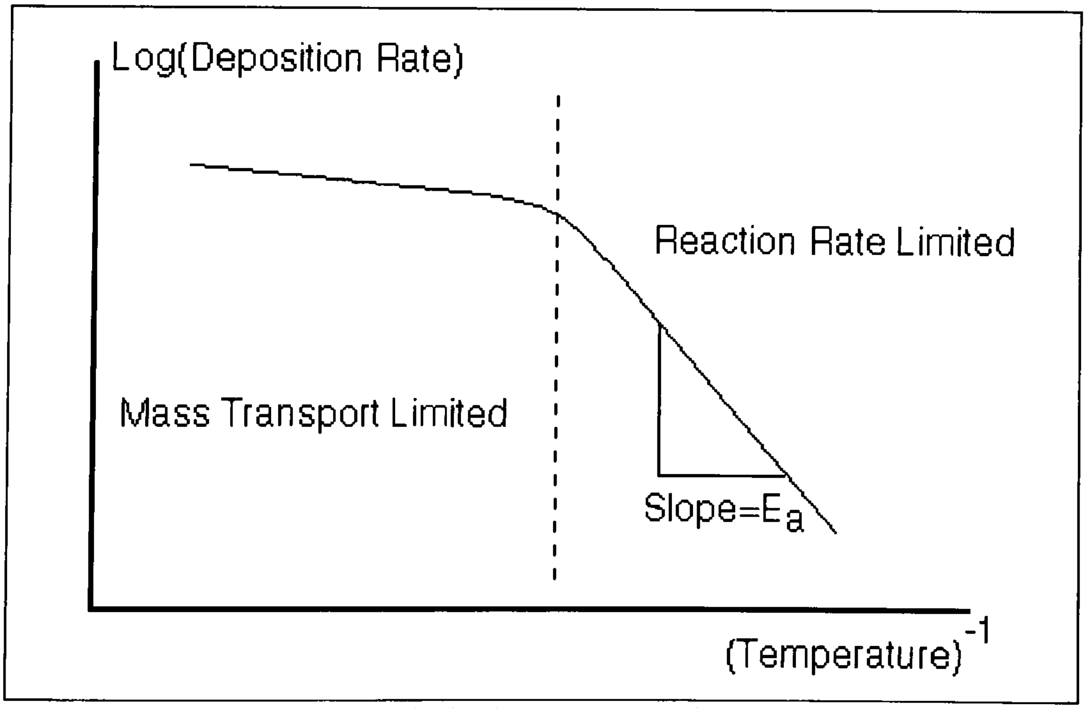

Figure 2. Arrhenius plot for deposition rate (After John L. Vossen and Werner Kern, "Thin Film Processes" [30]).

The deposition rate curve shown in Figure 2 corresponds to the theoretical curve. Actual experimental curves could vary in shape if other processing limits exist. It should be pointed out that the slope in the reaction rate limited region is approximately equal to the activation energy.

The temperature dependence of CVD reactions is generally expressed by the Arrhenious equation [27]:

$$R = A \exp\left[\frac{-qE_a}{kT}\right] \qquad (2.6)$$

where R is the deposition rate, E_a is the activation energy in eV, T is the absolute temperature in degrees Kelvin, k is the Boltzmann's constant, q is the electronic charge and A is the frequency factor. When the deposition rate is plotted against the inverse of deposition temperature as shown on Figure 2, the slope of the line in the reaction rate limited region is equal to the activation energy of the reaction. The frequency factor, A, is dependent on the surface concentration of the rate limiting reactant.

2.4 Transport Phenomena in CVD :

Transport phenomena in fluids are related to the nature of the fluid flow. The parameters that affect fluid flow are [28]:

1. Velocity of flow.
2. Temperature and temperature distribution in the system.
3. Pressure in the system.
4. Geometry of the system.

Gaseous flow in the CVD reactors obeys the universal laws of fluid dynamics. In general, there will be a gradient in gas concentration, temperature and flow velocity from the outside of the reactor to the center (assuming horizontal chambers). Most of the changes will occur within the fluid dynamic boundary layer. The boundary layer thickness will be dependent on the fluid flow velocity. As the velocity increases, the boundary layer gets smaller. The boundary layer thickness can be approximately by the Reynold's number [1,30]:

$$d = (X / R_e)^{(1/2)} \; ; \; R_e = (\rho u X) / \eta \qquad (2.7)$$

where R_e is the Reynold's number, X is a length characteristic of the flow system (such as the diameter of a flow tube), u is the flow velocity, ρ is the mass density and η is the viscosity. The same type of equations can be derived to describe the change in concentration and temperature in the system.

For comparison, at 760 mTorr, the diffusivity of the reaction species is generally three order of magnitude greater compared to that of the atmospheric conditions (760 Torr) [8, 30]. The velocity of the reactant species at 760 mTorr is also increased , whereas the density and Reynolds number are greatly reduced. The boundary layer at lower pressure is thicker than at atmospheric, but it does not offset the large increase in diffusivity of the species. Therefore, low pressure deposition greatly enhances the mass transfer making most LPCVD systems operate in the reaction rate limited region. By the same logic, the spacing between the wafers has also great effect on the deposition rate [17, 18, 19]. The larger the spacing, the greater the deposition rate since more species are available per wafer (generally it is a linear relationship). Without the mass transfer enhancement provided by the low pressure conditions, it would not be possible to place the wafers in the vertical standing position used in the LPCVD systems.

2.5 Processing Factors of CVD and Morphology :

The above sections presented the principles behind CVD processes. The object of this section is to discuss the factors described in the previous section and their effects on the morphology of the deposited film.

By changing the chemical equilibrium conditions described on pages 1-2, it is possible to control the direction of reaction. Several options can be employed [8]:

1. Removing or adding reactants or products.
2. Changing the partial pressure of the gaseous reactants and products.
3. Changing the temperature.
4. Adding catalysts.

Consider the following chemical reaction,

$$A + B \rightleftharpoons C + D \qquad (2.8)$$

What would happen if the concentrations were altered during reaction ? At equilibrium, the forward reaction rate (K_f, left to right) is equal to the reverse reaction rate (K_r, right to left). However, if the concentration of the products were decreased, the reaction would respond by increasing K_f. This response is described by the LeChatelier's Principle. The principle states that *if a system in chemical equilibrium is altered by the change of some conditions, chemical reaction occurs to shift the equilibrium composition in a way that attempts to reduce that change of condition* [51]. In CVD systems, products can be removed and/or reactants can be increased to increase the forward reaction rate. These conditions are especially true in Low Pressure CVD systems where the chamber is under vacuum and the concentrations of reactants are kept constant. The trade off in this type of situation would be the economical use of reactant gas and the resulting film thickness or deposition rate.

A change in pressure will also change the reaction direction. Change in pressure also obeys the LeChatelier's principle. In atmospheric CVD reactors, the partial pressure of a reactant may be changed only by dilution although total pressure remains constant. However, in LPCVD systems, the chamber pressure may be adjusted and therefore the partial pressures of the reactant species are altered. A change in partial pressures will offset the equilibrium condition. In general, as the pressure decreases in LPCVD systems, the forward reaction rate (K_f) increases, because the reaction products are constant removed [30].

A CVD reaction can occur under atmospheric pressure conditions. However, when CVD reactions are exposed to low pressure conditions, the chemical equilibrium of the reaction is changed to favor the forward reaction. At low pressure, contamination is also reduced. In CVD systems, contamination can be of several types. Undesirable species, such as hydrogen or nitrogen, exist under atmospheric pressure. These species could get trapped in the film deposited under atmospheric conditions. At the same time, homogeneous reactions may create contamination within the system regardless of the pressure. But under vacuum conditions, the homogeneous reaction products are constantly removed from the chamber. Therefore, contamination due to homogeneous reaction is reduced. As the linewidths of integrated circuits decrease, the contamination issue plays a much more important role [4].

Temperature change has a double effect on the reaction rates since many gaseous reactions and the equilibrium constants are all temperature dependent. To determine the shift in the reaction direction caused by temperature change, the heat of reaction must be added to the equilibrium equation 2.8. In the case of endothermic reactions, K_f is increased with increasing heat of reaction and vice versa for exothermic reactions.

A catalyst is a substance that increases the rate of reaction but it is not consumed by it. In this case, unlike the other three options, the addition of a catalyst does not offset the equilibrium equation. The catalyst just speeds up the reaction process, but it does not change the nature nor the concentration of the outcome. However, due to the nature of the gases used typically in CVD systems, catalysts are generally not used for safety reasons.

2.6 Morphology of CVD Films :

The morphology of CVD films is dependent on the starting surface conditions and the deposition rate. On the previous pages, the influence of many processing factors on the deposition rate were presented. In this section of the report, qualitative analysis of the morphology of CVD films will be presented.

The morphology of the film is closely related to the kinetics of the film growth. Therefore, it is important to understand how the film is formed as reactant species arrive at the surface. The reaction steps which were listed on page 5, are now analyzed in detail [27]:

1. Transport of reacting gaseous species to the substrate: The reactant species are transported to the surface along with inert gas used as the transport medium. The flow rate and the arrival rate determine whether the reaction is mass transport limited or reaction rate limited. During the transport, it is important to minimize the homogeneous type of reaction. If homogeneous type of reaction is the dominant reaction, the desired

product will be formed in the gaseous phase. When these gaseous product species arrive at the surface, they will solidify and form the film. However, due to low kinetic energy and the fact that the reaction has already taken place prior to deposition, the resulting film will be porous and have poor adhesion.

2. Adsorption of the species on the surface: In order to form the film, the reactant species must impinge on the surface and products must be nucleated and agglomerated. The atoms arriving from the vapor phase will not all stick to the surface. Those atoms that do condense onto the surface will migrate over the surface prior to bonding. The higher the substrate temperature, the greater the mobility of the atom. The extra energy available will allow the atoms to arrange themselves in a more "orderly" fashion. If deposition of nuclei from homogeneous reaction occurs, the film surface will have rough topography. The initial surface topography and crystal orientation will also have an effect on the resulting film. In general, different crystal orientation and topography provide different numbers of adsorption sites for the atoms.

3. Heterogeneous reaction on the surface: Only after the reactant species arrive and are adsorbed by the surface, can the heterogeneous reaction take place. The reaction rate will determine the deposition rate, but high deposition rate also will favor the formation of amorphous films. High deposition rate implies low mobility of the reactant species, because the reactant species at the surface are trapped immediately by the newly arrived species. Therefore each monolayer of the reactant species has less time to relax into a crystalline lattice before it is covered by the next monolayer.

Figure 3 shows the different type of films that can be formed depending on the substrate temperature and the deposition rate. In the high deposition rate and high substrate temperature region, the resulting film tends to have polycrystalline structure. A high substrate temperature allows formation of amorphous film at the surface. The process can be viewed as a combination of film deposition and annealing. The same morphology may be obtained by depositing an amorphous film (low substrate temperature) and subsequently exposing the film to a high temperature annealing step.

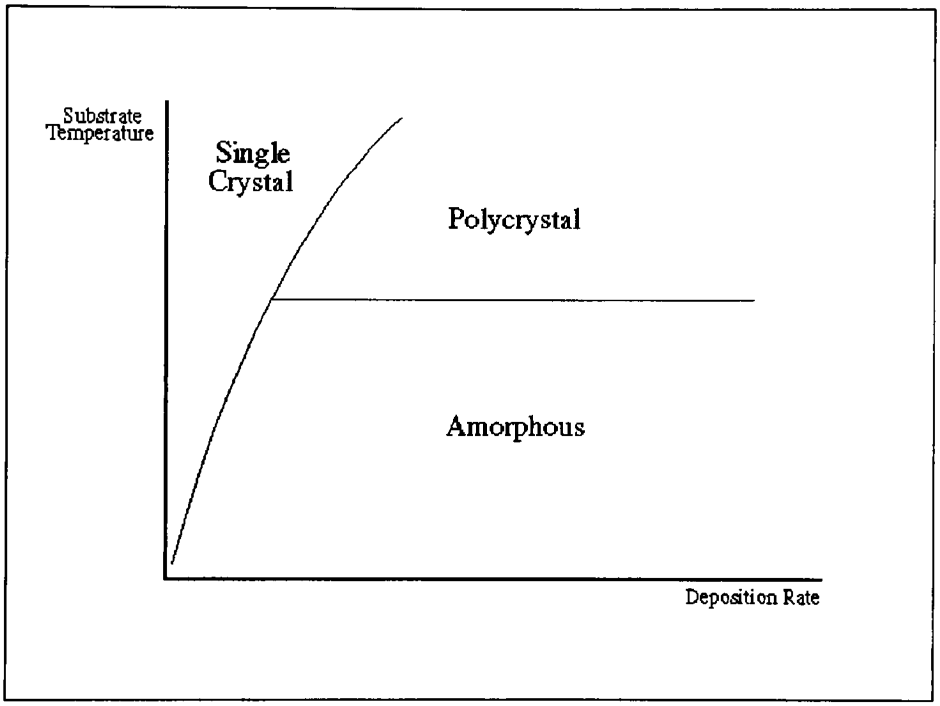

Figure 3. Relationship between film crystal structure, deposition rate and temperature.

4. Desorption of gaseous reaction by-products: the by-products of the heterogeneous reaction must leave the surface. If desorption does not occur, the by-product will be trapped in the film and, depending on the nature of the by-product, chemical reactions or changes in electrical properties might emerge later on.

5. Transport of reaction by-products away from the surface: Once the by-products have been released from the surface, they should be transported away from

the film. Film contamination due to presence of by-products could cause changes in the morphology of the film in an unpredictable manner.

The process described above refers to the undoped CVD deposition processes. In the case of doped thin films, the presence of doping species will influence the deposition rate and therefore the morphology of the resulting film will vary accordingly. Depending on the chemicals involved, the doping species can enhance or retard the deposition rate. In the case of phosphorous doped polysilicon, for example, the adsorption of phosphine forms a thin layer on the substrate and inhibits subsequent adsorption and heterogeneous reaction [7, 28].

Different surface crystal orientation provides a different number of sites at which the arriving species can nucleate. In the case of a silicon, <111> orientation provides the largest possible number of crystal sites, therefore the deposition rate is highest for a <111> orientated silicon substrate. Surface defects, like dopants, can act as growth catalysts or inhibitors. Pronounced surface topography will cause localized disturbances in the gas flow pattern. This results generally in non-uniform film and/or poor step coverage [1, 7, 8].

2.7 Alternative Methods to CVD Oxide :

As mentioned in the introduction, the CVD oxide films are used primarily in the microelectronic industry as insulating films. Alternative methods and materials have been developed to suit specific process needs. The different methods of chemical and physical vapor deposition (PECVD, LPCVD, PHCVD, Sputtering) are just few of the process alternatives available. The resulting films from these processes are similar in nature, they differ only in deposition rate and processing conditions (mainly temperature). Spin-on-glass and polyimide are material alternatives to CVD oxide.

The different process alternatives are classified into chemical and physical depositions. All CVD processes are based on the principles described on the previous pages. The addition of plasma, low pressure or laser enhances the deposition process by either increasing the deposition rate or decreasing contamination. The processing temperature is important because it has direct effect on the underlying films as well as on the impurities species in the substrate. By applying laser or plasma, the thermal energy needed for chemical reaction is reduced. In PECVD systems, the reaction species are more energetic due to the interaction with the plasma. Therefore deposition can take place at lower processing temperature. At the same time, the deposition rate is generally increased by increasing the pressure and the voltage applied on the plasma.

Spin-on-glass (SOG) is an organometallic material used most commonly as an insulation film or etch barrier [27, 28]. SOG is composed of silicon-oxygen backbone polymers dissolved in organic solvents. The material is spin coated onto the substrate and the solvent is removed by a heat process. The film properties are similar that of CVD or thermal oxide. However, a small percentage of carbon remains trapped in the film due to the metallic polymer. SOG processes require less equipment capital than CVD oxide processes, but the process time is significantly longer than CVD oxide. The process itself is more complicated and there are more parameters that must be controlled. Typical problems with SOG includes film cracking and contamination from the spin coating procedure. Most recently, better SOG materials have been redesigned and some of these problems have been reduced. SOG is still widely preferred in the multilayer photoresist processes where the underlying material cannot tolerate temperature above 250 °C.

Organic materials such as polyimide are also suitable to be employed as insulation films [28]. Polymers are used mainly in the integrated circuit manufacturing process as photoresist material for defining geometries on the wafer substrate. Traditional polyimide differs from photoresist in the sense that polyimide lacks of a photoactive compound. Polyimide can also tolerate higher temperature compared to photoresist. Polyimide is applied to the wafer in the same fashion as SOG. After the spin coating process, polyimide films are heat treated to evaporate the solvent and to give the film more stability. In general, the material is treated at approximately 300 to 450 °C for a period of 30 to 60 minutes. Just as for SOG, there are many process parameters that must be controlled to provide proper polyimide films. The heat cycle is nearly equivalent to the process time for CVD oxide. The latest development in the polyimide material arena has been photosensitive polyimide polymers. By making polyimide photosensitive, the deposition and the photolithography procedure are reduced in length and complexity. However, the overall process remains complex and many process parameters still need tight control to provide consistent results.

The CVD oxide process does indeed appear to be very attractive due to its process simplicity. Gas concentrations and temperature are the only process parameters that need attention. Since the process is generally carried out in a controlled environment (plasma or vacuum), contamination and other process parameters are reduced or eliminated. Therefore in theory, PECVD is the most appropriate process technique for oxide deposition available today. Since the chemical process in PECVD is similar to that of LPCVD, by studying LPCVD one can understand the basic principles of CVD oxide processes.

Section 3 : LPCVD Systems for Low Temperature Oxide Films

This section describes the particular CVD system at RIT used for this project and the processing details of oxide deposition using silane and oxygen. The basic principles of CVD presented in the previous section will be used in some occasions to interpret the process parameters of LPCVD.

3.1 General System Description :

The CVD system used for this project was the model 500 LPCVD system manufactured by the Advanced Crystal Sciences Corporation [25]. The system consists of a quartz reaction chamber, a three zone heating system, a mechanical rotary pumping station, a controlled-combustion decomposition and oxidation system, several mass flow controllers, and a process controller. This particular unit lacks an automatic loading system, therefore all loading operations were performed manually. Figure 4 shows a block diagram of the system [25].

The LPCVD system at RIT was used prior to this project for polysilicon and silicon nitride thin film depositions. The gases that were available were dichlorosilane, silane, nitrogen and ammonia. An oxygen gas delivery system was added to the unit for the LTO process. All three processes coexist in the same system at the present time. Each thin film deposition process possesses its own dedicated quartz reaction chamber, which is exchanged for each deposition process.

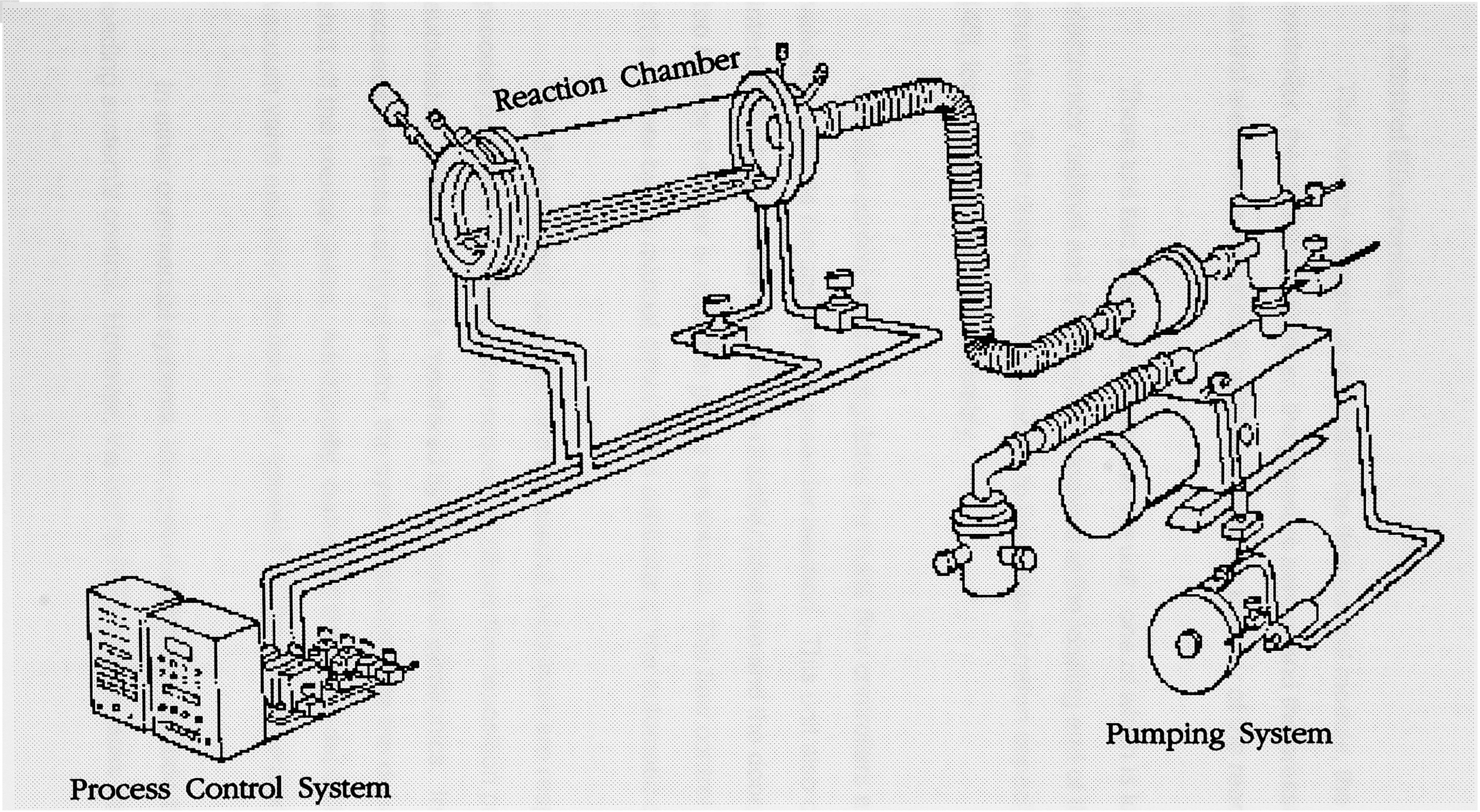

Figure 4. ACS Model 500 Block Diagram
(After ACS 500 System User Manual [25]).

3.2 Control Electronics :

The control electronics consist of the flow control module, the direct digital controller, the control sequencer, the pressure sensor and the pressure displays. The control electronics are housed within a cabinet at the rear of the reaction chamber.

There are two pressure displays in the unit; one of which is located in the control electronics' cabinet and the second is located at the loading end of the reaction chamber. Both displays are connected to the same Baratron capacitance manometer [45], located near the door assembly.

The flow control module regulates the mass flow controllers and the gas control valves to provide the appropriate gases for reaction. This unit also contains the safety interlock features which monitor the chamber pressure and the door. If the pressure is too high or the door is open the gases are shut off. The flow control module can be driven either by the manual direct digital controller or the automatic control sequencer.

The direct digital controller and the control sequencer are responsible for the process parameters. The control sequencer allows the deposition process to be automated. The pressure is monitored by the control electronics. In the event that it exceeds the limits set by operator, the system will terminate the deposition process and shut off the source gases. Additionally, during the automatic deposition process the vacuum valve and door interlock are regulated by the control sequencer.

In other commercial systems, the control electronics include the automatic loading system's control. However, the unit at RIT currently lacks this feature. A new three tube LPCVD system with automatic loading is being installed which should be operational in the beginning of 1992.

3.3 Vacuum System and CDO System :

A mechanical two-stage Leybold-Heraeus rotary pump [46] is employed in the LPCVD unit at RIT. The base pressure in the system is typically in the 20 milliTorr range. The vacuum system also includes an oil filtration system and a particle trap. The pump oil is recirculated and filtered by the filtration system to provide proper pump operating conditions. Particles created in the process chamber are removed by the particle trap before entering the rotary pump. The pump oil and the particle filter are changed approximately every twelve months.

The unit at RIT includes a Controlled-Combustion Decomposition and Oxidation (CDO) system which is not shown in figure 4. This particular unit is manufactured by the Innovative Engineering, Inc. CDO systems process the exhaust gases before they enter the main exhaust systems [25]. The exhaust gases are exposed to high temperature (approximately 850 °C) and are diluted by nitrogen gas. CDO systems remove and/or neutralize the byproducts and the residual gases by means of combustion and decomposition. Without CDO, the byproducts or the residual gases could accumulate and react in the main exhaust system causing explosion or fire. At RIT, the exhaust gases are vented to the house air scrubber after the CDO system.

3.4 Three Zone Furnace :

The reaction quartz chamber is heated by a three zone diffusion furnace. The LPCVD unit at RIT uses three controllers and thermocouples to provide proportional feedback control. The furnace lacks of a temperature monitor during the deposition process. The setpoints are controlled manually and the temperature profile in the chamber is obtained prior to each deposition run. The temperature profile measurements were made while the system was under vacuum using a profiling tube placed down the center of the chamber. The temperature and the profile were assumed to remain unchanged throughout the deposition process. Actual wafer surface temperature probably differs slightly; the degree of inaccuracy is unknown.

3.5 Wafer Boat :

The wafers were loaded into enclosed LTO boats for the deposition process. The boat is not completely enclosed, rather both the boat and the lid are open at each end to allow for gas flow. The boat has additional openings on the bottom to allow gas entrance near the wafers. Two boats were used per deposition run. The boats and the lids are made of quartz material. Each boat can hold up to14 wafers standing in the vertical position. The spacing between wafers (including wafer to wafer between boats) is 9 millimeters. The space between the enclosed boat and the reaction chamber is approximately 5 to 10 millimeters. The LPCVD unit at RIT lacks gas injectors into the reaction chamber. Figure 5 shows a cross-sectional view of the reaction chamber with the enclosed LTO boat loaded with a three inch wafer.

The quartz boats and lids were cleaned by immersing them into a buffered hydrofluoric acid bath. Cleaning was only required when the amount of homogeneous reaction byproduct on the boat (in the form of white powder and/or thin film) was significant. The dummy wafers were cleaned using the same procedure. Cleaning of the boats and the lids usually reduced the apparent leak rate of the system. It appears that the homogeneous film tends to trap moisture and particles, resulting in outgassing. The same logic applies to the cleaning of the quartz furnace tube.

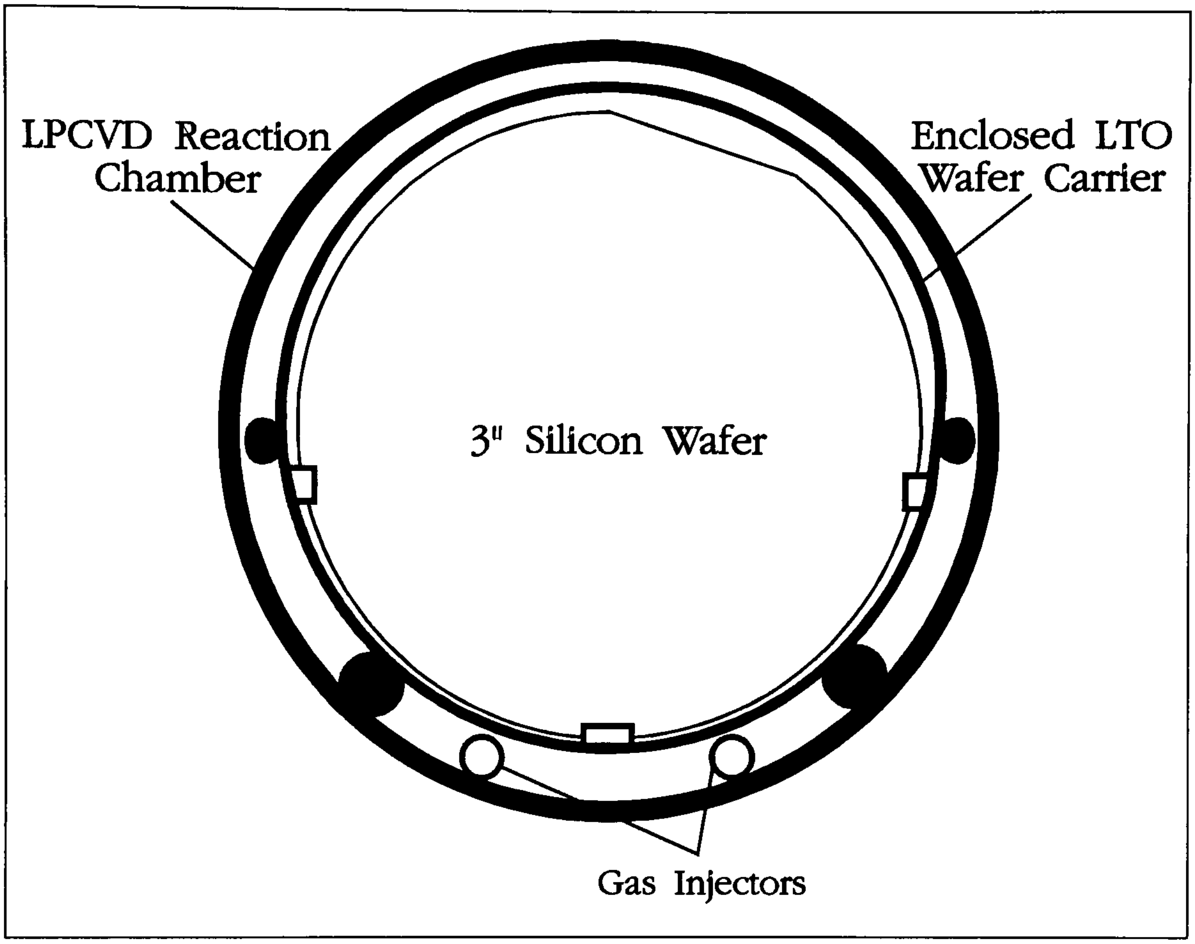

Figure 5. Reaction Chamber with LTO Boat

The enclosed quartz boats are commonly used in LTO processes to accelerate the velocity of the reactant species near the wafers in order to minimize the amount of homogeneous reaction occurring [24, 26]. The gas injectors mentioned before are a set of quartz tubes that transport the source gases (oxygen and silane) separately in LTO systems. The injectors only contain openings near the enclosed wafer boats. The injectors significantly reduce the amount of homogenous reaction and provide better flow dynamics of the gases near the substrate surfaces [24, 26]. Therefore, the uniformity within wafer and from wafer to wafer is generally improved with gas injectors. Figure 5 shows the general location of the gas injectors. Once again, the LPCVD system at RIT does not have the gas injectors.

3.6 Low Temperature Oxide using LPCVD System :

The chemical reaction which produces silicon dioxide film from silane and oxygen gases is described in the following steps [42]:

1. Initiation with excited oxygen radical, represented by square brackets, to form silyl radical:

$$SiH_4 + [O] \rightleftharpoons [SiH_2] + H_2O \qquad (3.1)$$

2. Branching to form an intermediate Si-H-O compound:

$$SiH_2 + O_2 \rightleftharpoons [SiH_2O] + [O] \qquad (3.2)$$

$$SiH_2O + O_2 \rightleftharpoons [SiH_2O_2] + [O] \qquad (3.3)$$

3. Regenerating and terminating:

$$[SiH_2O_2] + O_2 \rightleftharpoons SiO_2 + H_2O + [O] \qquad (3.4)$$

4. Overall reactions are:

$$SiH_4\,(g) + O_2\,(g) \rightleftharpoons SiO_2\,(s) + 2H_2\,(g) \qquad (3.5)$$

and / or

$$SiH_4\,(g) + 2O_2\,(g) \rightleftharpoons SiO_2\,(s) + 2H_2O\,(g) \qquad (3.6)$$

depending on the process conditions, especially the gas flow ratio.

As it can be seen from above, several species are in the chamber while the reaction is taking place. Even the byproducts are composed of several different species. Under normal LPCVD operating conditions, the reaction is in the forward direction and the reaction byproducts are removed by the vacuum system. The silicon dioxide film is deposited onto the substrate and the interior of the reaction chamber, wherever the temperature and gas concentrations are sufficient for the reaction to occur.

Silane gas is used by the semiconductor industry in numerous processes. Silane gas, when exposed to room moisture, is pyrophoric. In the LTO process, it appears that a dangerous situation is being created. The hydrogen byproduct from the silane/oxygen reaction is highly flammable, making the reaction violent and explosive under normal atmospheric conditions. Oxygen is one of the common species present in the room moisture; causing violent results when mixed with silane to produce silicon dioxide and hydrogen. Under LPCVD conditions, the reaction rate of silane and oxygen is regulated both by the gas flow and the deposition pressure. The reaction is therefore under controlled and the amount of hydrogen released by the reaction is kept to a safe level. As long as the concentration of hydrogen is kept low, hydrogen will not be able to ignite.

The process parameters that affect the resulting silicon dioxide film are the deposition temperature, oxygen/silane flows and the chamber pressure (partial pressures of source gas). The spacing between wafers, the chamber dimensions and the shape of the wafer boat influence the uniformity of the film, but they do not significantly affect the deposition rate nor the film physical characteristics [42].

The deposition rate determines the morphology of the deposited film. Generally, LPCVD oxide is in the amorphous state and its physical characteristics are similar to that of thermally grown oxide [16, 20]. The low pressure enhances the forward direction reaction by changing the equilibrium condition (removing reaction byproducts). The dimensions of the enclosed wafer carrier and the reaction chamber itself, cause an increase in gas flow velocity near the wafers (see Figure 5).

The LPCVD oxide deposition from silane/oxygen can take place at any temperature above 300 °C. 420 °C and 900 °C are two temperatures that are commonly used. The deposition temperature must often be kept low because of other films present on the substrate, for example with multilayer metal processes. Oxide obtained from deposition in the temperature range of 400 °C to 500 °C is considered to be Low Temperature Oxide. Index of refraction, film stoichiometry, density and etch rate are all dependent on deposition temperature. At higher deposition temperature, the film tends to be denser. In Sections 5 and 6, the relationship between these properties will be discussed.

Section 4 : Experimental Design and Response Surface Methodology

The method of trial and error has been employed from the beginning of scientific research. The initial conditions were chosen either arbitrary or based on some already known facts. If the experiment involved one single variable, the methodology is to measure the response as the variable takes several values within the experimental range. A mathematical expression can then be written to describe the process and the optimization process is purely mechanical computation.

If two independent variables are involved in the experiment, a similar two-step approach can be taken: hold the first variable fixed, vary the second, then hold the second fixed and vary the first. Each step yields a mathematical equation and the process is simply the product of the two independent equations. Optimization can be carried out by solving the two equations. When two or more dependent variables are involved the optimization process becomes much more complicated. The experimental factors interact with each other and the trial and error methodology simply cannot keep up with the mixed experimental solutions. Therefore, a systematic approach to modeling the system and optimizing the responses is needed. Statistical Experiment design and Response Surface Methodology (RSM) can be used in these situations.

By using statistical experimental design and response surface methodology, today's scientist can accurately and efficiently study and analyze a complex process with a minimum number of tests. A properly designed experiment selectively collects the data within a range of the experimental conditions. The data are then used to predict the results (responses) at specified process conditions. Numerous statistical designs have been developed over the years. It is not the scope within of this project to present the different approaches that are available. The author of this paper has chosen a central composite design and a 2^3 factorial design to analyze the deposition rate and index of refraction of silicon dioxide films deposited by LPCVD. Therefore, in the following pages we will concentrate on the description of the factorial design, the central composite design and their characteristics [11, 12, 13, 14].

4.1 Factorial Design :

In the two factorial design, each experimental factor only occurs at two levels (values). This type of design is useful when not much is known about the experiment [13]. The two level factorial will provide a good base to build other more complex designs. However, the two level factorial design lacks of enough information to generate contour plots. A 2^3 factorial design consists of eight runs which correspond to the eight corners of the square design space. Repeated sets of runs can be performed to assure the results. Analysis of the data is done by plotting the responses versus two or more factors, generating a two or a three dimensional graph. The model will be able to provide an estimate of the differences, trends and similarities between the dependent variables and the responses.

Factorial designs are important and useful for their simplicity. They also allow the researcher to see the trends and the patterns followed by the responses. They also provide a good estimate of the constants in the model with small or as small of variance as any other experimental design. The models derived form factorial designs are generally simple and the calculations to derive the model is not as complicated as the other experimental designs [13].

4.2 Central Composite Design :

A general description of the central composite design's construction is shown below. This description was taken from "Statistical Design & Analysis of Experiment" (page 217) by Robert L. Mason, Richard F. Gunst and James L. Hess [13]. Additional comments (square brackets) were added to clarify the definition.

> 1. *Construct a complete or fractional 2^k factorial layout* [for k variables], *depending on the need for efficiency and the ability to ignore interaction effects.*
>
> 2. *Add 2k axial, or start, points along the coordinate axes. Each pair points is denoted, using coded levels* [+1 or -1, instead of real experimental values, such as 400 °C or 500 °C], *as follows:*
>
> $$(\pm a,\ 0,\ 0,\ \ldots,\ 0),$$
> $$(0,\ \pm a,\ 0,\ \ldots,\ 0),$$
> $$(0,\ 0,\ 0,\ \ldots,\ \pm a),$$
>
> *where a is a constant which can be chosen to make the design rotatable or to satisfy some other desirable property.*
>
> 3. *Add m repeat observations at the design center* [repeat runs are added to observe the reproducibility of the process]*:*
>
> $$(0,\ 0,\ 0,\ \ldots,\ 0).$$
>
> 4. *Randomize* [to eliminate possible errors from the experimental setup] *the assignment of factor-level combinations to the experimental units or to the run sequence, whichever is appropriate.*

When *a* = 1, the design is called a face-centered cube design. The face centered design uses only three levels of factors. Generally other central composite design, where a is not equal to one, five levels of factor are required. For example, if a had value of 1.5, the five factorial levels would be -1.5, -1, 0, 1 and 1.5.

4.3 LTO Experimental Design Details :

In this experiment, four repeat runs at the design center were chosen to study the repeatability of the process. The face-centered cube design was chosen due to temperature control limitations on the LPCVD system at RIT (the temperature controllers are limited to 400 °C, at the low end). The total number of runs was 18 (2^3 + 2x3 + 4). The following table summarizes the experimental factors (conditions) used for this experiment:

Experimental Factor	Range
Deposition Temperature	400 to 500 °C
Deposition Time	30 to 90 minutes
Gas Ratio (Oxygen / Silane)	1.2 to 1.8

Table 1. Experimental Conditions.

Deposition rate and index of refraction were used as the experimental responses. The measurement techniques and data collection procedure are presented in the following section. Figure 6 shows the face-centered composite design used for this experiment.

During the course of the experiment, it was found that the data generated from the central composite design did not appear to correlate at all. Therefore, a two-level factorial design was used instead to complete the experiment. More on this topic is presented in Section 6.

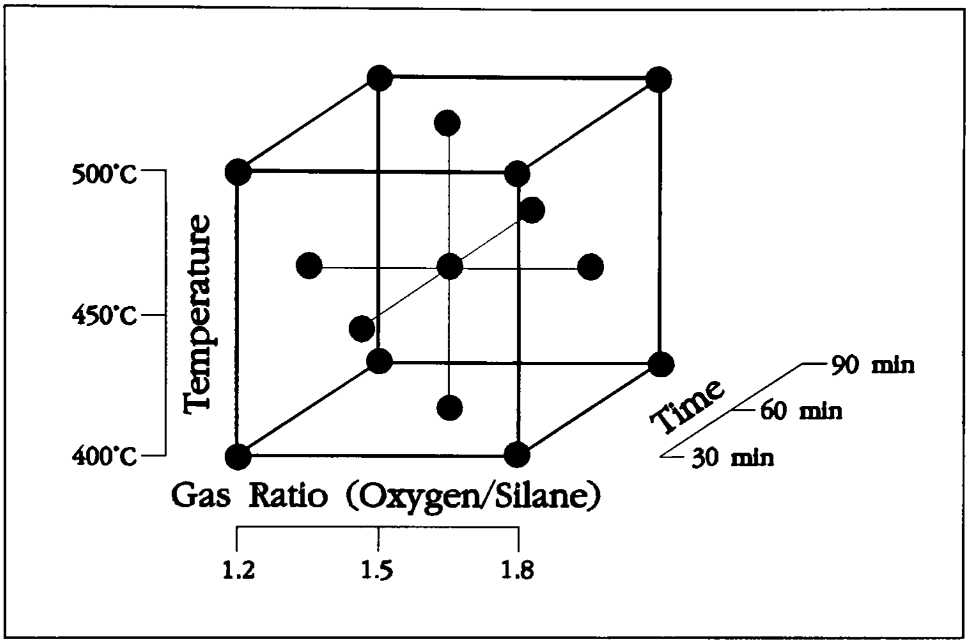

Figure 6. (Face-centered Central Composite Design)

The oxygen-silane gas ratio is calculated by dividing the gas flow of oxygen to that of silane. For safety reasons, the gas flow of silane was kept at a constant value (40 sccm). The gas flow of oxygen was varied from 48 sccm to 72 sccm. The deposition pressure in the chamber, at the 1.5 gas ratio, was approximately 200 mTorr. The deposition pressure upper safety limit was determined to be 400 sccm for the four inch diameter furnace at RIT. At higher pressures, the pyrolytic reaction takes place too rapidly which could lead to fire in the reaction chamber. The gas flows were regulated by mass flow controllers with accuracies on the order of 0.1 sccm.

The four repeat runs at the design center were chosen so that the reproducibility of the process could be studied. The six axial or star points provide the information required to produce more accurate response surfaces. The central composite design used in this project required fewer runs to obtain the same amount of information compared to the traditional 3x3 factorial design. The 3x3 factorial design would have required 27 test runs to cover the same experimental range. Furthermore, the 3x3 factorial would not have provided information on the reproducibility of the process.

The design and data analysis were performed with the Design-Expert and Design-Ease software written by STAT-EASE, Inc. [43], software program made available through the department of Quality and Applied Statistics at RIT. They are IBM/PC compatible and are available directly from STAT-EASE, Inc. The design and data summary for this project are included in the index section. Refer to section 6 for the analysis of the trend plots generated.

Section 5 : Experimental Procedure and Analytical Techniques

The experimental designs used in this project were described in the previous section. The procedure is presented in this section. The changes made to the original design during the course of the experiment are presented in this section along with the appropriate justification for the changes. Other experimental facts, such as the deposition pressure or the actual temperature readings, are also shown in the following pages.

Several analytical tools were employed to characterize the silicon dioxide films. The film thicknesses were measured using three different techniques: surface profilometry, ellipsometry and reflectance spectroscopy. The indices of refraction were determined using ellipsometry. Brief descriptions of each system are provided in Section 5.4. FTIR spectra were obtained using a Perkin Elmer FTIR spectrometer model 1750 with an Attenuated Total Reflectance (ATR) cell, a description of which is presented in Section 5.5. Other miscellaneous analytical techniques are presented in Section 5.6.

5.1 Experimental Design Modifications :

A central composite design was initially chosen for this project. This design consisted of 18 test runs which included four repeat runs at the design center. The design was divided into two separate experimental blocks. The initial intent was to evaluate the data after completing the first experimental block of ten runs. The first experimental block represented the eight corner runs, as shown on Figure 6, plus two center runs. A complete list of the process conditions of the central composite design is shown in Table 2.

Run #	Block	Temp. (°C)	Time (Minutes)	Flow Ratio
1	1	400	30	1.8
2	1	450	60	1.5
3	1	500	30	1.8
4	1	400	90	1.2
5	1	500	90	1.2
6	1	400	30	1.2
7	1	500	30	1.2
8	1	450	60	1.5
9	1	400	90	1.8
10	1	500	90	1.8
11	2	450	90	1.5
12	2	450	60	1.8
13	2	400	60	1.5
14	2	450	60	1.5
15	2	450	60	1.2
16	2	500	60	1.5
17	2	450	60	1.5
18	2	450	30	1.5

Table 2. Original Central Composite Design.

The results of the first block were analyzed using the Design-Expert software and it was found that there was no correlation between the experimental factors and the responses. This indicated that the experimental design should be reconsidered. The second block of the central composite design would have provided more detail on the correlations if they existed. The axial runs would have provided information to generate contour plots. Since no correlation was seen from the collected data, it was unnecessary to complete the original design. A simpler design was needed to re-evaluate the situation. A 2^3 factorial design was chosen to complete the experiment. The results from the central composite design were kept and the corner runs were repeated using a 2^3 factorial design. The modified experimental design and the process parameters are shown in Table 3.

Run #	Block	Temp. (°C)	Time (Minutes)	Flow Ratio
1	1	400	30	1.8
2	1	450	60	1.5
3	1	500	30	1.8
4	1	400	90	1.2
5	1	500	90	1.2
6	1	400	30	1.2
7	1	500	30	1.2
8	1	450	60	1.5
9	1	400	90	1.8
10	1	500	90	1.8
11	2	400	30	1.8
12	2	500	90	1.2
13	2	400	30	1.2
14	2	400	90	1.8
15	2	500	90	1.8
16	2	400	90	1.2
17	2	500	30	1.8
18	2	500	30	1.2

Table 3. Modified Experimental Design (2^3 Factorial) Design.

The modified design repeated the corner runs so that the results from the first block could be confirmed and any previous process errors could be detected. The center points were omitted for simplicity. The new design should allow clarification about whether the factors are insignificant to the responses or whether the process is not in control. Refer to Section 4 for the description of the designs used. By dividing the original design into two blocks, it was possible to detect the problem prior to the completion of all eighteen runs. Without the modification described above, the experiment would have most likely led to inconclusive results. Additional test runs would have been needed to analyze the results.

5.2 Experimental Procedure :

The substrates used were three inch silicon n-type wafers [44]. These wafers were control wafer grade and they were unused prior to this experiment. All wafers were etched in the BOE bath for two minutes, rinsed in deionized (DI) water for five minutes and spun dried prior to the deposition. Since the wafers were unused, no gross organic contamination needed to be removed and therefore, only the BOE bath was used to remove possible particle contamination on the surface.

Twenty-eight wafers were used per deposition run. Measurements were only performed on ten wafers. Eighteen dummy wafers were loaded with the test wafers to provide the same gas flow conditions in the chamber from run to run. The wafers were positioned as shown in Figure 7. The gases entered the chamber at the front of the reaction chamber. The vacuum pump was connected to the rear of the chamber. The center of the two wafer boats corresponded with the center of the three zone diffusion furnace.

The temperature measurements were performed prior to each deposition run with the reaction chamber under vacuum conditions. The temperature was monitored for at least one hour prior to deposition, to allow the chamber and the thermocouples to reach thermal equilibrium. The temperature settings and the thermocouple readings in the three zones were recorded and are shown in Table 4.

The wafers were loaded manually with a push/pull quartz rod. The test wafers were replaced after each deposition run. The dummy wafers, the boats and the lids were cleaned using BOE approximately every four runs. The furnace tube was cleaned three times in between the eighteen test runs.

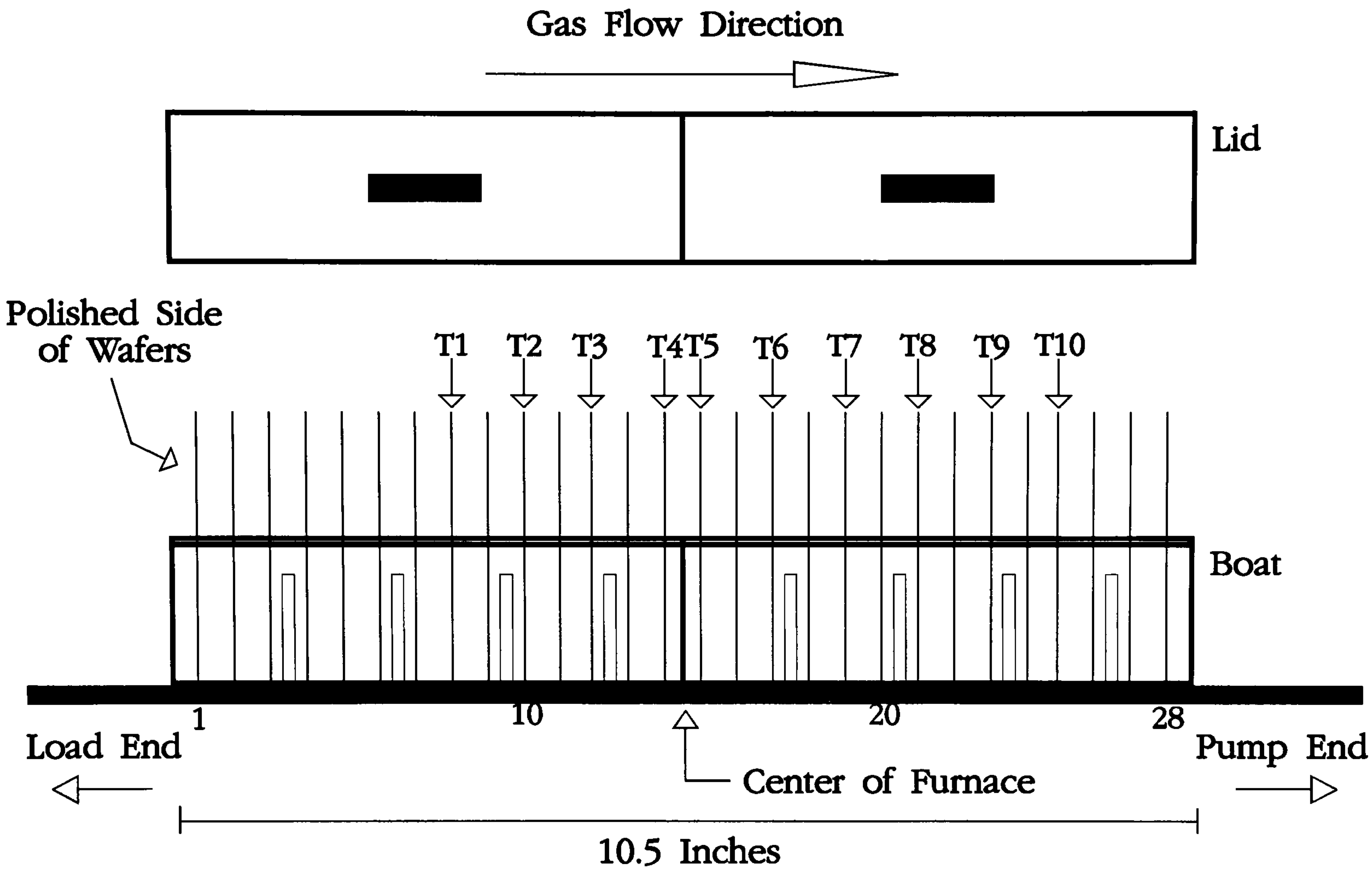

Figure 7. LTO Experimental Load Configuration.
The test wafers are labeled T1 to T10, the other wafers are dummies used to simulate a production run.

Run #	Temp. Load	Setting Load	Temp. Center	Setting Center	Temp. Pump	Setting Pump
1	405	185	399	012	397	540
2	454	158	449	060	448	556
3	505	154	500	109	500	543
4	410	176	400	013	402	545
5	504	152	498	107	497	545
6	398	181	400	011	407	535
7	504	148	501	110	506	536
8	454	157	449	061	453	553
9	408	178	398	012	402	537
10	505	154	500	108	505	543
11	406	185	402	009	402	540
12	507	143	503	105	505	540
13	405	161	400	009	397	543
14	407	161	400	009	401	543
15	505	152	501	106	502	542
16	400	165	400	010	398	542
17	500	150	500	110	503	543
18	499	150	500	110	502	542

Table 4. Deposition Temperature Measurements and Settings. All temperature readings are expressed in °C. The temperature remained constant within ±1 °C during runs.

The control sequencer program used is shown in the Appendix A. A brief summary of the process is shown below:

Process Step	Time
Pump Down 1	15 min
Leak Check	1 min
Pump Down 2	5 min
Gas Ramp Up	2 min
Deposition	Varied
Gas Ramp Down	2 min
Post Pump	5 min
Pump Purge	2 min
Pump Down 3	5 min
Backfill	3 min

Table 5. Summary of Process Sequence

Once the wafers were loaded into the chamber and the system was near the base pressure (approximately 20 mTorr), the automatic control sequencer was turned on. The sequencer controlled the vacuum valve, the gas valves and the time for each process step. Each step had a default abort sequence, outlined in the Appendix A. During the initial pump down (Pump Down 1), the system was brought to base pressure and followed by a leak check. During the leak check, the sequencer closed the vacuum valve for one minute and the pressure differential was recorded manually. This pressure differential corresponded to the leak rate of the system. As long as leak rate was sufficiently low (less than 15 mTorr per minute), the process continued.

The system was then re-evacuated to base pressure prior to the deposition. Due to the lack of "soft start" mass flow controllers, the oxygen and the silane gases were ramped up manually to the set points. Oxygen was ramped up first, followed by silane. Without the ramping step, the pressure in the chamber could have exceeded the upper limit when the mass flow controllers were enabled by the sequencer. The ramping step added extra process control over the initial gas flow conditions. After the deposition run was completed, the gases were again ramped down manually. The deposition time for the different runs are in Table 3.

The remaining steps removed the residual source gases from the chamber and purged the system with nitrogen prior to venting the system to atmospheric pressure. The wafers were then removed manually by using a quartz push/pull rod.

During the course of the entire process, the operator could have aborted or held the run by switching to manual mode on the direct digital controller and putting the automatic sequencer on hold. It is essential that the vacuum valve be in the on position prior to switching to manual mode. Otherwise, the chamber could be vented to atmospheric pressure conditions while silane gas was still in it.

5.3 Observations During Deposition :

The partial pressure of the chamber during deposition did not correspond to the sum of the individual partial pressures of oxygen and silane. At a flow rate of 40 sccm, silane gas, by itself, had a partial pressure of approximately 150 mTorr. At a flow rate of 60 sccm, oxygen gas, by itself, had a partial pressure of approximately 200 mTorr. When the two gases were combined, the total pressure was approximately 225 mTorr. During ramp up, the pressure was observed to drop slightly when the silane gas was first turned on with oxygen already in the chamber. The pressure would then increase slowly by about 5 to 10 mTorr after approximately five minutes. During the remaining of the deposition time, the pressure was constant. A summary of the observed deposition conditions are shown in Table 6.

It is not a surprise that the deposition pressure was not equal to the sum of the individual partial pressures since the reaction was indeed taking place and many reaction species were all present at the same time in the chamber. It is difficult to predict the pressure without having knowledge of the reaction species in the chamber. However, the sum of all the partial pressures of the species in the chamber must equal to the deposition pressure. At the present time, it was not possible to determine the species in the chamber.

The initial pressure drop, when the silane gas was turned on, indicates the initiation of the deposition process. Once the deposition reaction started, one to two minutes were required to reach equilibrium pressure.

Run #	Date	Temp. °C	Time Minutes	Flow Ratio	Base P. (mTorr)	Dep. P. (mTorr)	Leak Rate
1	8/17/91	400	30	1.8	20	245	1.6
2	8/17/91	450	60	1.5	19	225	3.0
3	8/17/91	500	30	1.8	21	250	10.0
4	8/18/91	400	90	1.2	21	200	4.0
5	8/18/91	500	90	1.2	23	200	12.0
6	8/19/91	400	30	1.2	21	195	3.8
7	8/19/91	500	30	1.2	22	205	7.0
8	8/19/91	450	60	1.5	21	220	4.8
9	8/20/91	400	90	1.8	22	250	3.8
10	8/20/91	500	90	1.8	24	255	11.0
11	8/23/91	400	30	1.8	21	250	6.0
12	8/24/91	500	90	1.2	24	205	8.7
13	8/24/91	400	30	1.2	22	200	9.0
14	8/24/91	400	90	1.8	22	250	10.5
15	8/24/91	500	90	1.8	23	250	14.5
16	8/25/91	400	90	1.2	23	200	3.5
17	8/25/91	500	30	1.8	23	250	10.0
18	8/25/91	500	30	1.2	26	200	9.0

Table 6. Summary of Process Conditions. Leak rates are expressed in units of mTorr per minute.

It was also observed that the homogeneous reaction tended to take place at higher gas flow ratio. This was seen from the white layer of film left in the reaction chamber after each deposition. The white film was much more noticeable after high flow ratio deposition runs. This white film had a direct effect on the pumping performance. After approximately four hour of accumulated deposition time, both the base pressure and the leak rate in the system tended to be higher. This was probably caused by the outgassing of the film formed from the homogeneous reaction. If the homogeneous reaction was minimized, the reaction chamber did not need as frequent cleaning.

The leak rate is therefore a good indicator of the furnace tube condition. Cleaning is recommended when the leak rate surpasses 15 mTorr per minute. The particle trap on the mechanical pump seemed to retain most of the homogeneous reaction products, since the pumping speed has remained almost constant after 18 test runs. The base pressure rose slightly during the start of this project; this could be an indication of the particle trap getting too dirty. These observations on the mechanical pump agree with those seen by other researchers.

5.4 Thickness Measurement Techniques :

The thickness measurement was a very important part of this project since one of the experimental responses, deposition rate, was a function of the thickness. Ellipsometry was the main measurement tool used to obtain both the index of refraction and film thickness of the resulting oxide films. Surface profilometer and reflectance spectroscopy were used to verify and adjust the readings obtained from the ellipsometer.

Ellipsometry uses the change of state of the polarization of light when it is reflected from a surface. The polarization state is defined by the relative amplitude and the phase difference of the parallel and perpendicular polarization components of the radiation. By analyzing the polarization state of the reflected radiation, one can determine the thickness of the film if the optical constants of the substrate and the angle of incidence were known. Two different ellipsometers were used: an Applied Material manual ellipsometer and a PLASMOS SD2000 automatic ellipsometer [48].

The PLASMOS SD2000 unit uses a 632.8 nm He-Ne laser light source. The incident angle was set at 70°. The system is linked to a IBM/PC compatible computer. All operation of the ellipsometer are controlled by a custom software package provided with the unit. The SD2000 unit is based on the principles of rotating analyzer. The polarizer is kept at a fixed angle of 45°. The analysis is performed by a permanently rotating polarizer with a photo-detector. The photo-detector reports the angle at which a minimum intensity was found and the built-in microprocessor determines the ellipsometer angles. These angles are then transfered to the computer for thickness and index of refraction computations. The SD2000 setup is shown on Figure 8. For a more detailed description of the system refer to the PLASMOS' operating manual [48].

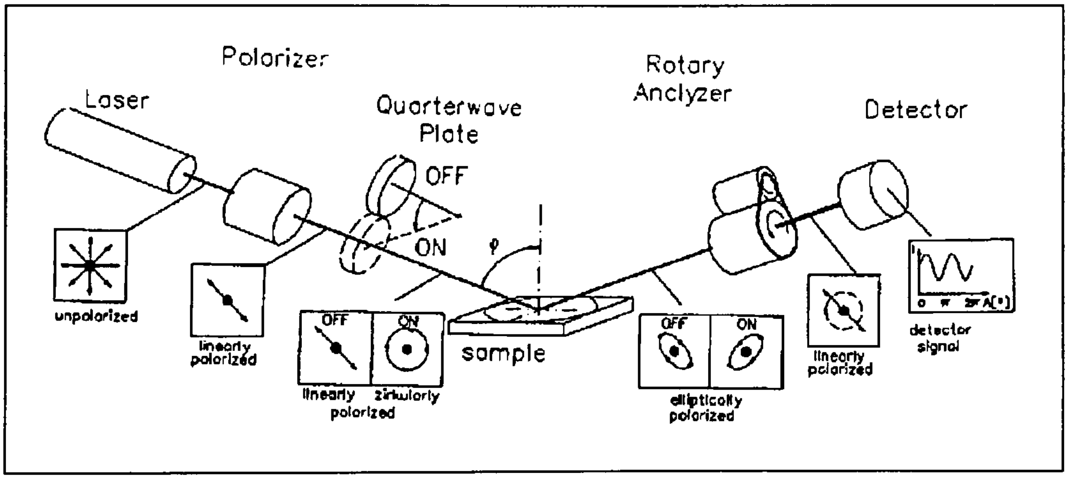

Figure 8. SD2000 Setup (After PLASMOS Thin Film Measurement Systems Operating Manual [48]).

A similar manual rotating analyzer ellipsometer was used to confirm the readings obtained from the PLASMOS SD2000 system. The analyzer and polarizer angles were read manually and then they were entered into a computer program. This program was developed by Frank McCrackin [49], for the National Bureau of Standards, to compute the film thickness and the index of refraction given the angles from the ellipsometer.

Surface profilometry requires a step in the film for the measurement. A profilometer drags a fine stylus along the surface with the step. The stylus provides the information by means of differential capacitance or inductance techniques. The signal change is recorded by a computer or displayed on a chart recorded. When the signal is recorded by a computer, the step can be further analyzed by manipulation of the data on the computer. A Sloan Dektak IIA and a Tencor Alpha-Step I profilometers were used. The step on the oxide films were created using conventional photolithography and BOE.

Reflectance spectroscopy analyzes the interference spectrum produced by differential reflections from top and bottom surfaces of a transparent film. The optical interference intensities versus wavelengths are used to determine the thickness. A Nanometrics NanoSpec/AFT Reflectance microspectrophotometer was used to confirm the ellipsometer readings. The standard program 1 for oxide film on silicon substrate and 10X magnification were used. A detail operating procedure of the NanoSpec/AFT can be found elsewhere [53].

5.5 Fourier Transform Infrared Spectroscopy :

Fourier Transform Infrared (FTIR) spectrometer is based on the Michaelson interferometer. FTIR interferometer utilizes a system of mirrors to direct the electromagnetic radiation (in this case, infrared light) onto the sample. When the electromagnetic radiation passes through the sample being analyzed, some of the frequencies are absorbed. The absorption is related to the molecular vibrational frequencies within the sample. Different molecular bonds will absorb at different frequencies. By analyzing the absorption bands in the infrared spectrum, the chemical bonds and some structural characteristics can be identified.

FTIR spectroscopy has been used widely in the study of polymers for many years. In the recent years, more research has been directed toward inorganic materials. Many scientists and engineers have used FTIR to identify certain materials and their crystalline structure. The microelectronic industry has employed this technique as a fast, non-destructive method of characterizing thin films. By a simple comparison test, a new material or a new process can be characterized against well-known materials. Silicon dioxide is a good example of this.

As mentioned in the introduction, silicon dioxide films created by new processes are generally compared to the thermally grown silicon dioxide films. FTIR provides the information needed for the comparison in most situations with the silicon dioxide films. As more research is done with FTIR, new facts about chemical composition, crystal structure and oxygen/silicon contents are being discovered. The FTIR was used in this project to identify the silicon dioxide films created by a LPCVD process. Some discoveries were made on the chemical composition of the created films. The FTIR results are contained in Section 6.

A Perkin Elmer FTIR spectrometer model 1750 was used. The spectra were obtained by using an Attenuated Total Reflectance (ATR) cell [50], also known as the Multiple Internal Reflection (MIR) cell. The ATR cells allows the study of surface properties. The ATR cells guides the radiation to the sample surface at some grazing angle of incidence. Silicon dioxide films were deposited on silicon substrates in this project. The transmission of infrared through the sample would have contained mostly information on the silicon substrate due to the thickness difference. Therefore, a multiple internal reflection technique was employed.

A multiple internal reflection technique utilizes a set of mirrors to direct the radiation into an internal reflection element, such as a crystal of KRS-5, Ge or ZnSe. The sample is placed against the crystal, the IR radiation is then reflected off the sample surface several times before leaving the crystal. The spectra are collected by a photodetector and the signal is send to a computer. A KRS-5 crystal of 45° entrance angle was used. The KRS-5 crystal used had an index of refraction of 2.37 and the transmission range was 4000 to 300 cm^{-1}. Figure 9 shows an ATR cell with the mirror elements.

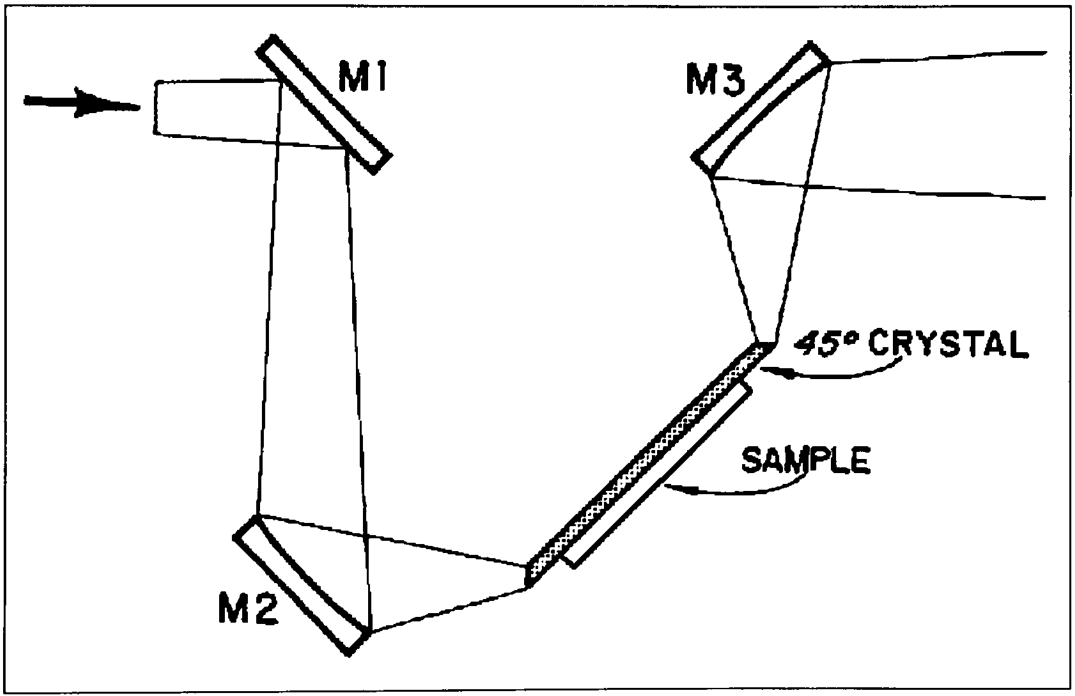

Figure 9. Optical Diagram of the ATR Accessory (After Perkin Elmer, Multiple Internal Reflection Accessory Instructions [50]).

The signal from the MIR or ATR cell is directly proportional to the number of times that the radiation is reflected off the sample. The physical dimensions (thickness, width and angle of incident) of the crystal will determine the number of reflections. By using the 45° crystal, the number of reflections was estimated to be approximately 25 for the setup used in this project [48]. The signal is also affected by the contact between the crystal and the sample. The objective in this project was to identify the silicon dioxide films and no quantitative results were derived from the spectra. Therefore, the intensities of the absorption peaks were not as important as their location and shape. The results are presented and discussed in section 6.

5.6 Other Analytical Techniques :

Besides film thicknesses, indices of refraction and FTIR spectra, the density, etch rate and dielectric constant of the optimum condition film were also determined. The analytical techniques used to obtain these properties are described in the next few paragraphs. Visual examination and Scanning Electron Microscope (SEM) procedures used were standard and will not be discussed here.

The density of the film was determined by measuring the weight of the wafer prior to the deposition run and after the BOE etch step. The weight was then recorded again after the deposition run. The density was then calculated as follows:

$$\text{Density} = \frac{\text{Weight After} - \text{Weight Before}}{2 \times \text{Wafer Area} \times \text{Oxide Thickness}} \qquad (5.1)$$

The deposited oxide films were assumed to be equal on both sides of the wafer. The oxide thickness was taken from the ellipsometer readings. This method can only yield a rough estimate of the density since neither the weight nor the area were accurate measurements. The analytical balance used was only accurate to the 1/1000 of a gram. The area of the wafer was not exactly the area of a three inch circle because of the major and the minor flats on the wafers. Poor uniformity also contributed to the calculation errors. However, this method did provide an estimate for the density of the deposited oxide films.

The etch rate was determined by step etching the oxide films in BOE [47]. The step etch was performed by lowering the wafer approximately half inch into the etcher every five seconds. The thickness loss was then determined by measuring the remaining thickness using the NanoSpec. Since comparisons were made within the same wafer, the measurement from the NanoSpec was accurate enough and ellipsometry measurements were not taken.

The dielectric constant was determined by using capacitance-voltage measurements. The dielectric constant of a film can be found by creating a capacitor with the film and measuring the capacitance. The capacitance of a parallel plate capacitor is defined as:

$$\text{Capacitance} = (\kappa\ \varepsilon_0\ A) / d \qquad (5.2)$$

where κ is the dielectric constant, ε_0 is the permittivity of free space (8.854×10^{-12} F/m), A is the area of the capacitor and d is the thickness of the dielectric material, in this case silicon dioxide. Once again the oxide thickness was obtained from the NanoSpec measurement. The capacitors created had the Metal-Oxide-Semiconductor (MOS) structure. The capacitors were made by applying standard microelectronic processing techniques, which can be found from some of the references listed at the end of this report [27, 28, 29].

Dielectric strength was found by applying voltage on the MOS structure until current flow was detected. The voltage, at which the current flow begins, divided by the thickness of the film corresponds to the dielectric strength of the material.

Additionally, five wafers were processed to create double metal structures using the LTO films as the insulating film. The procedure and the photolithography mask set were provided by Michael Bailey [52], details on his project can be found in his unpublished paper. The results and discussion of the double metal wafers are also presented in Section 6.

Section 6 : Results and Interpretation

The summaries of the experimental results are presented in this section. The complete tabulated data can be found in the Appendices B, C, D and E. Statistical software Design-Ease was used to model the deposition rate and the index of refraction. A more traditional statistical approach was taken to study film thickness uniformity.

6.1 Thickness and Index of Refraction Measurements :

The film thickness and the index of refraction measurements obtained from the PLASMOS SD2000 ellipsometer are tabulated in the Appendices B and C. A plot of film thickness and index of refraction versus wafer position is included along with each table. Each wafer had five measurements taken at fixed locations on the wafer. Figure 10 shows these locations. A transparent plastic template was used to locate the exact location for the measurements. The center location was position at the wafer's center and the four axial points were approximately one inch away from the center position.

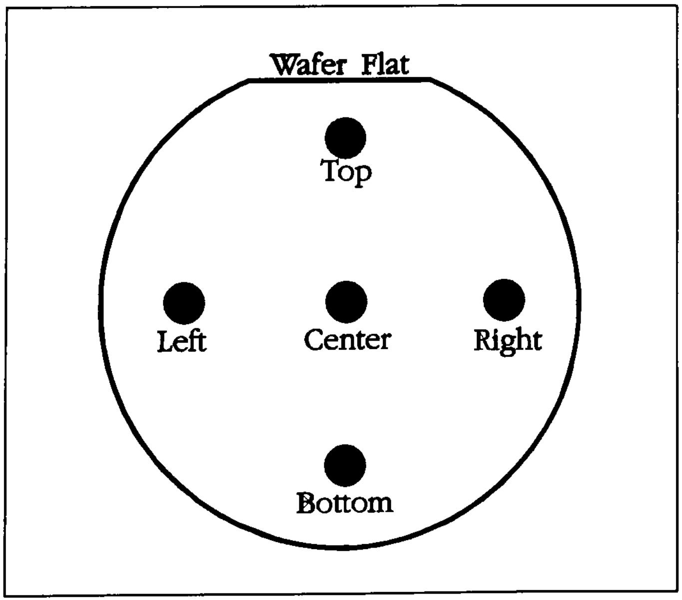

Figure 10. Wafer Measurement Locations.

For each wafer, an average value and standard deviation of five measurements were computed. For the entire test run, the wafer averages were averaged, to give the run averages, and the wafer standard deviation were averaged to give the run standard deviation. A summary of the results is shown in Tables 7 and 8. The values shown are the run averages and the run standard deviations. The deposition rate was calculated by dividing run average thickness to the deposition time. All values were rounded off to the nearest tens figures. Many other approaches could have been taken, such as the standard deviation of the measurements within a lot, the average of STD from wafer to wafer or the STD of the averages. For comparison reasons, any one of the above would have provided the information needed. The same run numbers as those used in the previous sections are shown in Tables 7 and 8. The runs with the same process conditions are indicated by the equal sign in the Run # column.

Run #	Process Conditions	Average Thickness (Å)	Thickness STD (Å)	Deposition Rate (Å/min)
1	400 / 30 / 1.8	820	110	27
3	500 / 30 / 1.8	1640	130	55
4	400 / 90 / 1.2	1930	200	22
5	500 / 90 / 1.2	4380	270	49
6	400 / 30 / 1.2	1200	30	40
7	500 / 30 / 1.2	2170	90	72
9	400 / 90 / 1.8	2920	150	32
10	500 / 90 / 1.8	4100	290	46
11=1	400 / 30 / 1.8	810	70	27
12=5	500 / 90 / 1.2	4240	160	47
13=6	400 / 30 / 1.2	1160	30	39
14=9	400 / 90 / 1.8	2930	170	33
15=10	500 / 90 / 1.8	3970	350	44
16=4	400 / 90 / 1.2	-----	-----	-----
17=3	500 / 30 / 1.8	1800	90	60
18=7	500 / 30 / 1.2	2100	50	70

Table 7. Summary of Thickness Measurement and Deposition Rate.

Run #	Process Conditions	Average Index of Ref.	Index of Ref. STD
1	400 / 30 / 1.8	1.438	0.025
3	500 / 30 / 1.8	1.448	0.018
4	400 / 90 / 1.2	1.449	0.017
5	500 / 90 / 1.2	1.444	0.012
6	400 / 30 / 1.2	1.459	0.001
7	500 / 30 / 1.2	1.432	0.003
9	400 / 90 / 1.8	1.434	0.046
10	500 / 90 / 1.8	1.416	0.052
11=1	400 / 30 / 1.8	1.445	0.016
12=5	500 / 90 / 1.2	1.440	0.012
13=6	400 / 30 / 1.2	1.458	0.001
14=9	400 / 90 / 1.8	1.432	0.045
15=10	500 / 90 / 1.8	1.421	0.043
16=4	400 / 90 / 1.2	-----	-----
17=3	500 / 30 / 1.8	1.450	0.012
18=7	500 / 30 / 1.2	1.451	0.008

Table 8. Summary of Index of Refraction Measurements

All the thickness and index of refraction measurements taken from the SD2000 ellipsometer were confirmed using a manual ellipsometer and two profilometers. The difference between the thickness readings is small and Table 9 shows these readings. The procedure followed to create the steps for the profilometer measurements was described in the previous Section.

Wafer #	SD2000	AlphaStep	Dektak IIA	NanoSpec
5	718	1200*	990	670
15	2410	2400	2737	2356
25	1825	1800	1907	1808
35	1951	1900	1993	1928
45	5382	5000	5788	5605
55	1276	1350	1247	1260
65	2205	2000	2217	2167
75	3284	3100	3188	3256
85	3198	3200	2733	3263
95	4938	5200	5676	5561

Table 9. Comparison between the Thickness Measurement Techniques.
*AlphaStep lacks of resolution for film thickness of 1000 Å or less.

The profilometer measurements were taken near the center of the wafer. The film thickness readings for SD2000 shown above correspond to the ellipsometer measurement taken at the wafer center point (single measurement). The NanoSpec readings correspond to the average of three measurements near the center of the wafer. The index of refraction at the center point of each specific wafer was entered into the NanoSpec to obtain the thickness reading. From the readings shown above, the film thickness measurements from the SD2000 ellipsometer can be considered representative.

6.2 Deposition Rate Model :

As mentioned previously, the software package Design-Ease was used to analyze the data. The average of deposition rate was computed by dividing the average thickness by the deposition time. This was the response used. Despite identical process conditions runs 3 and 14 gave very different thickness readings. Therefore, the results from these two runs were omitted from the statistical analysis. The program computed the coefficients for each experimental factor and the four interaction terms: Tt, TR, tR and TtR. T represents deposition temperature, t represents deposition time and R represents gas flow ratio. Analysis of variance allowed a residual variance and standard error to be computed. Effects which had standard deviation error less than the residual were considered insignificant and were omitted from analysis. The coefficient with the highest sum of squares was the most influential factor in the design.

A summary of the results from Design-Ease for deposition rate is shown in the Appendix F along with effect plots. The model for the deposition rate was determined to be:

$$\text{Dep. Rate} = -84.10 + (.40 \times T) + (.85 \times t)$$
$$- (29.83 \times R) - (3.12\text{x}10^{-3} \times T \times t) + (.28 \times t \times R) \qquad (6.1)$$

where T is the deposition temperature (in °C), t is the deposition time (in minutes) and R is the gas flow ratio.

Figure 11 shows the cube plot of the deposition rate as predicted by the model. Since the data points at the low temperature, low gas flow ratio and high deposition time region (run 3 and 14) were omitted when the model was created, the plot is not valid near those process conditions region.

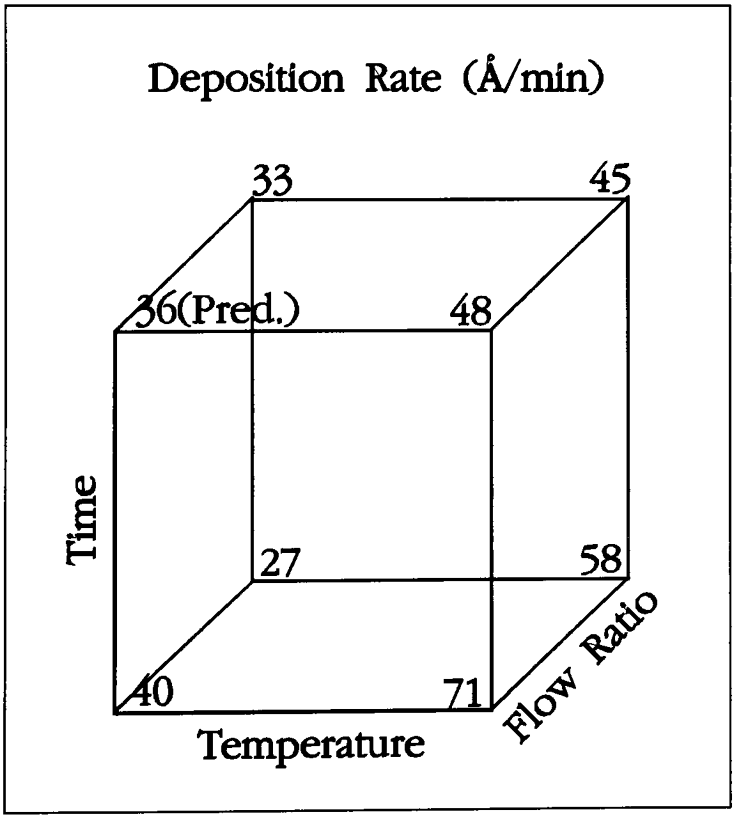

Figure 11. Cube Plot of Predicted Deposition Rate.

Figure 12 shows the effect plot of deposition rate versus temperature, which basically corresponds to the projection of the cube design space onto one single dimension. This plot is similar to the Arrhenius plot except that the T-axis is inverted. The slope of this plot is a function of the activation energy of the process.

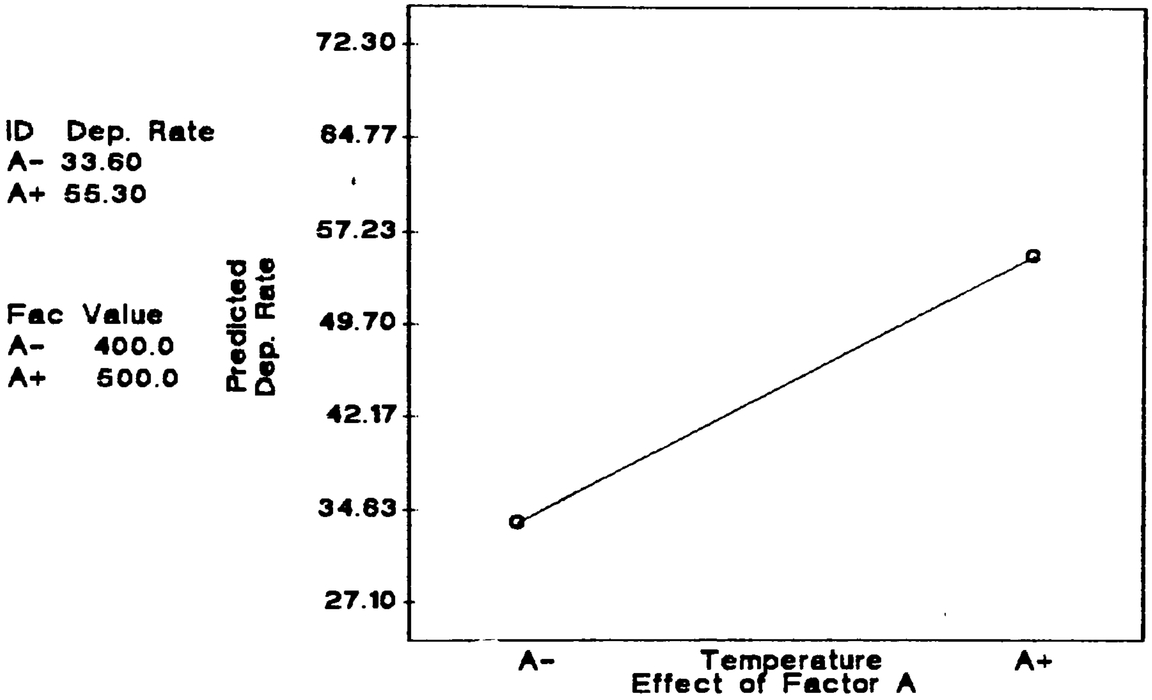

Figure 12. Effect Plot of Deposition Rate versus Temperature.

The apparent activation energy was estimated by the following Arrhenius formula (assuming that the reaction obeys Arrhenius equation) [30]:

$$E_a = \frac{k \ln \frac{R_2(T)}{R_1(T)}}{\frac{1}{T_1} - \frac{1}{T_2}} \qquad (6.2)$$

where k is the Boltzmann's constant (8.62x10^{-5} eV/°K). The apparent activation energy was found to be .089 eV for the LTO process presented here. The activation energy for thermally grown oxide is reported to be 1.9 to 2.0 eV. The activation energy of CVD silicon dioxide has found to be less than .4 eV from literature [28]. The low value indicates the dominance of surface reactions. This result agrees with the results found in the literature.

It has been reported that the deposition rate has a complicated dependency on the oxygen/silane gas ratio. At a constant temperature, as the gas flow ratio increases the deposition rate increases rapidly and then it drops off after reaching a maximum value. It has been reported that the surface reaction is the cause for the decrease in deposition rate. As the ratio of oxygen/silane is increased, the surface becomes saturated by oxygen molecules and the reaction is inhibited. It was observed in this experiment that the deposition rate does indeed drop off toward the high gas flow ratio end. From the data collected (including the two center runs), the optimum gas flow ratio appears to be within the experimental design range. However, without further investigation the exact ratio at which the deposition rate is at a maximum cannot be predicted. The additional axial runs from the original central composite design might be able to provide the answer to this question.

Figure 13 shows the interaction plot of deposition rate versus time and gas flow ratio averaged over high and low temperatures. At low deposition time (30 minutes), the gas flow ratio had more pronounced effect on the deposition rate. Although the overall deposition rate was higher at the low deposition times. The process appeared to be a self limiting reaction process. Therefore, the surface condition must be changing with respect to time. The general decreasing trend of the deposition rate (seen on Figure 13) as the gas flow ratio was increased was caused by the increase of homogeneous reactions. As the homogeneous reaction rate increased, less amount of reactant species was available to create the desired silicon dioxide film through heterogeneous reactions.

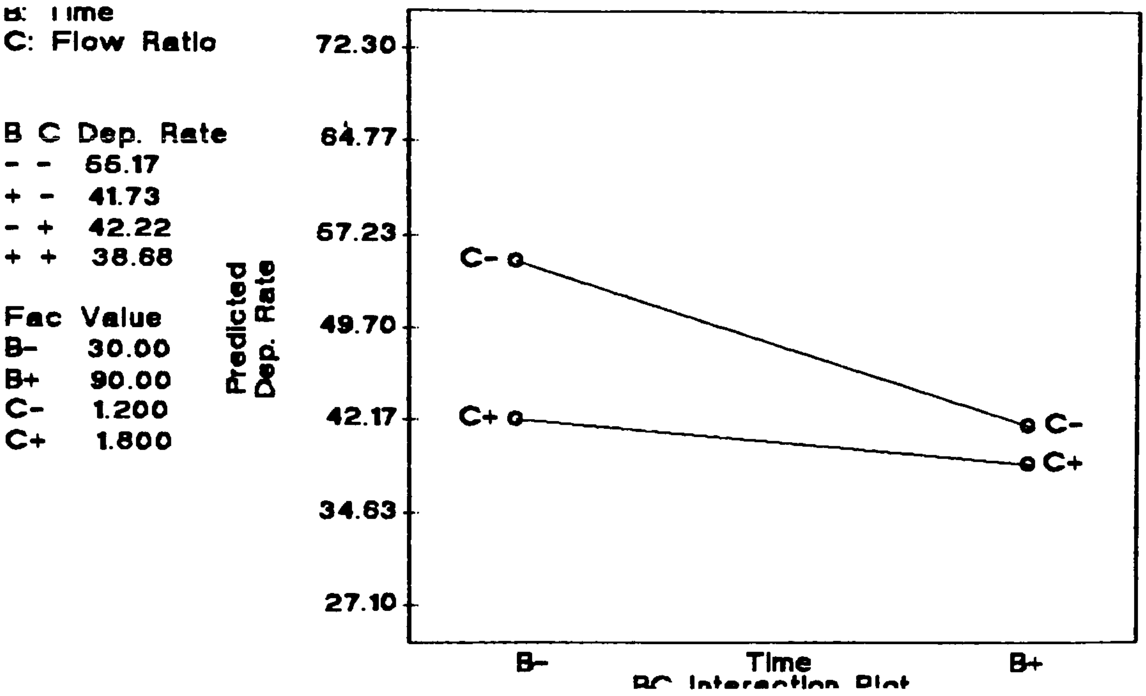

Figure 13. Gas Flow Ratio and Time Interaction Plot. The predict value for deposition rate at low flow ratio and low deposition time is questionable since results from runs 4 and 16 were employed to determine this plot.

From the cube plot, Figure 11, the gas flow ratio phenomena mentioned above was also observed. The maximum deposition rate seems to be near the high temperature and low gas flow ratio region. However, the high temperature might not be suitable in some processes. Compromise between temperature tolerance and deposition rate must be made.

6.3 Index of Refraction Model :

A similar procedure as the one used for the deposition rate model was followed to obtained the model for the index of refraction. The summary sheets from Design-Ease for the index of refraction is shown in Appendix G. Although a model was determined for the index of refraction, the reader is cautioned about these results. The standard deviation for the measurements were large compared to the variation predicted by the model, therefore the model should only be used to interpret the results from this project.

The index of refraction was found to be dependent of the deposition temperature, the deposition time, the gas flow ratio and the interaction between the time and the gas flow ratio. The temperature had a very weak influence on the index of refraction. The governing equation was determined to be :

$$\begin{aligned} \text{Index} = 1.48 - (7.70\text{x}10^{-5} \text{ x } T) + (4.03\text{x}10^{-4} \text{ x } t) \\ + (4.38\text{x}10^{-3} \text{ x } R) \quad (4.06\text{x}10^{-4} \text{ x } t \text{ x } R) \end{aligned} \qquad (6.3)$$

where T is the temperature (in °C), t is time (in minutes) and R is gas flow ratio. The overall average index of refraction was found to be 1.44. The index of refraction for silicon dioxide is 1.458 at a wavelength of 632.8 nanometers [28]. Silicon dioxide films with index of 1.46 and higher are usually silicon rich with high film density. At indexes of 1.44 or lower, the films are more porous. In general, CVD oxides tend to have lower indexes of refraction [28].

Figure 14 shows the interaction plot of gas flow ratio and deposition time. The index of refraction decreased with both increase in deposition time and gas flow ratio. The deposition time had a larger effect with large gas flow ratio. At higher gas flow ratio, the homogeneous reaction was enhanced by the increase in the amount of reaction species available. Therefore, the silicon dioxide films prepared became more porous as indicated by the index of refraction readings.

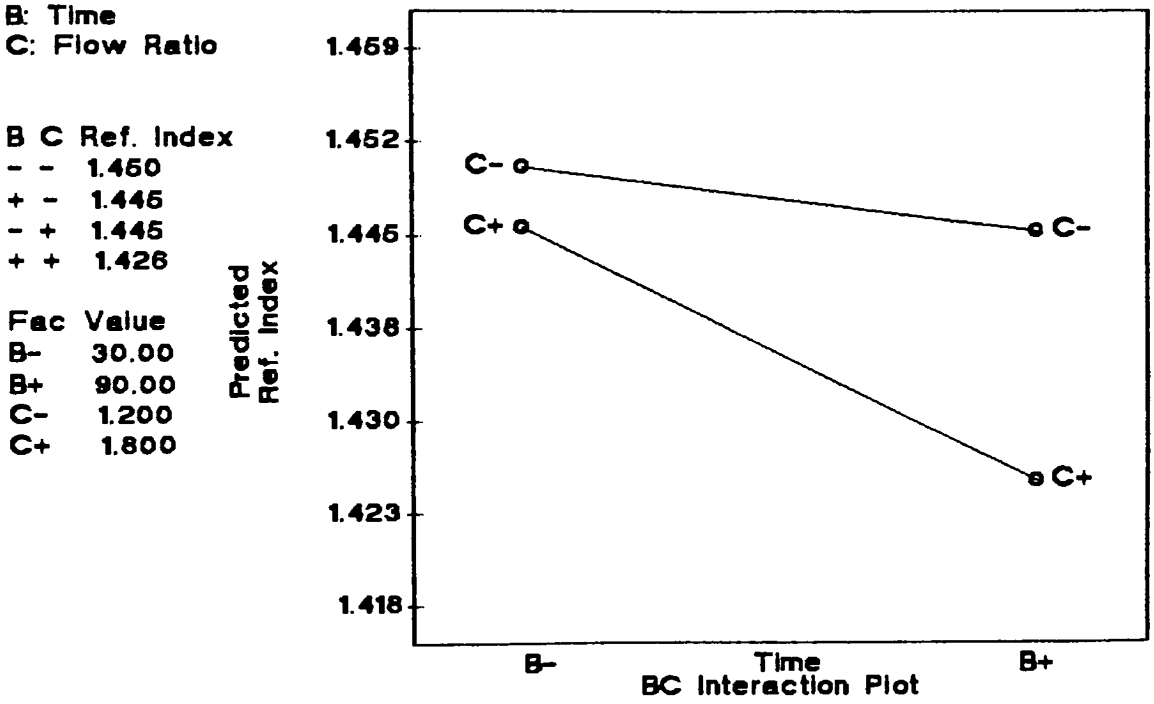

Figure 14. Gas Flow Ratio and Time Interaction Plot.

The crystal structure of CVD films is generally amorphous. However, the degree of "disorder" in relation to the process conditions is usually unknown. Some researchers have suggested a short term "order" within the amorphous structure of oxide films [35]. As the deposition time increases, the film becomes thicker and the overall "disorder" might increase as a result of the change in surface condition. The initial reactant species arriving at the surface encounter a very regular structure. As the deposition continues on, the structure at the surface starts to become more and more "disordered". The disorder in the structure contributes to the porous structure and therefore reducing the index of refraction. This phenomenon was also observed from the data collected in this project.

6.4 Thickness Uniformity Issue :

Film uniformity within the wafer, from wafer to wafer and from run to run are desirable characteristics in any type of film deposition processes. Film thickness variation within the wafer in the LTO process is ordinarily caused by nonuniform or poor gas flow near the wafer surface. Film thickness variation from wafer to wafer is usually caused by a gas distribution gradient in the reaction chamber. The uniformity from run to run is dependent on the entire process and all the parameters. To find conditions which minimize the film thickness variation, the previous experimental design approach can be employed. Once that a model is established, optimum conditions can be found by determining the minimum variation.

A more classic approach was taken for the film uniformity issue in this project. For each deposition run, the averages of the thickness readings for a wafer were plotted versus the position in the chamber such as shown in Figure 15 (Appendix B contains all the plots). The plots were then examined for repeating patterns from run to run and at different process conditions. The uniformity, or the lack of it, from wafer to wafer and from run to run were then recorded. The film uniformity within wafers was examined by looking at the film thickness standard deviations listed in the tables (Appendix B).

The deposition rate repeatability was found to be better than average. Plots of thickness versus position for each pair of runs sharing the same deposition conditions were very similar for seven out of the eight process conditions. The repeatability of the results indicated that the overall process was well behaved and under control. In other words, the process parameters (wafer location, temperature, time and gas flow) can be reproduced with ease.

If the reaction rate is high and the gas flow in the chamber is not sufficient to create the same gas distribution throughout the chamber, a gradient in the deposition rate will be observed. Usually, the deposition rate is lower away from the point where the gases enter the chamber and near the vacuum pump. This phenomena is commonly known as the gas depletion effect. Gas depletion was observed for the high temperature (500 °C) depositions. Figure 15 shows a typical film thickness gradient in a wafer lot caused by the gas depletion effect. There was as much as 2000 Å film thickness difference between the wafers near the load end and the wafers near the pump end under high temperature conditions. The depletion effect could be eliminated either by increasing the gas flow or the reaction rate near the pump end. In order to fully characterize the depletion effect, the process conditions would be kept constant (probably at the optimum condition) and the temperature gradient across the chamber would be systematically varied within a range. The variation from wafer to wafer could then be recorded and optimized.

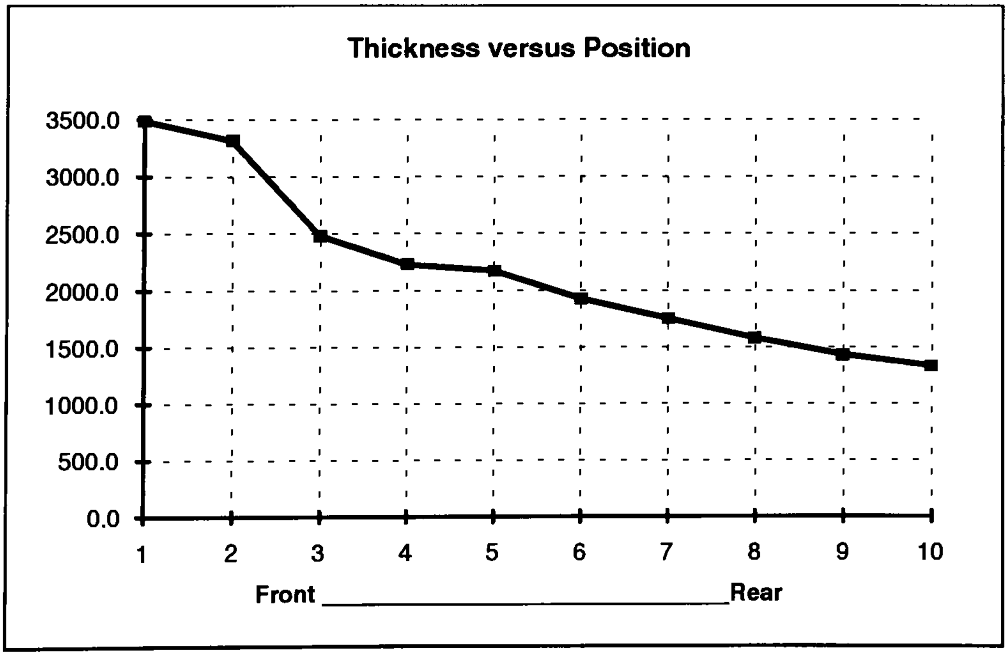

Figure 15. Gas Depletion Effect (Test Run 7).
Other test runs were qualitatively similar at high temperatures.

It was observed that for depositions at lower temperature conditions (400 °C), the film thickness gradient tended to have a "concave up" shape. Figure 16 illustrates the problem. The film thickness was higher at the two ends and there was a minimum near the center region.

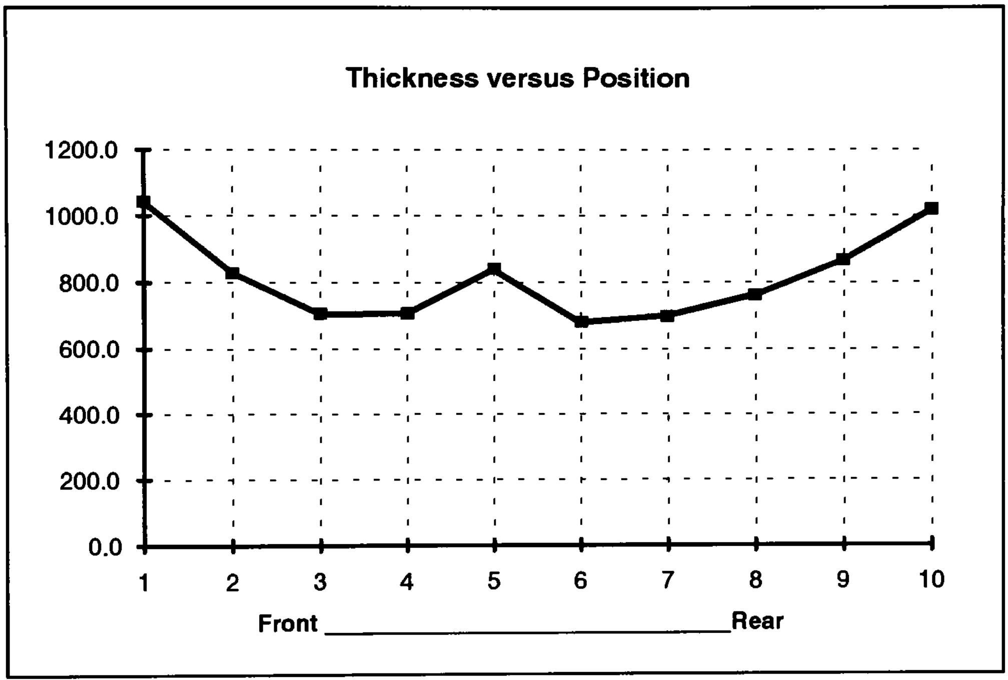

Figure 16. Film Thickness Gradient for 400 °C Depositions (Test Run 1).

The local maximum for position 5 seen in Figure16 was observed in most of the test runs. The change appeared at the same location each time and corresponded to the first wafer in the second LTO boat (refer to Figure 7). Any change in the gas flow between the two boats can cause variation in the deposition. When the wafer boats were inserted into the furnace tube, the gap between the boats and the lids was kept at a minimum. However, once that they were in the chamber, it was nearly impossible to determine if there was any spacing between them. It appears that there was a significant spacing in most of the deposition runs, therefore the problem might be inherent to the design of the boats and not related to the process procedure.

The best uniformity from wafer to wafer was found for those samples prepared under the 400 °C, 90 minutes and 1.8 gas flow ratio conditions, although the variation for the index of refraction under those conditions was intolerable. On the other hand, the variation for the index of refraction was at its minimum for the runs performed under low gas flow ratio conditions at any deposition temperature.

The best film uniformity within the wafer was found to be for those wafers located between the test wafer positions 3 to 9 in the LTO boats (see Figure 7). A total of 13 wafers can be placed in these positions. The film thickness variation within the wafer in these locations was generally less than 5%. During this project, the wafers were placed facing the load end of the furnace. It was noticed that the uniformity within the wafer was much better on the back side. It is therefore recommended that the wafers be placed facing away from the load end. The major flat of the wafers was always positioned toward the top of the furnace.

6.5 FTIR Results :

A considerable amount of research has been performed in the last decade on the characterization of silicon dioxide films by their IR spectra. The IR spectra have been to used to detect the different bonds that exist in the films and the stoichiometry of the films [16, 32, 33, 34, 35, 36]. The IR spectra were used in this project to simply verify that the films are silicon dioxide and to draw conclusions on relationships between the process conditions and the film stoichiometry.

The strength of the absorption peaks were found to be highly sensitive to the contact conditions between the sample and the crystal in the ATR cell. The contact conditions were not kept the same throughout the measurements taken here. Therefore, only the location and the shape of the absorption peaks are discussed.

Wafers located in the seventh position from each test run, as shown in Figure 7, were selected for the FTIR spectroscopy. All the spectra collected are presented in the Appendix E. The process conditions and the wafer ID are listed on top of each spectrum plot. The first two plots in the Appendix E correspond to the bare substrate (with approximately 20 to 30 Å of native oxide) used throughout the experiment. Figure 17 is a representative plot of FTIR spectrum for bare silicon wafer. The next six plots in the Appendix E correspond to the thermally grown oxide using both wet and dry oxygen growth methods and the remainder are the LTO oxide spectra.

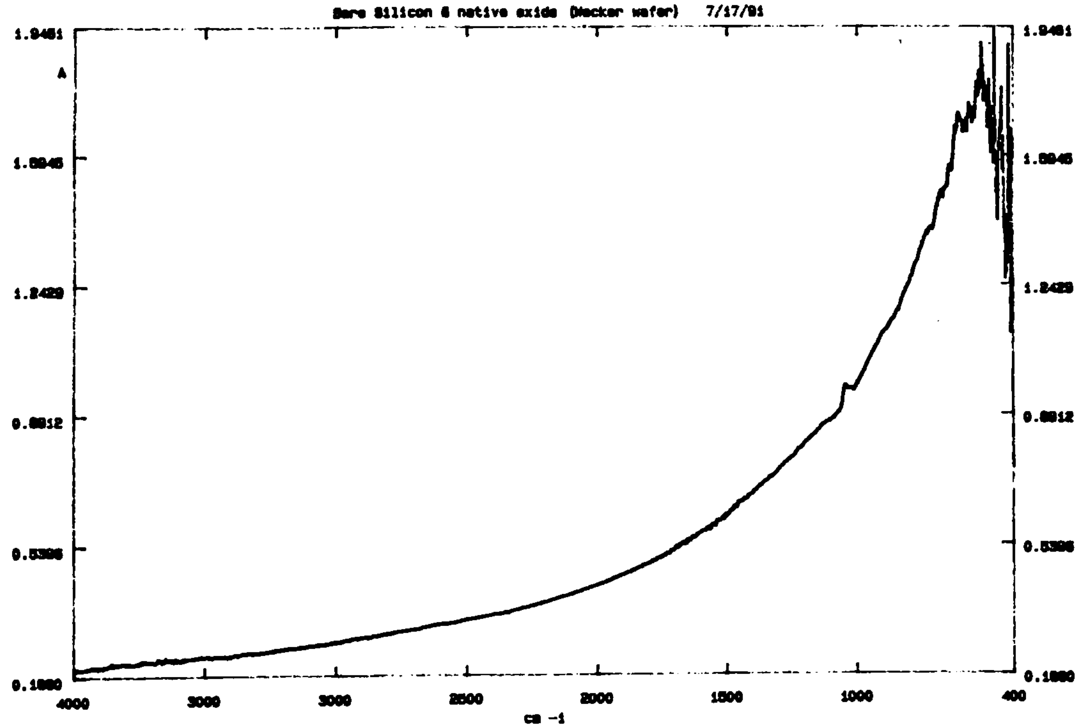

Figure 17. FTIR of Wacker Bare Silicon Wafer.

There are three vibration bands for the silicon dioxide films which can be seen from IR spectra [34]. The three vibrations correspond to the rocking, stretching and bending modes of the oxygen atom in the Si-O-Si bonding arrangement. The bending and the rocking bands overlaps each other below the frequency of 1000 cm^{-1}. The oxygen stretching mode absorbs in the 1075 cm^{-1} to 1150 cm^{-1} frequency range. The stretching mode absorption peak is the one generally used to characterize silicon dioxide films.

The stretching mode vibration of the oxygen atoms is coupled with the vibration of the silicon atoms. The oxygen and the silicon atoms vibrate at opposite phase with the respect to each other. Furthermore, all the oxygen atoms around a silicon atom vibrate in phase with each other. However, in order to maintain the center of mass, some of the oxygen atoms must vibrate in phase with the silicon atoms. The stretching mode absorption band is therefore characterized by the in and out of phase oxygen motions. Vibration at the lower energy band (1075 cm^{-1}) corresponds to the in phase motion of the oxygen atoms and vibration at the higher energy band (1150 cm^{-1}) corresponds to the out of phase motion. The difference between these two motion produces the absorption peak or peaks in the 1075 cm^{-1} to 1150 cm^{-1} region [34].

The dry oxygen grown oxide exhibited an even distribution of the in and out of phase vibrations (Figure 18 is an example of even distribution). The wet oxygen grown oxide had an uneven distribution (Figure 19 is an example of uneven distribution). The wet oxide was slightly dominated by the out of phase oxygen stretching motion (indicated by the shoulder peak toward the higher frequency). When comparing the two thermally grown oxides, it can be said that the dry oxide possessed a more even distribution of equal bonds throughout the film whereas the wet oxide did not. An even distribution would also implies less stress in the film since the bonds are all equal in strength.

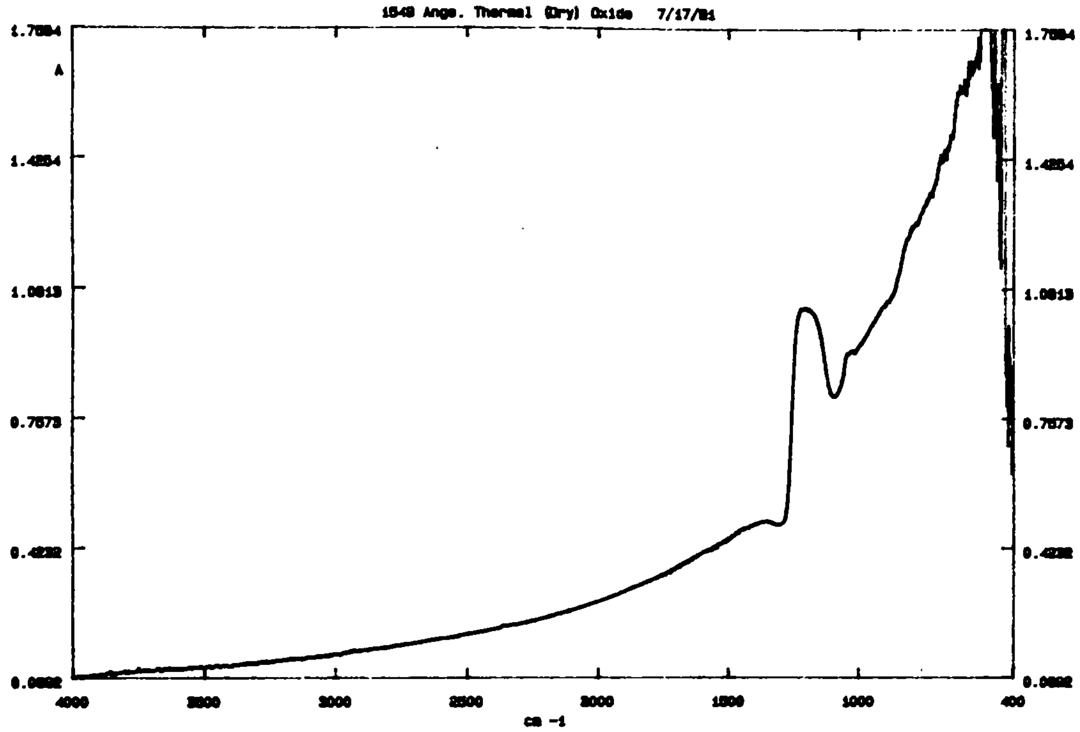

Figure 18. Example of Silicon Dioxide FTIR Even Distribution Spectrum.

The spectra obtained from the LTO oxides exhibited uneven distribution just like the wet oxide. The peaks were much more pronounced for the samples prepared at high temperatures. From the theory and the model, it is known that deposition rate is directly proportional to the temperature. Therefore, at higher temperature, the morphology of the films would be more disordered. The pronounced absorption peaks, therefore, correspond to disorder in the oxide films structure. Furthermore, the optical characteristics of the film were equally affected by the change in morphology; this agrees with the trend seen from the films' indices of refraction readings.

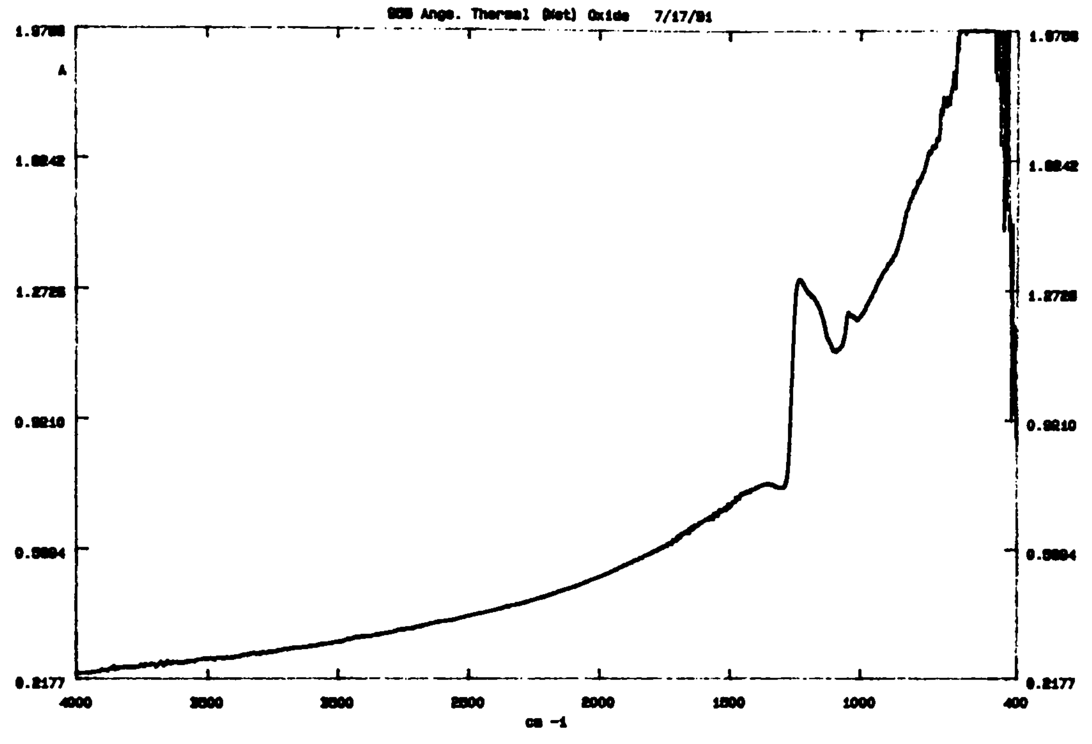

Figure 19. Example of Silicon Dioxide FTIR Uneven Distribution Spectrum.

The shift of the vibration frequency is generally due to change in the SiO_x composition [34]. As x gets smaller than 2, the silicon atoms have higher probability of having one or more silicon atom neighbors and therefore the Si-O-Si stretching mode is shifted toward lower frequencies. This shift toward lower frequency was observed on those samples prepared at high gas flow rate ratio. This result also agrees with the models and the other conclusions drawn previously. Therefore, at high gas flow ratios, the oxide films contained less oxygen than those at lower gas flow ratios. The closer x is to 2, the more similar is the LTO oxide films characteristics to those of thermally grown oxides.

6.6 Film Density :

A final confirmation run was performed, five double metal process wafers, three wafers with LTO oxide films and two bare silicon wafers were placed between the test wafer positions 5 to 9. The film density, etch rate, dielectric constant and dielectric strength were computed with these wafers. A few observations from the double metal process wafers were recorded. The deposition rate from this final run agrees with the predict value by the model (actual value = 37 Å/min and predicted value = 38 Å/min).

The film density is another property that serves as an indicator of the film quality. In general, oxide films with higher density are denser in structure and more resistant. The density of thermally grown oxide is approximately 2.27 [28]. The LTO oxide density reported is near 2.10. Higher LTO oxide density can be obtained by heat treating the film at 1000 °C to 1100 °C. Due to the poor uniformity in many of the samples, the density was only computed for four samples at several deposition conditions, all of which had low deposition temperature. The average density was found to be 2.12.

6.7 BOE Etch Rate :

Different authors use different etch chemicals to compare the etch rate of oxide films. Since the LTO oxide film presented here will be etched in regular stocked BOE solutions, the etch rate was determined using this chemical.

The etch rate was determined by creating four steps using the BOE bath. The etch rate was found to be approximately 5500 Å per minute. Although this value cannot be compared to values reported by other authors, it is similar to the etch rate of spin-on-glass.

6.8 Dielectric Constant and Dielectric Strength :

Dielectric constant was determined by using capacitance-voltage (CV) technique. The capacitance of a MOS structure,with the LTO oxide as the insulating material,was found. The dielectric constant was then calculated by using equation 5.2. The dielectric constant was determined to be 3.9. The reported value for dielectric constant is 3.9 for thermally grown silicon dioxide films and 4.3 for LTO oxide films [28]. Figure 20 shows the CV plot for the LTO oxide film. Further CV analysis can be performed to investigate device characteristics of the oxide film. Due to the extent of the analysis, it was not investigated in this project.

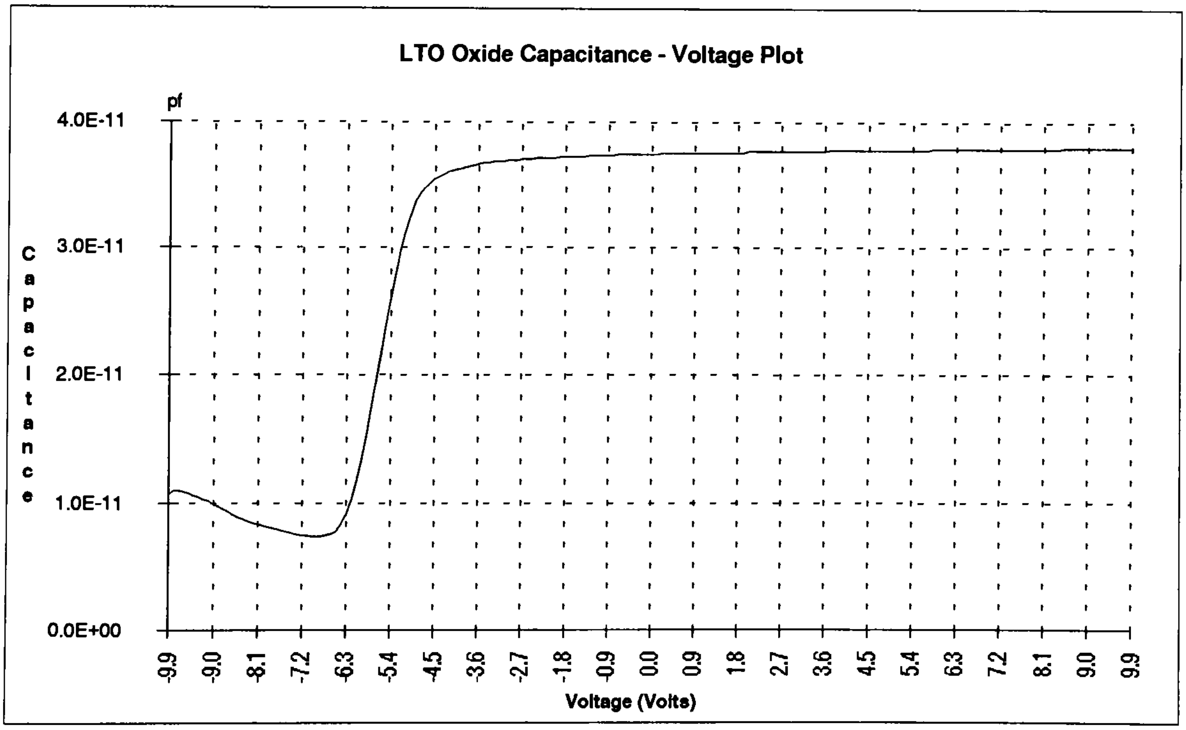

Figure 20. Capacitance-Voltage Plot for LTO Oxide MOS Structure.

Dielectric strength was found to be greater than 4.6×10^6 volts per centimeter. Dielectric strength for LTO oxide is reported to be 8×10^6 volts per centimeter [28].

6.9 Multilayer Metallization Results :

The same process procedure as the one employed by Michael Bailey was used to create the double metal structures. The metal 1 aluminum film, the metal 2 aluminium film and the LTO oxide film had an approximate thickness of .5 microns, .7 microns and .22 microns respectively. The aluminum was deposited by DC sputtering technique.

The resistivity of via chain structures were measured and the resistivity values per contact cut (CC) was determined by dividing the total resistance by the number of contact cuts per via chain (40). The results are shown in Table 10.

Contact Cut Dimensions	Resistance (ohms per CC)
6 μm x 6 μm	.31
10 μm x 10 μm	.24
20 μm x 20 μm	.21
30 μm x 30 μm	.23

Table 10. Double Metal Process Resistivity per Contact Cut Readings.

The resistivity values were low and no significant difference was observed among the larger contact cuts (greater or equal to 10 μm x 10 μm). The resistivity of 6 μm x 6 μm contact cuts was slightly higher compared to the others. These values are in agreement with Michael Bailey's findings [52].

Figure 21 and 22 are Scanning Electron Microscope (SEM) pictures of the double metal structures. Both pictures were taken at 5K magnification. Figure 21 shows a contact cut through the oxide film and the underlying metal 1 film. It can be observed that metal 1 was attacked by the BOE solution when the contact cuts were etched. Figure 22 shows a metal 2 line over a metal 1 line and an oxide contact cut.

The two metal lines were connected through the contact cut shown in the left upper corner of the picture. Some photoresist scumming can be seen in both pictures.

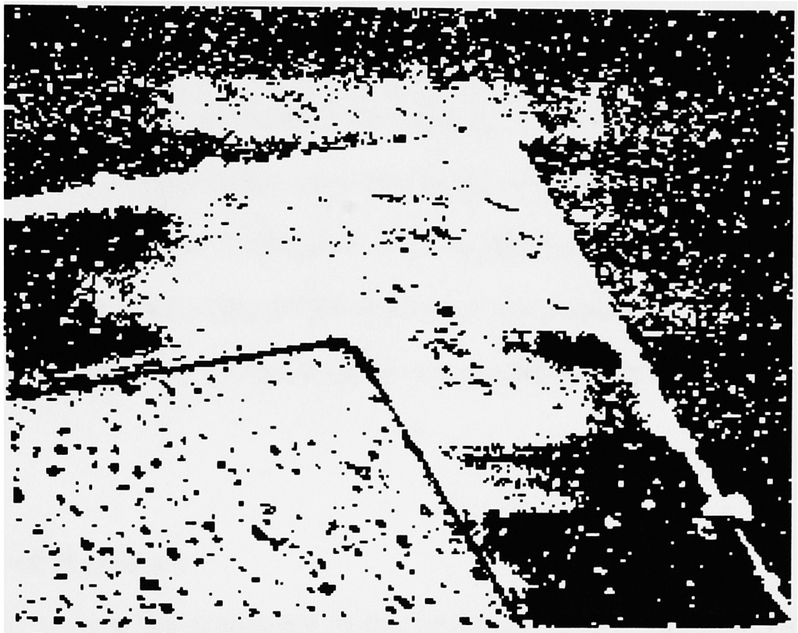

Figure 21. SEM Picture of Metal 1 and LTO Oxide Contact Cut.

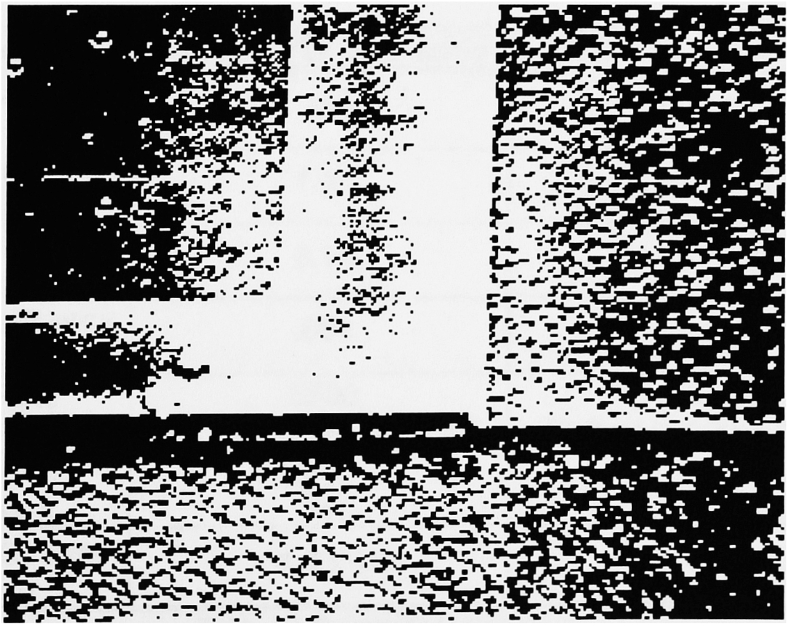

Figure 22. SEM Picture of Metal 1, Metal 2 and LTO Oxide.

Section 7 : Summary and Recommendations

The objective of this project was to study the effect of the process parameters in a LTO system and develop a baseline process for use in multilayer metallization processes. Models for deposition rate and index of refraction were derived. Fundamental LTO oxide film properties: density, activation energy, dielectric constant, dielectric strength, etch rate and FTIR spectrum were found. The fundamental properties were found to be in remarkably close agreement with the reported values in the literature.

7.1 Summary of Results :

Table 10 shows the summary of the findings. The deposition rate listed refers to the average deposition rate calculated by Design-Ease computer software.

Properties	Chen's LTO (This work)	Reported Values [28]
Deposition Rate (Å/min)	46	50 - 150
Index of Refraction	1.44	1.44 - 1.46
Density (gram/cm^3)	2.12	2.10 - 2.20
Activation Energy (eV)	.089	.4
Etch Rate (Å/min)	5500 Etched in Buffered HF	60 Etched in 100:1 DI:HF
Dielectric Constant	3.93	4.3
Dielectric Strength (V/cm)	> 4.6 x 10^6	8 x 10^6

Table 10. Summary of Results

The statistical model for deposition rate was found to be:

$$\text{Dep. Rate} = -84.10 + (.40 \times T) + (.85 \times t) - (29.83 \times R) - (3.12\times10^{-3} \times T \times t) + (.28 \times t \times R)$$

The model for index of refraction was found to be:

$$\text{Index} = 1.48 - (7.70\times10^{-5} \times T) + (4.03\times10^{-4} \times t) + (4.38\times10^{-3} \times R) - (4.06\times10^{-4} \times t \times R)$$

In the above equations, T is the deposition temperature (in °C), t is the deposition time (in minutes) and R is the gas flow ratio.

7.2 Conclusions :

The objective of this project was to characterize the LTO process at RIT and to create a baseline LTO process suitable for multilayer metallization processes. The process was studied within the temperature range of 400 °C to 500 °C, within the deposition period of 30 to 90 minutes and within the gas flow ratio or 1.2 to 1.8. A statistical model was derived and presented. The phenomena and the film properties seen in the project agree with those reported by other reserchers.

The LTO baseline process conditions recommended, based on the results of this project, are: 400 to 410 °C deposition temperature and 1.2 oxygen/silane gas flow ratio. Deposition time will be dependent on the film thickness required. To achieve a thickness of 5000 Å, the deposition time will be approximately 3 hours. Under these conditions, the uniformity within wafer, from wafer to wafer (within the 13 wafer positions listed in the previous Section) and from run to run will be within 5% to 8%. The films properties will be similar to those listed on the previous page.

7.3 Recommendation for Future Work :

The deposition rate must be further characterized with the respect to gas flow ratio. The deposition rate remains unpredictable near the low temperature, low gas flow ratio and high deposition time region. Completion of the original central composite design might be the answer. The deposition rate can be further enhanced by increasing the gas flows. Precautions must be taken so that the deposition pressure does not excess the 350 mTorr safety limit.

Uniformity from wafer to wafer can be improved further by the addition of gas injectors in the system, although the physical dimensions of the existing system might not allow this addition. The gas injectors will improve uniformity and, at the same time, reduce homogeneous reactions and therefore improving the quality of the oxide film.

Further study of inorganic material using FTIR spectroscopy is needed and desired. Quantitative correlation between the fundamental properties and the absorption peaks should be established for the LTO process. FTIR technique can also be employed to characterize and study other organic and inorganic materials used in the microelectronic manufacturing field.

Section 8 : Appendices

Appendix A :

LTO Process Specification Form

MODE 1																								
SEG. NO. (S=)	ENTER																							
	OUTPUT (OUT ?)																INPUT (INP ?)							
	0	1	2	3	4	5	6	7	8	9	A	B	C	D	E	F	0	1	2	3	4	5	6	7
0		X																						
1			X															X						
2							X												X					
3			X					X												X				
4			X			X		X	X											X				
5			X			X		X	X											X				
6			X			X		X	X											X				
7			X					X												X				
8		X	X																					
9			X																					
A		X																						
B																								
C																								
D																								
E																								
F																								

	MODE 2			MODE 3	
		ENTER			
CYCLE DESCRIPTION	CYCLE NO.	SEG. NO. (S=)	ABORT TO (A=)	CYCLE NO.	TIME MINUTES (ttt.t)
IDLE	0	0	0	0	0
PUMP1	1	1	8	1	15.0
LEACK CHECK	2	2	1	2	1.0
PUMP 2	3	3	8	3	5.0
RAMP UP	4	4	7	4	2.0
DEPOSITION	5	5	7	5	
RAMP DOWN	6	6	7	6	2.0
POST PUMP	7	7	9	7	5.0
PUMP PURGE	8	8	9	8	2.0
PUMP 3	9	9	10	9	5.0
BACKFILL	10	10	0	10	3.0
	11			11	
	12			12	
	13			13	
	14			14	
	15			15	

OUTPUTS

(1) N_2 PROCESS
(2) VACUUM
(3) SiH_2Cl_2
(4) NH_3
(5) SiH_4
(6) ENABLE LEAK DETECTOR
(7) ENABLE DOOR PRES. DETECTOR
(8) OXYGEN

INPUTS

1. DOOR SENSOR
2. LEAK PRESSURE SENSOR
3. OVER PRESSURE SENSOR

PROGRAMMING HINTS

MODE 1 - Select Mode 1 & load all outputs & inputs as shown to the assigned segment numbers.

MODE 2 - Select recipe no.0 then select mode 2. Load all seg. no.'s & abort cycles to the specified cycle no.'s. Load all seg. no.'s & abort cycle shown before proceeding to mode 3.

MODE 3 - Select mode 3 & load specified time to each applicable cycle upon completion of mode 3. Toggle switch to reset system is now ready for operation.

Appendix B :

Tabulated Data and Plots of Film Thickness From SD2000 Ellipsometer

Thickness for Run #1 : 400 °C, 30minutes, Gas Ratio 1.8

Wafer #	Top	Left	Center	Right	Bottom	Average	STD
1	1608.9	802.1	897.5	1091.8	809.3	1041.9	337.8
2	983.5	904.9	766.5	708.6	783.9	829.5	111.9
3	861.7	635.1	679.6	664.7	682.6	704.7	89.7
4	614.5	610.9	681.4	746.2	875.6	705.7	110.0
5	1319.7	817.8	717.8	709.2	630.5	839.0	276.8
6	814.6	629.0	668.9	644.3	642.6	679.9	76.7
7	734.0	681.2	719.4	681.8	681.4	699.6	25.3
8	765.6	753.0	788.6	749.0	754.9	762.2	16.0
9	875.4	850.0	895.0	858.1	854.5	866.6	18.6
10	1035.5	997.1	1047.5	1006.8	1004.3	1018.2	21.9
						814.7	108.5

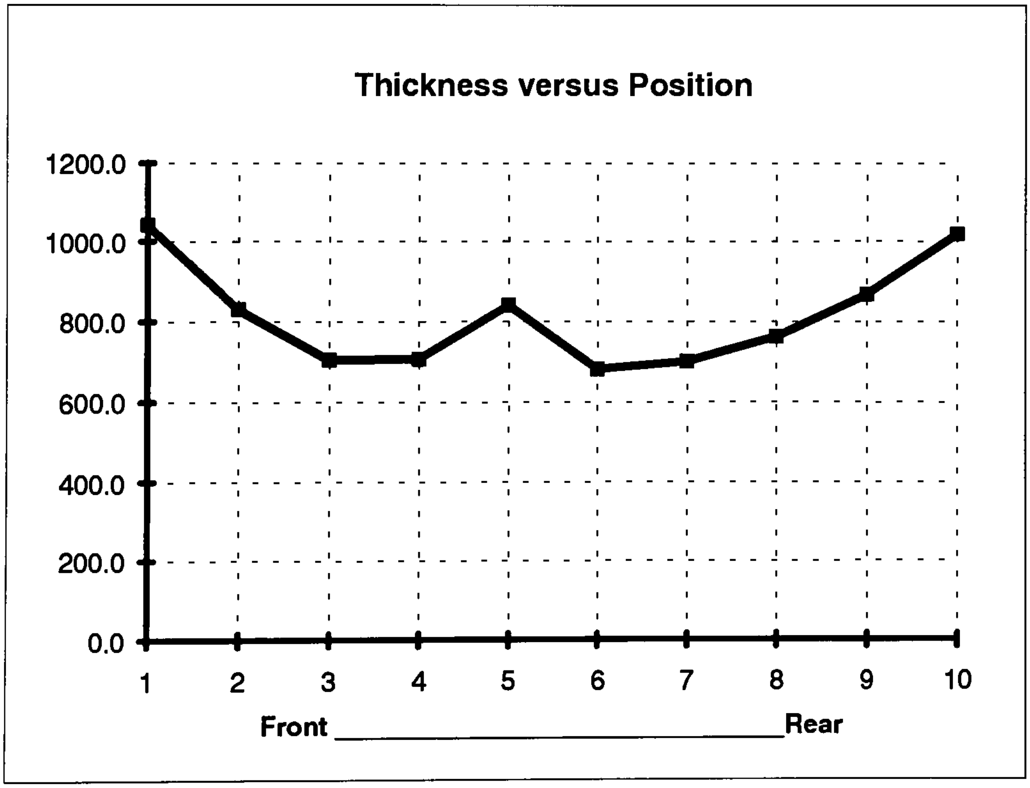

Thickness for Run #2 : 450 °C, 60 minutes, Gas Ratio 1.5

Wafer #	Top	Left	Center	Right	Bottom	Average	STD
11	1087.6	2073.4	136.6	351.1	3062.7	1342.3	1224.3
12	384.5	2394.0	2774.8	2587.3	2368.8	2101.9	974.0
13	2402.5	2330.0	2511.5	2329.7	2352.4	2385.2	76.6
14	2251.7	2256.4	2335.4	2208.6	2229.3	2256.3	48.2
15	2350.5	2302.4	2410.0	2261.4	2274.3	2319.7	61.0
16	2289.7	2146.1	2287.1	2167.7	2143.4	2206.8	75.1
17	2209.6	2144.2	2269.7	2149.8	2114.3	2177.5	62.1
18	2209.5	2118.2	2252.1	2149.3	2119.7	2169.8	59.0
19	2221.6	2152.8	2262.6	2161.3	2145.8	2188.8	51.0
20	2246.5	2207.1	2323.1	2265.1	2203.6	2249.1	48.9
						2139.7	268.0

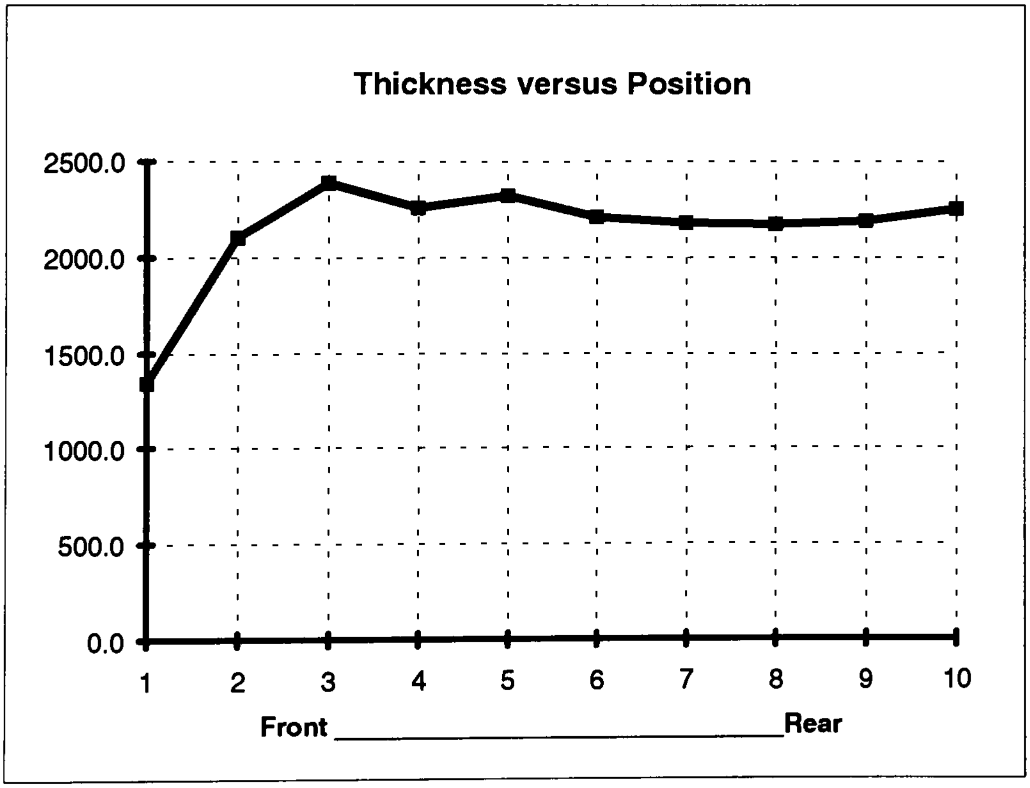

Thickness for Run #3 : 500 ˚C, 30 minutes, Gas Ratio 1.8

Wafer #	Top	Left	Center	Right	Bottom	Average	STD
21	450.2	2310.1	2441.8	2341.8	2283.2	1965.4	849.2
22	2292.7	2120.5	2214.9	2131.9	2147.6	2181.5	72.1
23	2111.1	1932.6	2019.6	1930.6	1969.6	1992.7	75.4
24	1764.8	1811.5	1847.7	1786.1	1874.9	1817.0	44.7
25	1956.1	1737.7	1824.6	1740.2	1776.7	1807.1	90.4
26	1587.3	1552.3	1628.4	1570.2	1546.8	1577.0	32.8
27	1467.4	1427.5	1489.1	1439.5	1433.8	1451.5	26.0
28	1306.7	1387.2	1347.2	1304.0	1292.7	1327.6	39.2
29	1195.2	1170.4	1215.3	1184.2	1173.8	1187.8	18.2
30	1082.6	1055.9	1101.6	1081.9	1064.7	1077.3	17.7
						1638.5	126.6

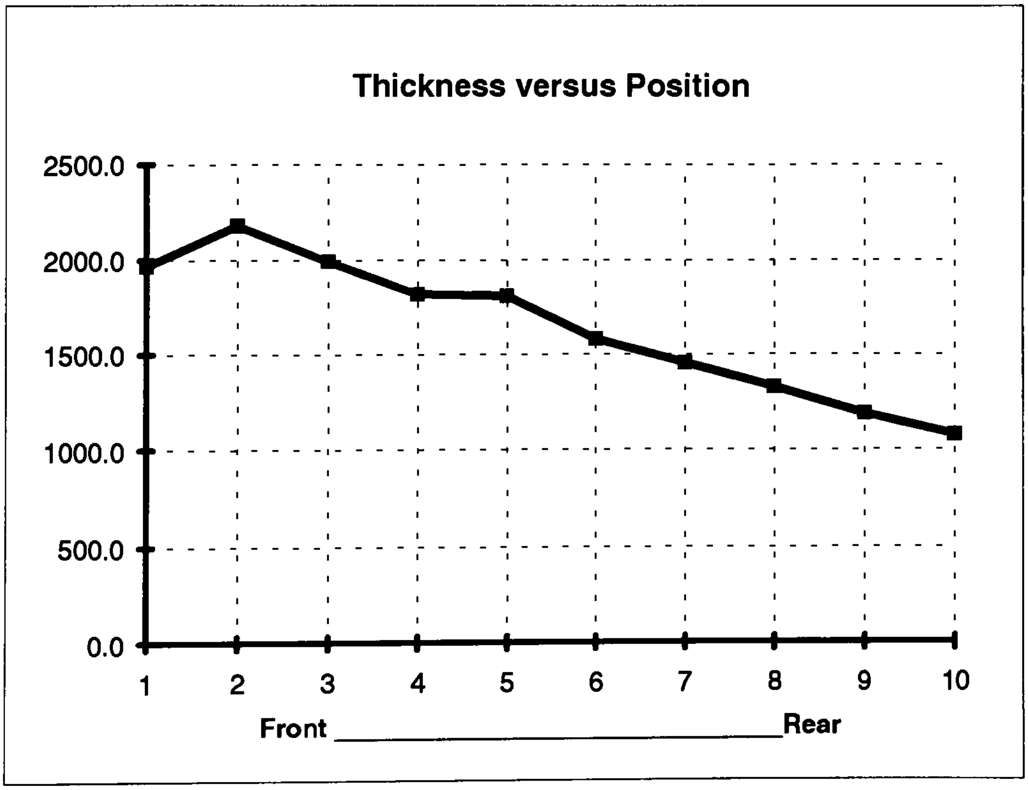

Thickness for Run #4 : 400 ˚C, 90 minutes, Gas Ratio 1.2

Wafer #	Top	Left	Center	Right	Bottom	Average	STD
31	450.8	2383.8	4430.2	2744.1	2540.2	2509.8	1414.1
32	2251.4	2069.7	2234.6	2119.7	2052.6	2145.6	92.5
33	1925.4	1776.1	1925.8	1801.1	1778.1	1841.3	77.6
34	1649.1	1602.3	1733.3	1631.1	1610.6	1645.3	52.5
35	1965.0	1784.2	1950.6	1782.1	1789.6	1854.3	94.7
36	1650.8	1619.9	1719.7	1627.1	1592.6	1642.0	48.1
37	1691.4	1677.7	1776.1	1680.3	1658.8	1696.9	45.8
38	1775.6	1777.5	1865.6	1772.1	1745.4	1787.2	45.7
39	1946.7	1939.8	2028.1	1936.8	1903.0	1950.9	46.4
40	2222.0	2220.4	2302.6	2231.0	2192.7	2233.7	41.1
						1930.7	195.8

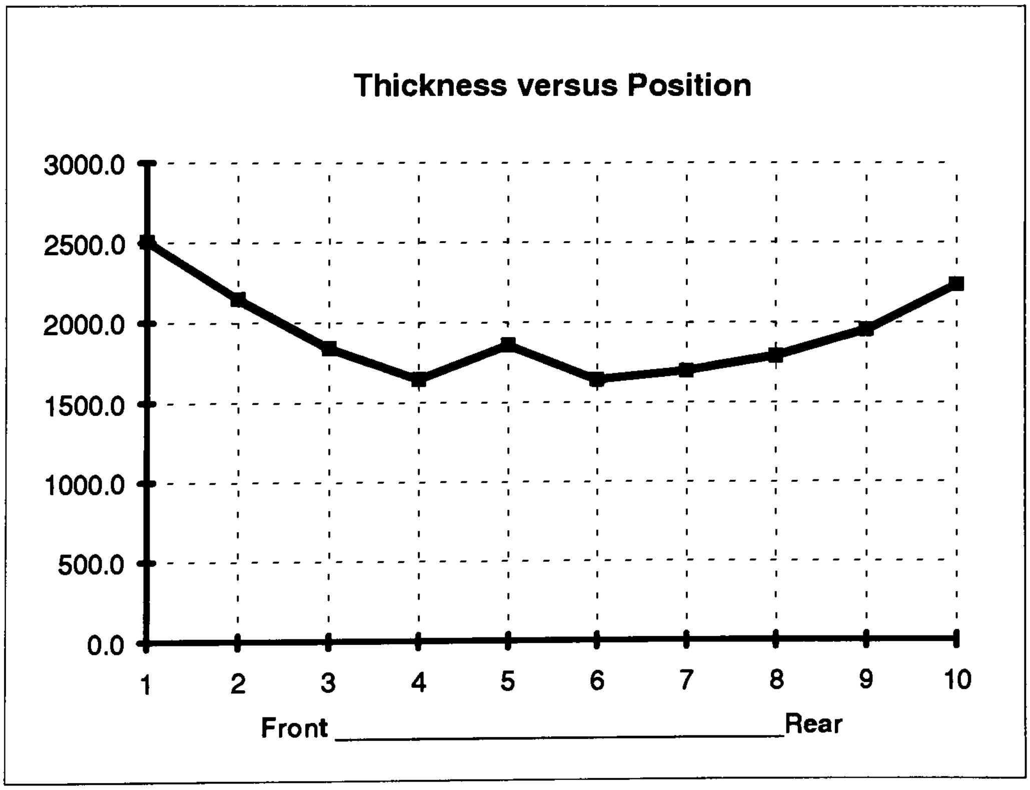

Thickness for Run #5 : 500 °C, 90 minutes, Gas Ratio 1.2

Wafer #	Top	Left	Center	Right	Bottom	Average	STD
41	3821.0	5224.4	6404.8	5797.4	5260.8	5301.7	956.9
42	4534.3	4227.2	4412.5	4325.9	4176.0	4335.2	143.8
43	3648.5	3358.5	3542.7	3463.0	3339.2	3470.4	129.2
44	4081.2	5766.9	4457.8	5614.9	5459.8	5076.1	756.1
45	4560.8	5627.8	5382.1	5512.7	5541.2	5324.9	436.2
46	4937.6	4799.4	4913.2	4811.8	4722.5	4836.9	88.2
47	4465.9	4349.8	4463.0	4391.1	4301.8	4394.3	71.4
48	4052.1	3944.9	4039.7	4001.9	3905.5	3988.8	62.5
49	3697.1	3619.6	3690.9	3666.6	3577.4	3650.3	50.9
50	3520.2	3441.8	3474.1	3461.3	3418.5	3463.2	38.2
						4384.2	273.3

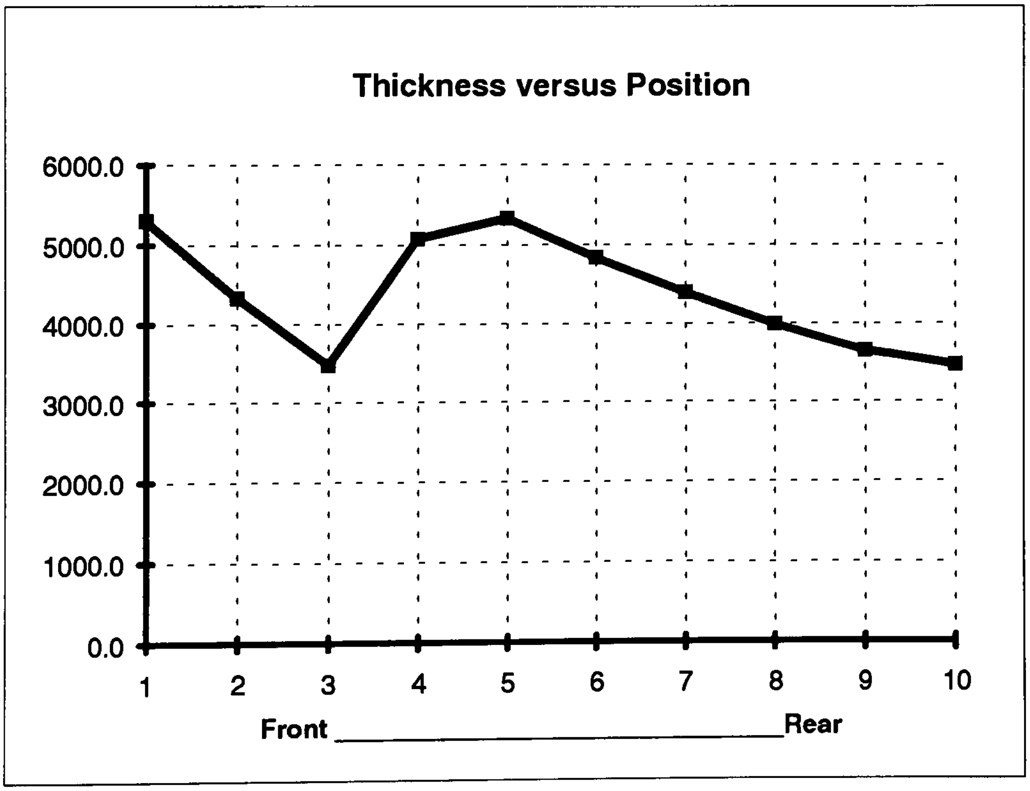

Thickness for Run #6 : 400 °C, 30 minutes, Gas Ratio 1.2

Wafer #	Top	Left	Center	Right	Bottom	Average	STD
51	1624.8	1439.1	1518.7	1453.2	1432.5	1493.7	80.9
52	1356.9	1292.7	1358.4	1314.1	1281.5	1320.7	35.7
53	1265.3	1209.4	1255.7	1210.4	1202.4	1228.6	29.4
54	1136.4	1148.1	1174.4	1136.4	1144.6	1148.0	15.6
55	1308.8	1245.2	1276.1	1208.8	1202.5	1248.3	45.0
56	1100.8	1078.7	1106.3	1079.2	1064.6	1085.9	17.2
57	1096.6	1066.9	1094.1	1074.3	1059.3	1078.2	16.5
58	1091.6	1063.8	1090.7	1078.3	1057.8	1076.4	15.4
59	1118.4	1091.0	1111.3	1099.8	1084.7	1101.0	13.9
60	1201.0	1164.0	1181.0	1177.2	1157.9	1176.2	16.8
						1195.7	28.6

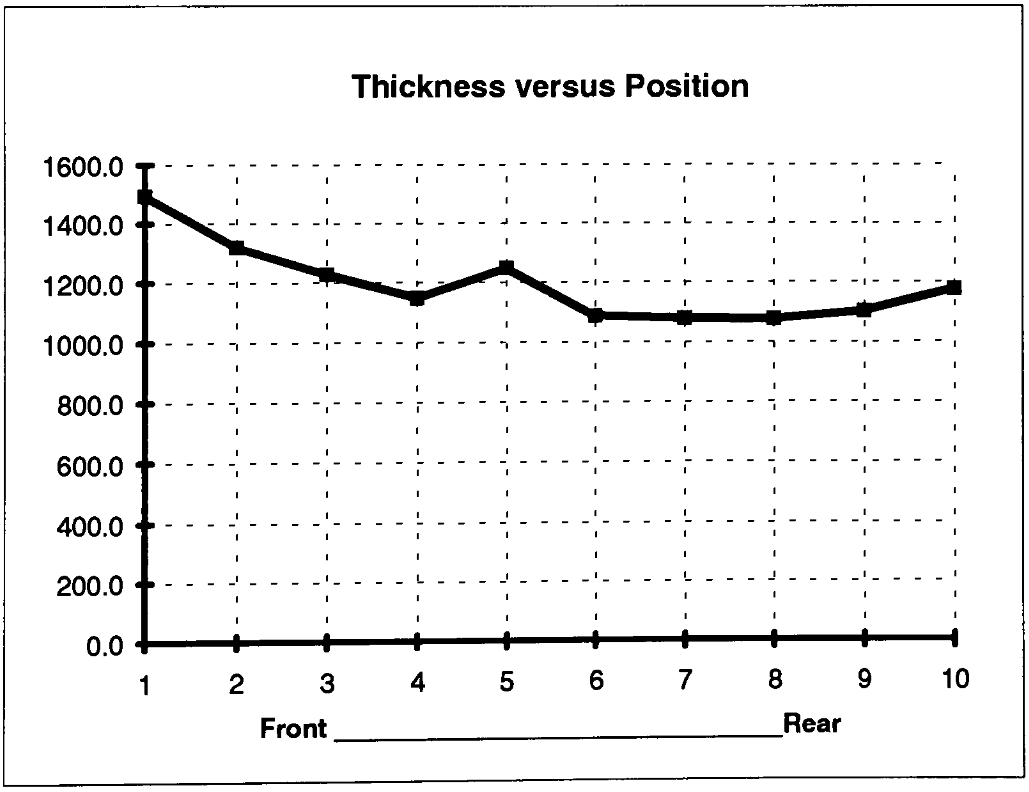

Thickness for Run #7 : 500 °C, 30 minutes, Gas Ratio 1.2

Wafer #	Top	Left	Center	Right	Bottom	Average	STD
61	3513.2	3517.7	3262.5	3500.7	3626.9	3484.2	133.9
62	4044.5	2911.9	3710.7	2955.1	2925.8	3309.6	532.0
63	2530.2	2390.8	2528.6	2558.5	2392.5	2480.1	81.6
64	2254.5	2220.6	2270.2	2216.5	2175.4	2227.4	36.9
65	2223.3	2139.6	2204.8	2162.3	2138.6	2173.7	38.6
66	1958.8	1920.8	1952.6	1918.0	1891.4	1928.3	27.6
67	1782.4	1749.3	1767.4	1737.1	1721.3	1751.5	24.1
68	1607.7	1571.9	1592.4	1576.6	1549.5	1579.6	22.0
69	1455.4	1435.5	1441.5	1435.4	1407.6	1435.1	17.4
70	1361.2	1327.7	1333.3	1329.3	1313.0	1332.9	17.6
						2170.3	93.2

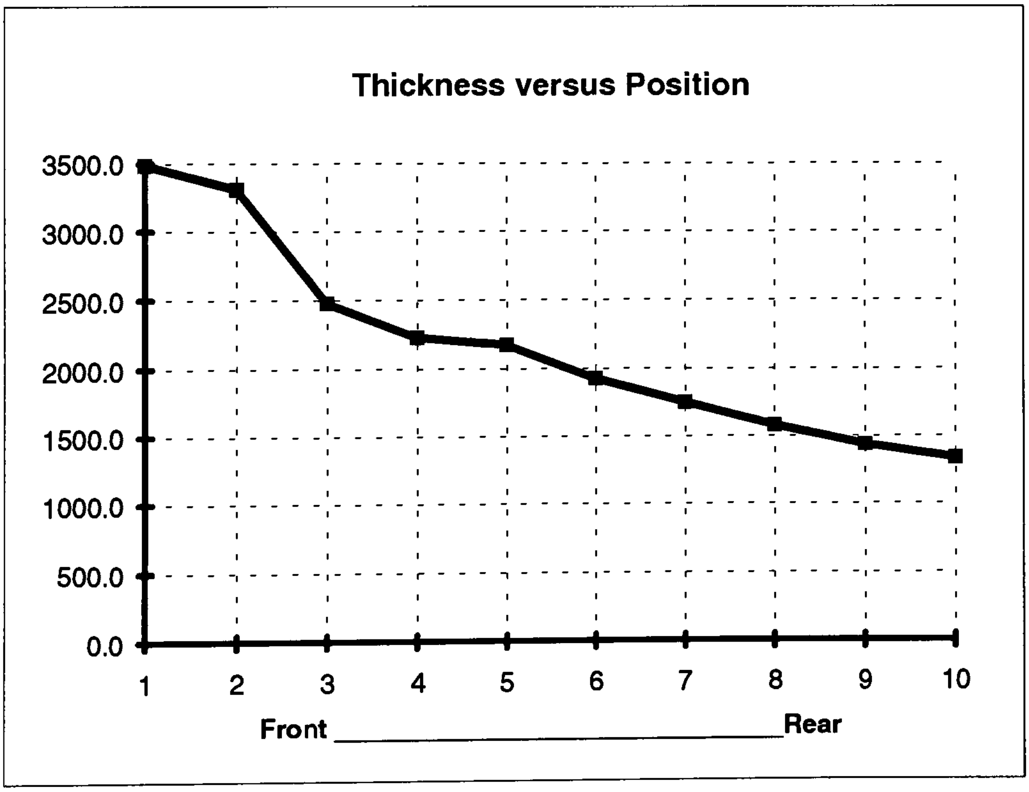

Thickness for Run #8 : 450 °C, 60 minutes, Gas Ratio 1.5

Wafer #	Top	Left	Center	Right	Bottom	Average	STD
71	4672.2	3670.2	3880.1	3823.7	3666.4	3942.5	418.6
72	3596.0	3642.2	3590.0	3474.4	3637.6	3588.0	67.8
73	3719.2	3315.0	3405.0	3385.9	3419.1	3448.8	156.3
74	3366.5	3387.6	3336.7	3535.9	3686.3	3462.6	146.7
75	3633.2	3435.0	3305.5	3243.4	3450.7	3413.6	150.6
76	3554.2	3589.9	3283.5	3456.6	4168.7	3610.6	333.8
77	3926.6	4646.8	3500.5	3810.4	5623.6	4301.6	850.1
78	4562.3	4478.8	3994.7	4805.5	5605.3	4689.3	590.6
79	5610.5	5438.0	5642.4	5564.6	5392.9	5529.7	109.1
90	4528.2	5597.9	5655.6	5605.5	5586.1	5394.7	485.1
						4138.1	330.9

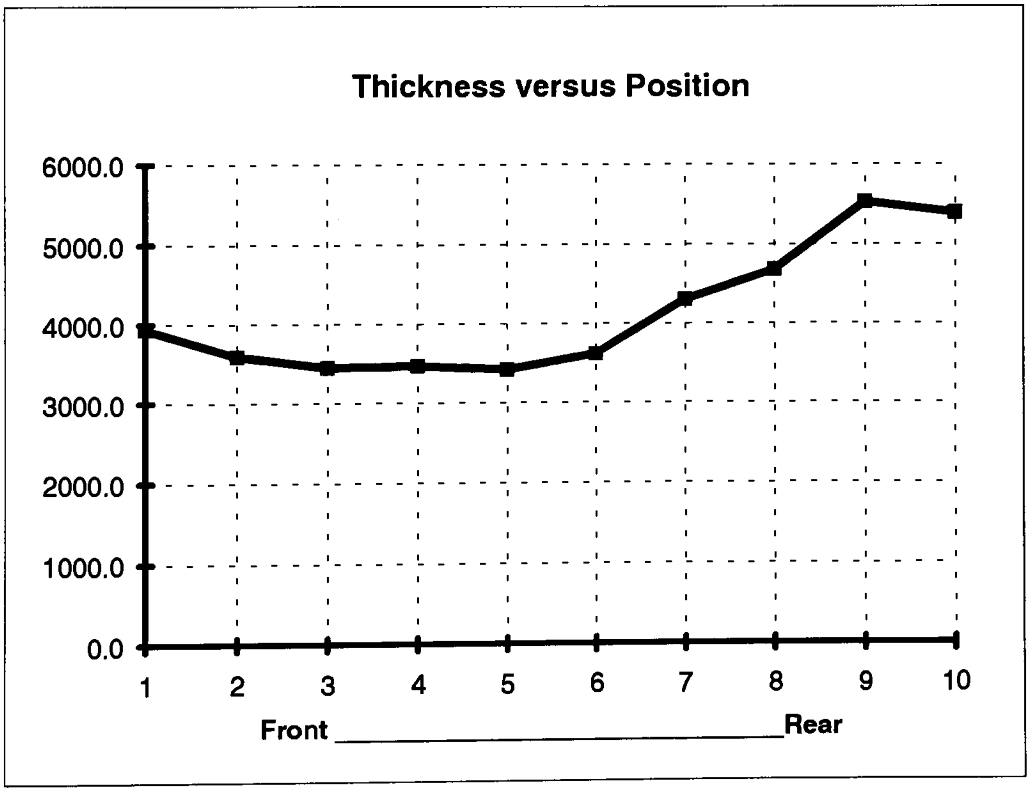

Thickness for Run #9 : 400 °C, 90 minutes, Gas Ratio 1.8

Wafer #	Top	Left	Center	Right	Bottom	Average	STD
81	3320.8	2941.7	2855.6	2867.1	2862.7	2969.6	199.4
82	3807.6	2903.7	2848.5	2850.6	2891.3	3060.3	418.4
83	3121.8	2904.1	2843.2	2848.3	2904.0	2924.3	114.2
84	2875.3	2994.6	2896.3	2893.1	3392.3	3010.3	218.6
85	3076.9	3233.2	3197.7	2893.6	2885.7	3057.4	163.8
86	2929.8	2881.5	2841.0	2854.7	2876.1	2876.6	33.9
87	2892.9	2853.1	2843.1	2849.0	2883.1	2864.2	22.3
88	2920.5	2872.0	2863.7	2847.6	3008.0	2902.4	65.0
89	2804.5	2873.8	2846.4	2840.9	2760.6	2825.2	43.8
90	2578.1	2505.4	2928.8	2937.4	2521.6	2694.3	219.7
						2918.5	149.9

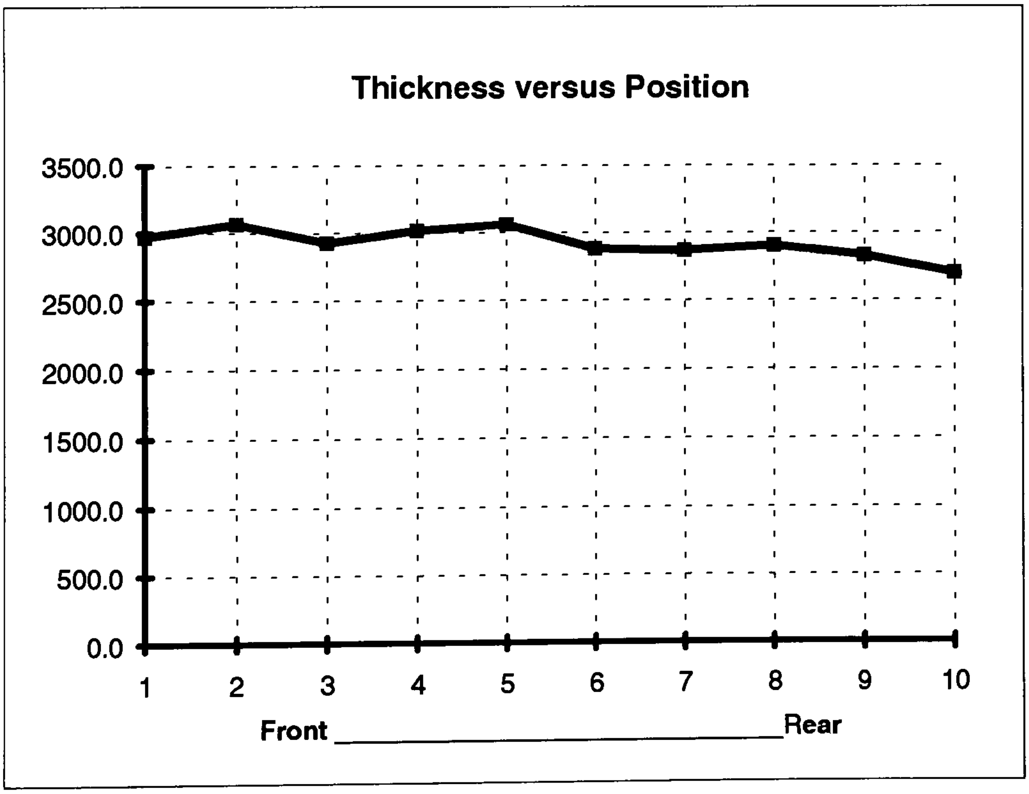

Thickness for Run #10 : 500 °C, 90 minutes, Gas Ratio 1.8

Wafer #	Top	Left	Center	Right	Bottom	Average	STD
91	4538.5	4581.7	4375.5	4069.2	4021.2	4317.2	260.5
92	4274.1	3966.7	3774.8	4017.7	3993.6	4005.4	178.3
93	4259.6	3786.2	3318.1	4482.3	4071.9	3983.6	451.3
94	3523.8	3599.4	2769.2	3378.2	5484.3	3751.0	1022.5
95	4189.1	5119.0	4938.1	5258.8	5050.2	4911.0	420.0
96	4679.9	4709.9	4910.1	4742.7	4722.9	4753.1	90.7
97	4671.1	4255.5	4431.3	4320.4	4256.4	4386.9	174.3
98	3948.4	3818.3	3965.7	3822.8	3903.4	3891.7	68.9
99	3564.9	3617.0	3554.6	3466.9	3516.0	3543.9	56.1
100	3574.5	3627.1	3324.5	3312.9	3660.4	3499.9	168.3
						4104.4	289.1

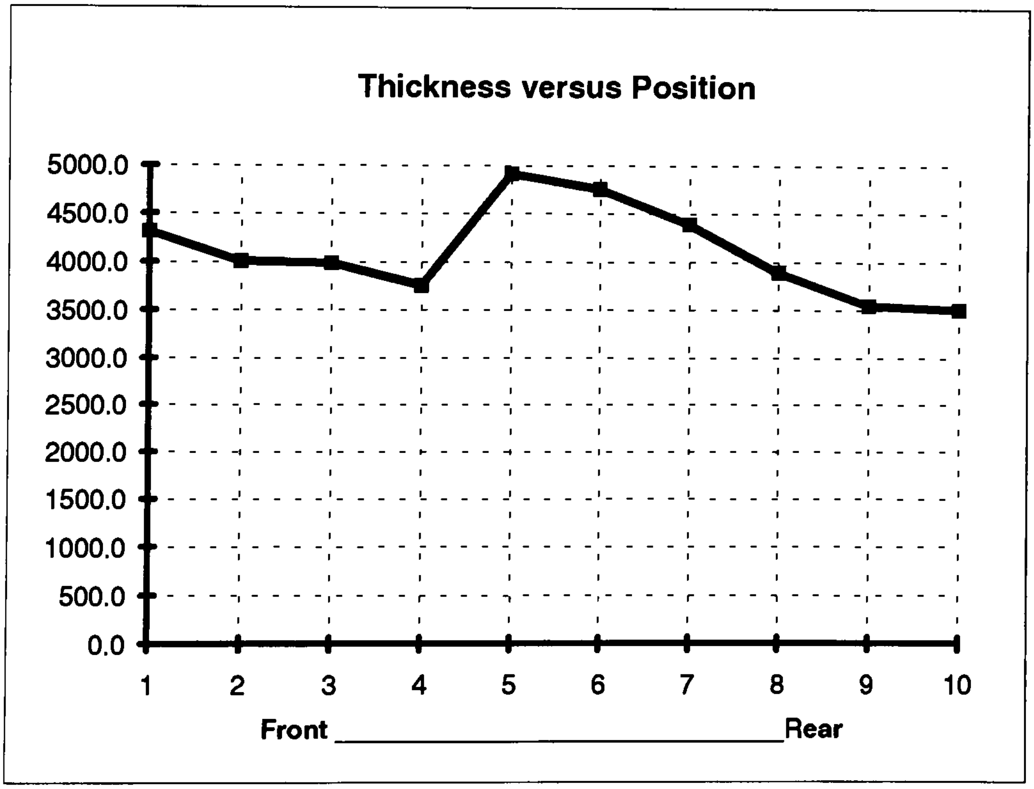

Thickness for Run #11 : 400 °C, 30 minutes, Gas Ratio 1.8

Wafer #	Top	Left	Center	Right	Bottom	Average	STD
101	1384.1	963.5	868.8	814.1	795.0	965.1	243.2
102	975.6	774.9	768.8	740.3	747.8	801.5	98.4
103	812.0	681.6	717.8	689.2	702.5	720.6	52.9
104	654.1	747.2	722.8	708.4	882.2	742.9	85.0
105	1123.3	804.9	818.4	750.3	747.5	848.9	156.7
106	720.6	685.0	711.4	680.0	677.4	694.9	19.7
107	741.6	714.8	745.6	722.6	709.8	726.9	16.0
108	793.8	757.8	802.2	777.6	780.7	782.4	17.0
109	863.8	855.0	891.4	866.8	863.8	868.2	13.7
110	985.9	968.1	1021.5	998.1	978.4	990.4	20.5
						814.2	72.3

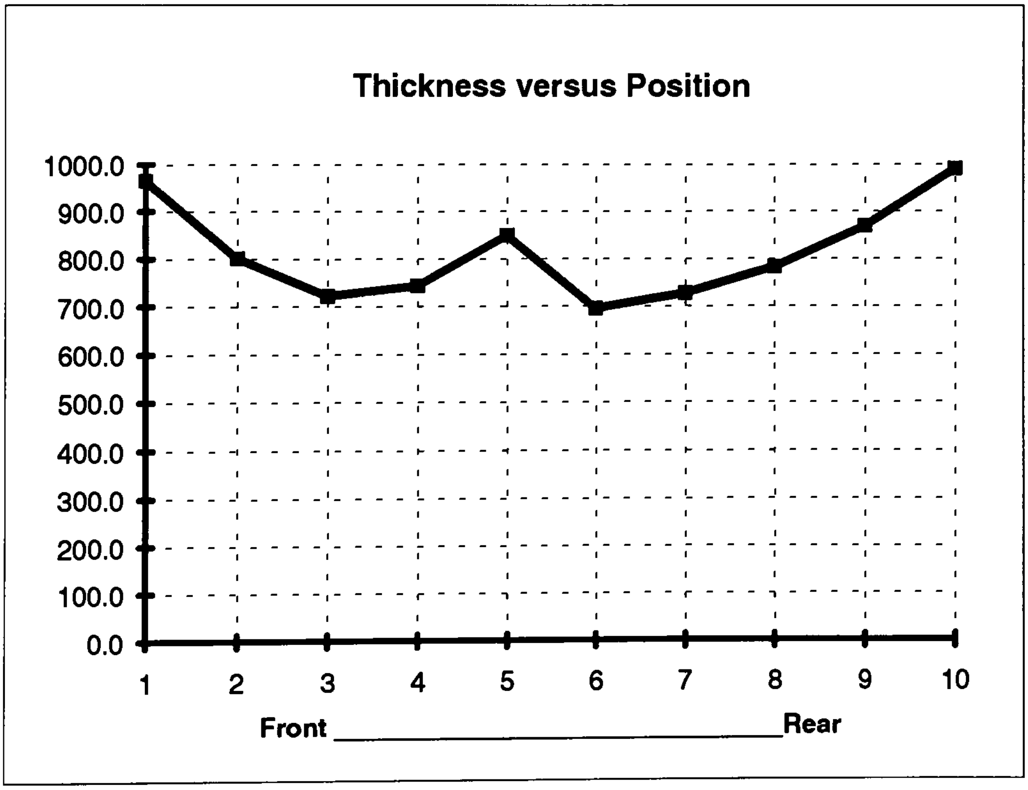

Thickness for Run #12 : 500 °C, 90 minutes, Gas Ratio 1.2

Wafer #	Top	Left	Center	Right	Bottom	Average	STD
111	5454.7	4540.1	4913.0	4785.9	4550.0	4848.7	374.1
112	4099.6	3725.0	3996.5	3852.7	3701.4	3875.0	172.0
113	3503.8	3616.1	3350.4	3362.4	4117.7	3590.1	314.6
114	5496.1	5276.8	5683.8	5337.4	5198.6	5398.5	193.3
115	5323.6	5126.3	5474.6	5245.3	5145.9	5263.1	142.4
116	4697.7	4523.7	4726.4	4646.0	4507.3	4620.2	100.0
117	4230.1	4110.9	4302.2	4209.9	4113.4	4193.3	81.6
118	3838.1	3712.9	3885.0	3848.2	3695.9	3796.0	85.7
119	3517.0	3414.8	3599.3	3506.0	3404.5	3488.3	80.4
120	3330.3	3288.4	3343.4	3316.9	3284.5	3312.7	25.8
						4238.6	157.0

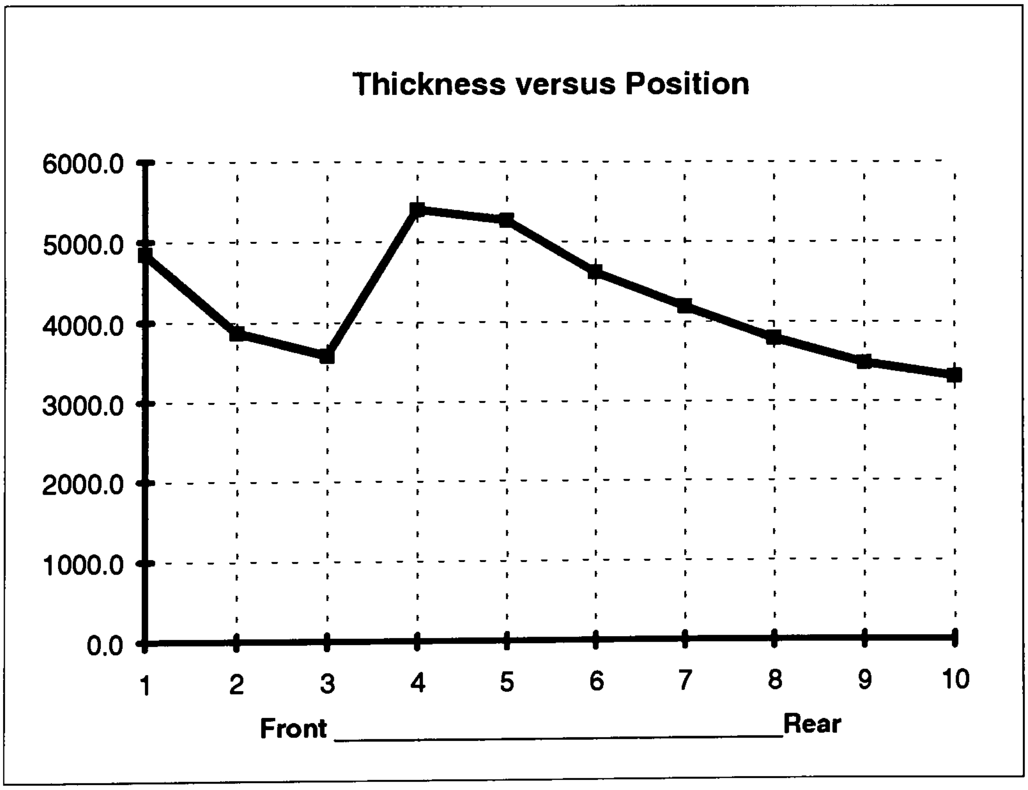

Thickness for Run #13 : 400 °C, 30 minutes, Gas Ratio 1.2

Wafer #	Top	Left	Center	Right	Bottom	Average	STD
121	1697.9	1497.6	1593.5	1521.0	1493.2	1560.6	86.6
122	1379.8	1334.2	1397.8	1350.7	1328.9	1358.3	29.7
123	1240.7	1188.8	1264.4	1231.8	1197.3	1224.6	31.3
124	1135.6	1122.4	1165.9	1131.5	1108.2	1132.7	21.3
125	1135.5	1124.5	1170.2	1139.6	1124.4	1138.8	18.8
126	1054.1	1026.8	1071.1	1061.6	1025.8	1047.9	20.6
127	1032.4	994.8	1039.4	1029.7	993.2	1017.9	22.1
128	1011.2	977.8	1018.3	1012.0	978.3	999.5	19.8
129	1020.4	990.9	1024.9	1020.7	985.6	1008.5	18.7
130	1088.7	1060.0	1084.0	1072.5	1049.7	1071.0	16.3
						1156.0	28.5

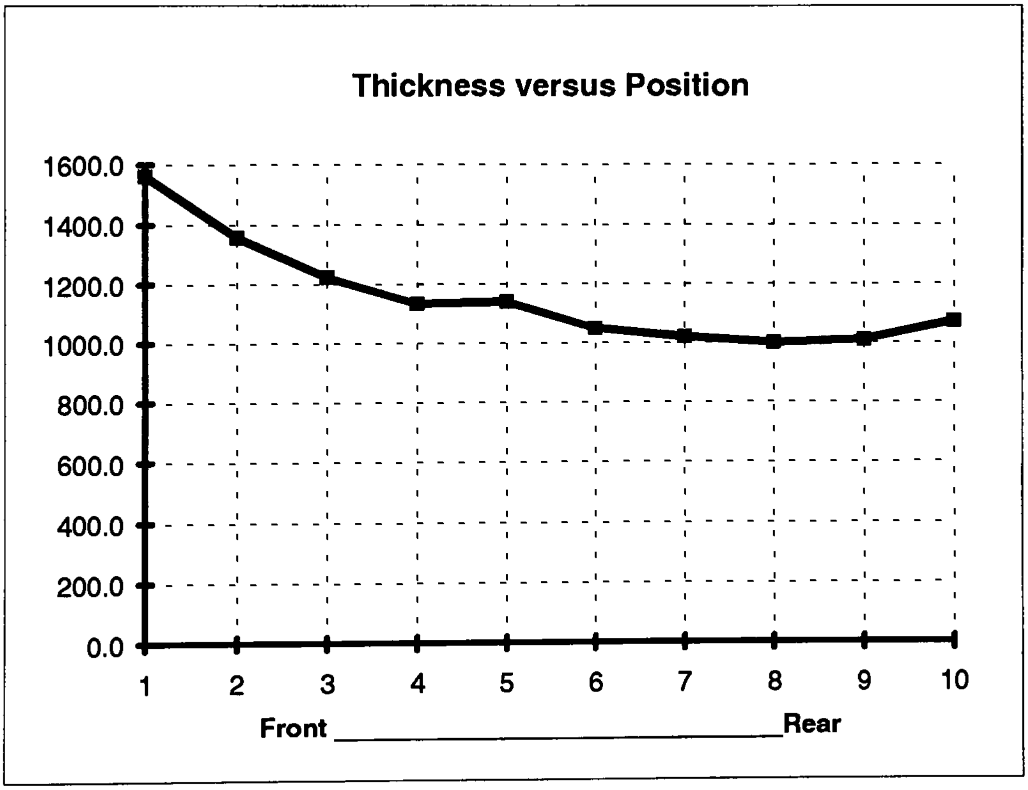

Thickness for Run #14 : 400 °C, 90 minutes, Gas Ratio 1.8

Wafer #	Top	Left	Center	Right	Bottom	Average	STD
131	4930.1	2978.0	2923.0	2966.6	2871.7	3333.9	893.3
132	3045.6	2927.9	2845.0	2857.2	2887.4	2912.6	80.9
133	3269.6	2852.7	2848.8	2852.4	2867.6	2938.2	185.4
134	2855.0	2921.7	2897.3	2923.9	2879.2	2895.4	29.2
135	3213.0	2877.5	2853.3	2870.7	2845.9	2932.1	157.6
136	2907.9	2853.9	2842.5	2847.0	2856.5	2861.6	26.5
137	3002.9	2858.7	2844.5	2850.6	2857.9	2882.9	67.3
138	2902.6	2860.9	2842.9	2855.9	2882.0	2868.9	23.5
139	2828.0	2857.7	2856.1	2850.8	2868.5	2852.2	15.0
140	2724.8	2730.9	3038.1	2975.5	2644.3	2822.7	172.9
						2930.1	165.2

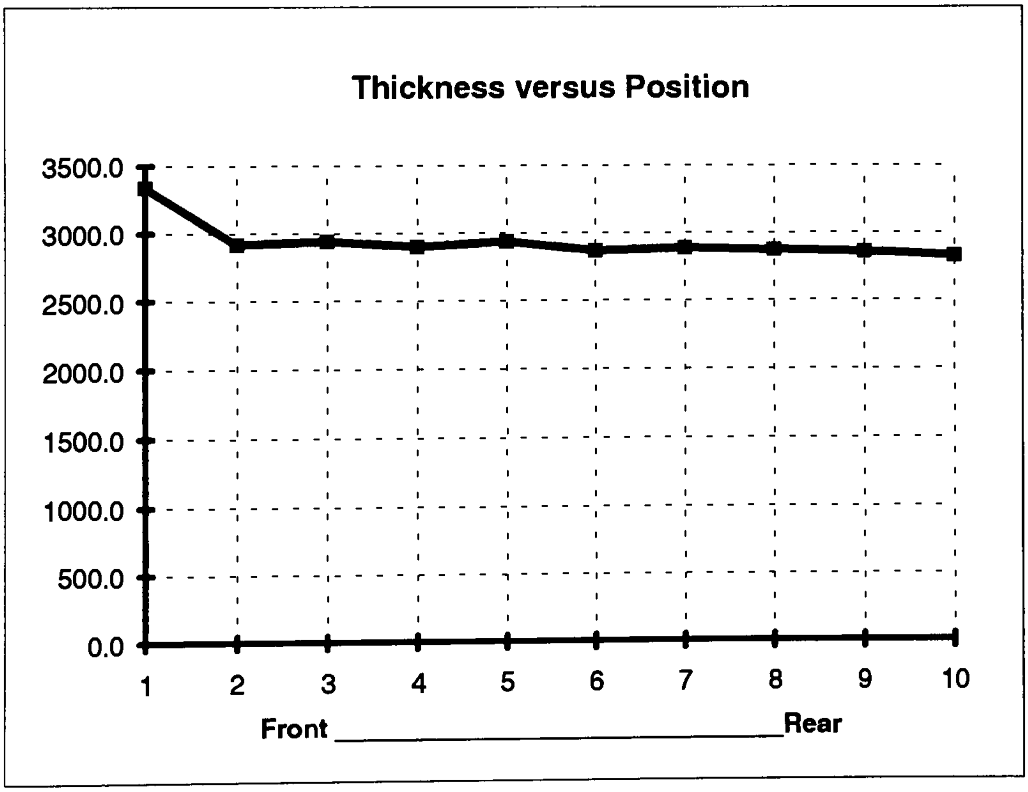

Thickness for Run #15 : 500 °C, 90 minutes, Gas Ratio 1.8

Wafer #	Top	Left	Center	Right	Bottom	Average	STD
141	4420.7	3891.4	3888.5	3724.7	4621.9	4109.4	388.5
142	3958.4	4609.6	4297.1	5031.1	4188.8	4417.0	415.6
143	3982.4	4114.6	4426.7	4191.9	4094.6	4162.0	165.8
144	4632.2	4691.6	4853.9	4837.8	5270.1	4857.1	249.5
145	5164.8	5008.9	4753.8	4524.0	4542.7	4798.8	283.4
146	4167.5	3933.4	4056.5	4332.1	4527.3	4203.4	233.0
147	4023.9	3552.0	3615.0	6403.1	3351.0	4189.0	1261.6
148	3745.2	3818.0	3310.2	3295.8	3647.0	3563.2	245.2
149	3133.0	2743.9	2892.0	3152.5	2790.6	2942.4	190.7
150	2392.2	2339.3	2486.3	2427.2	2422.5	2413.5	53.7
						3965.6	348.7

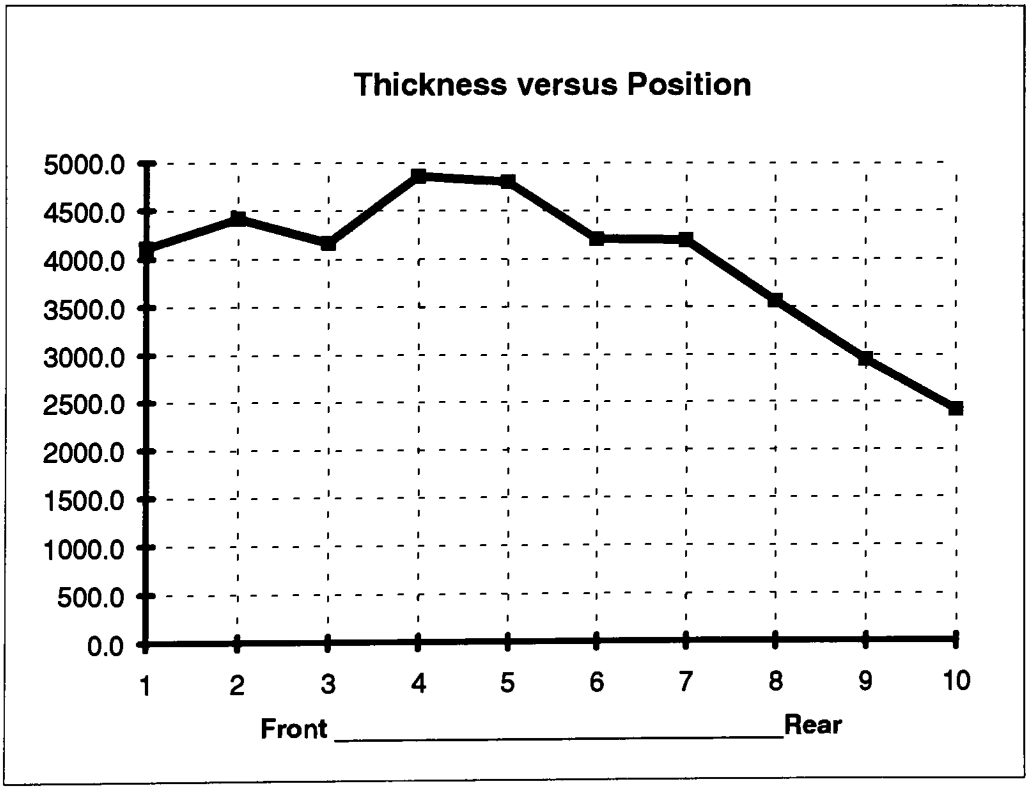

Thickness for Run #16 : 400 °C, 90 minutes, Gas Ratio 1.2

Wafer #	Top	Left	Center	Right	Bottom	Average	STD
151	1515.5	3612.8	3682.4	3559.8	3481.7	3170.4	928.0
152	3667.9	3451.9	3370.7	3315.7	3518.0	3464.8	137.2
153	3842.0	4373.4	3379.8	3995.6	3963.2	3910.8	357.3
154	4488.6	4455.3	3910.3	5135.5	5048.1	4607.6	499.1
155	4058.7	4772.8	3836.4	4280.3	4201.9	4230.0	347.2
156	4779.3	2392.8	3697.2	5256.0	3895.1	4004.1	1103.5
157	4661.2	3580.3	3538.7	4497.4	4198.6	4095.2	516.6
158	4061.5	4021.9	3029.9	5564.8	4758.4	4287.3	942.9
159	3919.4	4106.3	3132.0	5424.4	3582.5	4032.9	861.5
160	3424.6	3478.0	3362.1	3292.0	3454.4	3402.2	75.4
						3920.5	576.9

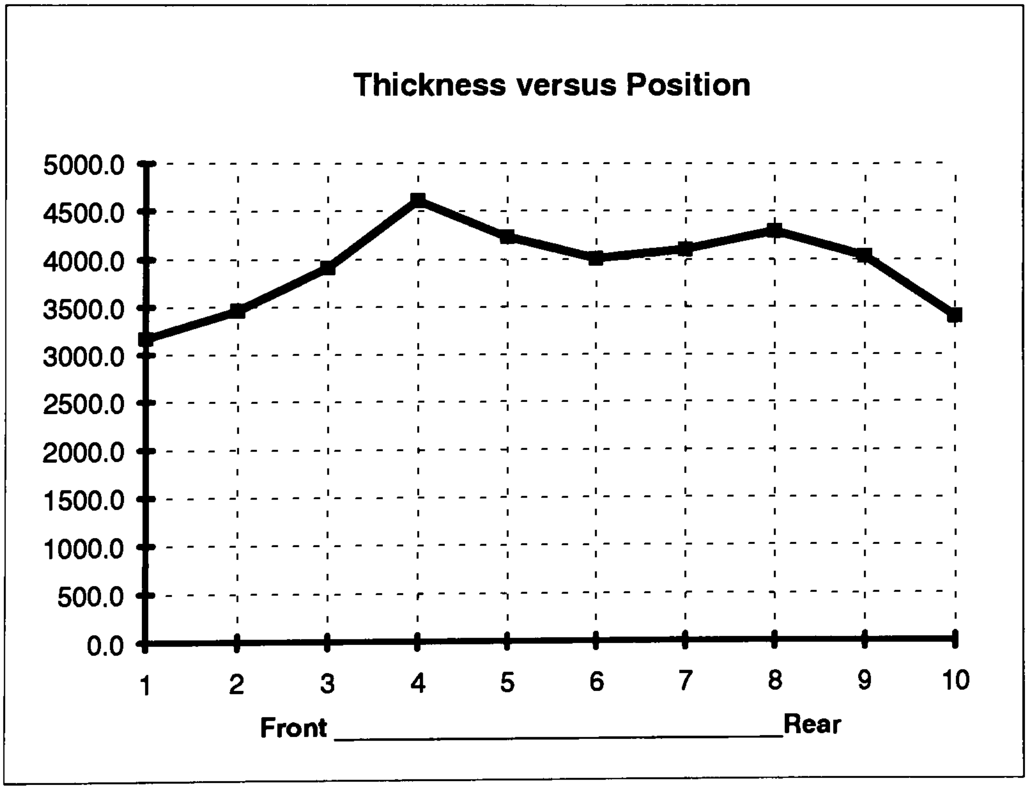

Thickness for Run #17 : 500 °C, 30 minutes, Gas Ratio 1.8

Wafer #	Top	Left	Center	Right	Bottom	Average	STD
161	3466.5	2490.4	2539.3	2402.0	2427.0	2665.0	451.2
162	2339.6	2216.8	2346.4	2255.1	2251.9	2282.0	57.8
163	2254.7	2062.2	2142.8	2098.2	2110.5	2133.7	73.5
164	1916.8	1910.4	1993.5	1999.2	2086.0	1981.2	71.8
165	2158.3	1948.4	2003.0	1917.1	1930.9	1991.5	98.8
166	1725.5	1679.7	1727.9	1685.2	1664.7	1696.6	28.5
167	1523.1	1529.9	1552.0	1499.3	1520.0	1524.9	19.0
168	1393.8	1347.1	1482.2	1358.2	1360.2	1388.3	55.3
169	1220.4	1227.9	1247.8	1219.0	1217.8	1226.6	12.5
170	1099.5	1109.1	1123.4	1099.0	1094.3	1105.1	11.6
						1799.5	88.0

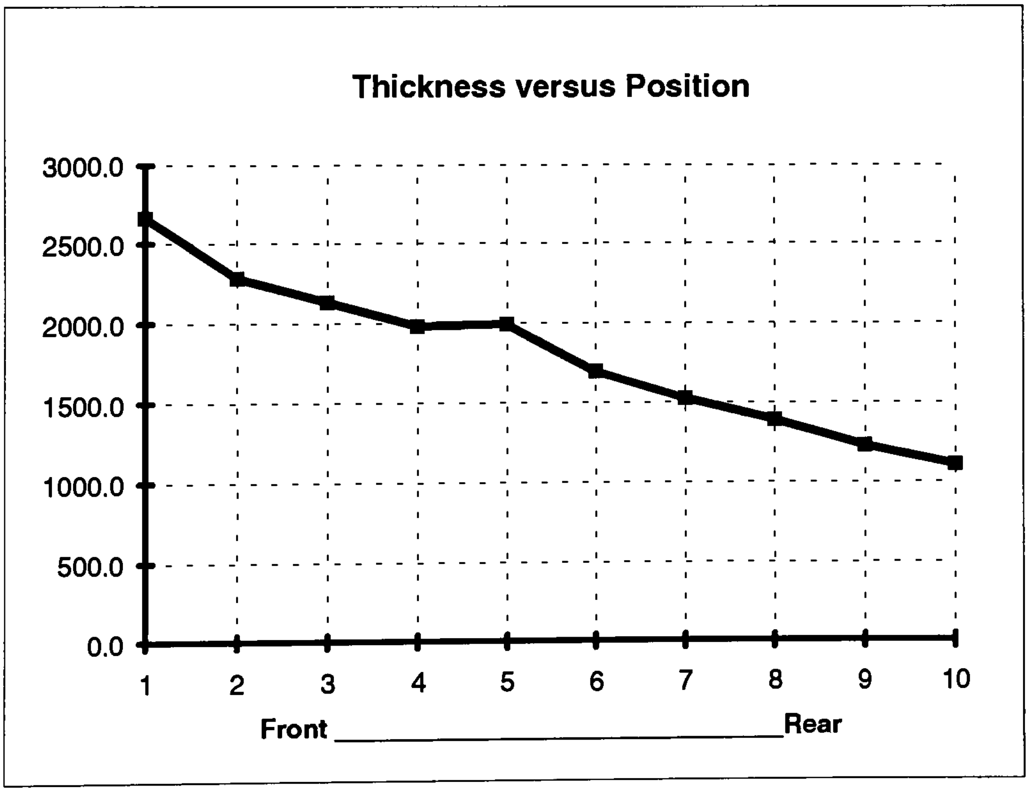

Thickness for Run #18 : 500 °C, 30 minutes, Gas Ratio 1.2

Wafer #	Top	Left	Center	Right	Bottom	Average	STD
171	3348.7	3301.7	3403.4	3316.1	3244.5	3322.9	58.7
172	3181.6	3041.1	3151.7	3048.8	3041.4	3092.9	68.2
173	2456.5	2379.8	2458.9	2464.9	2255.4	2403.1	89.6
174	2209.2	2214.5	2283.0	2220.3	2196.9	2224.8	33.7
175	2245.7	2196.6	2268.7	2193.6	2169.3	2214.8	41.0
176	1947.8	1943.1	1987.0	1935.8	1920.6	1946.9	24.7
177	1628.8	1620.9	1664.6	1632.0	1798.0	1668.9	74.1
178	1586.7	1495.3	1524.9	1483.6	1476.4	1513.4	45.0
179	1394.1	1397.0	1324.0	1397.2	1368.9	1376.2	31.5
180	1228.1	1223.4	1249.3	1233.9	1205.0	1227.9	16.1
						2099.2	48.3

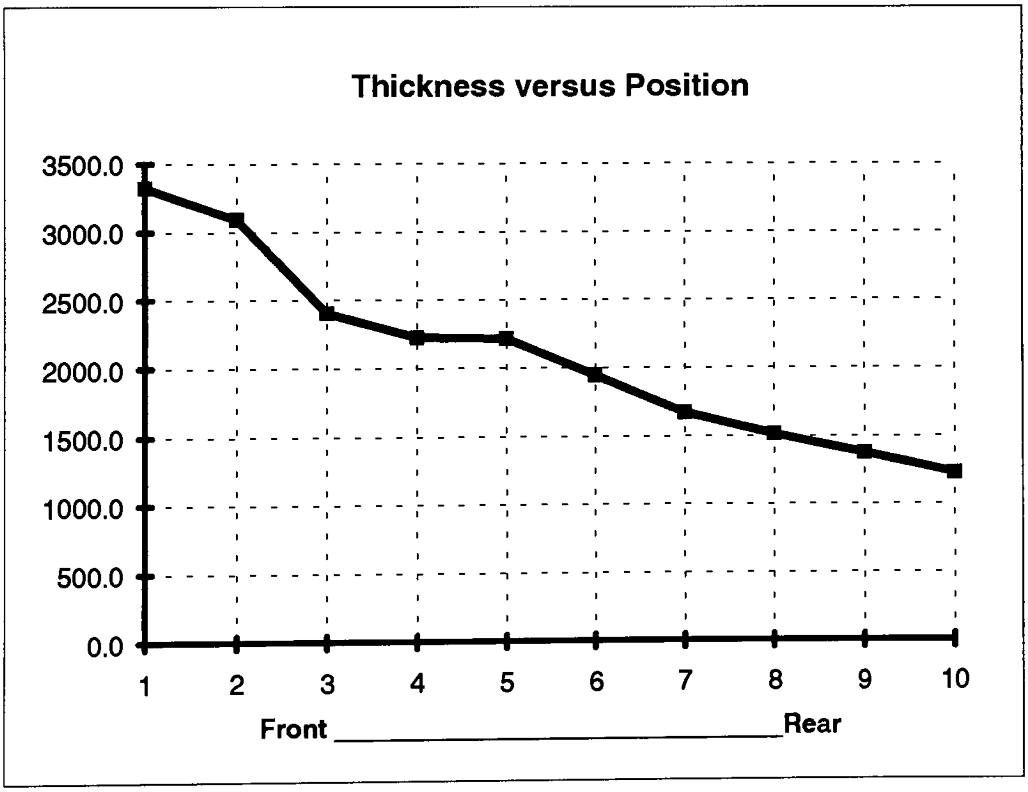

Appendix C :

Tabulated Data and Plot of Index of Refraction From SD2000 Ellipsometer

Index of Refraction for Run #1 : 400 °C, 30 minutes, Gas Ratio 1.8

Wafer #	Top	Left	Center	Right	Bottom	Average	STD
1	1.3002	1.4592	1.4480	1.3934	1.4546	1.4111	0.0674
2	1.3976	1.4029	1.4493	1.4508	1.4352	1.4272	0.0254
3	1.4061	1.4553	1.4584	1.4435	1.4373	1.4401	0.0209
4	1.4505	1.4491	1.4397	1.4062	1.3681	1.4227	0.0354
5	1.2995	1.4060	1.4383	1.4234	1.4534	1.4041	0.0611
6	1.4106	1.4596	1.4589	1.4492	1.4514	1.4459	0.0203
7	1.4407	1.4564	1.4600	1.4611	1.4533	1.4543	0.0082
8	1.4520	1.4579	1.4613	1.4594	1.4511	1.4563	0.0045
9	1.4537	1.4610	1.4616	1.4585	1.4559	1.4581	0.0034
10	1.4538	1.4597	1.4616	1.4609	1.4573	1.4587	0.0032
						1.4379	0.0250

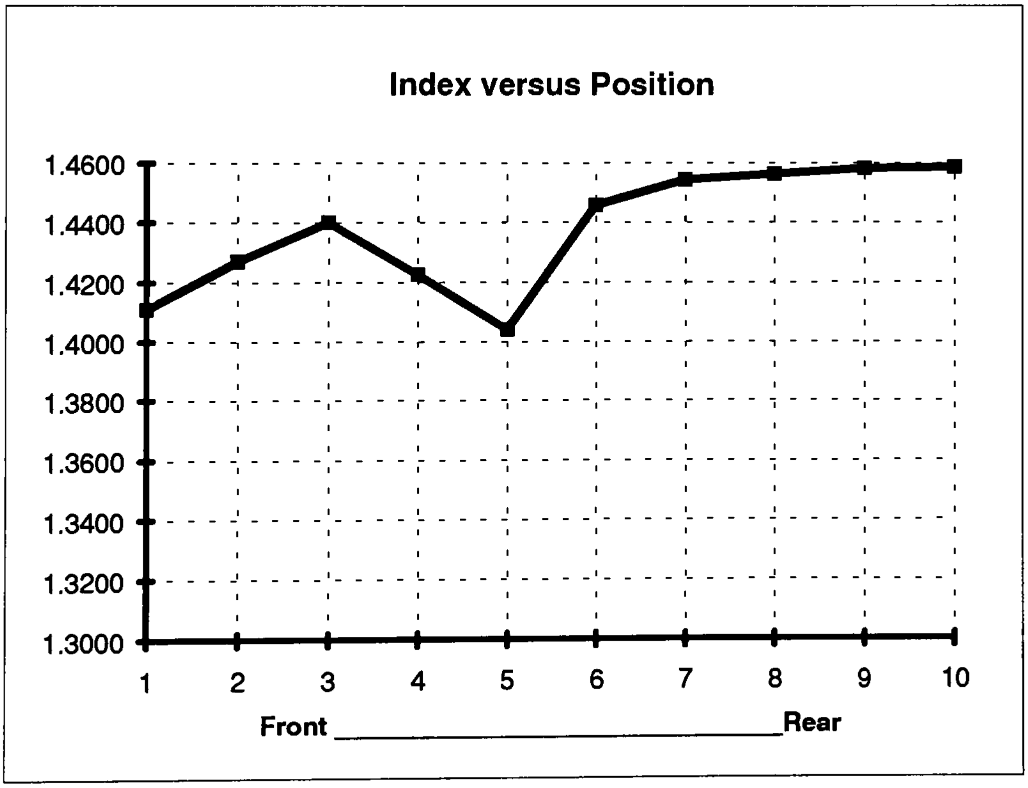

Index of Refraction for Run #2 : 450 °C, 60 minutes, Gas Ratio 1.5

Wafer #	Top	Left	Center	Right	Bottom	Average	STD
11	1.3906	1.4577	1.1000	1.1346	1.3671	1.2900	0.1616
12	1.1672	1.4794	1.4156	1.4301	1.4974	1.3979	0.1333
13	1.5577	1.4577	1.4474	1.4577	1.4536	1.4748	0.0465
14	1.4565	1.4740	1.4544	1.4498	1.4607	1.4591	0.0092
15	1.4995	1.4961	1.4562	1.4500	1.4637	1.4731	0.0231
16	1.4758	1.4568	1.4547	1.4532	1.4565	1.4594	0.0093
17	1.4580	1.4545	1.4548	1.4554	1.4540	1.4553	0.0016
18	1.4591	1.4554	1.4553	1.4563	1.4546	1.4561	0.0018
19	1.4598	1.4542	1.4553	1.4556	1.4537	1.4557	0.0024
20	1.4562	1.4604	1.4539	1.4480	1.4563	1.4550	0.0045
						1.4377	0.0393

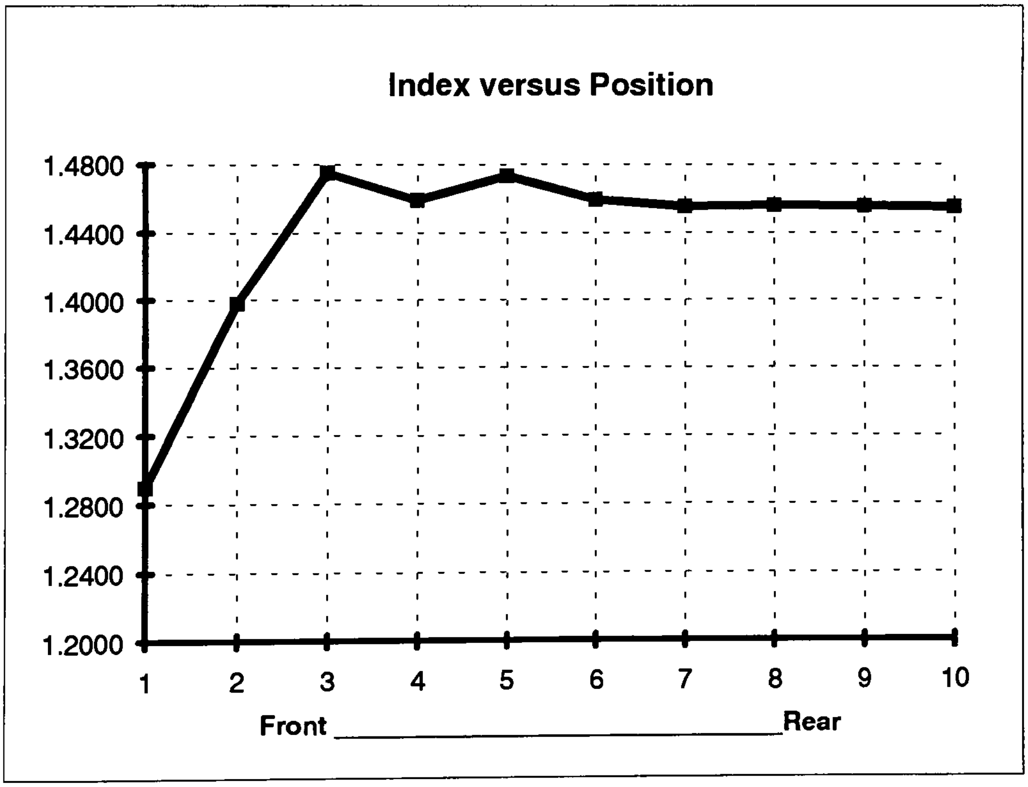

Index of Refraction for Run #3 : 500 °C, 30 minutes, Gas Ratio 1.8

Wafer #	Top	Left	Center	Right	Bottom	Average	STD
21	1.1450	1.4748	1.4524	1.4526	1.4628	1.3975	0.1415
22	1.4736	1.4558	1.4542	1.4498	1.4528	1.4572	0.0094
23	1.4438	1.4507	1.4542	1.4533	1.4490	1.4502	0.0041
24	1.4532	1.4487	1.4542	1.4510	1.4410	1.4496	0.0053
25	1.4390	1.4530	1.4551	1.4546	1.4495	1.4502	0.0067
26	1.4535	1.4554	1.4565	1.4559	1.4553	1.4553	0.0011
27	1.4518	1.4502	1.4564	1.4551	1.4518	1.4531	0.0026
28	1.4534	1.4556	1.4564	1.4567	1.4550	1.4554	0.0013
29	1.4517	1.4558	1.4567	1.4565	1.4555	1.4552	0.0020
30	1.4528	1.4564	1.4569	1.4566	1.4559	1.4557	0.0017
						1.4480	0.0176

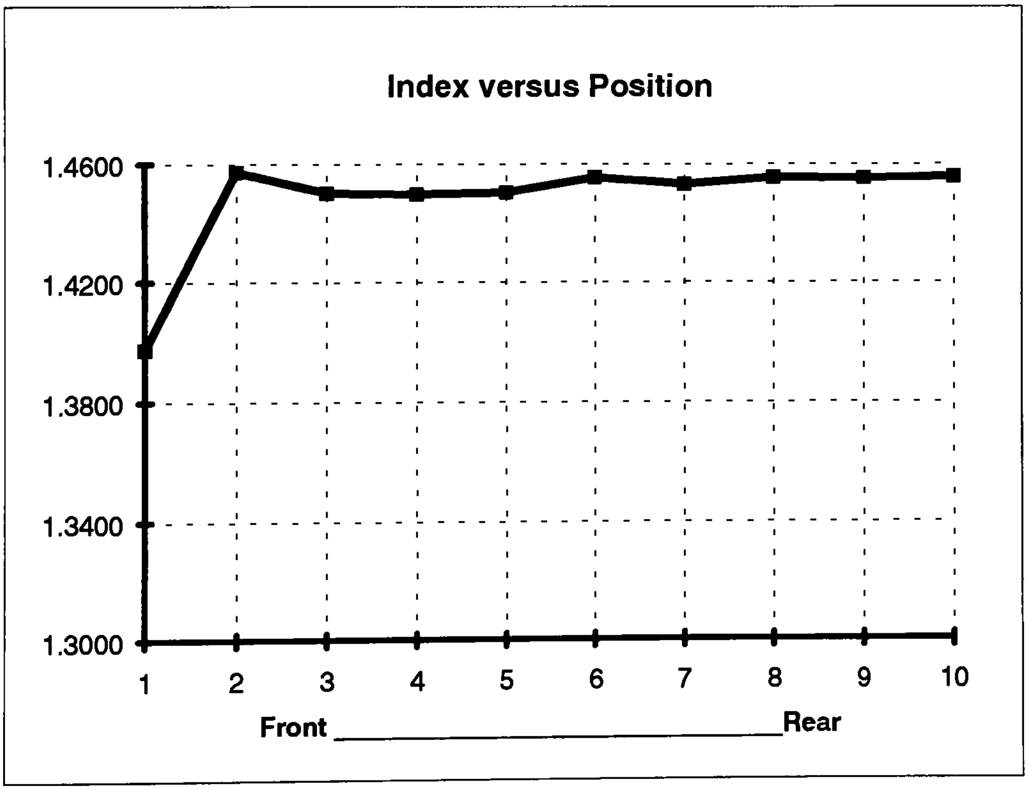

Index of Refraction for Run #4 : 400 °C, 90 minutes, Gas Ratio 1.2

Wafer #	Top	Left	Center	Right	Bottom	Average	STD
31	1.2657	1.5430	1.1675	1.4159	1.4622	1.3709	0.1520
32	1.4677	1.4548	1.4566	1.4558	1.4553	1.4580	0.0054
33	1.4505	1.4573	1.4574	1.4576	1.4569	1.4559	0.0031
34	1.4575	1.4581	1.4574	1.4575	1.4543	1.4570	0.0015
35	1.4509	1.4592	1.4585	1.4577	1.4583	1.4569	0.0034
36	1.4568	1.4590	1.4592	1.4585	1.4584	1.4584	0.0009
37	1.4571	1.4584	1.4588	1.4583	1.4584	1.4582	0.0006
38	1.4567	1.4578	1.4578	1.4581	1.4577	1.4576	0.0005
39	1.4561	1.4568	1.4569	1.4576	1.4565	1.4568	0.0006
40	1.4587	1.4545	1.4556	1.4564	1.4537	1.4558	0.0019
						1.4485	0.0170

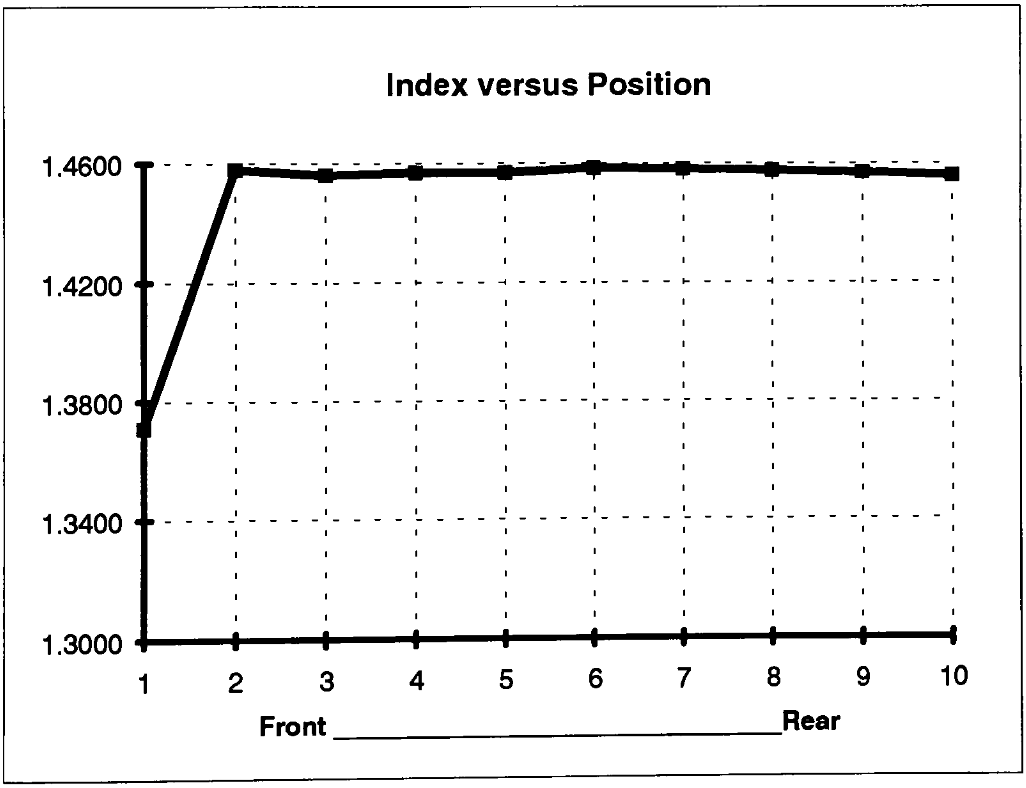

Index of Refraction for Run #5 : 500 °C, 90 minutes, Gas Ratio 1.2

Wafer #	Top	Left	Center	Right	Bottom	Average	STD
41	1.3008	1.4589	1.3449	1.4063	1.4541	1.3930	0.0690
42	1.4498	1.4510	1.4527	1.4452	1.4517	1.4501	0.0029
43	1.4454	1.4444	1.4550	1.4486	1.4438	1.4474	0.0046
44	1.4069	1.4124	1.4647	1.4323	1.4401	1.4313	0.0232
45	1.4576	1.4266	1.4288	1.4439	1.4328	1.4379	0.0129
46	1.4541	1.4541	1.4537	1.4549	1.4542	1.4542	0.0004
47	1.4549	1.4563	1.4554	1.4552	1.4550	1.4554	0.0006
48	1.4555	1.4574	1.4569	1.4563	1.4570	1.4566	0.0007
49	1.4562	1.4572	1.4583	1.4568	1.4578	1.4573	0.0008
50	1.4535	1.4520	1.4551	1.4521	1.4498	1.4525	0.0020
						1.4436	0.0117

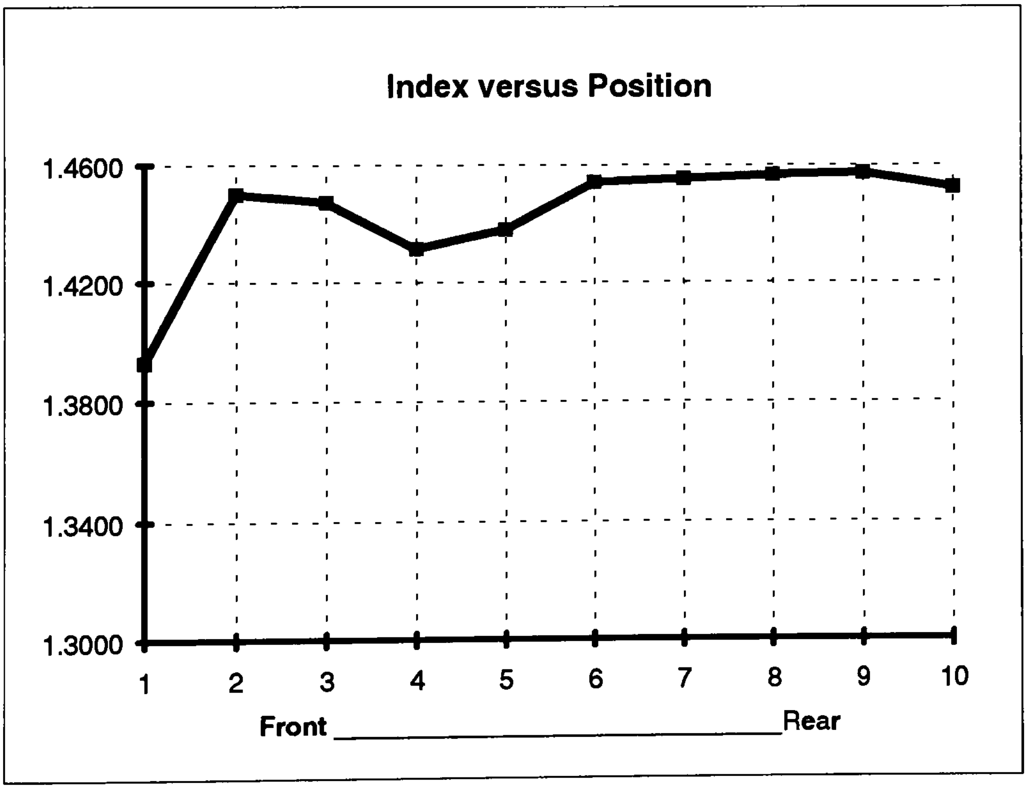

Index of Refraction for Run #6 : 400 °C, 30 minutes, Gas Ratio 1.2

Wafer #	Top	Left	Center	Right	Bottom	Average	STD
51	1.4525	1.4577	1.4595	1.4583	1.4556	1.4567	0.0027
52	1.4561	1.4595	1.4598	1.4590	1.4583	1.4585	0.0015
53	1.4543	1.4602	1.4599	1.4590	1.4597	1.4586	0.0025
54	1.4590	1.4601	1.4596	1.4580	1.4568	1.4587	0.0013
55	1.4546	1.4580	1.4597	1.4595	1.4590	1.4582	0.0021
56	1.4585	1.4598	1.4604	1.4596	1.4600	1.4597	0.0007
57	1.4586	1.4599	1.4597	1.4600	1.4597	1.4596	0.0006
58	1.4598	1.4600	1.4604	1.4601	1.4598	1.4600	0.0002
59	1.4599	1.4602	1.4603	1.4600	1.4602	1.4601	0.0002
60	1.4597	1.4610	1.4601	1.4596	1.4600	1.4601	0.0006
						1.4590	0.0012

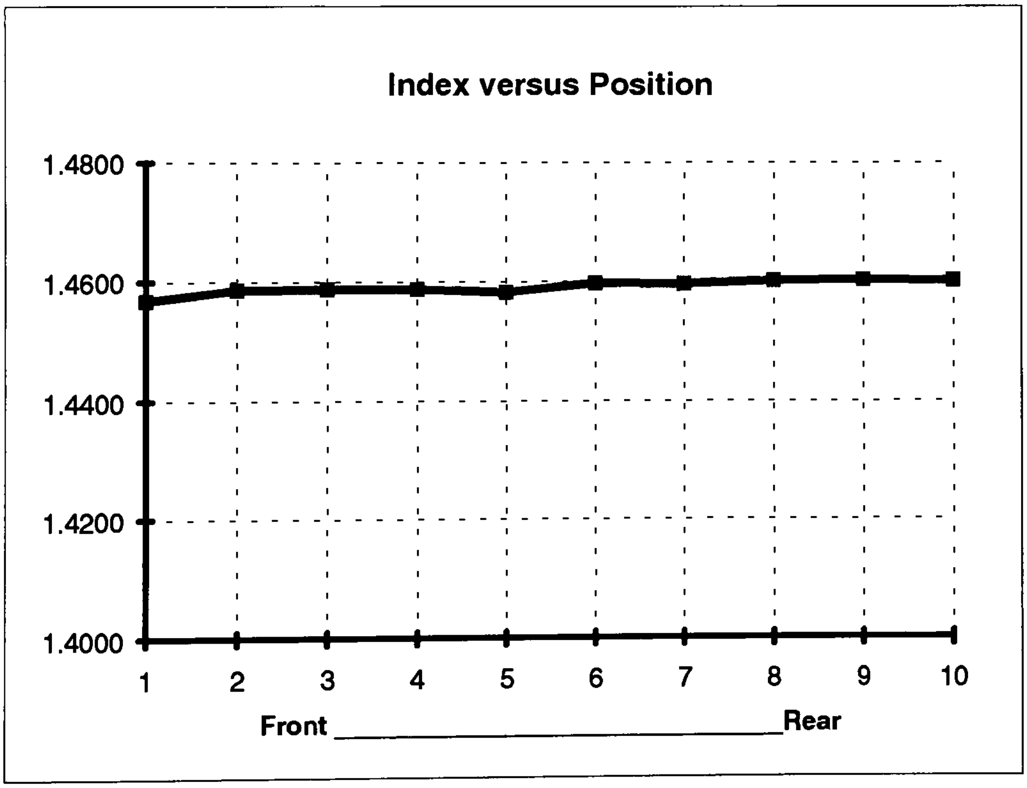

Index of Refraction for Run #7 : 500 °C, 30 minutes, Gas Ratio 1.2

Wafer #	Top	Left	Center	Right	Bottom	Average	STD
61	1.4012	1.3361	1.4141	1.3463	1.3072	1.3610	0.0452
62	1.2118	1.3912	1.2499	1.3830	1.3818	1.3235	0.0858
63	1.4460	1.4701	1.4452	1.4232	1.4632	1.4495	0.0183
64	1.4585	1.4504	1.4518	1.4583	1.4524	1.4543	0.0038
65	1.4542	1.4587	1.4530	1.4501	1.4553	1.4543	0.0032
66	1.4568	1.4547	1.4551	1.4563	1.4547	1.4555	0.0010
67	1.4556	1.4563	1.4561	1.4554	1.4558	1.4558	0.0004
68	1.4561	1.4568	1.4564	1.4557	1.4563	1.4563	0.0004
69	1.4560	1.4521	1.4555	1.4511	1.4538	1.4537	0.0021
70	1.4564	1.4572	1.4567	1.4562	1.4564	1.4566	0.0004
						1.4321	0.0160

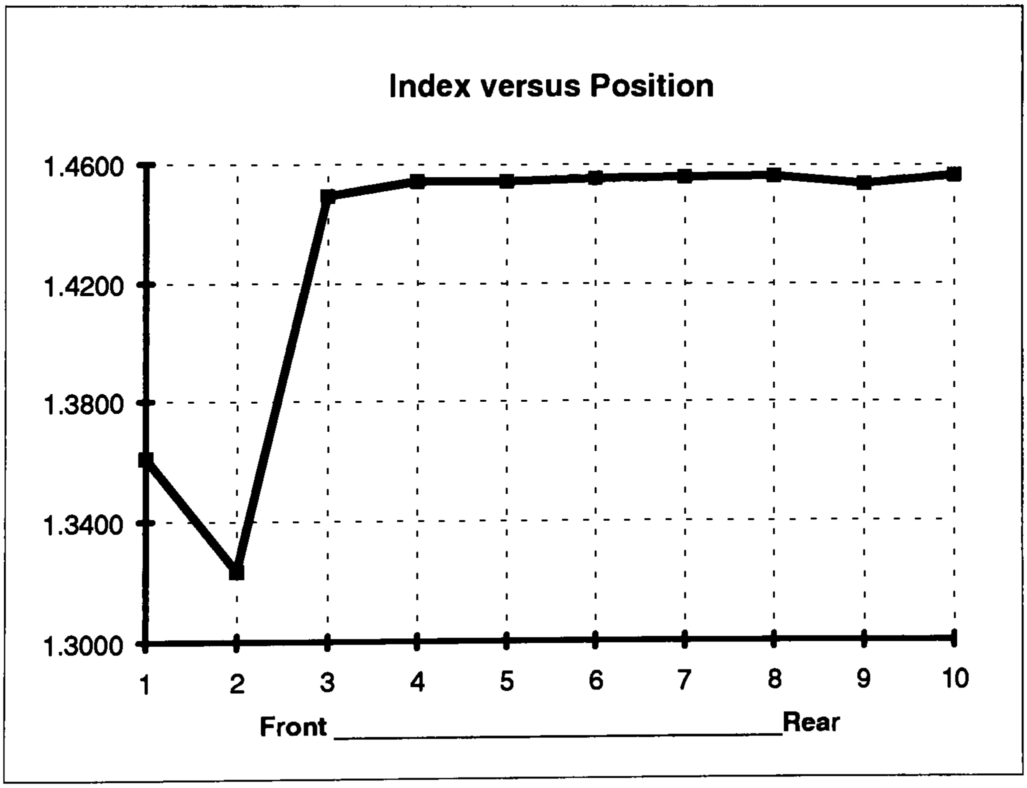

Index of Refraction for Run #8 : 450 °C, 60 minutes, Gas Ratio 1.5

Wafer #	Top	Left	Center	Right	Bottom	Average	STD
71	1.4316	1.4540	1.4551	1.4438	1.4514	1.4472	0.0098
72	1.4366	1.4277	1.4533	1.4463	1.4266	1.4381	0.0116
73	1.4187	1.4290	1.4527	1.4288	1.4117	1.4282	0.0155
74	1.4023	1.3958	1.4293	1.3700	1.3387	1.3872	0.0344
75	1.3866	1.3888	1.4373	1.4259	1.3812	1.4040	0.0257
76	1.3589	1.3198	1.4063	1.3502	1.2267	1.3324	0.0667
77	1.2708	1.1728	1.3369	1.2685	1.1016	1.2301	0.0926
78	1.1861	1.1857	1.2463	1.1561	1.1000	1.1748	0.0532
79	1.1000	1.1000	1.1000	1.1000	1.1000	1.1000	0.0000
80	1.1864	1.1000	1.1009	1.1000	1.1000	1.1175	0.0385
						1.3059	0.0348

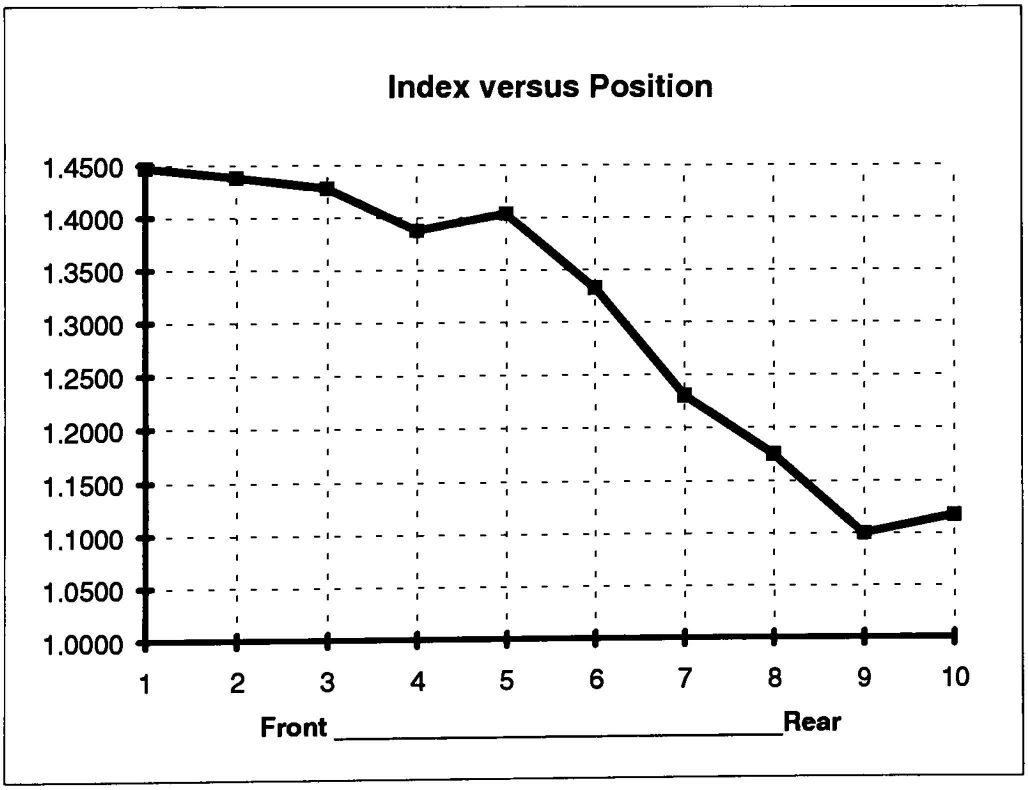

Index of Refraction for Run #9 : 400 °C, 90 minutes, Gas Ratio 1.8

Wafer #	Top	Left	Center	Right	Bottom	Average	STD
81	1.1120	1.4282	1.4528	1.4494	1.4507	1.3786	0.1494
82	1.2544	1.4389	1.4549	1.4543	1.4424	1.4090	0.0867
83	1.3821	1.4387	1.4565	1.4550	1.4388	1.4342	0.0304
84	1.4470	1.4140	1.4410	1.4419	1.3240	1.4136	0.0517
85	1.4276	1.4000	1.3646	1.4417	1.4440	1.4156	0.0335
86	1.4315	1.4452	1.4572	1.4531	1.4468	1.4468	0.0098
87	1.4419	1.4536	1.4565	1.4548	1.4448	1.4503	0.0065
88	1.4341	1.4480	1.4504	1.4552	1.4105	1.4396	0.0181
89	1.4683	1.4475	1.4556	1.4572	1.4821	1.4621	0.0134
90	1.5179	1.4869	1.4318	1.4294	1.5676	1.4867	0.0588
						1.4337	0.0458

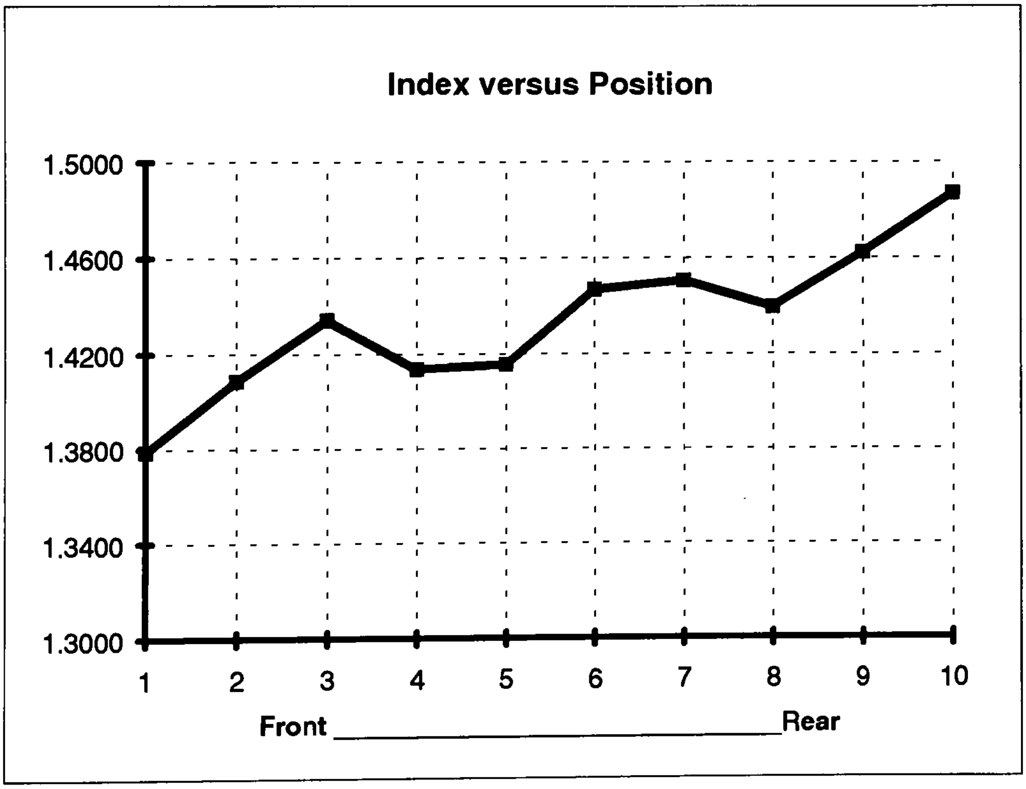

Index of Refraction for Run #10 : 500 °C, 90 minutes, Gas Ratio 1.8

Wafer #	Top	Left	Center	Right	Bottom	Average	STD
91	1.3077	1.4362	1.4610	1.4724	1.4613	1.4277	0.0684
92	1.4318	1.3945	1.4517	1.3695	1.3865	1.4068	0.0339
93	1.3394	1.2892	1.4311	1.3987	1.2816	1.3480	0.0660
94	1.4573	1.4927	1.4116	1.4180	1.1201	1.3799	0.1489
95	1.3114	1.4915	1.4338	1.4547	1.5114	1.4406	0.0783
96	1.5549	1.4472	1.4500	1.4491	1.4471	1.4697	0.0477
97	1.4263	1.4496	1.4527	1.4474	1.4500	1.4452	0.0107
98	1.4435	1.4493	1.4538	1.4529	1.4335	1.4466	0.0084
99	1.4323	1.4127	1.4528	1.4449	1.4260	1.4337	0.0158
100	1.3505	1.3280	1.4191	1.4000	1.3174	1.3630	0.0447
						1.4161	0.0523

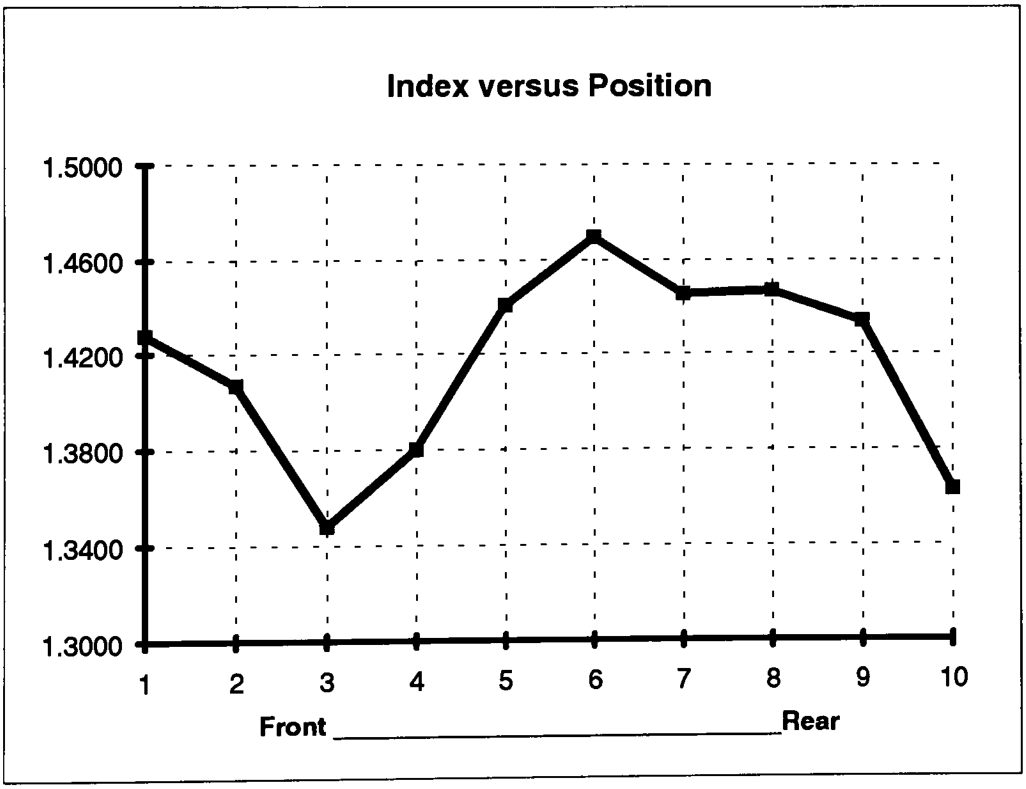

Index of Refraction for Run #11 : 400 °C, 30 minutes, Gas Ratio 1.8

Wafer #	Top	Left	Center	Right	Bottom	Average	STD
101	1.3463	1.4207	1.4564	1.4549	1.4581	1.4273	0.0479
102	1.4100	1.4347	1.4607	1.4565	1.4461	1.4416	0.0203
103	1.4270	1.4472	1.4598	1.4522	1.4475	1.4467	0.0122
104	1.4526	1.4258	1.4453	1.4377	1.3842	1.4291	0.0270
105	1.3840	1.4306	1.4506	1.4561	1.4503	1.4343	0.0298
106	1.4412	1.4436	1.4580	1.4567	1.4478	1.4495	0.0076
107	1.4458	1.4495	1.4602	1.4577	1.4529	1.4532	0.0059
108	1.4497	1.4535	1.4591	1.4596	1.4488	1.4541	0.0051
109	1.4565	1.4521	1.4598	1.4600	1.4520	1.4561	0.0039
110	1.4589	1.4565	1.4600	1.4601	1.4552	1.4581	0.0022
						1.4450	0.0162

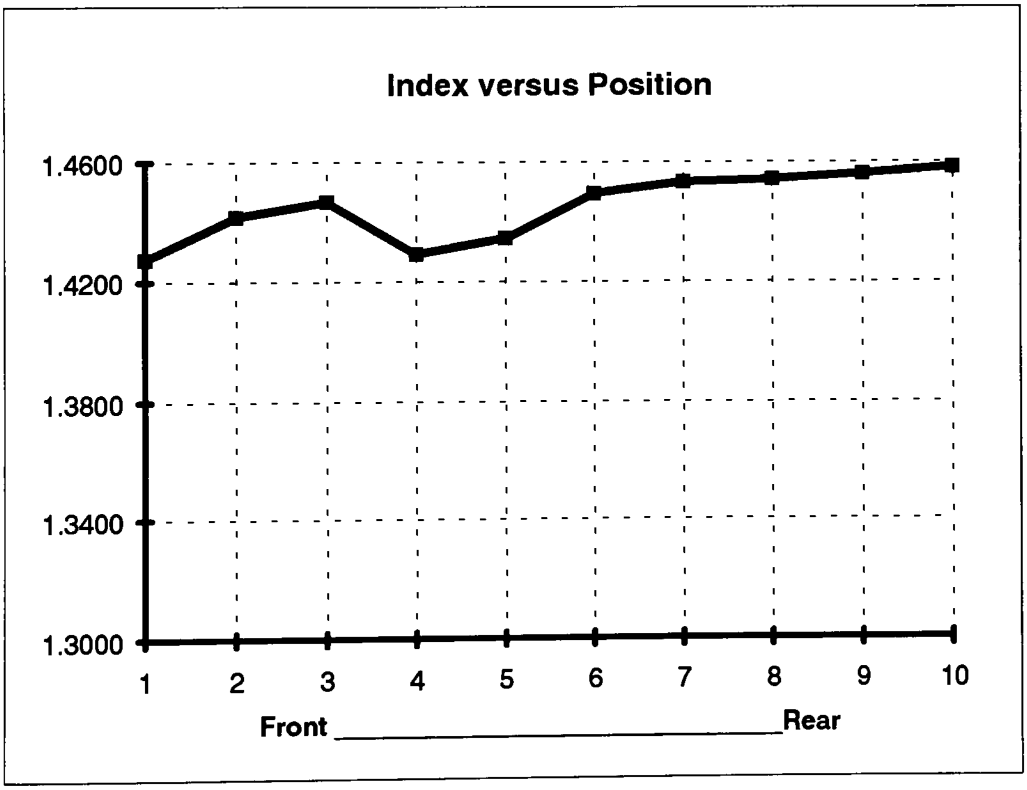

Index of Refraction for Run #12 : 500 °C, 90 minutes, Gas Ratio 1.2

Wafer #	Top	Left	Center	Right	Bottom	Average	STD
111	1.4511	1.4495	1.4503	1.4476	1.4491	1.4495	0.0013
112	1.4460	1.4489	1.4513	1.4498	1.4484	1.4489	0.0020
113	1.4130	1.3202	1.4347	1.3980	1.2371	1.3606	0.0814
114	1.4397	1.4466	1.4188	1.4492	1.4499	1.4408	0.0130
115	1.4576	1.4499	1.4361	1.4466	1.4501	1.4481	0.0078
116	1.4505	1.4537	1.4527	1.4517	1.4536	1.4524	0.0014
117	1.4530	1.4549	1.4533	1.4534	1.4543	1.4538	0.0008
118	1.4541	1.4576	1.4556	1.4542	1.4562	1.4555	0.0015
119	1.4492	1.4497	1.4538	1.4532	1.4482	1.4508	0.0025
120	1.4367	1.4263	1.4425	1.4438	1.4253	1.4349	0.0088
						1.4395	0.0120

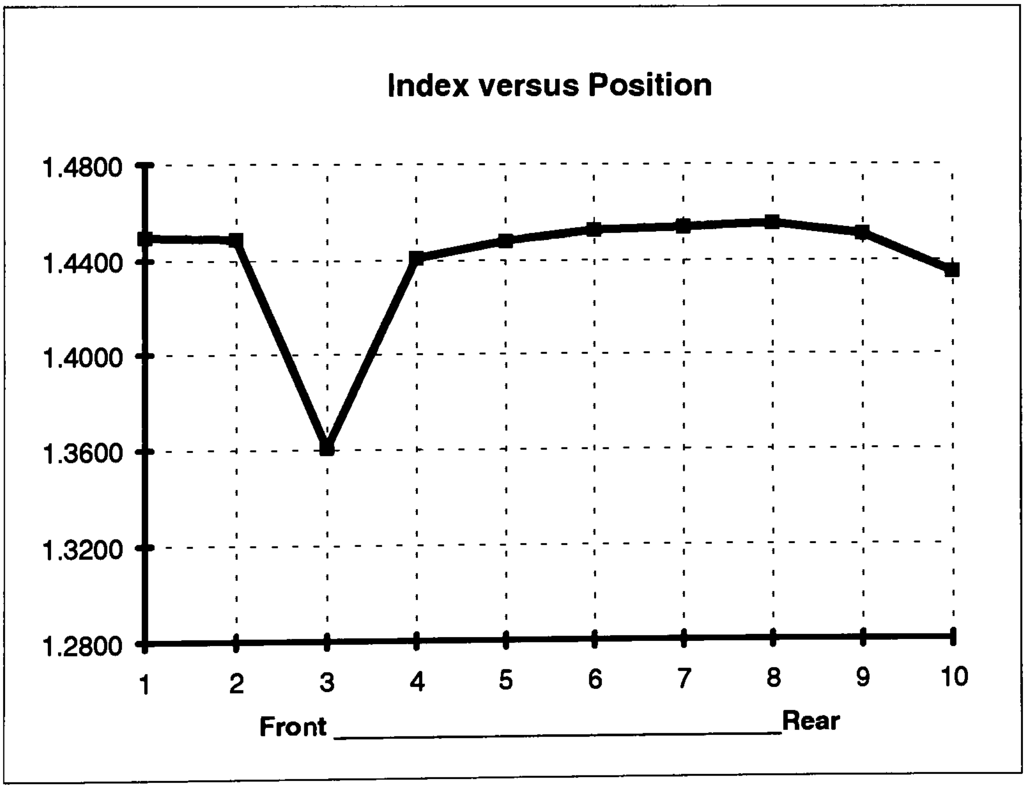

Index of Refraction for Run #13 : 400 °C, 30 minutes, Gas Ratio 1.2

Wafer #	Top	Left	Center	Right	Bottom	Average	STD
121	1.4500	1.4574	1.4579	1.4565	1.4574	1.4558	0.0033
122	1.4537	1.4585	1.4572	1.4580	1.4561	1.4567	0.0019
123	1.4542	1.4579	1.4591	1.4588	1.4582	1.4576	0.0020
124	1.4568	1.4585	1.4585	1.4577	1.4561	1.4575	0.0011
125	1.4561	1.4574	1.4594	1.4585	1.4588	1.4580	0.0013
126	1.4567	1.4577	1.4599	1.4585	1.4580	1.4582	0.0012
127	1.4565	1.4592	1.4592	1.4592	1.4597	1.4588	0.0013
128	1.4577	1.4591	1.4593	1.4597	1.4594	1.4590	0.0008
129	1.4587	1.4604	1.4595	1.4582	1.4590	1.4592	0.0008
130	1.4590	1.4592	1.4593	1.4590	1.4591	1.4591	0.0001
						1.4580	0.0014

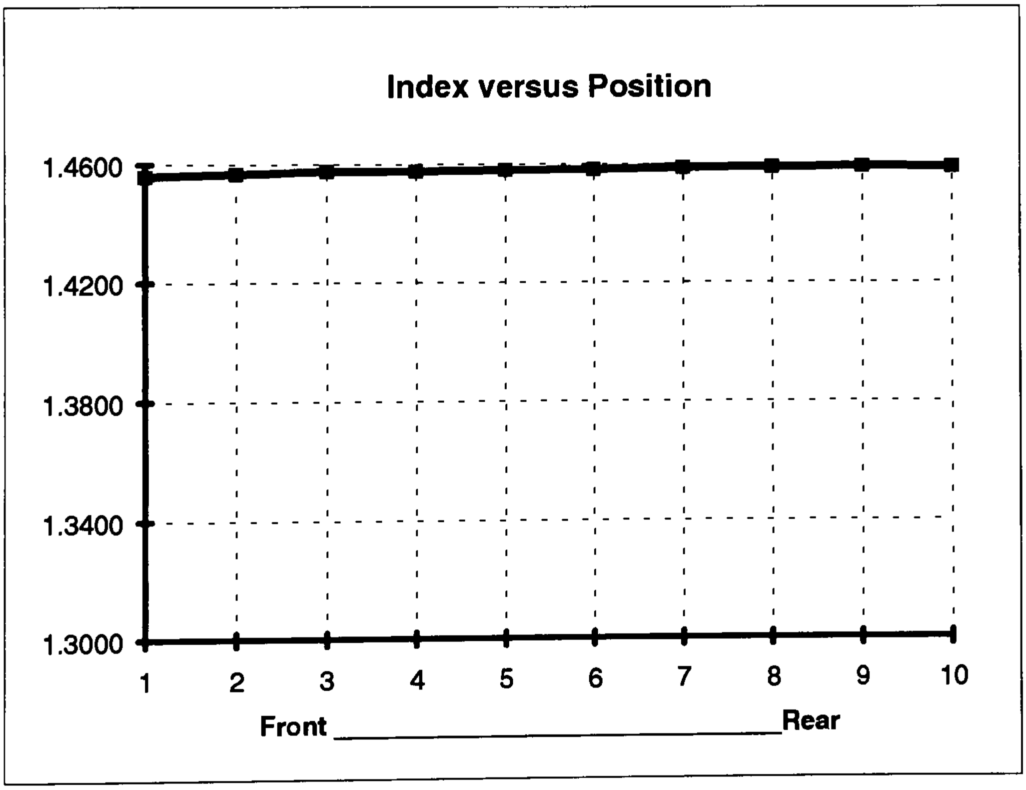

Index of Refraction for Run #14 : 400 °C, 90 minutes, Gas Ratio 1.8

Wafer #	Top	Left	Center	Right	Bottom	Average	STD
131	1.1379	1.4184	1.4334	1.4214	1.4481	1.3718	0.1313
132	1.4008	1.4321	1.4560	1.4524	1.4435	1.4370	0.0222
133	1.3489	1.4537	1.4572	1.4538	1.4493	1.4326	0.0469
134	1.4530	1.4338	1.4407	1.4312	1.2443	1.4006	0.0878
135	1.2685	1.4464	1.4535	1.4484	1.4557	1.4145	0.0817
136	1.4377	1.4533	1.4567	1.4551	1.4525	1.4511	0.0076
137	1.4118	1.4519	1.4561	1.4543	1.4521	1.4452	0.0188
138	1.4392	1.4512	1.4566	1.4527	1.4451	1.4490	0.0068
139	1.4611	1.4522	1.4527	1.4542	1.4490	1.4538	0.0045
140	1.4938	1.4918	1.4277	1.4191	1.5040	1.4673	0.0404
						1.4323	0.0448

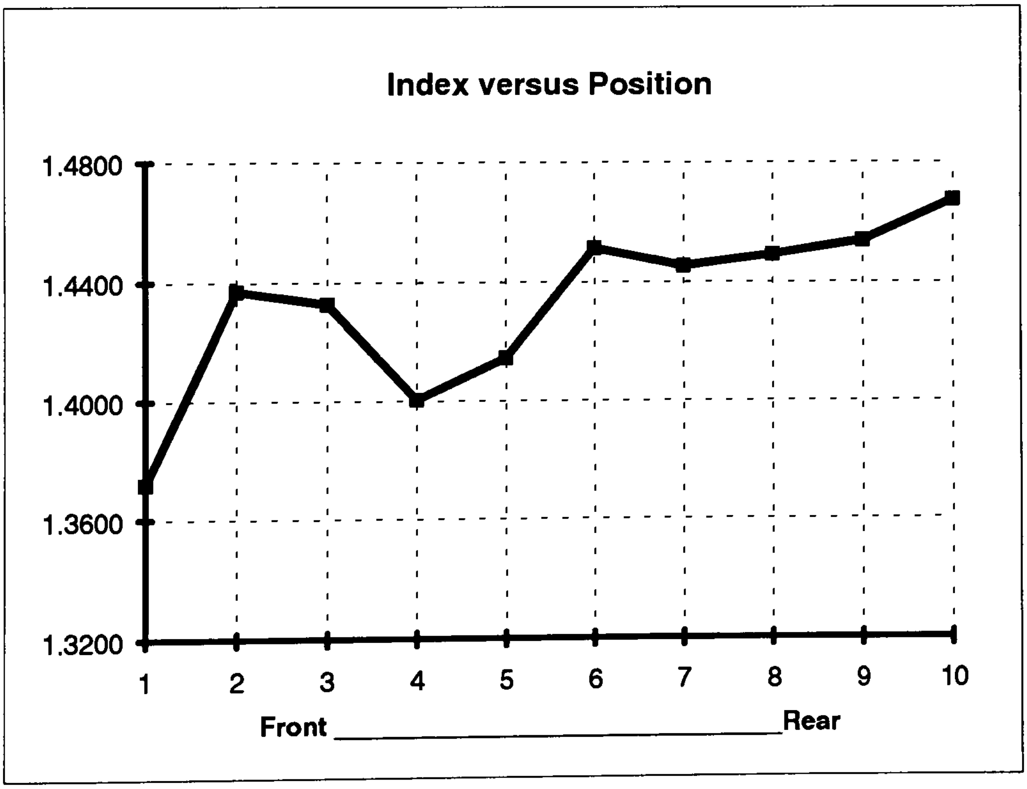

Index of Refraction for Run #15 : 500 °C, 90 minutes, Gas Ratio 1.8

Wafer #	Top	Left	Center	Right	Bottom	Average	STD
141	1.6857	1.4259	1.4418	1.4262	1.4337	1.4827	0.1137
142	1.3990	1.1845	1.4144	1.1476	1.2382	1.2767	0.1231
143	1.5427	1.4593	1.4452	1.4504	1.4883	1.4772	0.0402
144	1.4481	1.4433	1.4421	1.4351	1.4247	1.4387	0.0091
145	1.4521	1.4238	1.4452	1.4483	1.4476	1.4434	0.0112
146	1.4393	1.4451	1.4538	1.4529	1.4457	1.4474	0.0060
147	1.4206	1.4292	1.4524	1.4456	1.4378	1.4371	0.0127
148	1.3257	1.2927	1.4239	1.4017	1.3257	1.3539	0.0559
149	1.3540	1.4362	1.4059	1.3469	1.4331	1.3952	0.0426
150	1.4756	1.4551	1.4520	1.4525	1.4359	1.4542	0.0142
						1.4207	0.0429

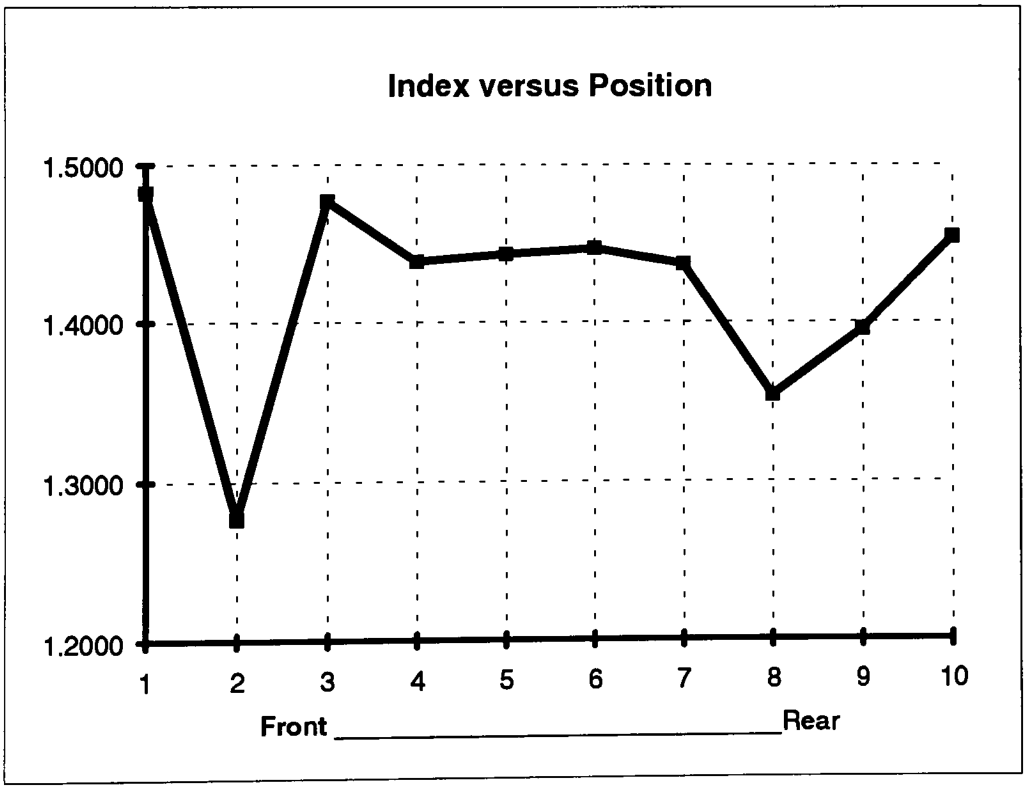

Index of Refraction for Run #16 : 400 °C, 90 minutes, Gas Ratio 1.2

Wafer #	Top	Left	Center	Right	Bottom	Average	STD
151	1.4221	1.4358	1.4565	1.4483	1.4470	1.4419	0.0133
152	1.4046	1.3870	1.4478	1.4261	1.3687	1.4068	0.0312
153	1.3042	1.2039	1.3880	1.2544	1.2578	1.2817	0.0692
154	1.2518	1.1964	1.2789	1.1378	1.1427	1.2015	0.0634
155	1.3172	1.1652	1.2965	1.2152	1.2246	1.2437	0.0623
156	1.2106	1.5785	1.3111	1.1067	1.8494	1.4113	0.3012
157	1.2173	1.2683	1.3363	1.1603	1.4308	1.2826	0.1052
158	1.2766	1.2094	1.4442	1.1041	1.6356	1.3340	0.2090
159	1.2971	1.2283	1.4150	1.1131	1.3007	1.2708	0.1107
160	1.3895	1.3602	1.4013	1.4183	1.3634	1.3865	0.0248
						1.3261	0.0991

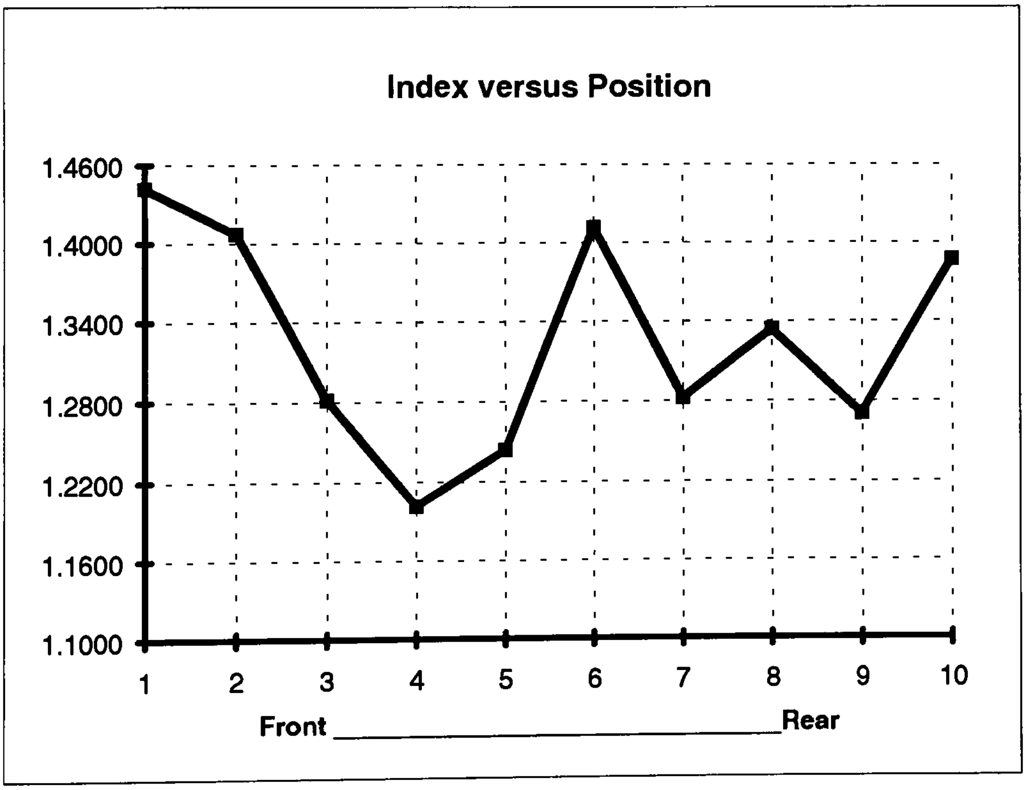

Index of Refraction for Run #17 : 500 °C, 30 minutes, Gas Ratio 1.8

Wafer #	Top	Left	Center	Right	Bottom	Average	STD
161	1.2959	1.4820	1.4650	1.4797	1.4544	1.4354	0.0788
162	1.4953	1.4556	1.4480	1.4518	1.4552	1.4612	0.0193
163	1.4565	1.4457	1.4548	1.4429	1.4476	1.4495	0.0059
164	1.4467	1.4507	1.4476	1.4393	1.4337	1.4436	0.0069
165	1.4404	1.4490	1.4525	1.4520	1.4497	1.4487	0.0049
166	1.4486	1.4544	1.4541	1.4516	1.4529	1.4523	0.0024
167	1.4511	1.4532	1.4545	1.4538	1.4529	1.4531	0.0013
168	1.4489	1.4536	1.4535	1.4543	1.4543	1.4529	0.0023
169	1.4521	1.4549	1.4545	1.4536	1.4535	1.4537	0.0011
170	1.4528	1.4556	1.4546	1.4536	1.4533	1.4540	0.0011
						1.4504	0.0124

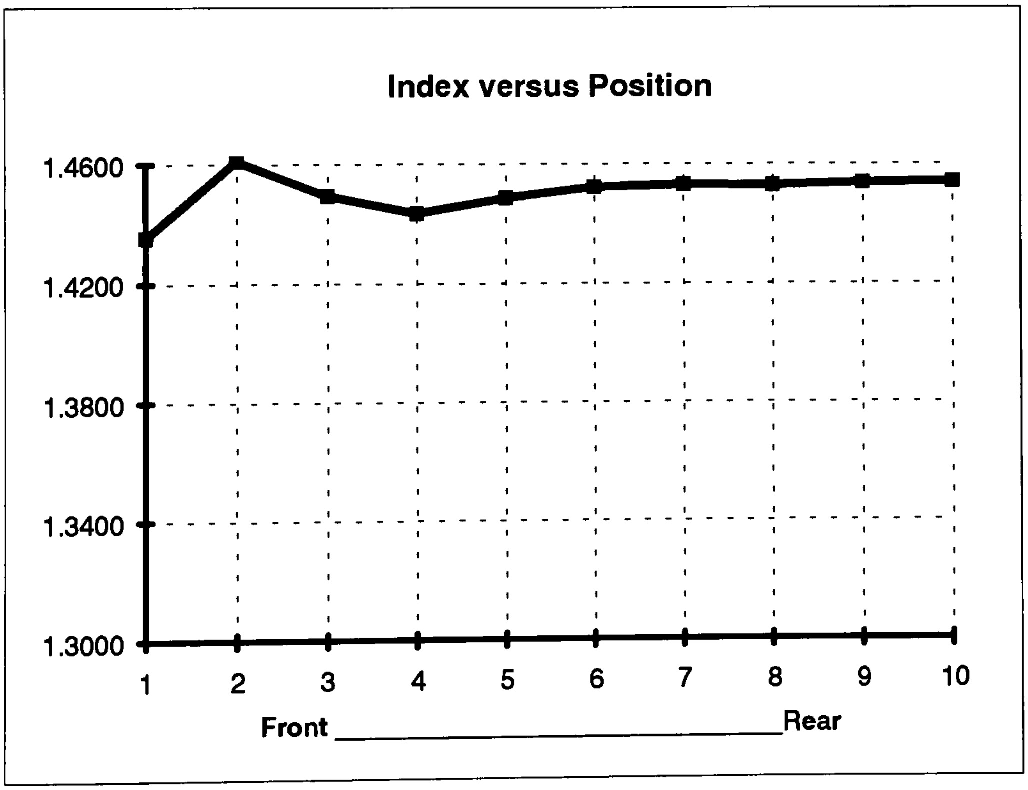

Index of Refraction for Run #18 : 500 °C, 30 minutes, Gas Ratio 1.2

Wafer #	Top	Left	Center	Right	Bottom	Average	STD
171	1.3127	1.4506	1.4646	1.4595	1.4507	1.4276	0.0645
172	1.4438	1.4530	1.4513	1.4522	1.4456	1.4492	0.0042
173	1.4427	1.4532	1.4528	1.4540	1.4531	1.4512	0.0048
174	1.4537	1.4552	1.4538	1.4505	1.4536	1.4534	0.0017
175	1.4517	1.4554	1.4544	1.4530	1.4545	1.4538	0.0015
176	1.4537	1.4553	1.4550	1.4544	1.4544	1.4546	0.0006
177	1.4480	1.4508	1.4550	1.4513	1.4542	1.4519	0.0028
178	1.4549	1.4563	1.4555	1.4551	1.4546	1.4553	0.0007
179	1.4560	1.4557	1.4562	1.4561	1.4555	1.4559	0.0003
180	1.4557	1.4565	1.4562	1.4558	1.4563	1.4561	0.0003
						1.4509	0.0081

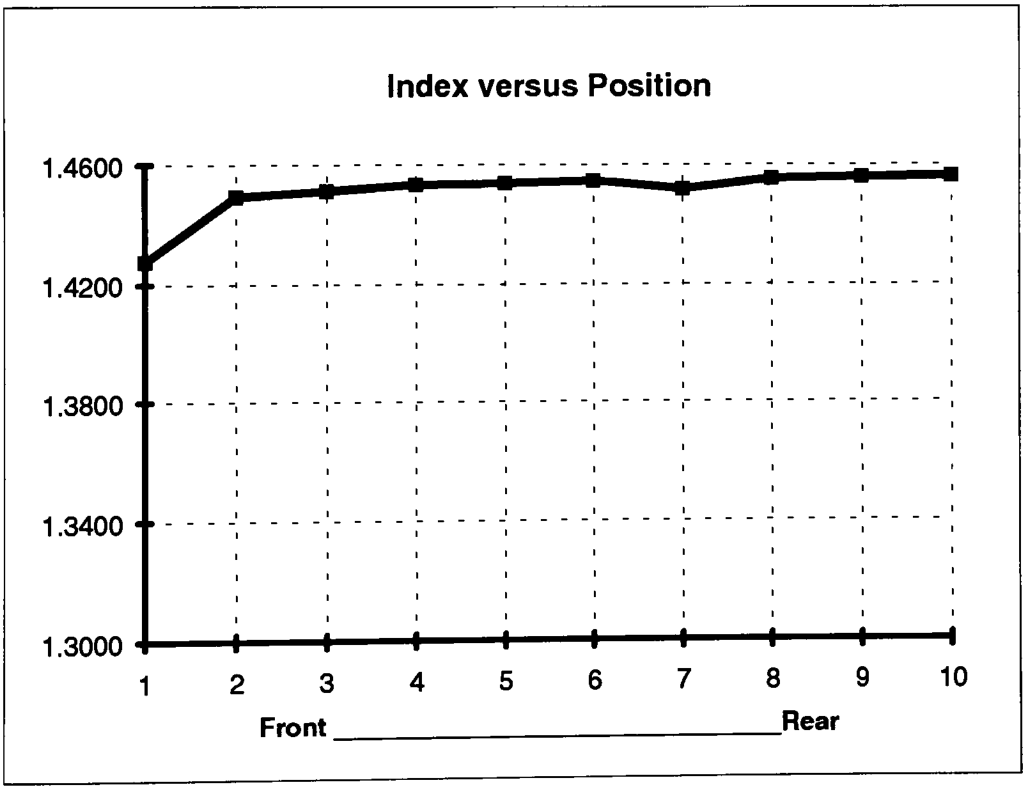

Appendix D :

Sloan Dektak IIA Plots

25

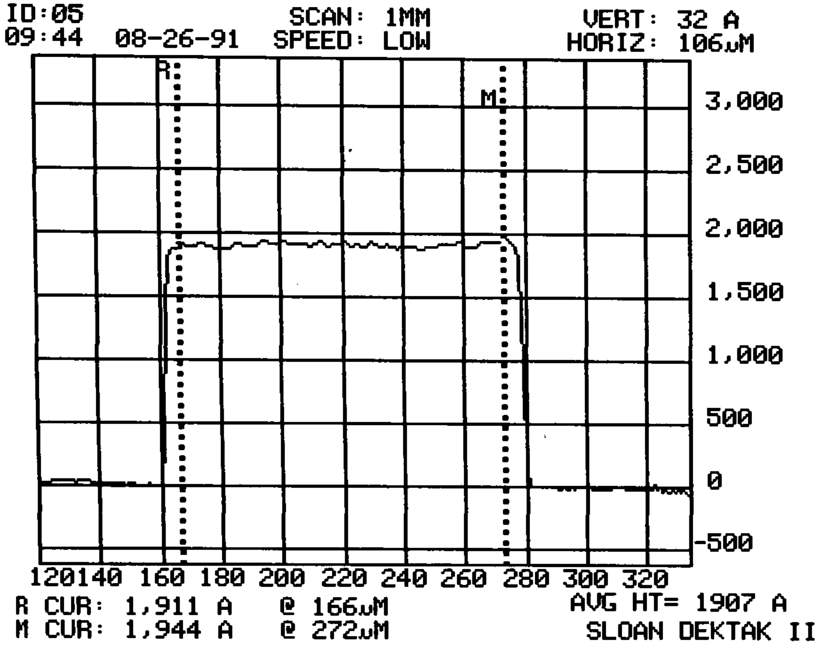
ID:05
09:44 08-26-91
SCAN: 1MM
SPEED: LOW
VERT: 32 A
HORIZ: 106µM
R
M
3,000
2,500
2,000
1,500
1,000
500
0
-500
120 140 160 180 200 220 240 260 280 300 320
R CUR: 1,911 A @ 166µM
M CUR: 1,944 A @ 272µM
AVG HT= 1907 A
SLOAN DEKTAK II

5

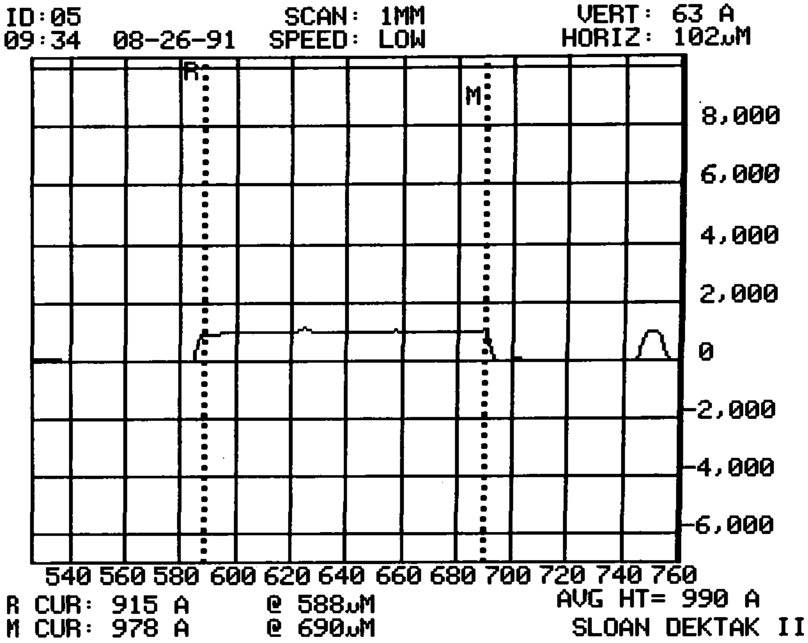
ID:05
09:34 08-26-91
SCAN: 1MM
SPEED: LOW
VERT: 63 A
HORIZ: 102µM
R
M
8,000
6,000
4,000
2,000
0
-2,000
-4,000
-6,000
540 560 580 600 620 640 660 680 700 720 740 760
R CUR: 915 A @ 588µM
M CUR: 978 A @ 690µM
AVG HT= 990 A
SLOAN DEKTAK II

35

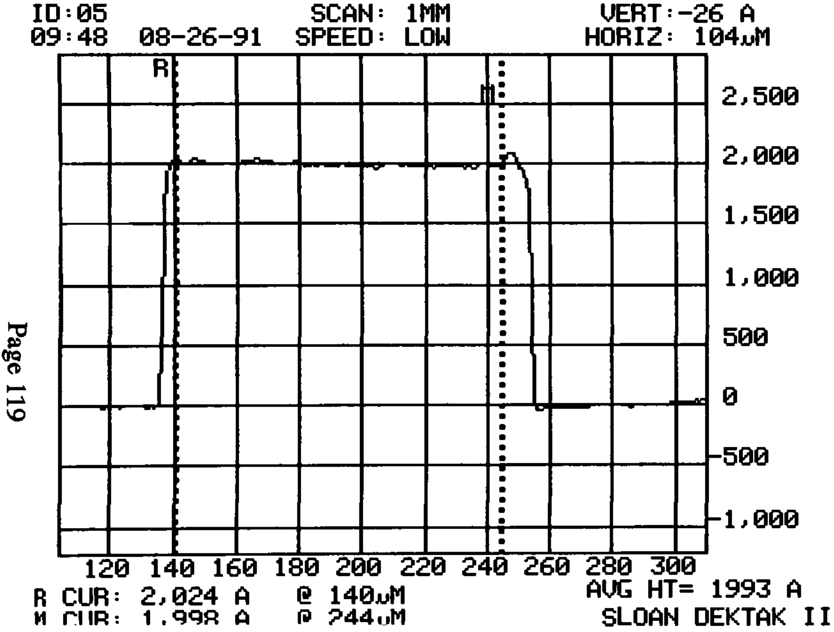
ID:05
09:48 08-26-91
SCAN: 1MM
SPEED: LOW
VERT: -26 A
HORIZ: 104µM
R
M
2,500
2,000
1,500
1,000
500
0
-500
-1,000
120 140 160 180 200 220 240 260 280 300
R CUR: 2,024 A @ 140µM
M CUR: 1,998 A @ 244µM
AVG HT= 1993 A
SLOAN DEKTAK II

15

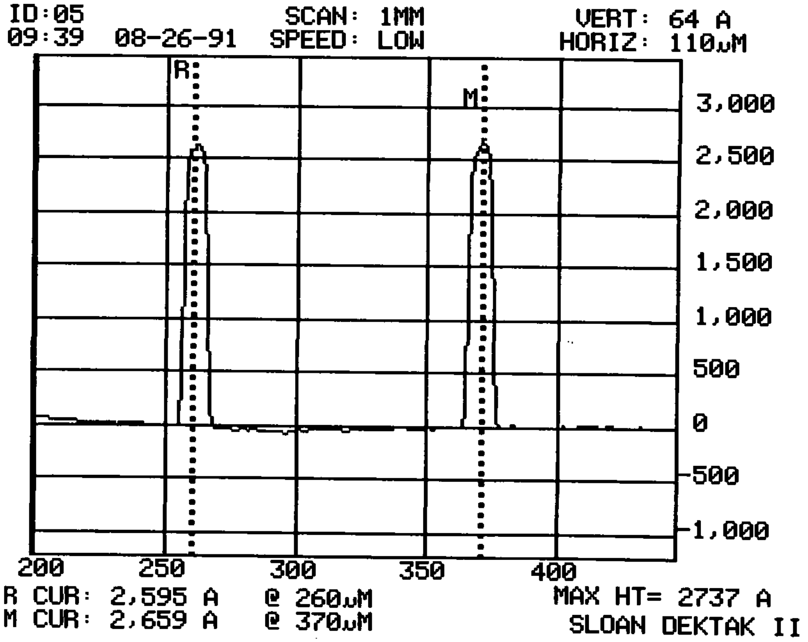
ID:05
09:39 08-26-91
SCAN: 1MM
SPEED: LOW
VERT: 64 A
HORIZ: 110µM
R
M
3,000
2,500
2,000
1,500
1,000
500
0
-500
-1,000
200 250 300 350 400
R CUR: 2,595 A @ 260µM
M CUR: 2,659 A @ 370µM
MAX HT= 2737 A
SLOAN DEKTAK II

45

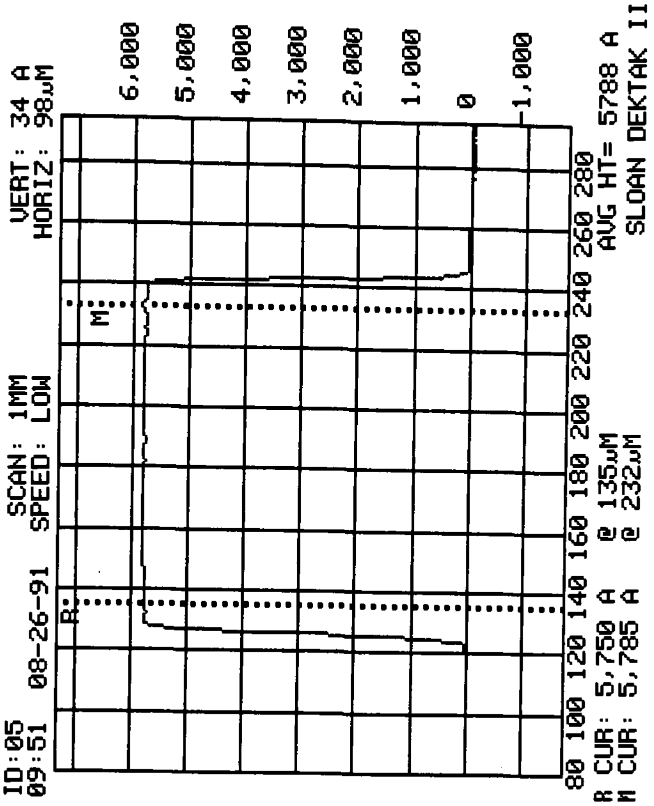

ID:05 08-26-91
09:51
SCAN: 1MM
SPEED: LOW
VERT: 34 A
HORIZ: 98uM
6,000
5,000
4,000
3,000
2,000
1,000
0
-1,000
R
M
80 100 120 140 160 180 200 220 240 260 280
R CUR: 5,750 A @ 135uM
M CUR: 5,785 A @ 232uM
AVG HT= 5788 A
SLOAN DEKTAK II

55

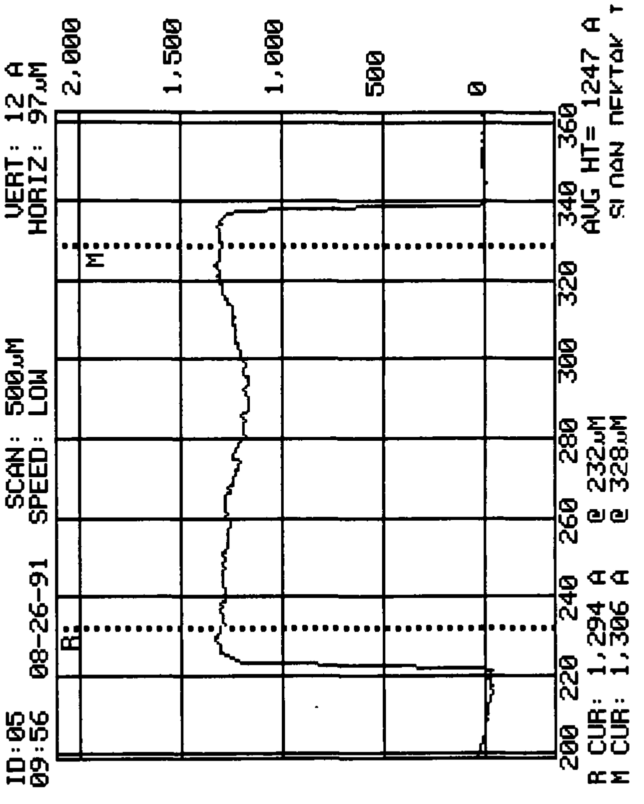

ID:05 08-26-91
09:56
SCAN: 500uM
SPEED: LOW
VERT: 12 A
HORIZ: 97uM
2,000
1,500
1,000
500
0
R
M
200 220 240 260 280 300 320 340 360
R CUR: 1,294 A @ 232uM
M CUR: 1,306 A @ 328uM
AVG HT= 1247 A
SLOAN DEKTAK II

5

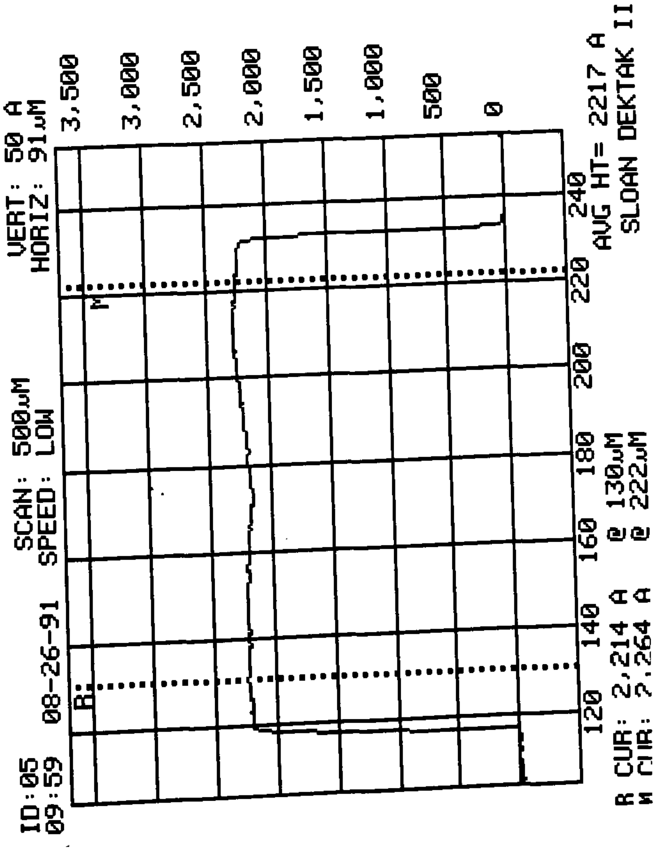

ID:05 08-26-91
09:59
SCAN: 500uM
SPEED: LOW
VERT: 50 A
HORIZ: 91uM
3,500
3,000
2,500
2,000
1,500
1,000
500
0
R
M
120 140 160 180 200 220 240
R CUR: 2,214 A @ 130uM
M CUR: 2,264 A @ 222uM
AVG HT= 2217 A
SLOAN DEKTAK II

75

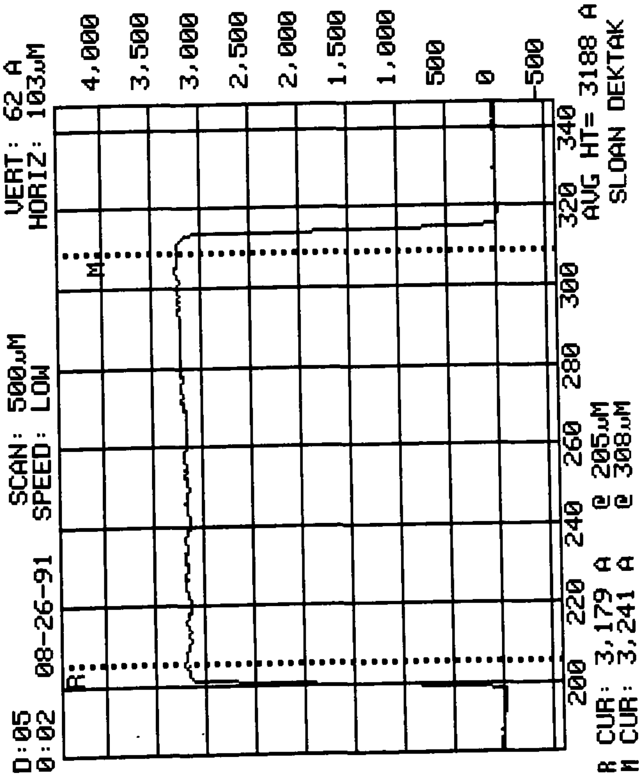

ID:05 08-26-91
10:02
SCAN: 500uM
SPEED: LOW
VERT: 62 A
HORIZ: 103uM
4,000
3,500
3,000
2,500
2,000
1,500
1,000
500
0
-500
R
M
200 220 240 260 280 300 320 340
R CUR: 3,179 A @ 205uM
M CUR: 3,241 A @ 308uM
AVG HT= 3188 A
SLOAN DEKTAK II

85

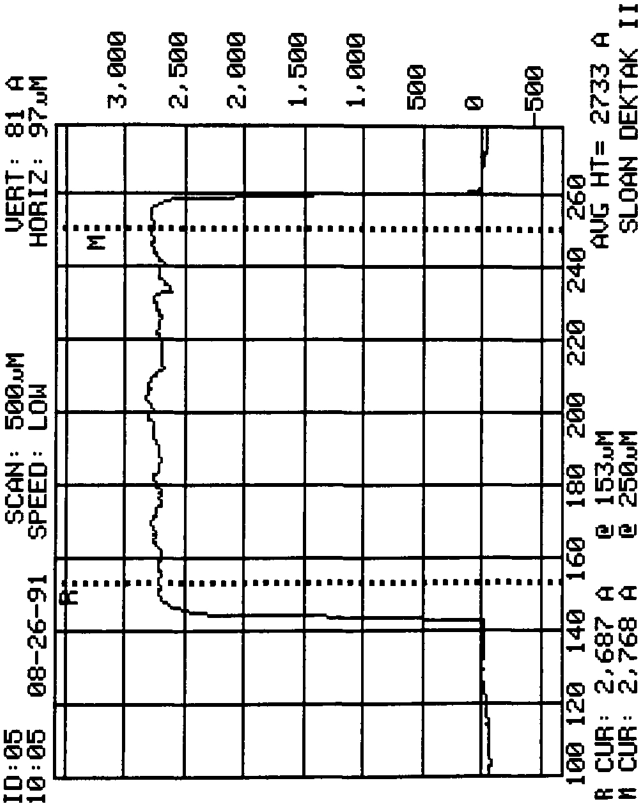
ID:05 08-26-91 SCAN: 500µM VERT: 81 A
10:05 SPEED: LOW HORIZ: 97µM
3,000
2,500
2,000
1,500
1,000
500
0
-500
R:
M:
100 120 140 160 180 200 220 240 260
R CUR: 2,687 A @ 153µM
M CUR: 2,768 A @ 250µM
AVG HT= 2733 A
SLOAN DEKTAK II

95

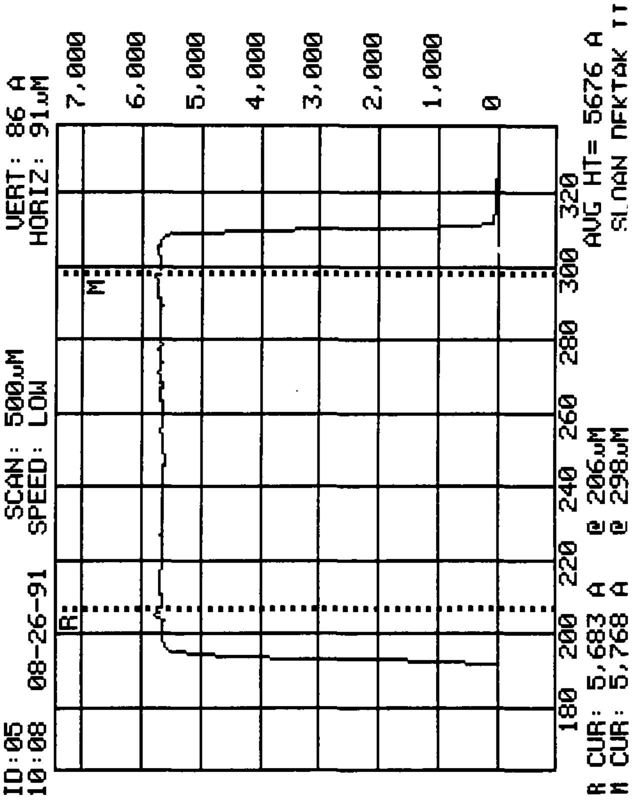
ID:05 08-26-91 SCAN: 500µM VERT: 86 A
10:08 SPEED: LOW HORIZ: 91µM
7,000
6,000
5,000
4,000
3,000
2,000
1,000
0
R:
M:
180 200 220 240 260 280 300 320
R CUR: 5,683 A @ 206µM
M CUR: 5,768 A @ 298µM
AVG HT= 5676 A
SLOAN DEKTAK II

Appendix E :

FTIR Spectra
From Perkin Elmer
Model 1750

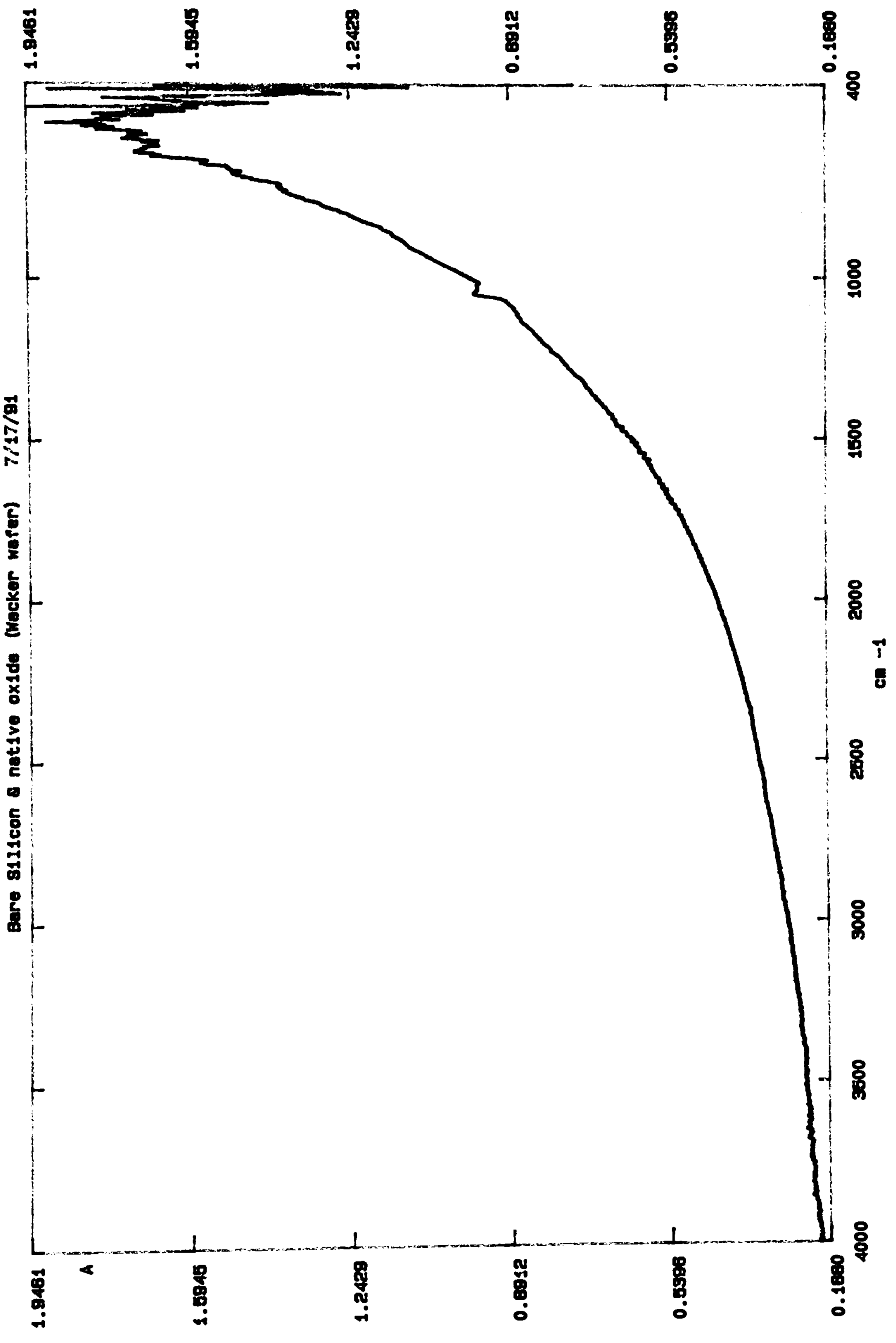
Bare Silicon & native oxide (Wacker wafer)   7/17/91
A
1.9461
1.5945
1.2429
0.8912
0.5396
0.1880
4000
3500
3000
2500
2000
1500
1000
400
cm -1

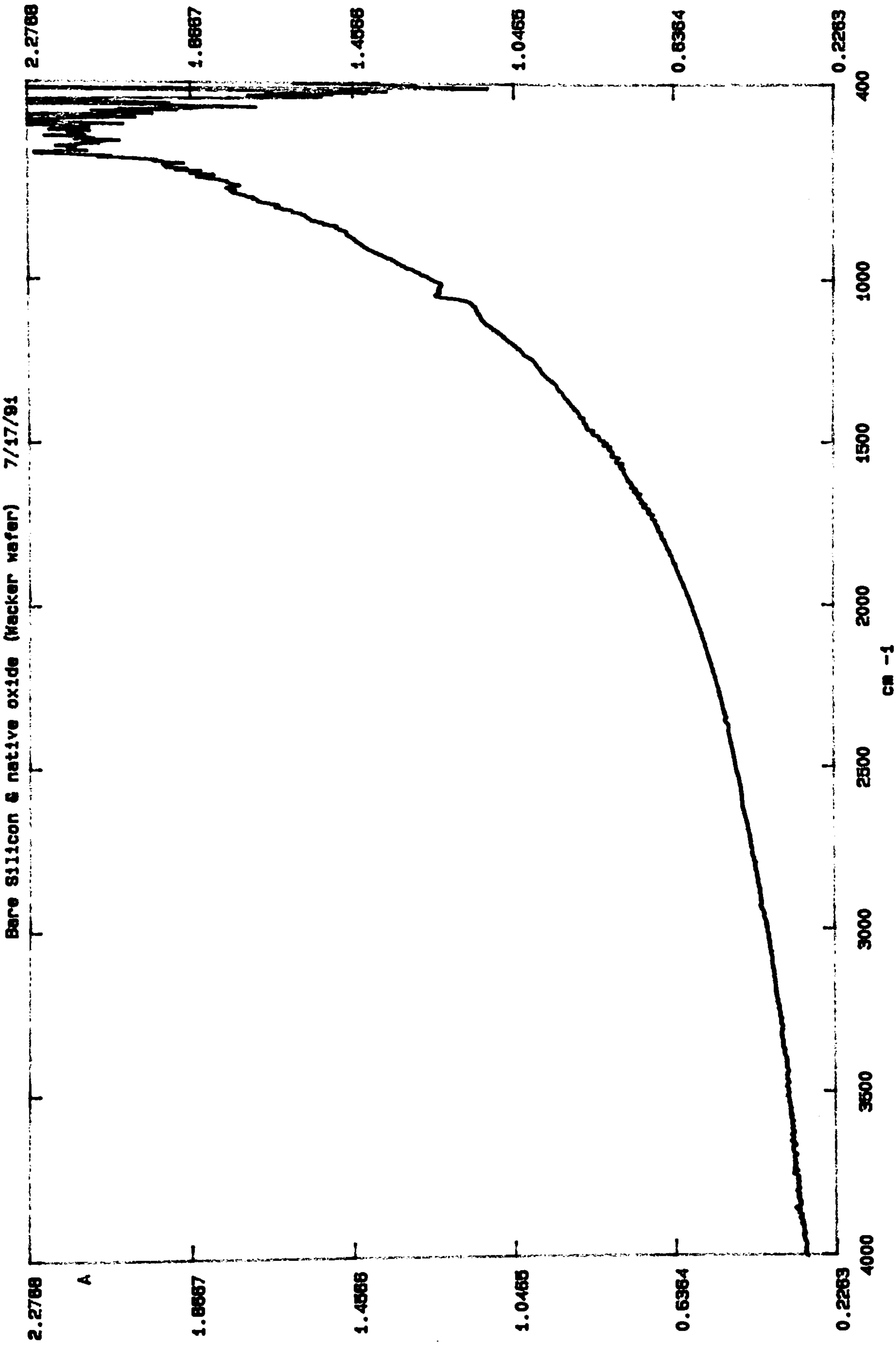

Bare Silicon & native oxide (Wacker wafer) 7/17/91

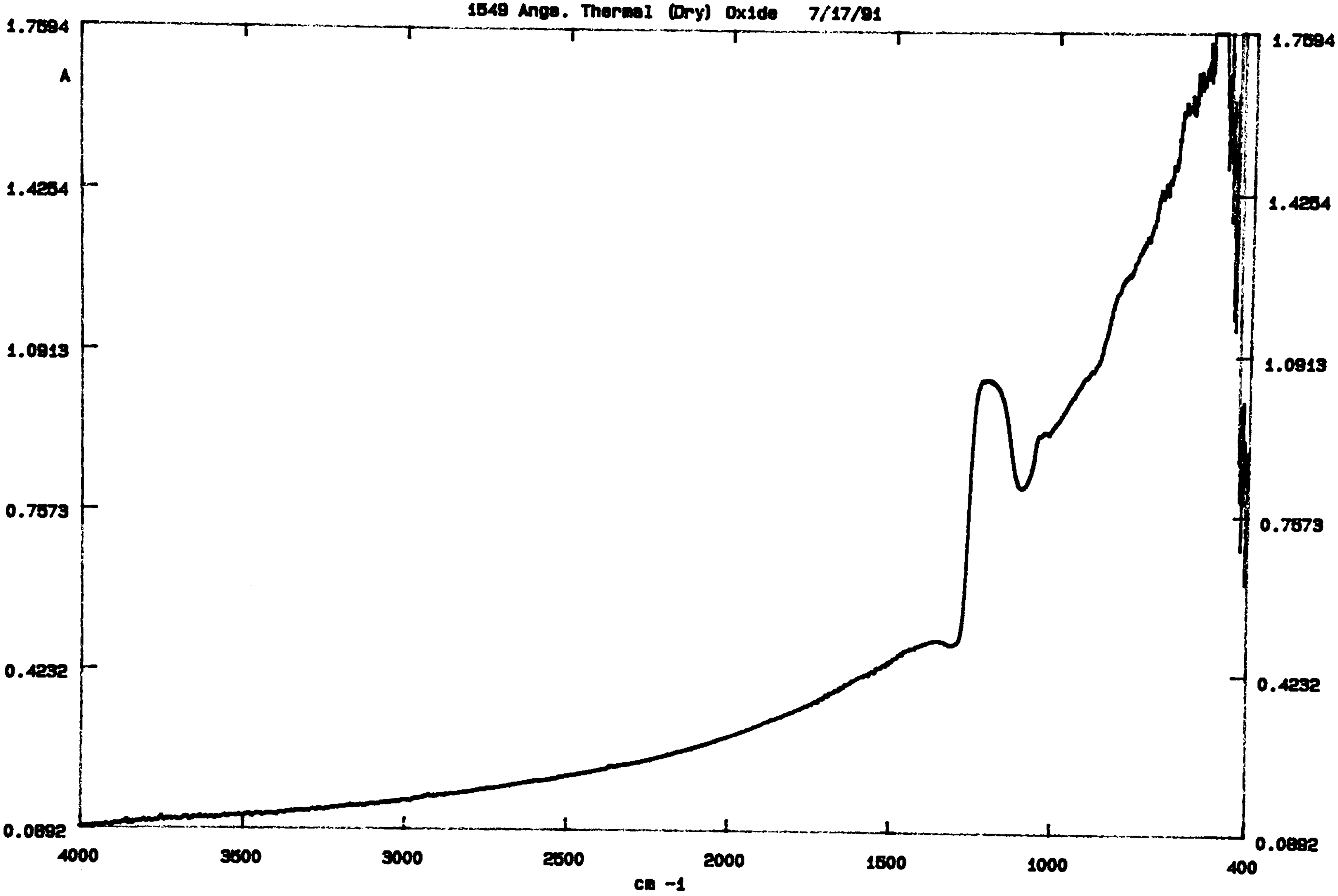
1549 Angs. Thermal (Dry) Oxide 7/17/91
A
1.7594
1.4254
1.0913
0.7573
0.4232
0.0892
4000
3500
3000
2500
2000
1500
1000
400
cm -1

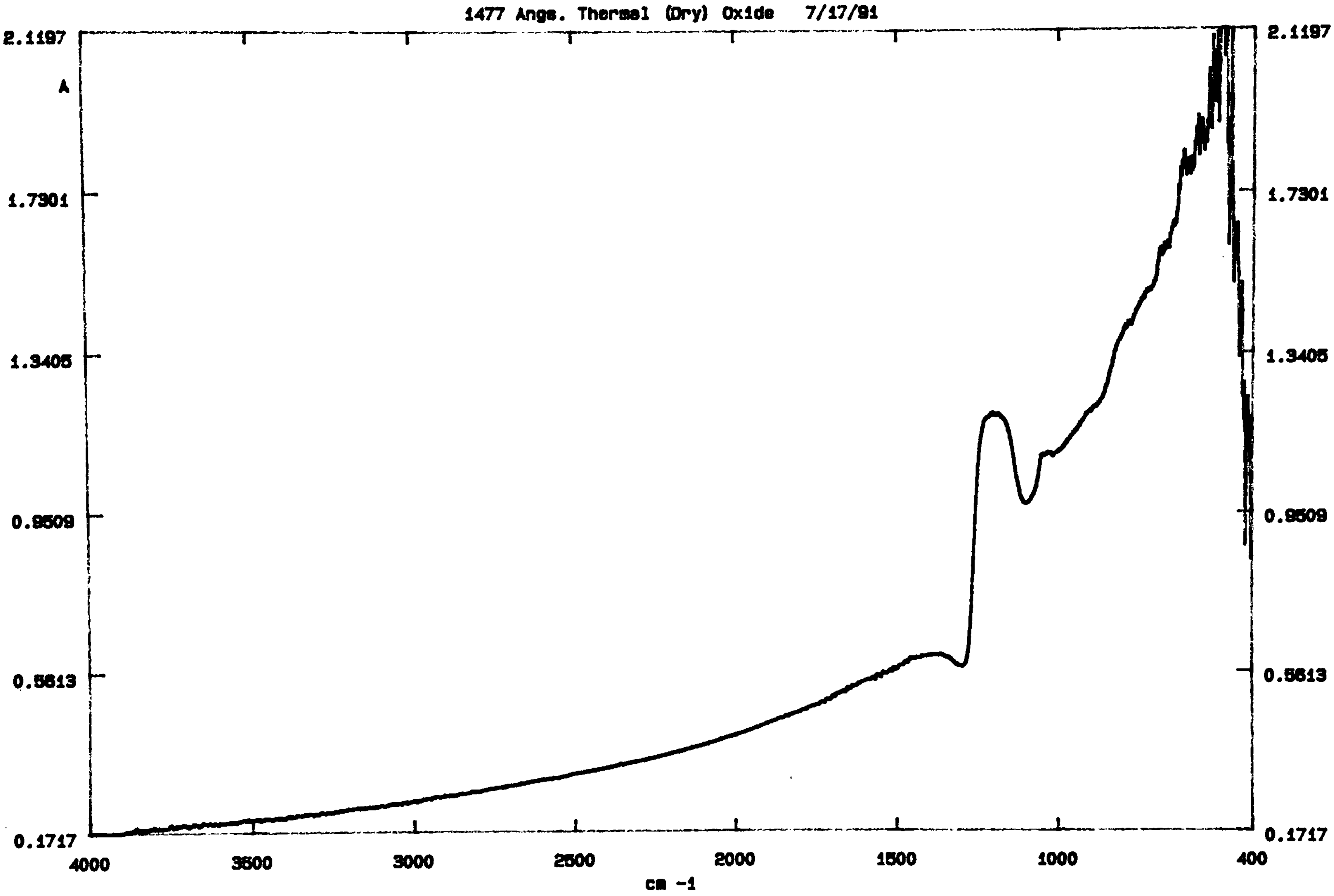
1477 Angs. Thermal (Dry) Oxide 7/17/91

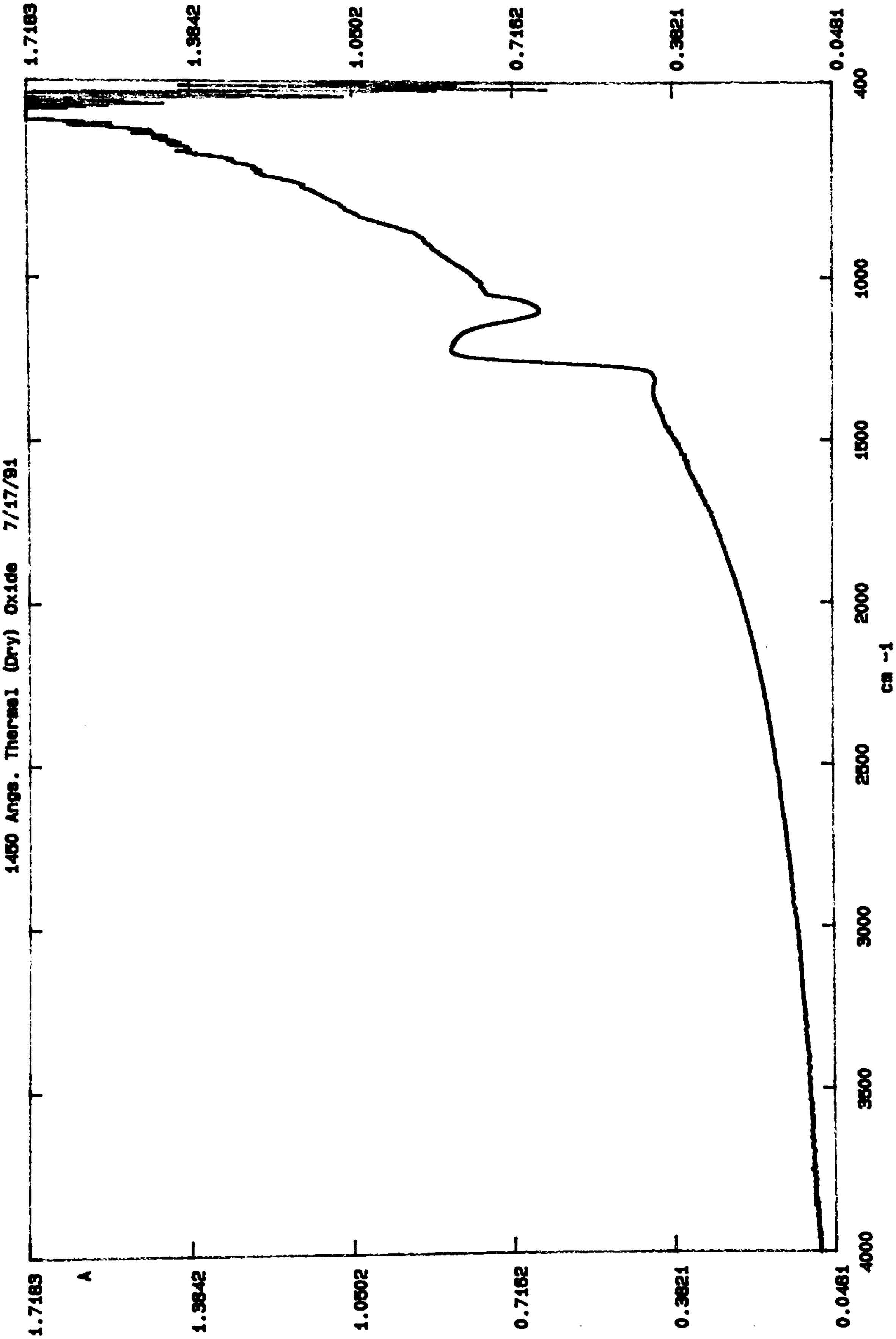
1450 Angs. Thermal (Dry) Oxide 7/17/91
A
1.7183
1.3842
1.0502
0.7162
0.3821
0.0481
4000
3500
3000
2500
2000
1500
1000
400
cm -1

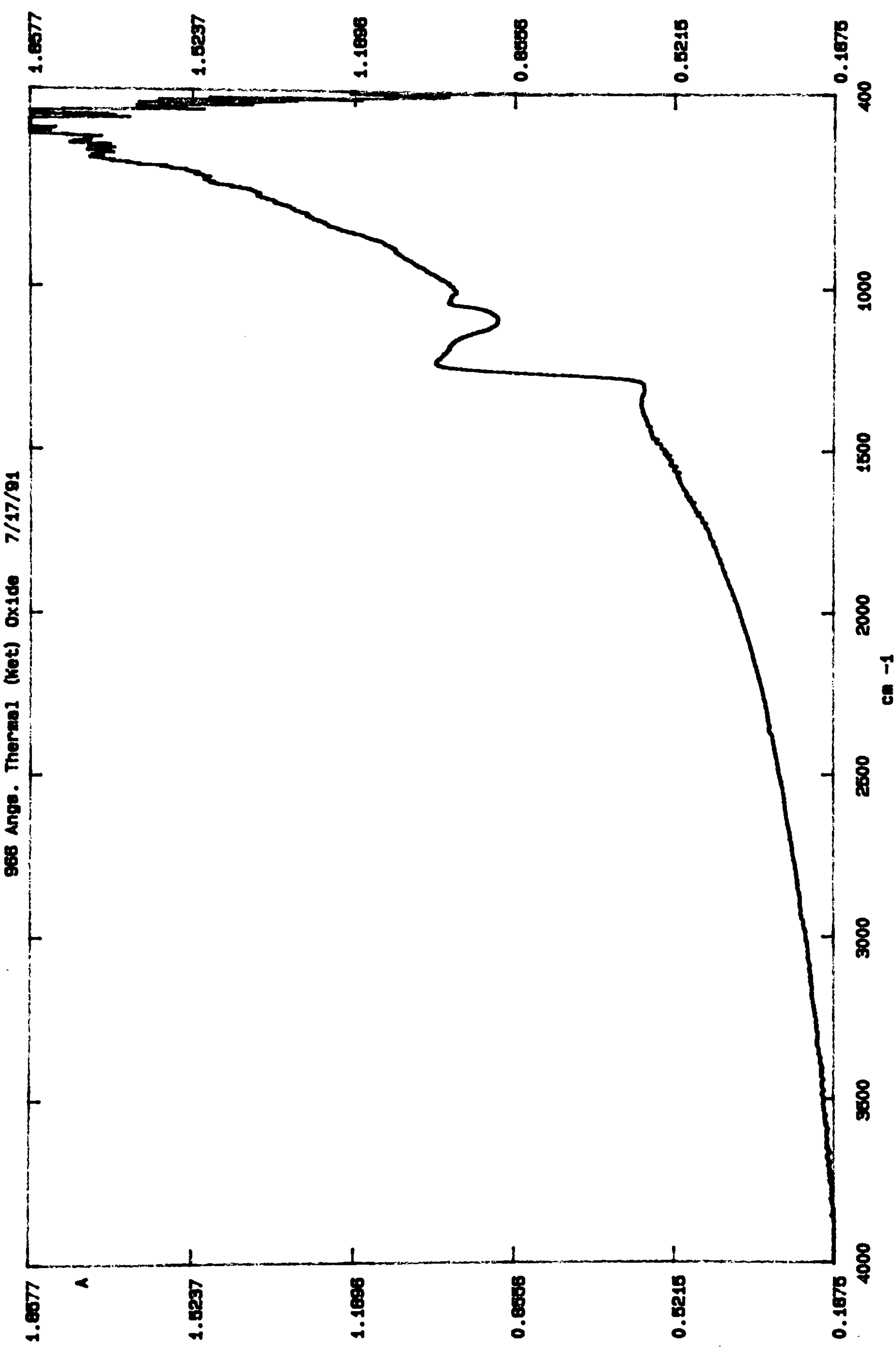
966 Angs. Thermal (Wet) Oxide 7/17/91

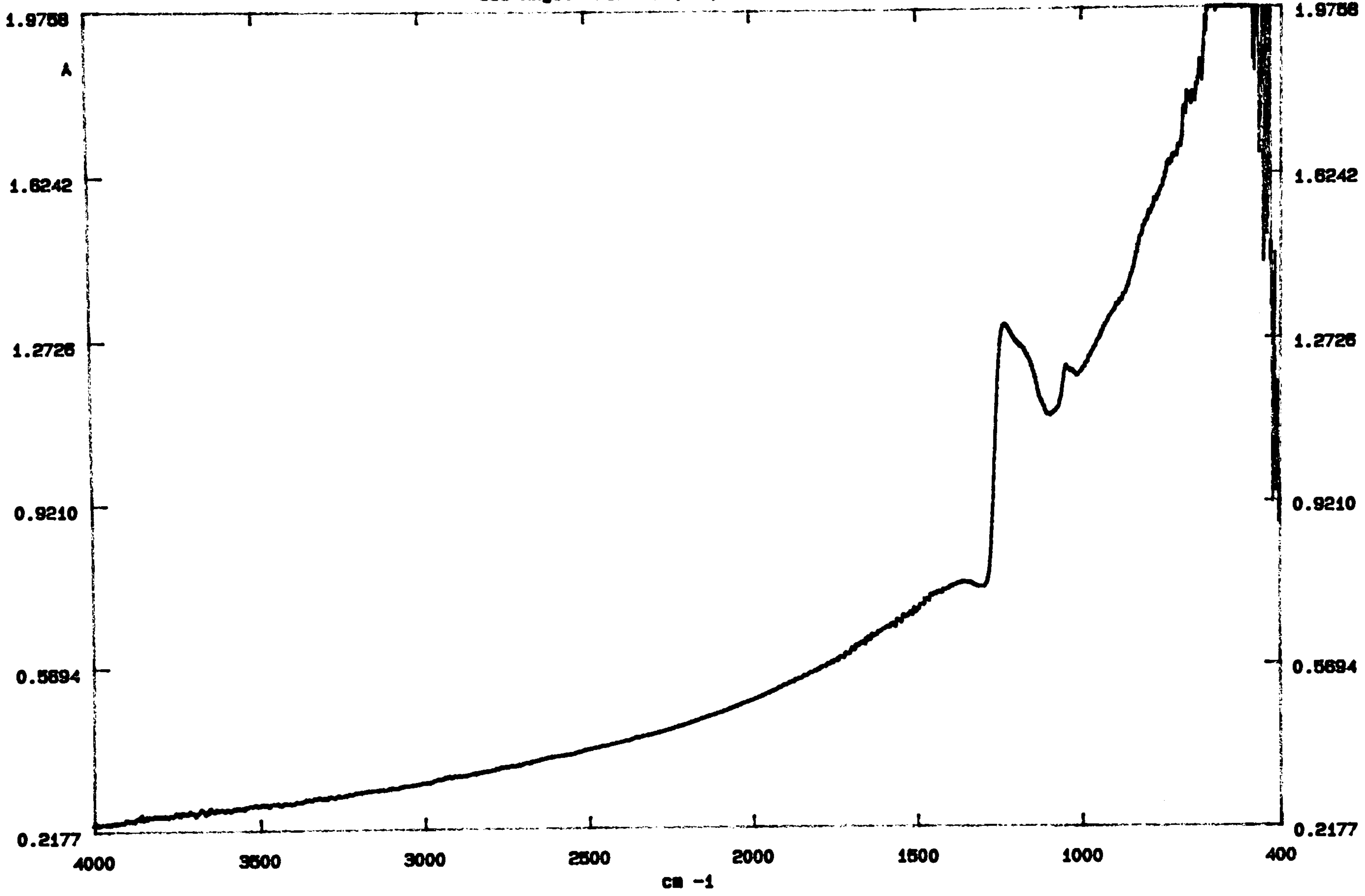

959 Angs. Thermal (Wet) Oxide 7/17/91

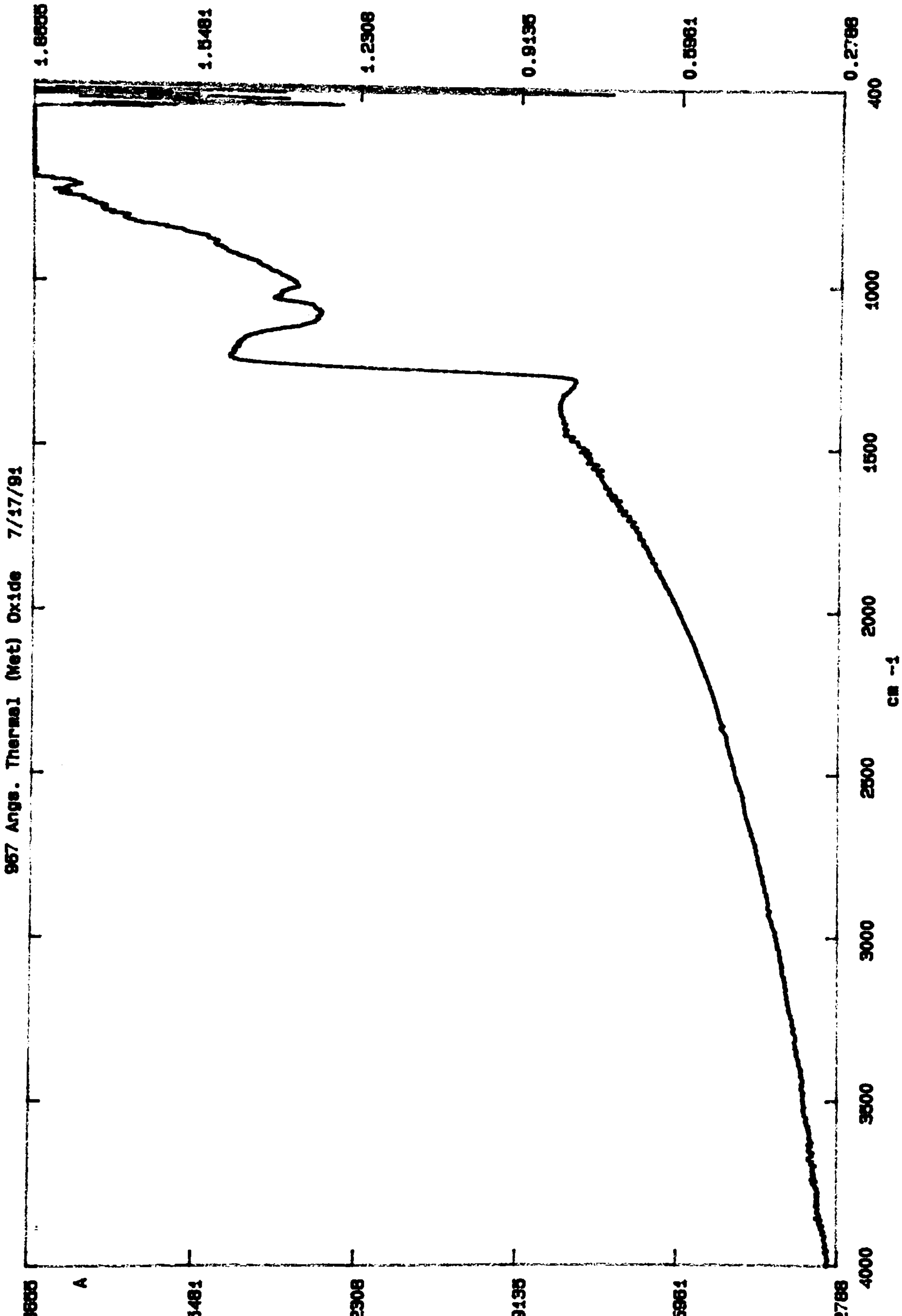

967 Angs. Thermal (Wet) Oxide 7/17/91

LTO Wafer 7, 400C, 30min, 1.8 Flow Ratio

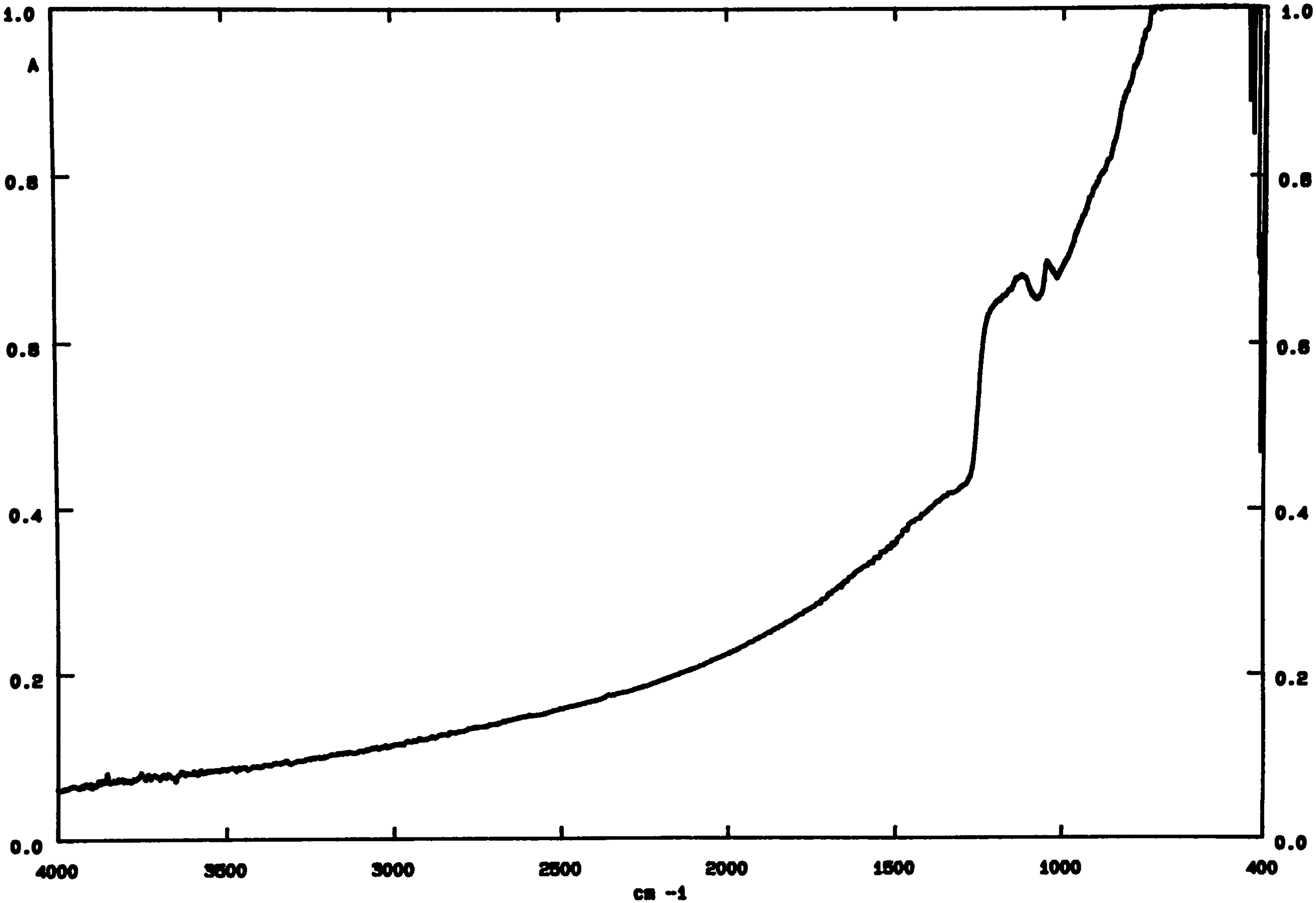

SAMPLE:
SCANS: 10
RESOLUTION:

DATE: 91/06/28
TIME: 13:13.17

1.5

LTO Wafer 17, 450C, 60min, 1.8 Flow Ratio

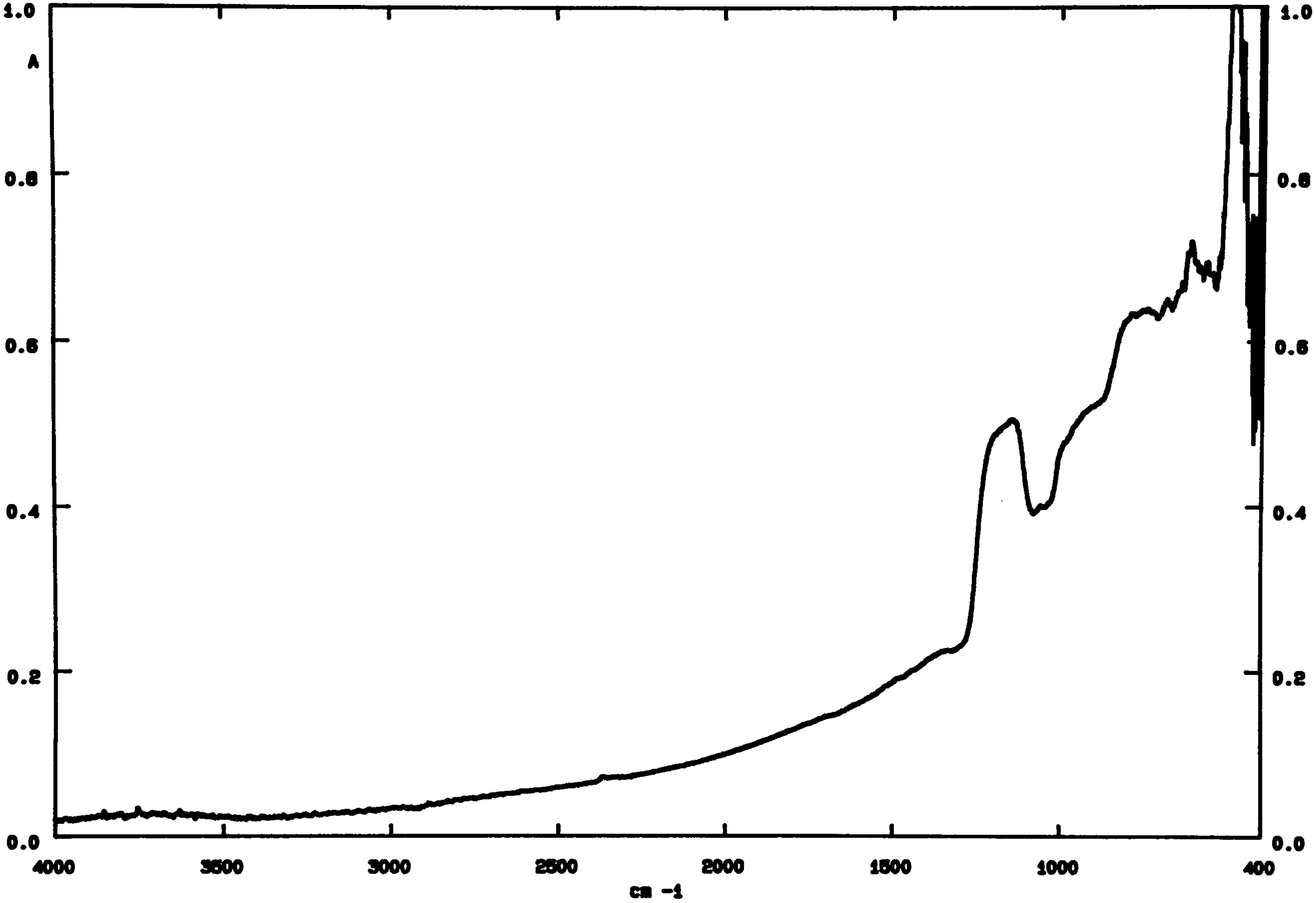

SAMPLE:
SCANS: 10
RESOLUTION:

DATE: 91/08/28
TIME: 13:36.20

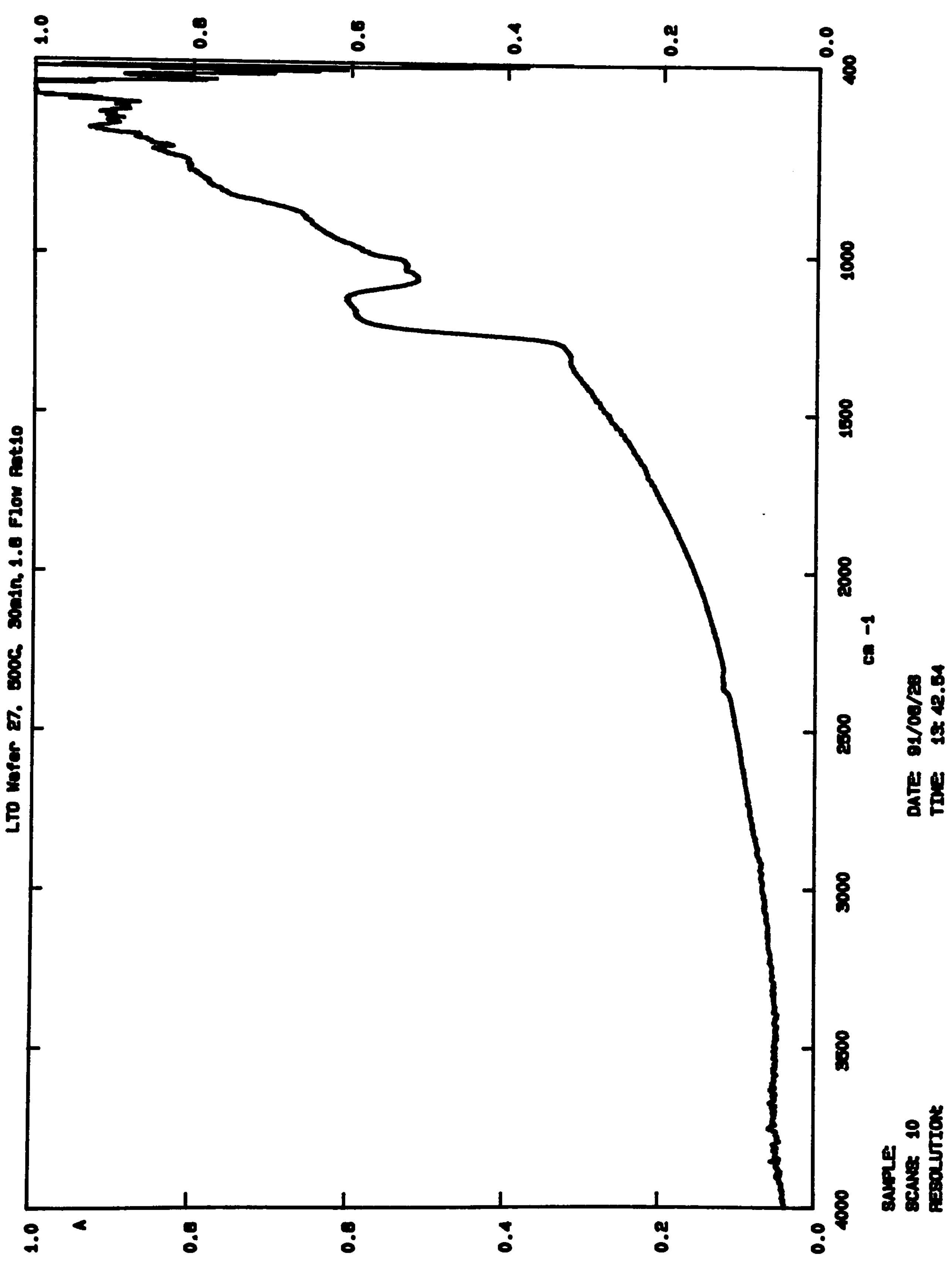
LTD Wafer 27, 500C, 30min, 1.8 Flow Ratio
A
1.0
0.8
0.6
0.4
0.2
0.0
4000
3500
3000
2500
2000
1500
1000
400
cm -1
SAMPLE:
SCANS: 10
RESOLUTION:
DATE: 91/08/28
TIME: 13:42.54

LTO Wafer 37, 400C, 90min, 1.2 Flow Ratio

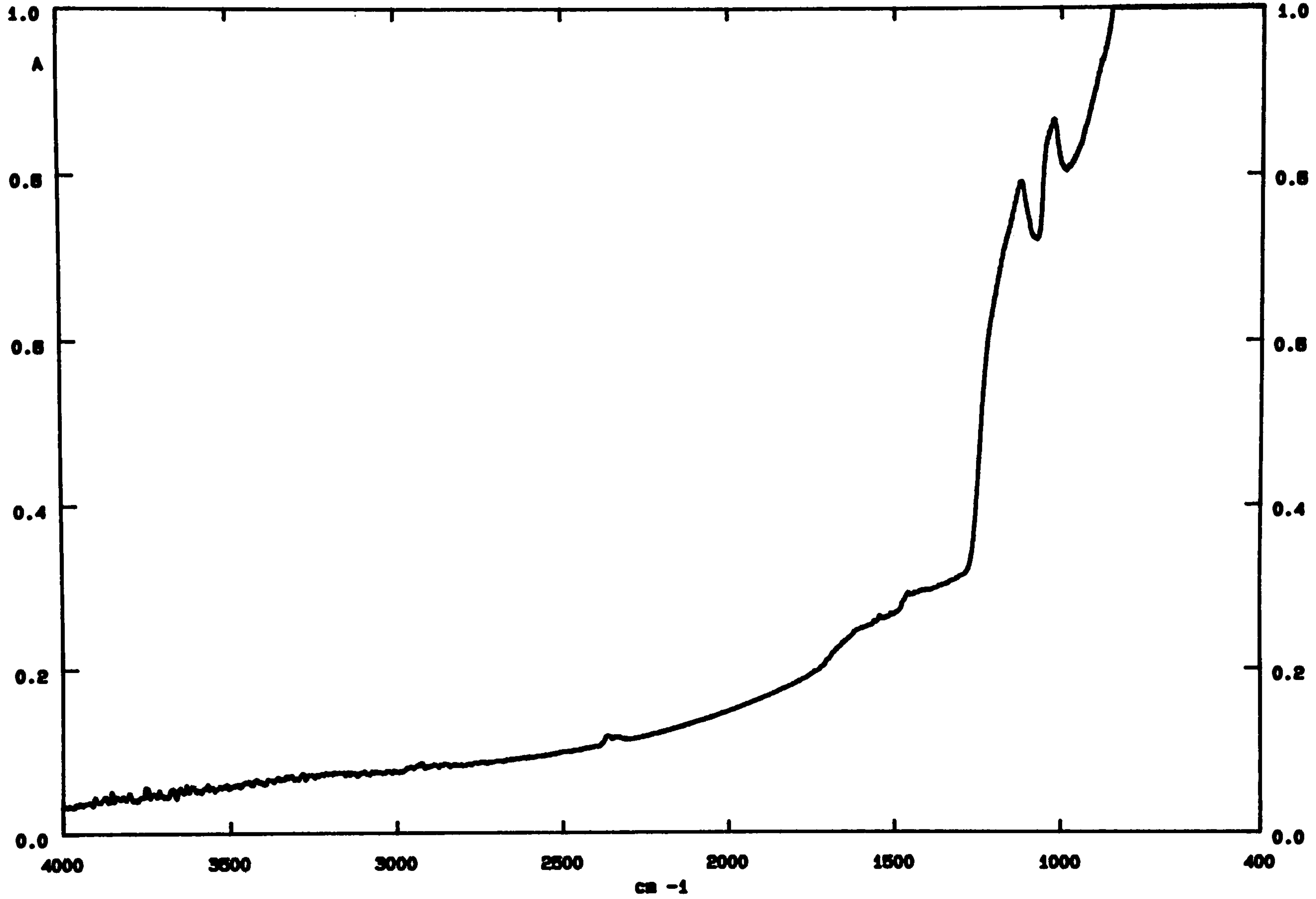

SAMPLE:
SCANS: 10
RESOLUTION:

DATE: 91/08/28
TIME: 13:59.10

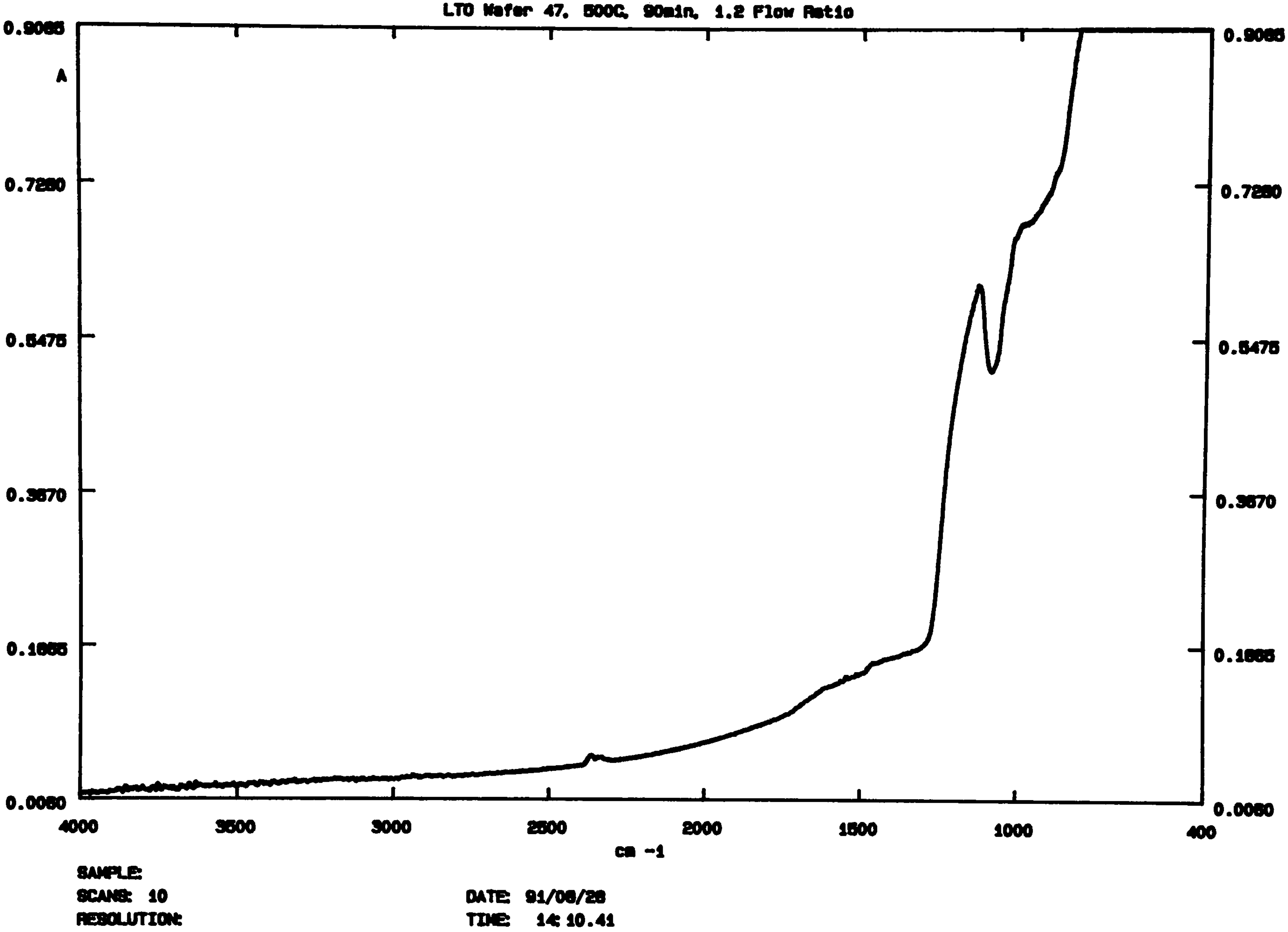
LTO Wafer 47, 500C, 90min, 1.2 Flow Ratio
A
0.9085
0.7280
0.5475
0.3670
0.1865
0.0060
4000
3500
3000
2500
2000
1500
1000
400
cm -1
SAMPLE:
SCANS: 10
RESOLUTION:
DATE: 91/08/28
TIME: 14:10.41

LTO Wafer 57. 400C, 30min, 1.2 Flow Ratio

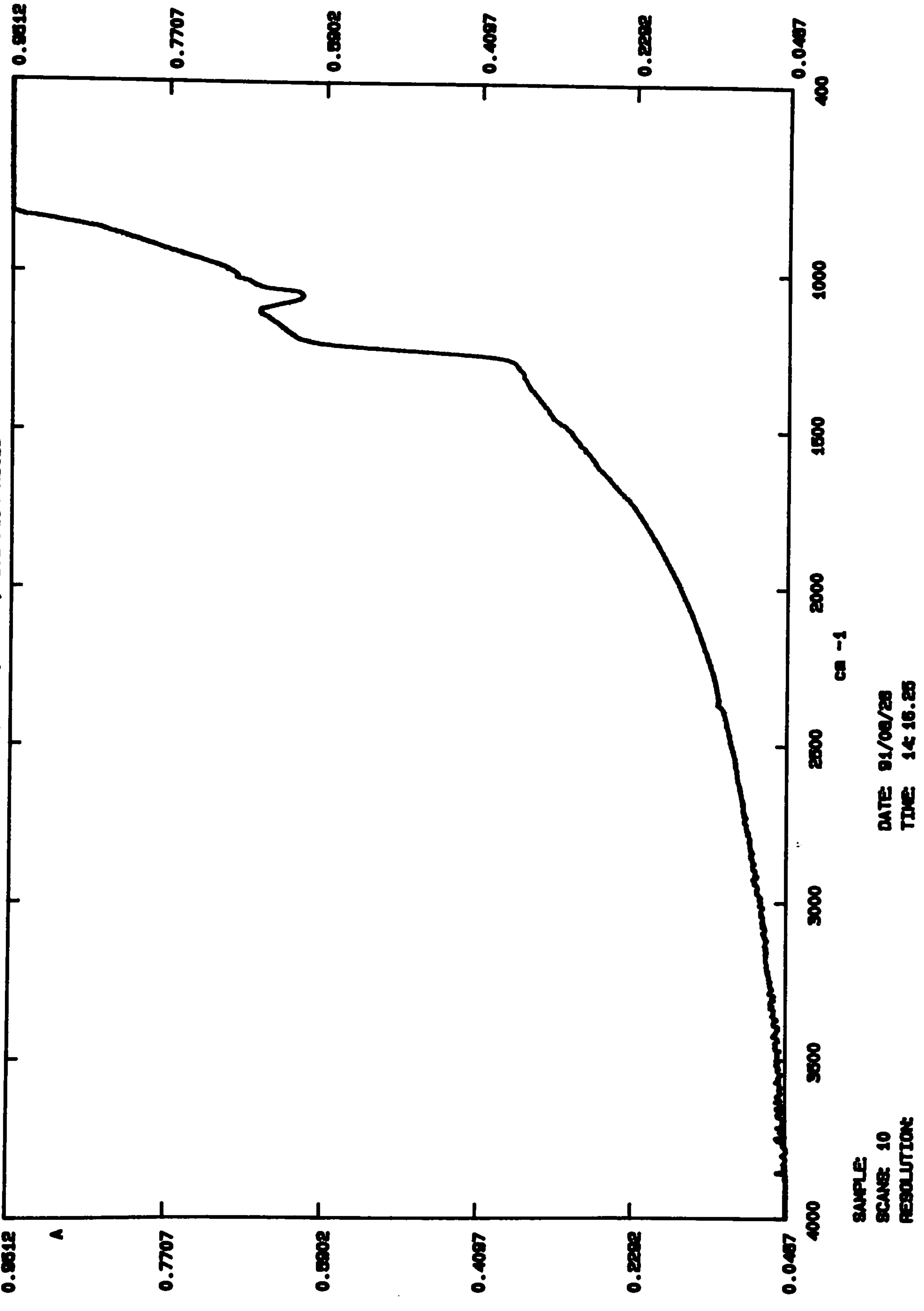

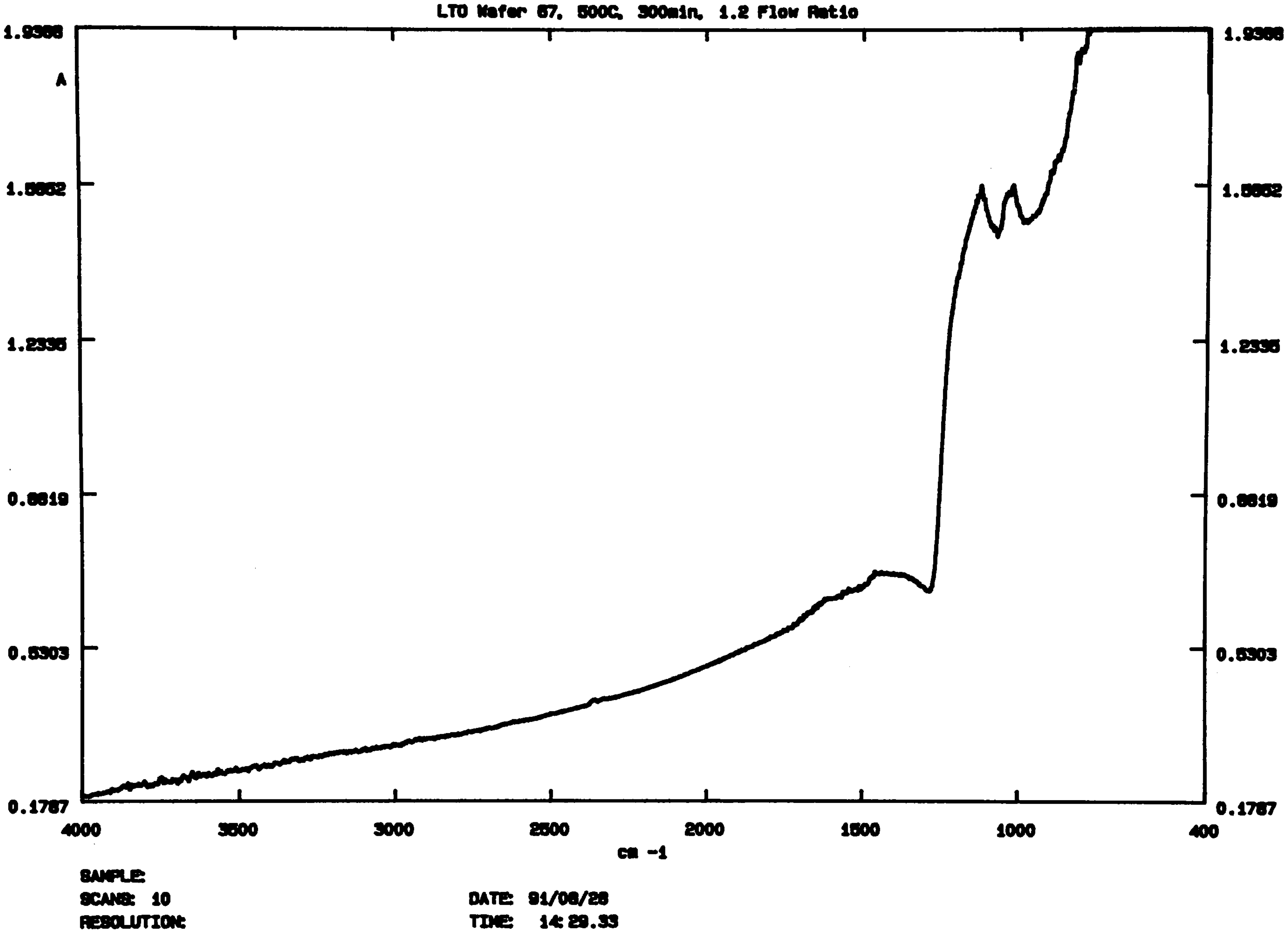
LTO Wafer 67, 500C, 300min, 1.2 Flow Ratio
A
1.9368
1.5852
1.2335
0.8819
0.5303
0.1787
4000
3500
3000
2500
2000
1500
1000
400
cm -1
SAMPLE:
SCANS: 10
RESOLUTION:
DATE: 91/06/28
TIME: 14:29.33

LTO Wafer 77, 450C, 60min, 1.5 Flow Ratio

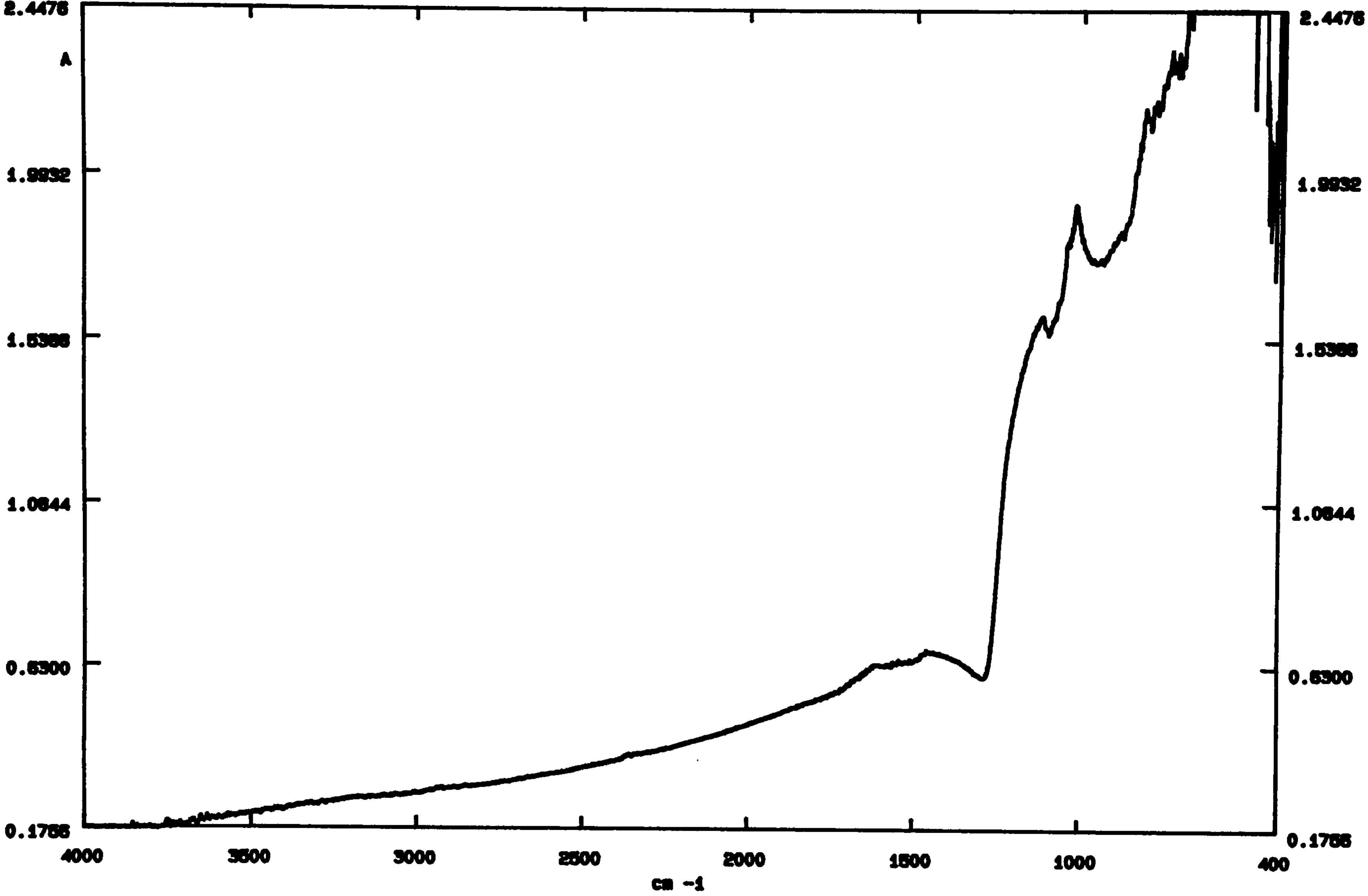

SAMPLE:
SCANS: 10
RESOLUTION:

DATE: 91/06/28
TIME: 14:36.57

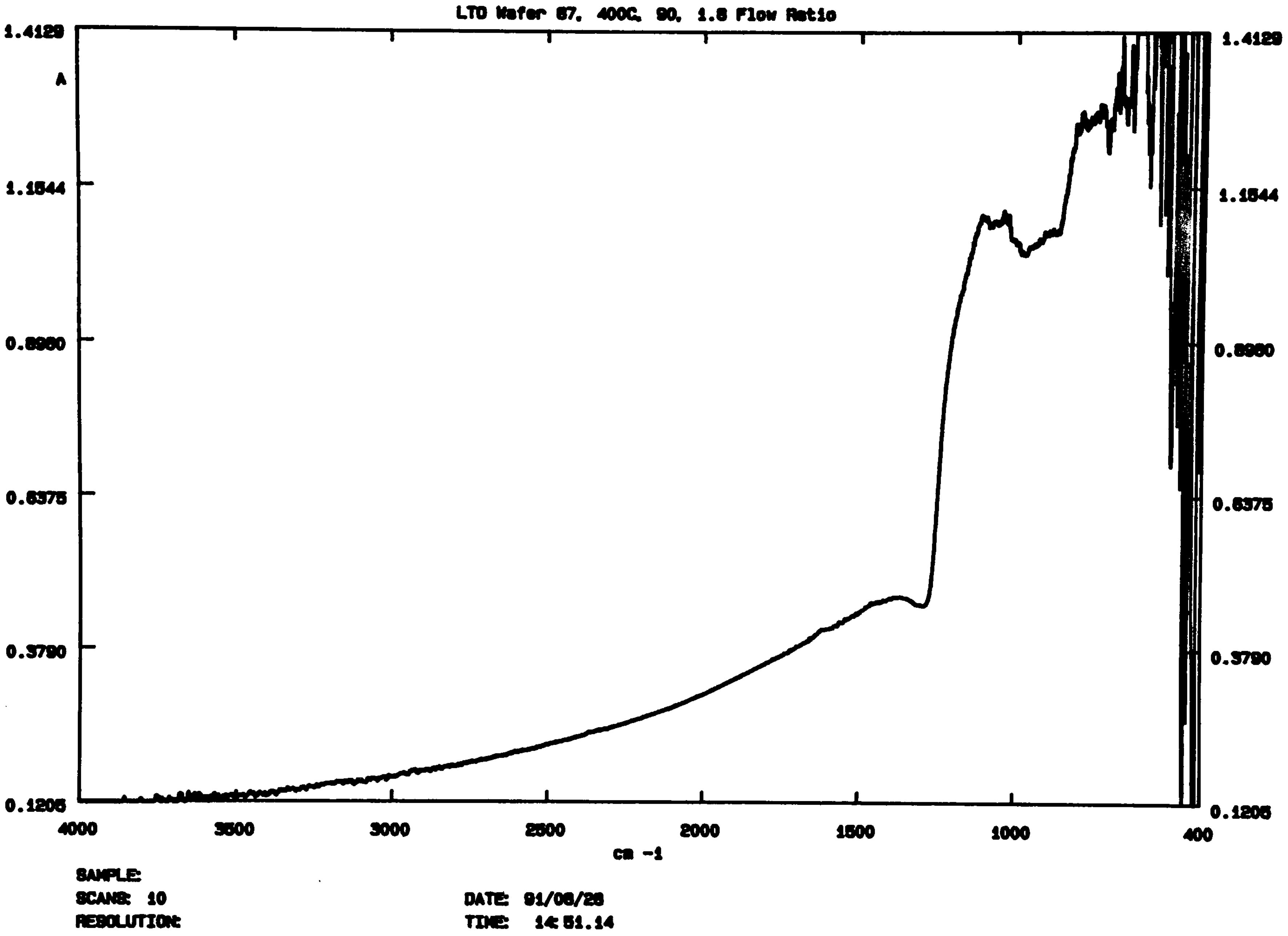
LTO Wafer 87, 400C, 90, 1.8 Flow Ratio
A
1.4129
1.1544
0.8960
0.6375
0.3790
0.1205
4000
3500
3000
2500
2000
1500
1000
400
cm -1
SAMPLE:
SCANS: 10
RESOLUTION:
DATE: 91/06/28
TIME: 14:51.14

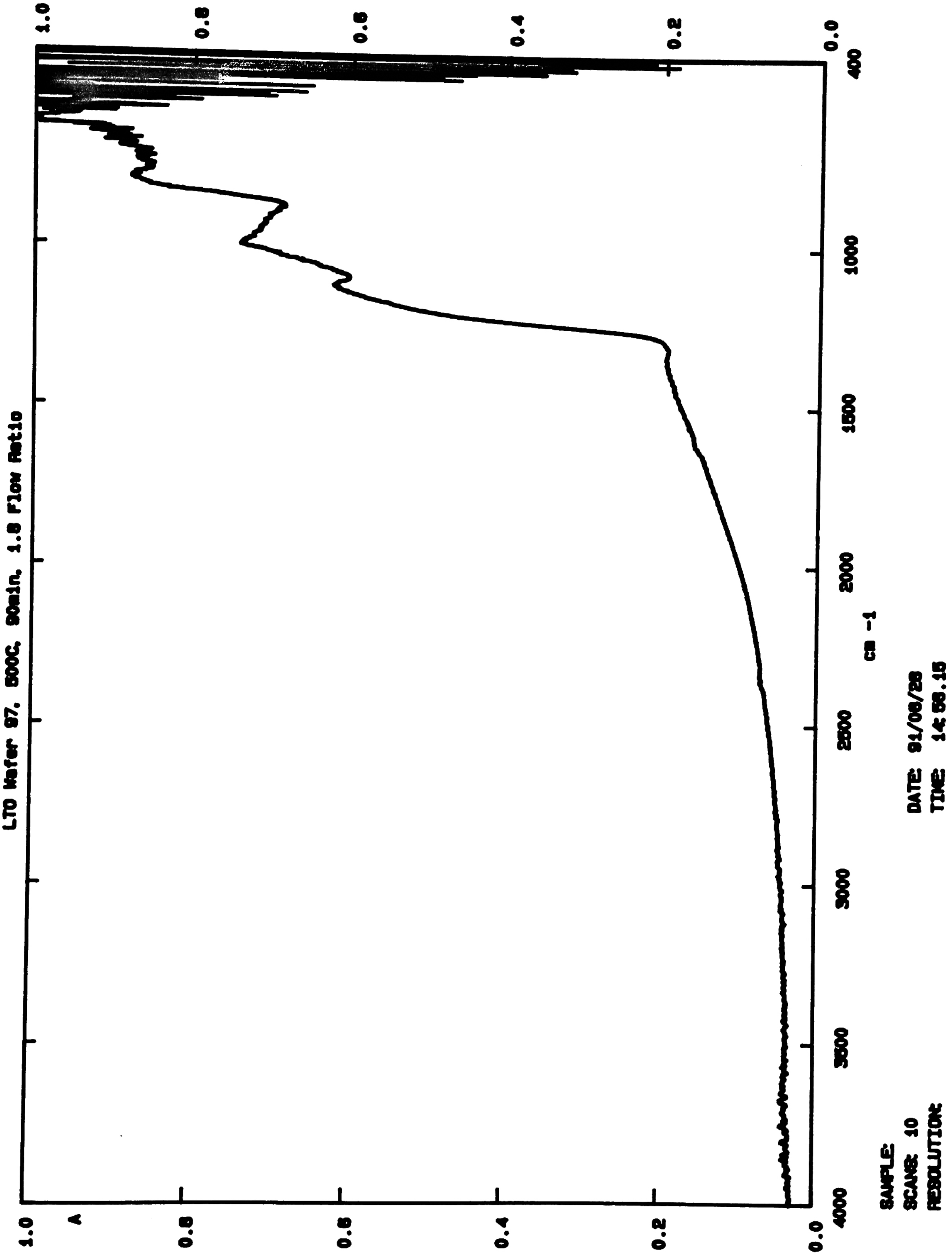
LTO Wafer 97, 500C, 90min, 1.8 Flow Ratio
A
1.0
0.8
0.6
0.4
0.2
0.0
4000
3500
3000
2500
2000
1500
1000
400
cm -1
SAMPLE:
SCANS: 10
RESOLUTION:
DATE: 91/08/28
TIME: 14:58.15

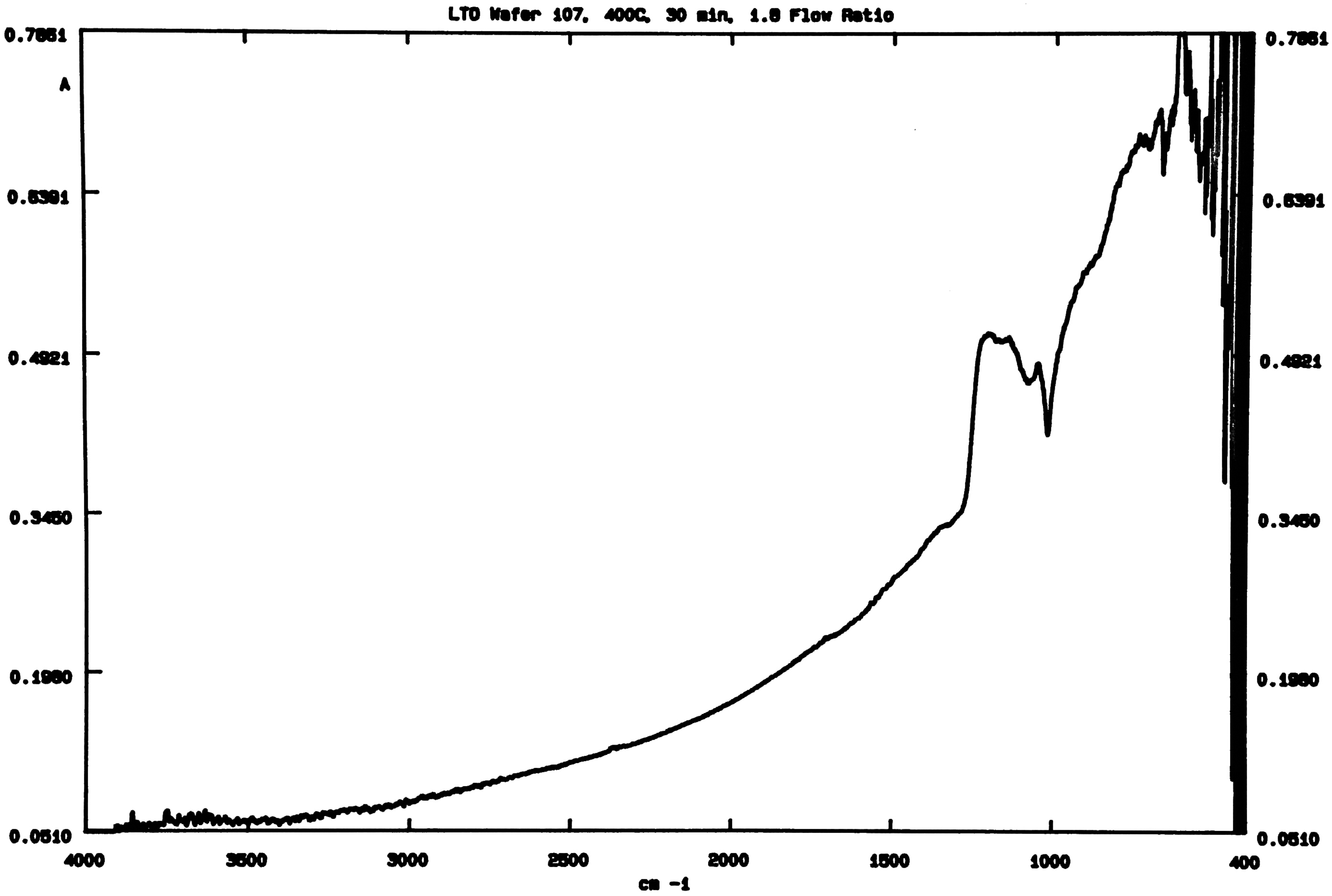

SAMPLE:
SCANS: 10
RESOLUTION:

DATE: 91/08/28
TIME: 15:08.49

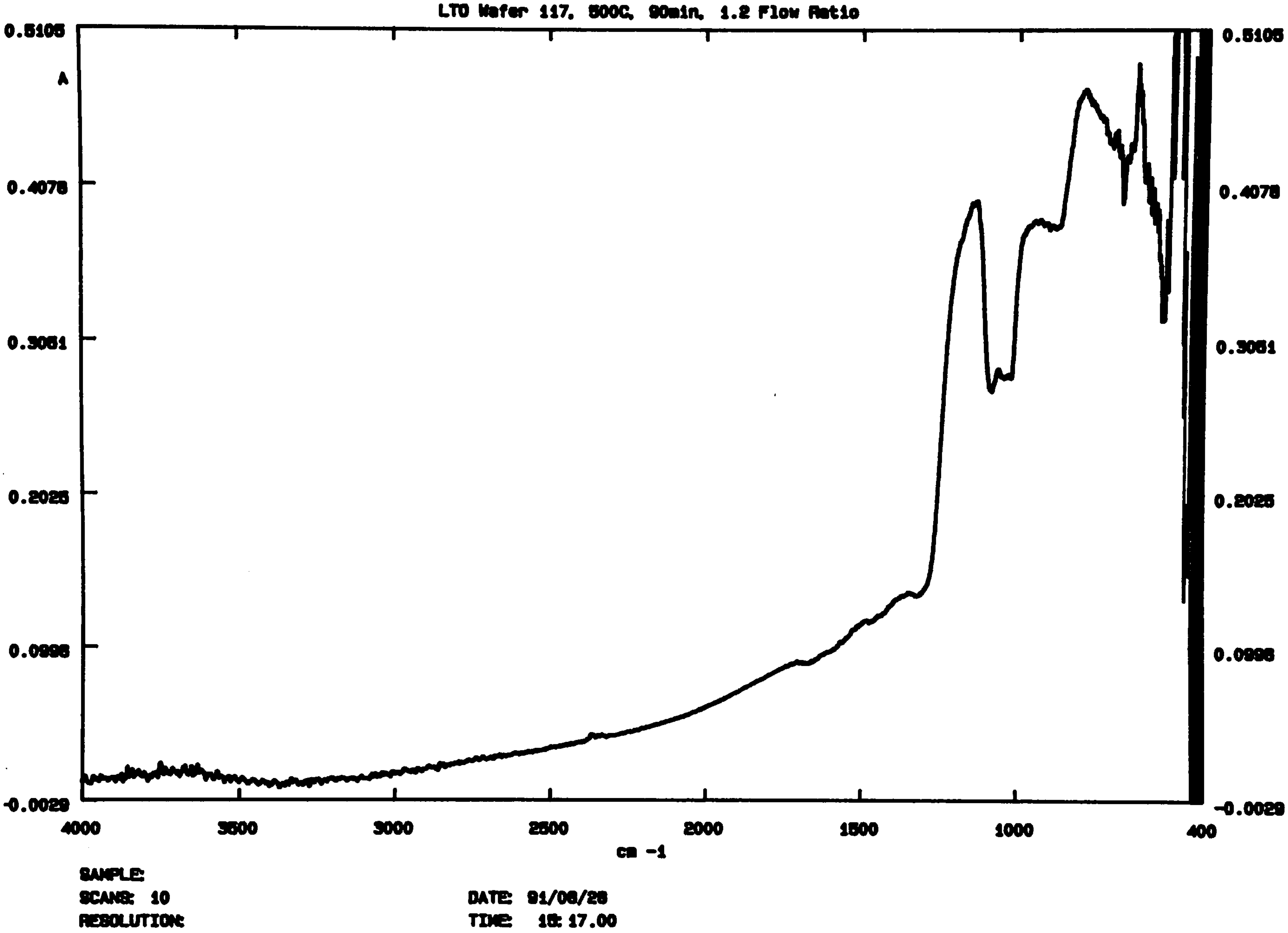
LTO Wafer 117, 500C, 90min, 1.2 Flow Ratio
A
0.5105
0.4078
0.3051
0.2025
0.0998
-0.0029
4000
3500
3000
2500
2000
1500
1000
400
cm -1
SAMPLE:
SCANS: 10
RESOLUTION:
DATE: 91/08/28
TIME: 15:17.00

LTO Wafer 127, 400C, 30min, 1.2 Flow Ratio

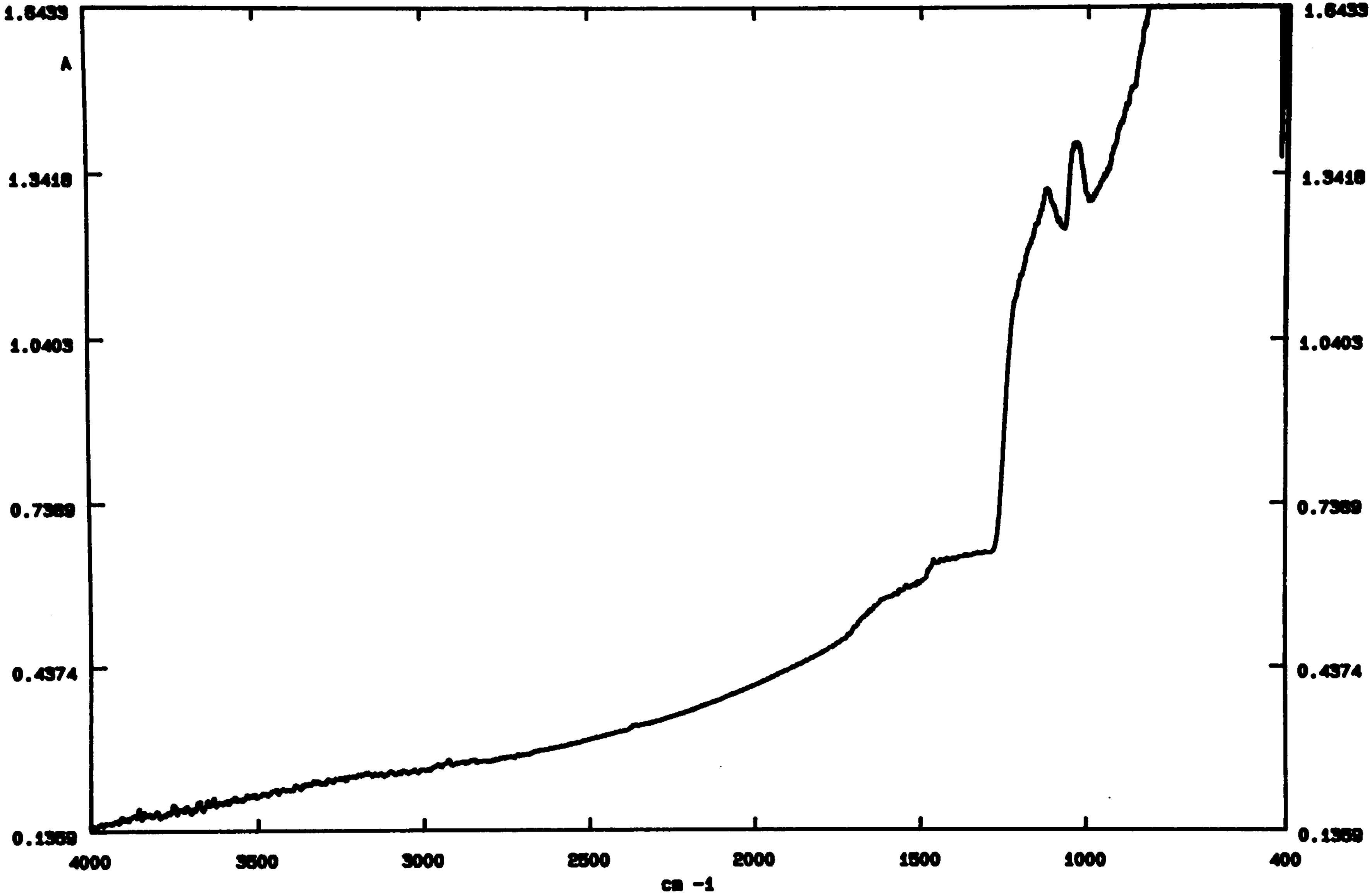

SAMPLE:
SCANS: 10
RESOLUTION:

DATE: 91/08/28
TIME: 15:32.17

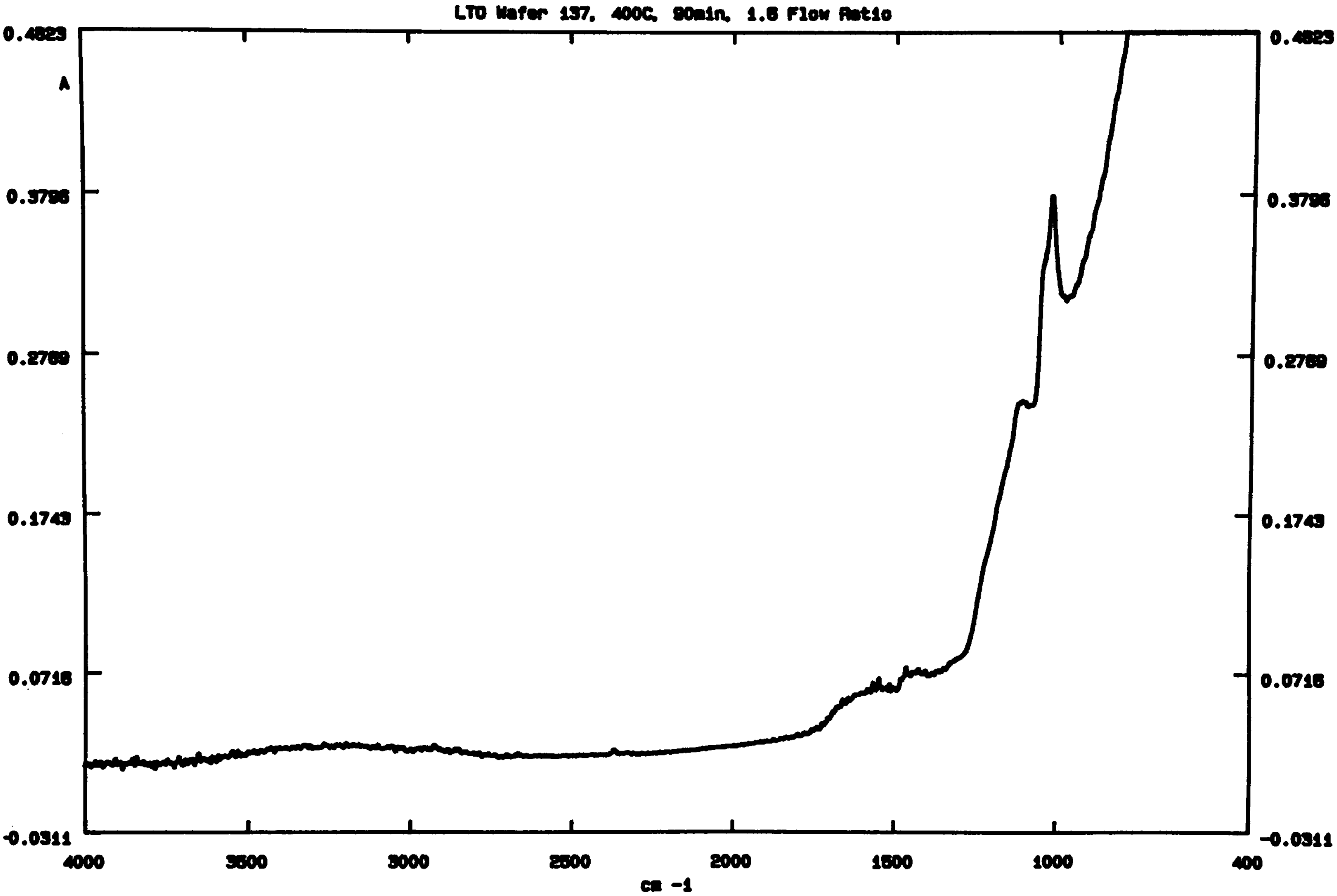

SAMPLE:
SCANS: 10
RESOLUTION:

DATE: 91/06/26
TIME: 15:47.09

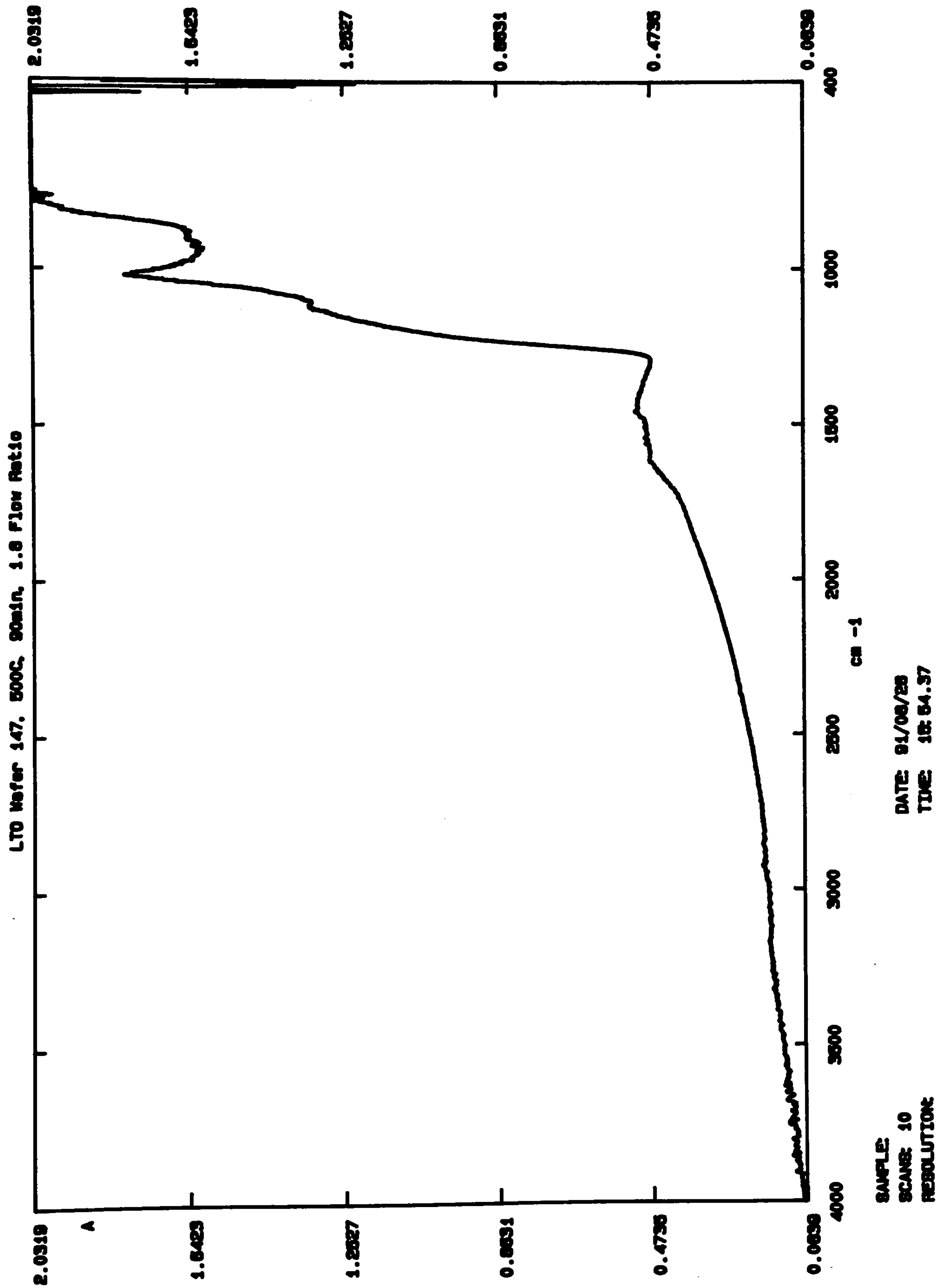
LTO Wafer 147, 500C, 90min, 1.8 Flow Ratio
A
2.0319
1.6423
1.2527
0.8631
0.4735
0.0839
4000
3500
3000
2500
2000
1500
1000
400
cm -1
SAMPLE:
SCANS: 10
RESOLUTION:
DATE: 91/08/28
TIME: 15:54.37

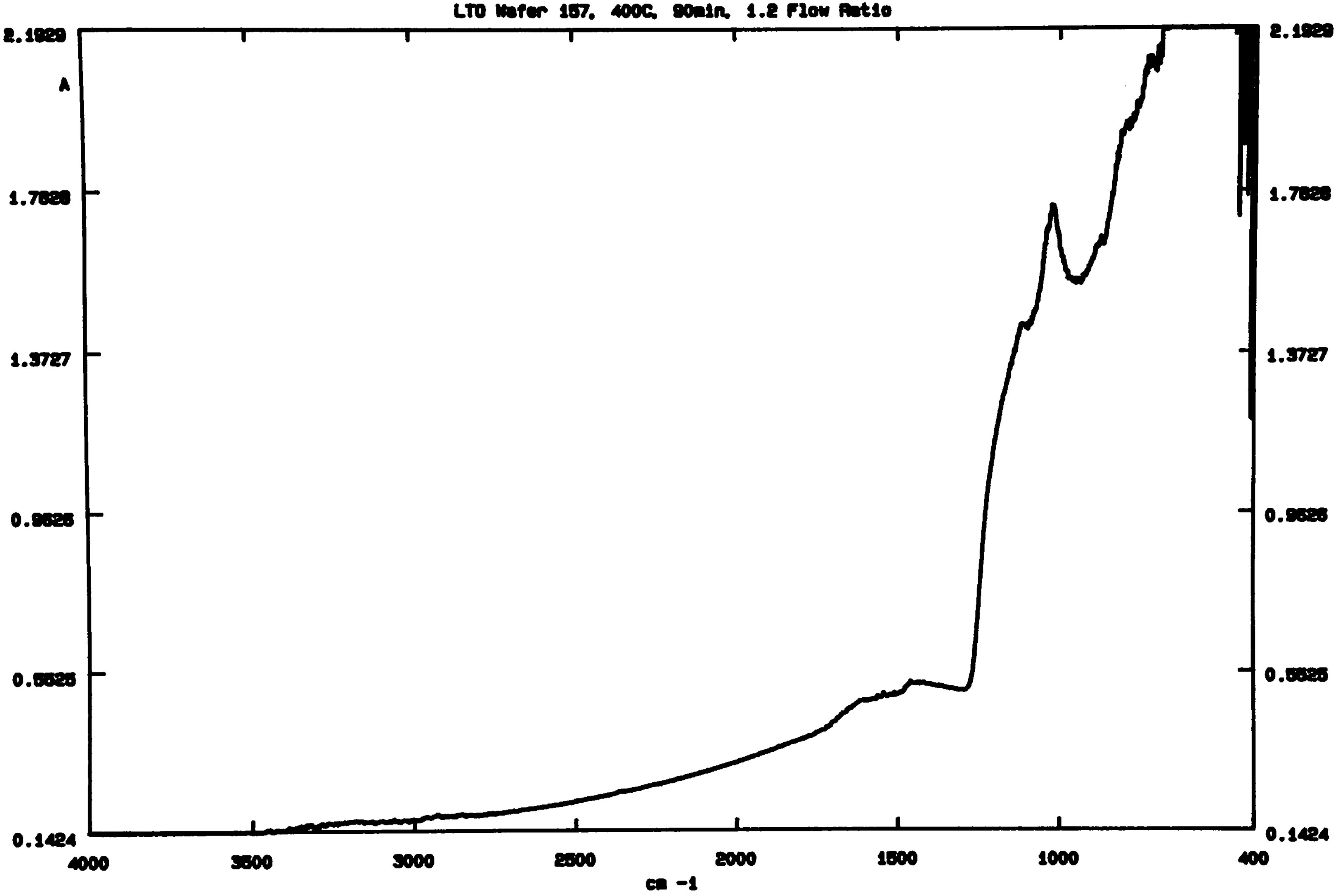

SAMPLE:
SCANS: 10
RESOLUTION:

DATE: 91/08/28
TIME: 16:01.55

LTO Wafer 167, 500C, 30min, 1.8 Flow Ratio

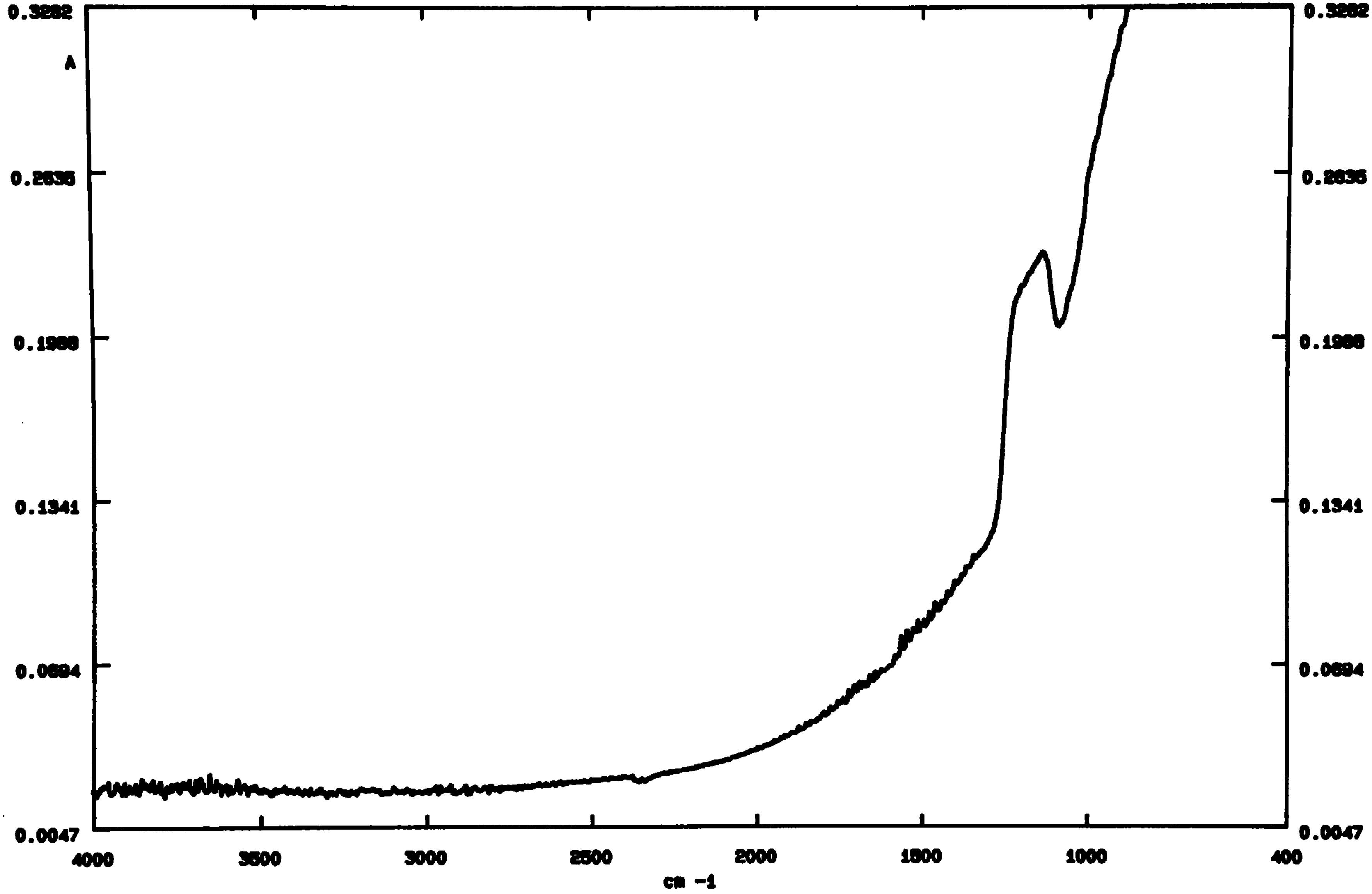

SAMPLE:
SCANS: 10
RESOLUTION:

DATE: 91/08/28
TIME: 16:09.03

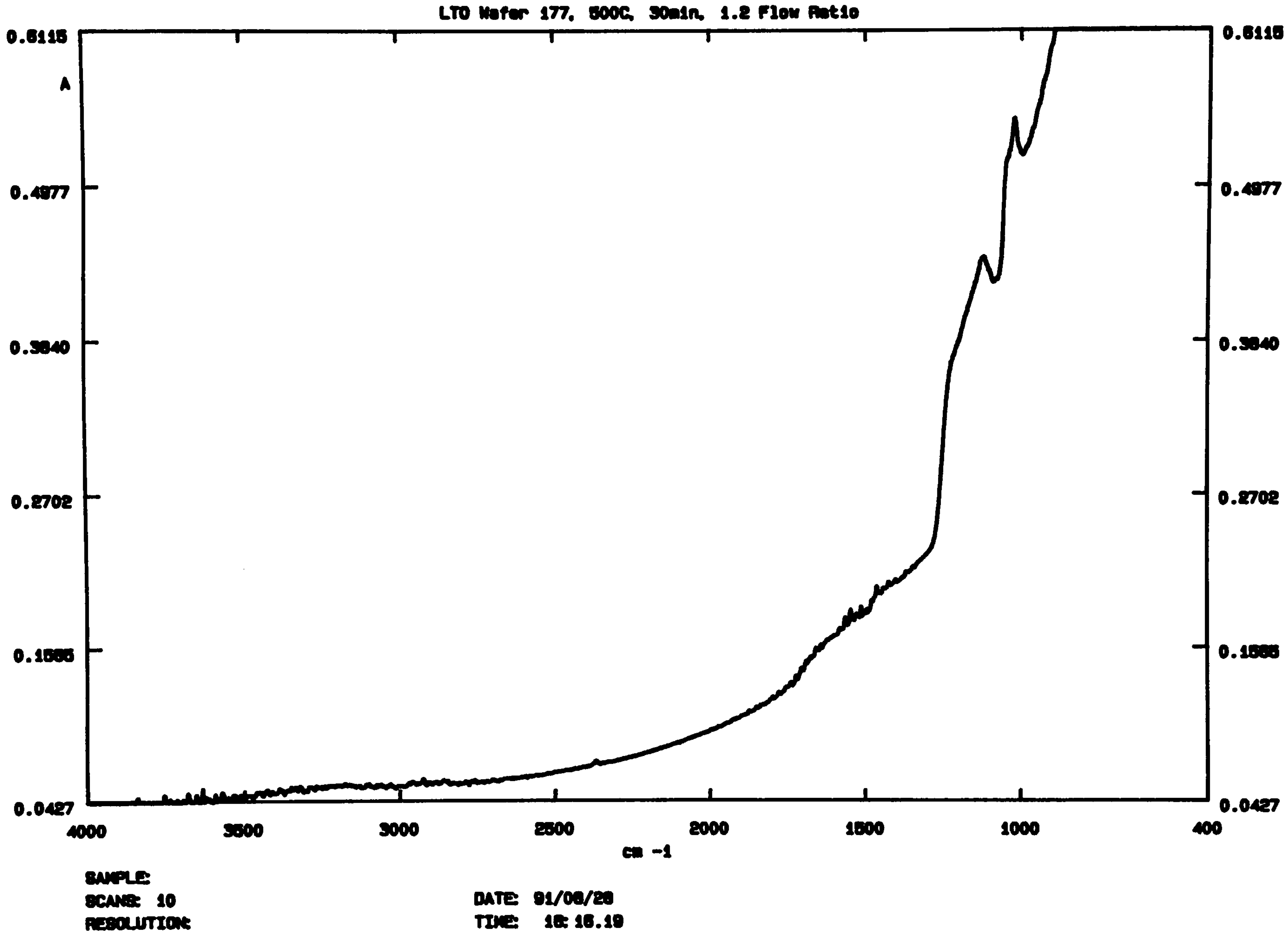
LTO Wafer 177, 500C, 30min, 1.2 Flow Ratio
A
0.6115
0.4977
0.3840
0.2702
0.1565
0.0427
4000
3500
3000
2500
2000
1500
1000
400
cm -1
SAMPLE:
SCANS: 10
RESOLUTION:
DATE: 91/08/28
TIME: 16:16.19

Appendix F :

Summary Sheet and Effect Plots for Deposition Rate

```
===========================================================================
Response: LTO Deposition Rate
===========================================================================
VAR     VARIABLE            UNITS                -1 LEVEL       +1 LEVEL
A       Temperature         Degree C              400.000        500.000
B       Time                Minutes                30.000         90.000
C       Flow Ratio                                  1.200          1.800

                                        STANDARDIZED          SUM OF
          VARIABLE     COEFFICIENT         EFFECT            SQUARES
   OVERALL AVERAGE         45.7214
                 A         11.4000        22.8000           1663.488
                 B         -4.8000        -9.6000            294.912
                 C         -3.4500        -6.9000            152.352
                AB         -4.4500        -7.0361            158.420
                AC         -0.4500        -0.7115              1.620
                BC          2.7000         4.2691             58.320
               ABC         ALIASED

===========================
Model selected for Factorial:
===========================

Results of Factorial Model Fitting    ANOVA for Selected Model

                   SUM OF                    MEAN          F
 SOURCE           SQUARES      DF           SQUARE       VALUE      PROB > F
MODEL            2695.209       5          539.042       193.8       0.0001
RESIDUAL           22.255       8            2.782
LACK OF FIT         1.620       1            1.620      0.5496       0.4826
PURE ERROR         20.635       7            2.948
COR TOTAL        2717.464      13

  ROOT MSE        1.66790              R-SQUARED      0.9918
  DEP MEAN       45.72143          ADJ R-SQUARED      0.9867
      C.V.          3.65%
  Predicted Residual Sum of Squares (PRESS) = 60.465

                COEFFICIENT              STANDARD    t FOR H0
   VARIABLE       ESTIMATE      DF         ERROR   COEFFICIENT=0  PROB > |t|
  INTERCEPT       44.45000       1        0.51069
          A       10.85000       1        0.51069        21.25        0.0001
          B       -4.25000       1        0.51069       -8.322        0.0001
          C       -4.00000       1        0.51069       -7.833        0.0001
         AB       -4.67500       1        0.51069       -9.154        0.0001
         BC        2.47500       1        0.51069        4.846        0.0013

Final Equation in Terms of Uncoded Variables:

      Dep. Rate = -84.10000
                 + 0.40400 * Temperature
                 + 0.84833 * Time
                 -29.83333 * Flow Ratio
                 - 0.00312 * Temperature * Time
                 + 0.27500 * Time * Flow Ratio

 Obs      ACTUAL     PREDICTED                        STUDENT  COOK'S      t    Run
 Ord       VALUE        VALUE      RESIDUAL    LEVER    RESID    DIST   VALUE   Ord
   1     38.5000      39.6500       -1.1500    0.375   -0.872   0.076  -0.858    11
   2     39.9000      39.6500        0.2500    0.375    0.190   0.004   0.178     5
   3     72.3000      70.7000        1.6000    0.375    1.213   0.147   1.257     6
   4     70.0000      70.7000       -0.7000    0.375   -0.531   0.028  -0.506    16
   7     47.1000      47.9000       -0.8000    0.500   -0.678   0.077  -0.654    10
   8     48.7000      47.9000        0.8000    0.500    0.678   0.077   0.654     4
   9     27.2000      26.7000        0.5000    0.375    0.379   0.014   0.358     1
  10     27.1000      26.7000        0.4000    0.375    0.303   0.009   0.285     9
  11     60.0000      57.7500        2.2500    0.375    1.706   0.291   2.001    15
  12     54.6000      57.7500       -3.1500    0.375   -2.389   0.571  -4.174     2
  13     32.4000      32.5000       -0.1000    0.500   -0.085   0.001  -0.079     7
  14     32.6000      32.5000        0.1000    0.500    0.085   0.001   0.079    12
  15     45.6000      44.8500        0.7500    0.500    0.636   0.067   0.610     8
  16     44.1000      44.8500       -0.7500    0.500   -0.636   0.067  -0.610    13
```

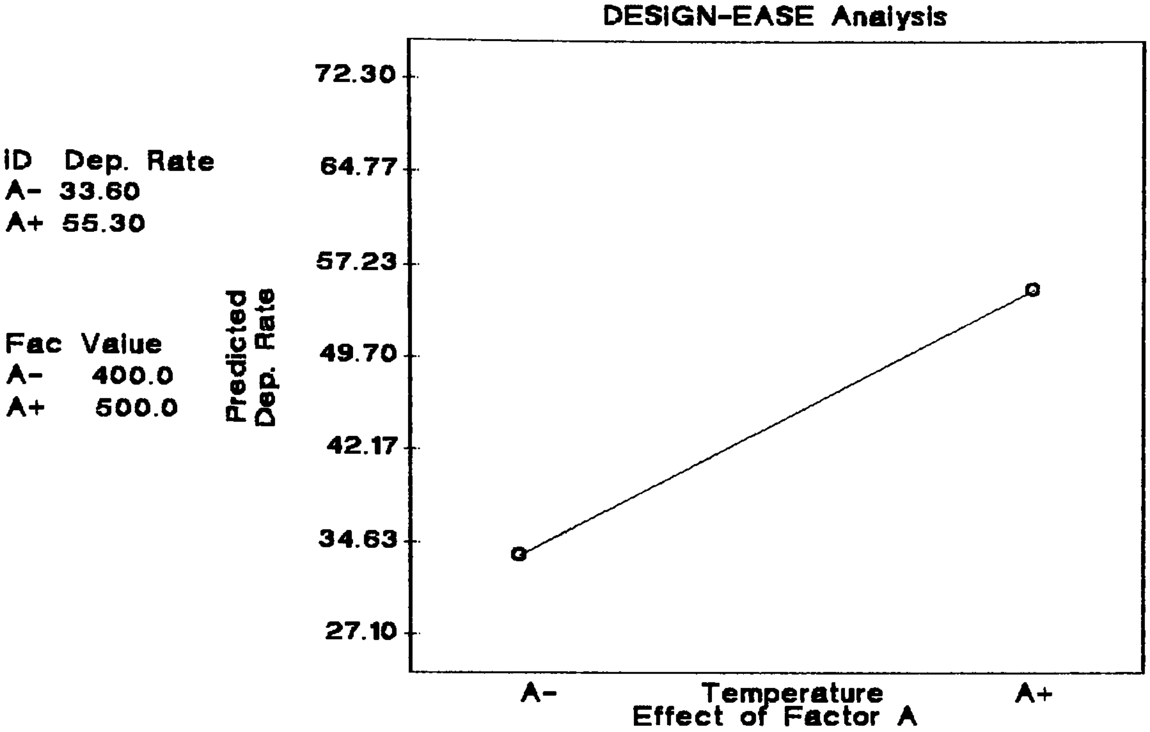
DESIGN-EASE Analysis
ID Dep. Rate
A- 33.60
A+ 55.30
Fac Value
A- 400.0
A+ 500.0
Predicted Dep. Rate
72.30
64.77
57.23
49.70
42.17
34.63
27.10
A-
Temperature
A+
Effect of Factor A

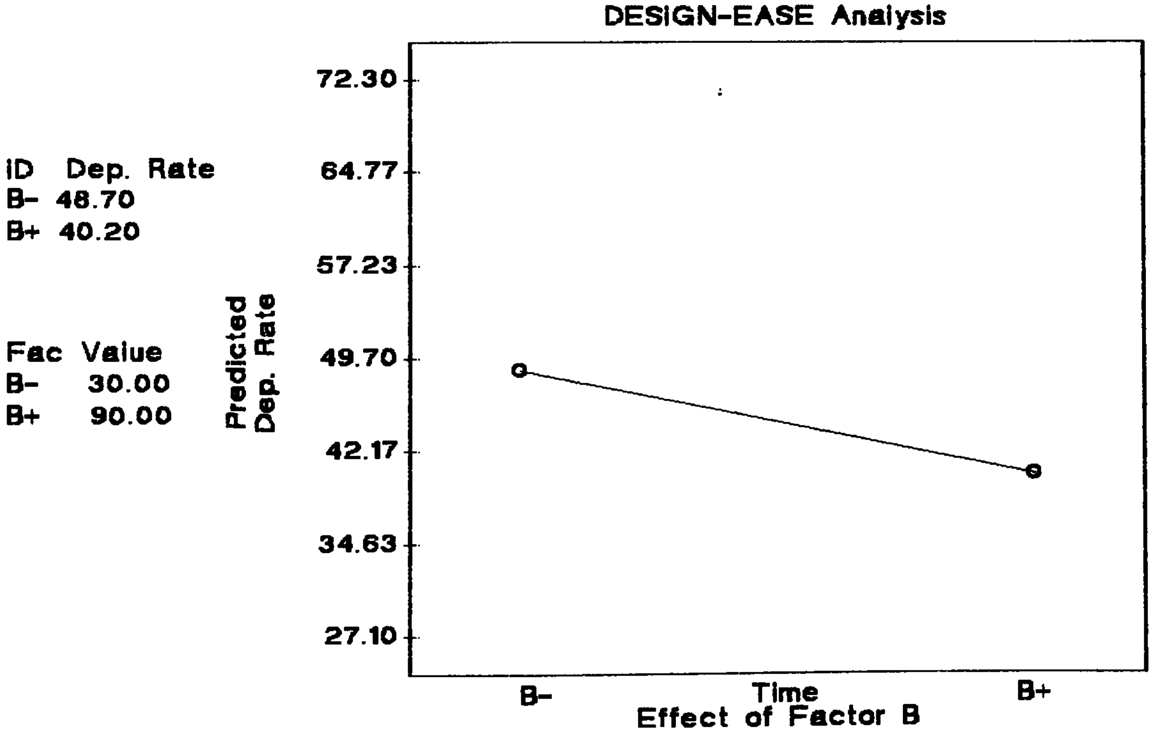
DESIGN-EASE Analysis
ID Dep. Rate
B- 48.70
B+ 40.20
Fac Value
B- 30.00
B+ 90.00
Predicted Dep. Rate
72.30
64.77
57.23
49.70
42.17
34.63
27.10
B-
Time
B+
Effect of Factor B

ID	Dep. Rate
C-	48.45
C+	40.45

Fac	Value
C-	1.200
C+	1.800

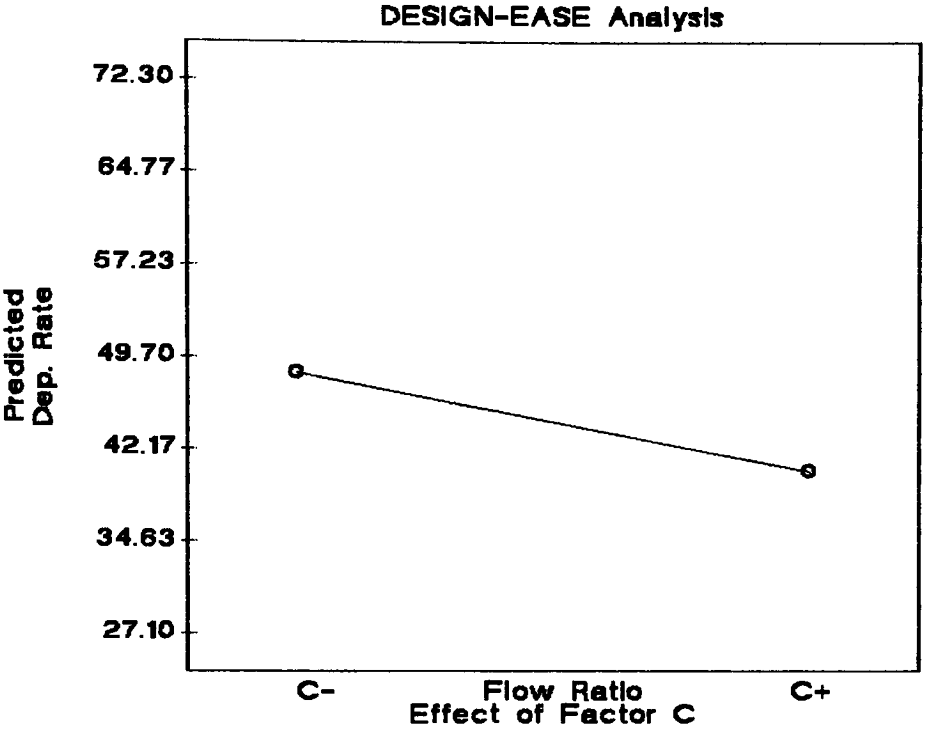

A: Temperature
B: Time

A	B	Dep. Rate
-	-	33.17
+	-	64.22
-	+	34.03
+	+	46.37

Fac	Value
A-	400.0
A+	500.0
B-	30.00
B+	90.00

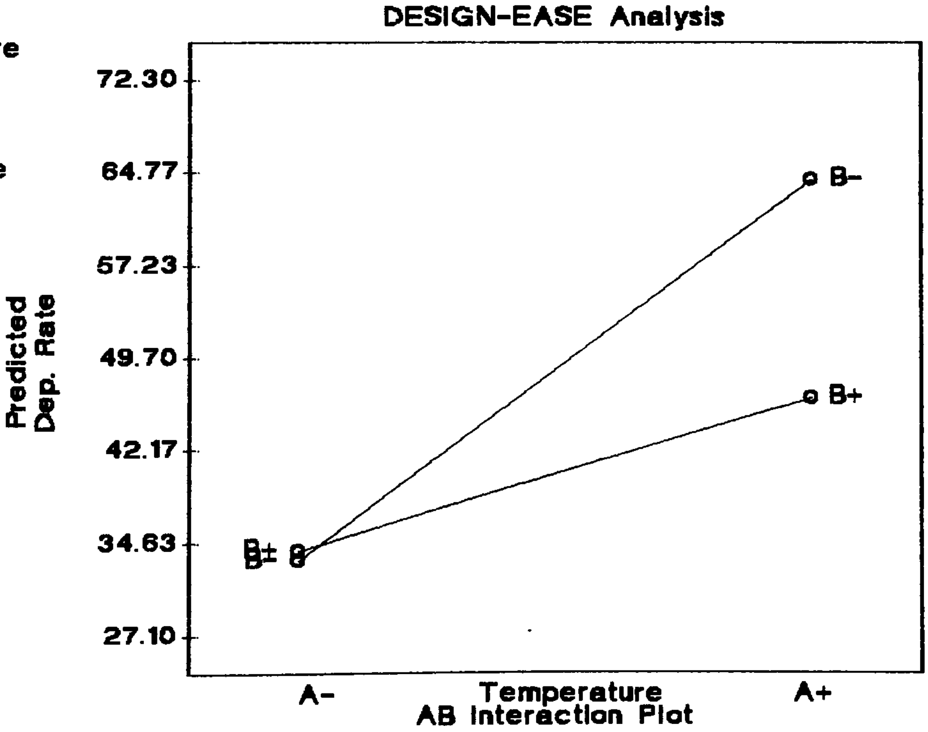

B: Time
A: Temperature

B	A	Dep. Rate
-	-	33.17
+	-	34.03
-	+	64.22
+	+	46.37

Fac	Value
B-	30.00
B+	90.00
A-	400.0
A+	500.0

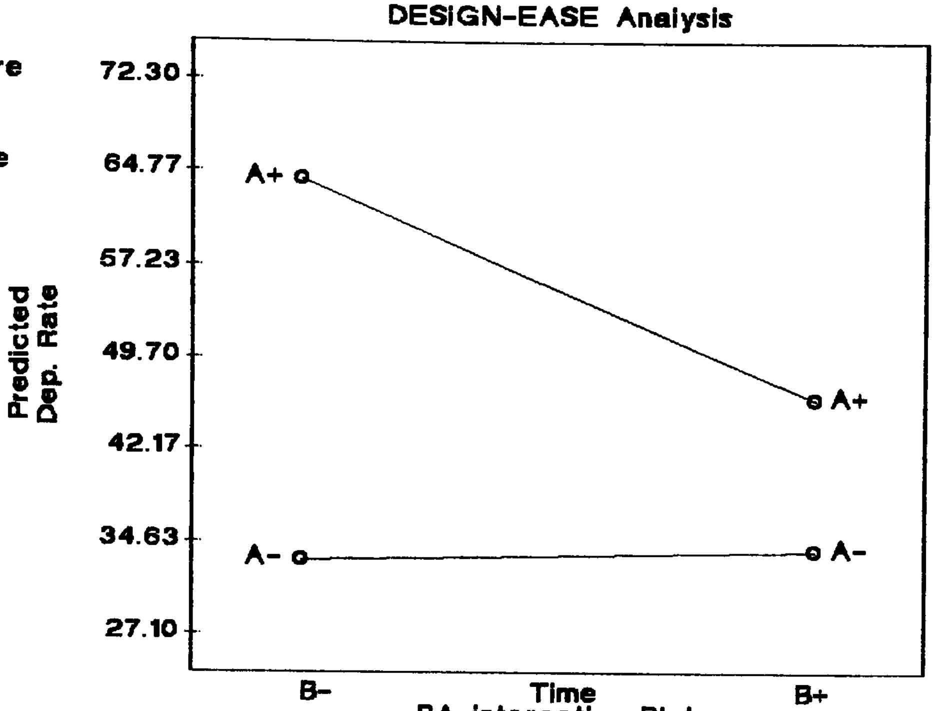

BA Interaction Plot

B: Time
C: Flow Ratio

B	C	Dep. Rate
-	-	55.17
+	-	41.73
-	+	42.22
+	+	38.68

Fac	Value
B-	30.00
B+	90.00
C-	1.200
C+	1.800

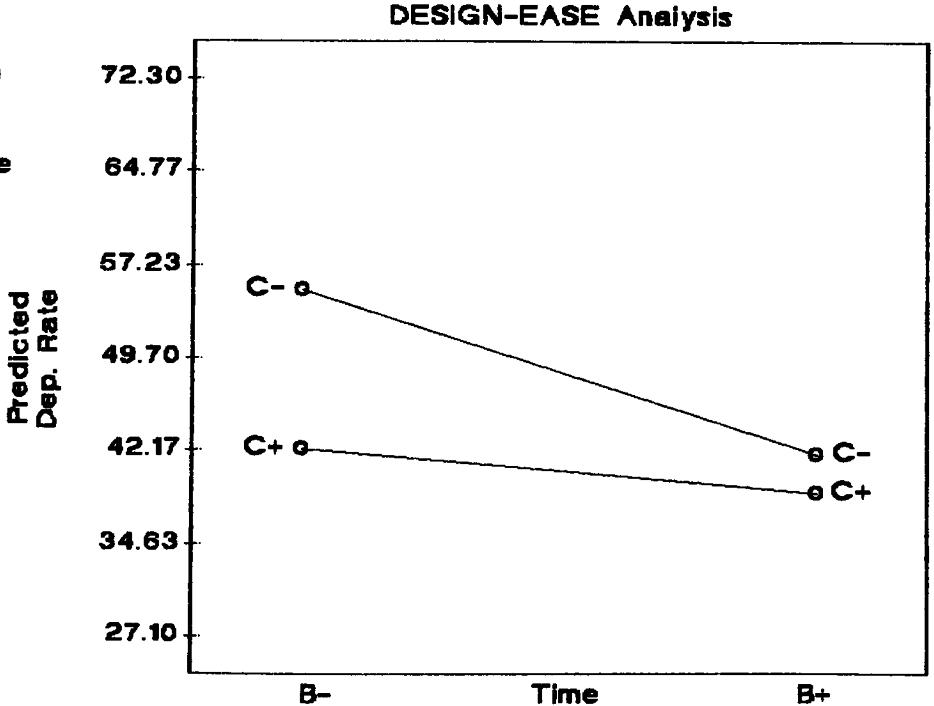

BC Interaction Plot

C: Flow Ratio
B: Time

C	B	Dep. Rate
-	-	55.17
+	-	42.22
-	+	41.73
+	+	38.68

Fac	Value
C-	1.200
C+	1.800
B-	30.00
B+	90.00

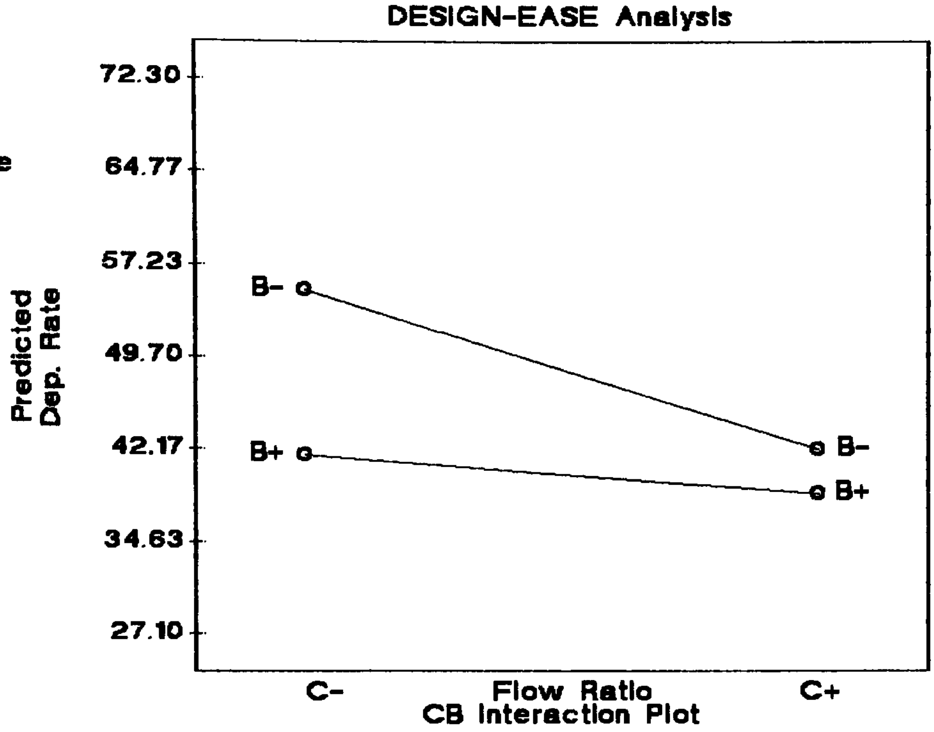

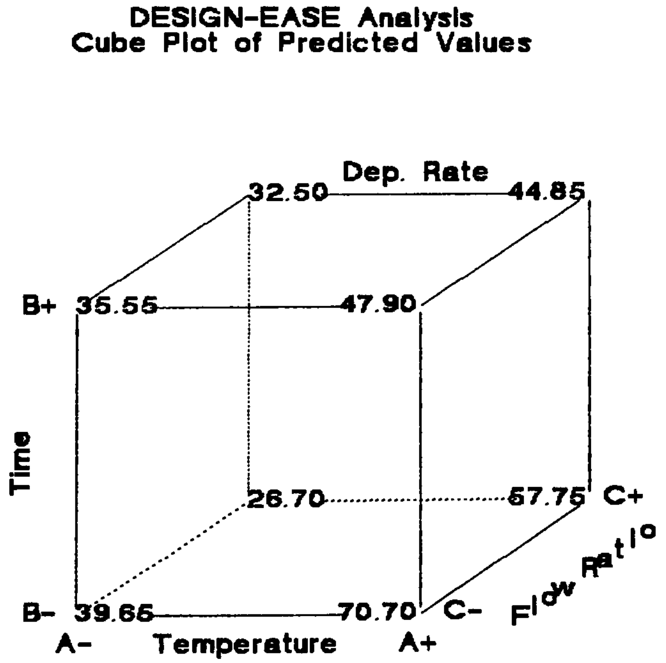

Appendix G :

Summary Sheet and Effect Plots for Index of Refraction

```
==============================================================================
Response: LTO Index of Refraction
==============================================================================
VAR     VARIABLE            UNITS                  -1 LEVEL       +1 LEVEL
A       Temperature         Degree C               400.000        500.000
B       Time                Minutes                 30.000         90.000
C       Flow Ratio                                   1.200          1.800

                                         STANDARDIZED         SUM OF
          VARIABLE       COEFFICIENT        EFFECT            SQUARES
     OVERALL AVERAGE        1.44101
                   A       -0.00353       -0.00707           0.000184
                   B       -0.00647       -0.01293           0.000617
                   C       -0.00568       -0.01137           0.000477
                  AB       -0.00193       -0.00382           0.000054
                  AC        0.00253        0.00500           0.000092
                  BC       -0.00406       -0.00801           0.000237
                 ABC       -0.00411       -0.00807           0.000241

 ============================
 Model selected for Factorial:
 ============================

  Results of Factorial Model Fitting   ANOVA for Selected Model

                  SUM OF                   MEAN         F
   SOURCE         SQUARES       DF        SQUARE      VALUE       PROB > F
 MODEL           0.001573        4      0.000393      6.565        0.0074
 RESIDUAL        0.000599       10      0.000060
 LACK OF FIT     0.000374        3      0.000125      3.872        0.0638
 PURE ERROR      0.000225        7      0.000032
 COR TOTAL       0.002172       14

   ROOT MSE      0.007740                R-SQUARED     0.7242
   DEP MEAN      1.441013            ADJ R-SQUARED     0.6139
       C.V.           0.54%
   Predicted Residual Sum of Squares (PRESS) = 0.001292


                COEFFICIENT                STANDARD    t FOR H0
     VARIABLE     ESTIMATE        DF         ERROR    COEFFICIENT=0   PROB > |t|
    INTERCEPT     1.441501         1       0.002021
            A    -0.003839         1       0.002021       -1.899        0.0867
            B    -0.006161         1       0.002021       -3.049        0.0123
            C    -0.005989         1       0.002021       -2.963        0.0142
           BC    -0.003651         1       0.002021       -1.807        0.1010

  Final Equation in Terms of Uncoded Variables:

       Ref. Index = 1.481803
                    -0.000077 * Temperature
                    +0.000403 * Time
                    +0.004379 * Flow Ratio
                    -0.000406 * Time * Flow Ratio

                                                         STUDENT COOK'S     t     Run
   Obs       ACTUAL      PREDICTED                         RESID   DIST    VALUE   Ord
   Ord        VALUE        VALUE      RESIDUAL    LEVER
    1       1.45800      1.45384      0.00416    0.318    0.651   0.040    0.631   11
    2       1.45900      1.45384      0.00516    0.318    0.808   0.061    0.792    5
    3       1.43210      1.44616     -0.01406    0.318   -2.200   0.452   -2.906    6
    4       1.45090      1.44616      0.00474    0.318    0.741   0.051    0.724   16
    6       1.44800      1.44882     -0.00082    0.455   -0.143   0.003   -0.136    3
    7       1.43950      1.44114     -0.00164    0.364   -0.266   0.008   -0.253   10
    8       1.44360      1.44114      0.00246    0.364    0.398   0.018    0.381    4
    9       1.43790      1.44916     -0.01126    0.318   -1.762   0.290   -2.014    1
   10       1.44500      1.44916     -0.00416    0.318   -0.651   0.040   -0.632    9
   11       1.45040      1.44149      0.00891    0.318    1.395   0.182    1.474   15
   12       1.44800      1.44149      0.00651    0.318    1.019   0.097    1.021    2
   13       1.43370      1.42954      0.00416    0.318    0.651   0.040    0.631    7
   14       1.43230      1.42954      0.00276    0.318    0.432   0.017    0.414   12
   15       1.41610      1.42186     -0.00576    0.318   -0.901   0.076   -0.892    8
   16       1.42070      1.42186     -0.00116    0.318   -0.182   0.003   -0.173   13
```

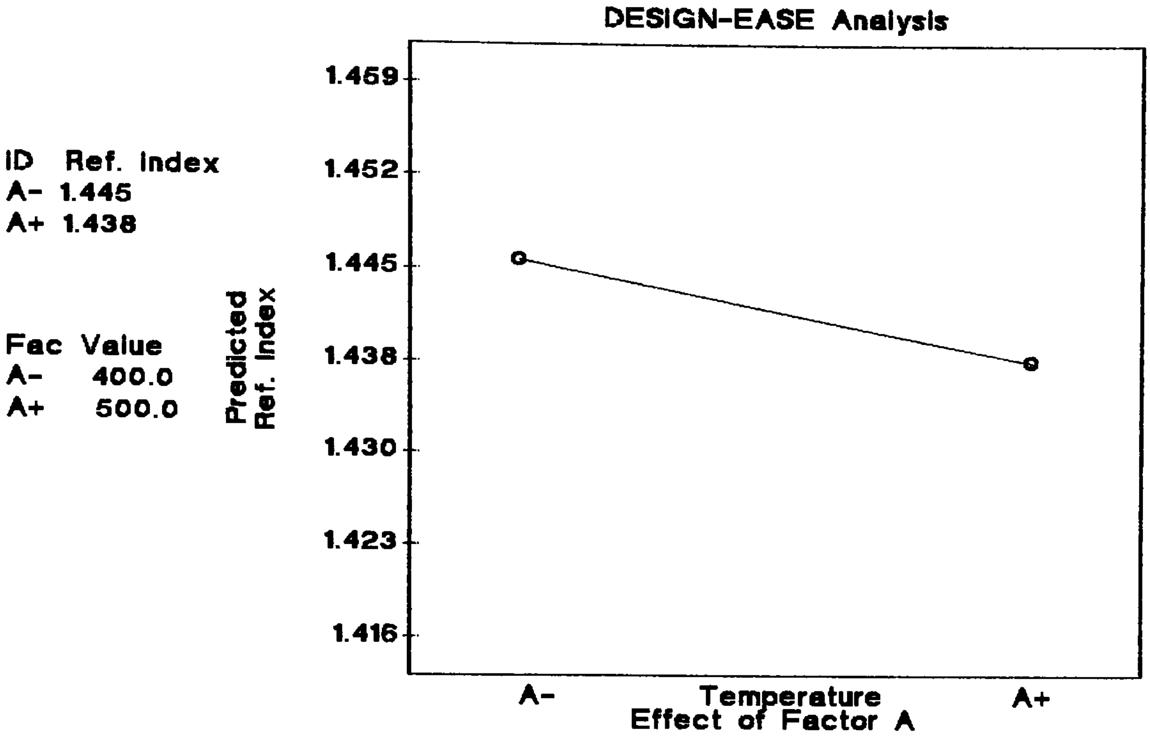

ID	Ref. Index
A-	1.445
A+	1.438

Fac	Value
A-	400.0
A+	500.0

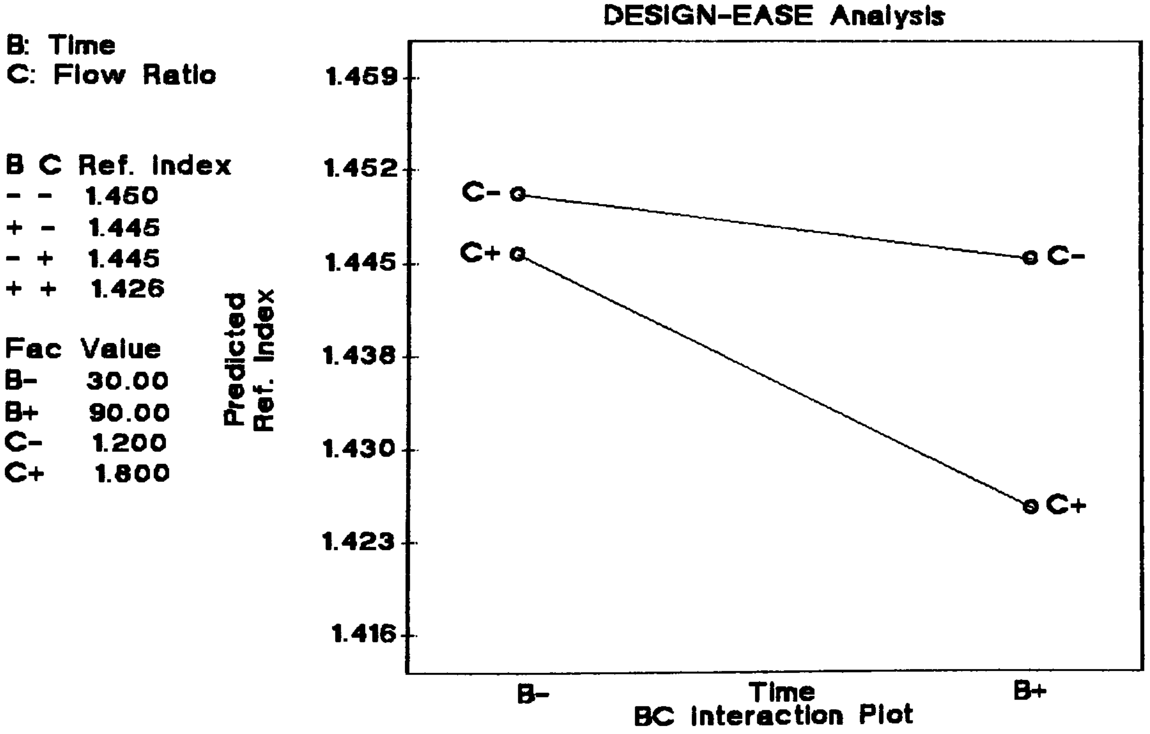

B: Time
C: Flow Ratio

B	C	Ref. Index
-	-	1.450
+	-	1.445
-	+	1.445
+	+	1.426

Fac	Value
B-	30.00
B+	90.00
C-	1.200
C+	1.800

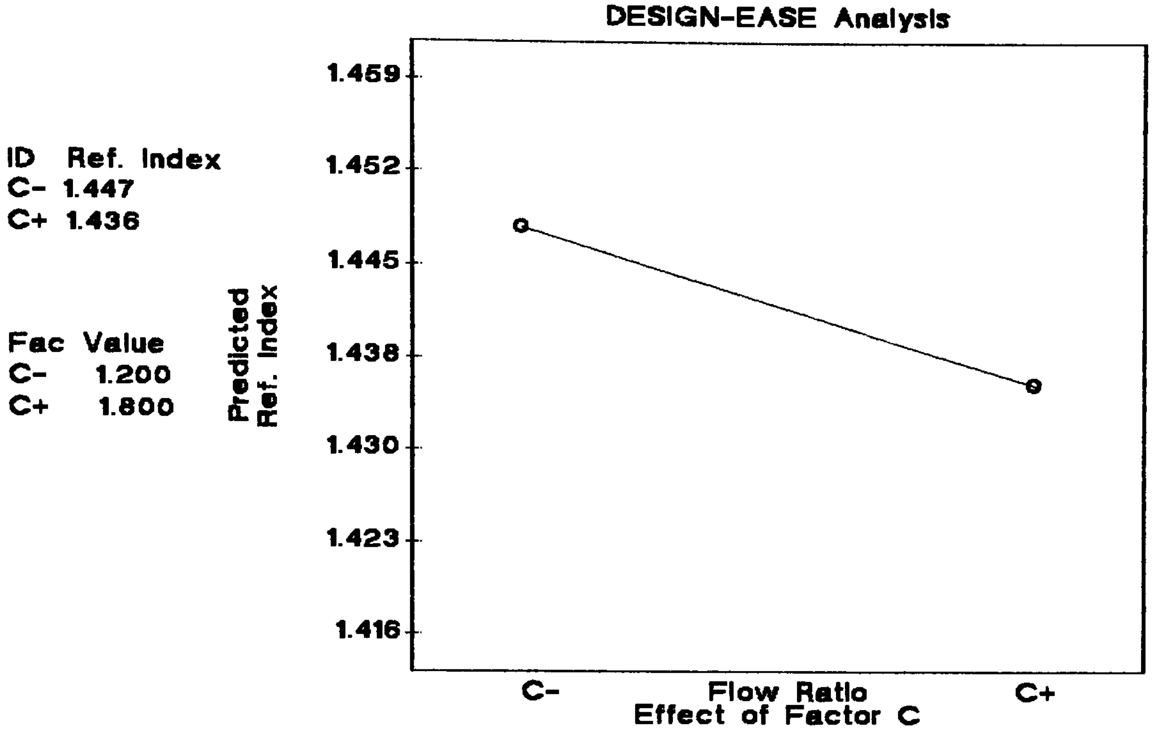
DESIGN-EASE Analysis
ID Ref. Index
C- 1.447
C+ 1.436
Fac Value
C- 1.200
C+ 1.800
Predicted Ref. Index
1.459
1.452
1.445
1.438
1.430
1.423
1.416
C-
Flow Ratio
C+
Effect of Factor C

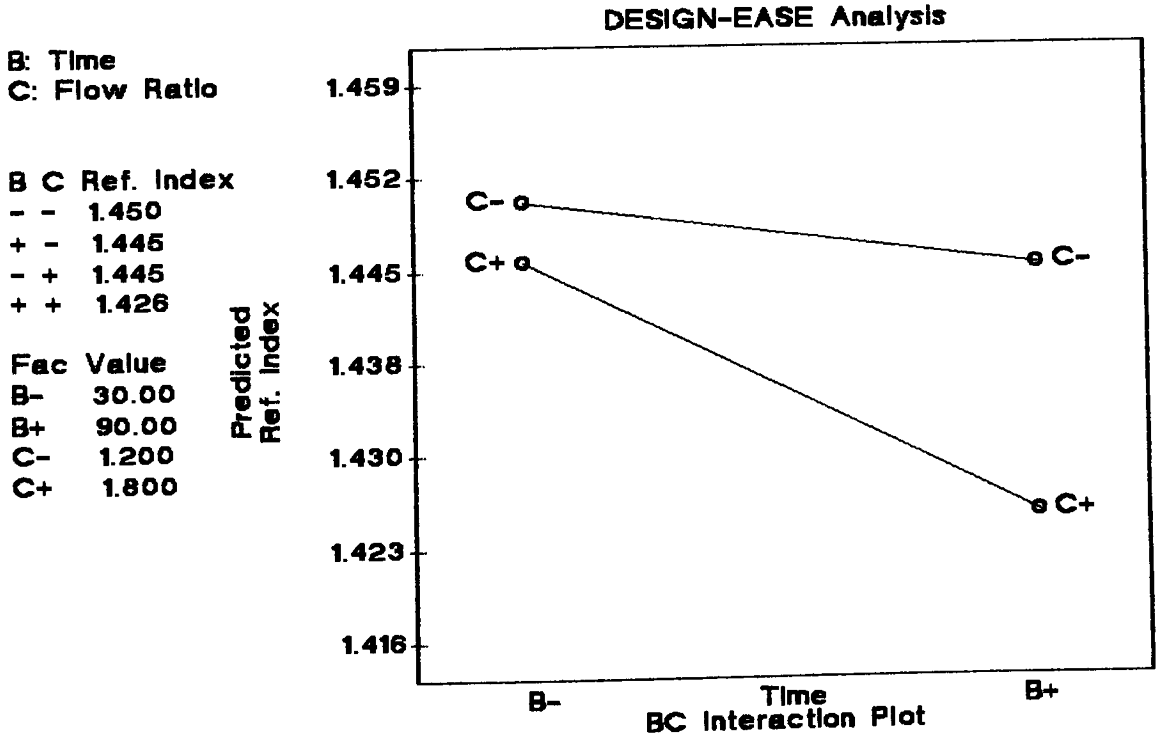
DESIGN-EASE Analysis
B: Time
C: Flow Ratio
B C Ref. Index
- - 1.450
+ - 1.445
- + 1.445
+ + 1.426
Fac Value
B- 30.00
B+ 90.00
C- 1.200
C+ 1.800
Predicted Ref. Index
1.459
1.452
1.445
1.438
1.430
1.423
1.416
C-
C+
C-
C+
B-
Time
B+
BC Interaction Plot

C: Flow Ratio
B: Time

C	B	Ref. Index
-	-	1.450
+	-	1.445
-	+	1.445
+	+	1.426

Fac	Value
C-	1.200
C+	1.800
B-	30.00
B+	90.00

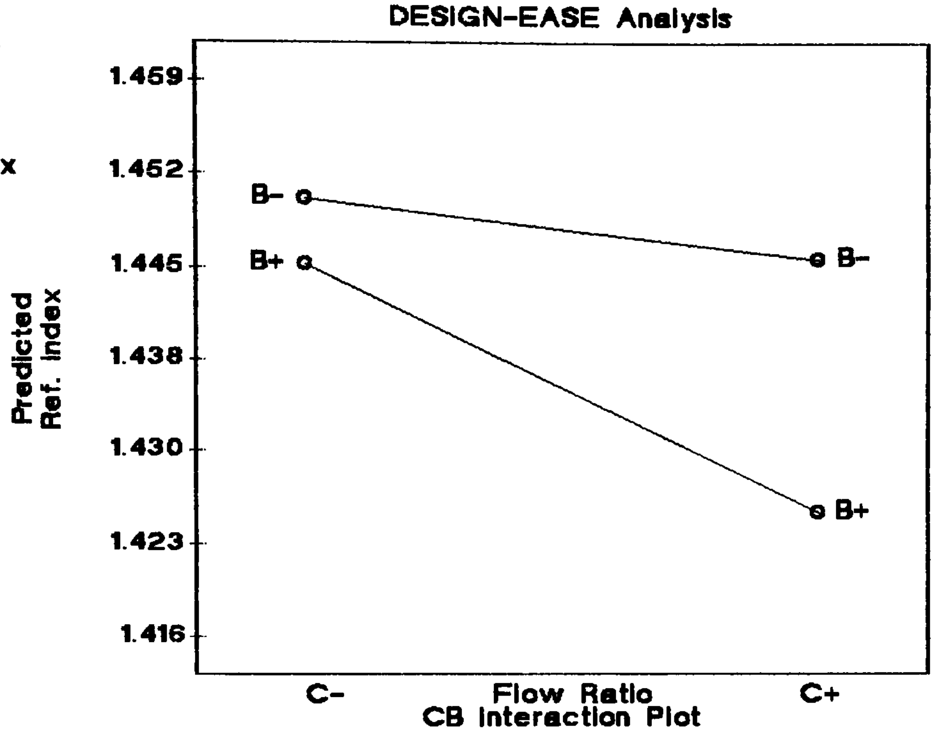

DESIGN-EASE Analysis
Cube Plot of Predicted Values

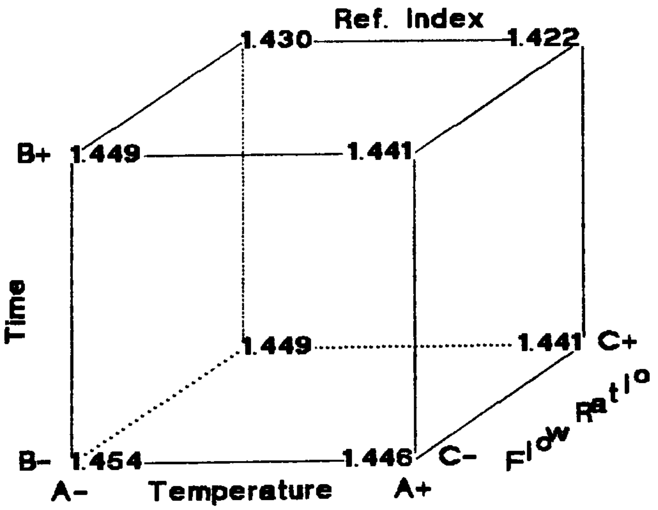

Appendix H :

Current vs Voltage Plots of Double Metal Via Chains

****** GRAPHICS PLOT ******

30X30 VIA CHAIN

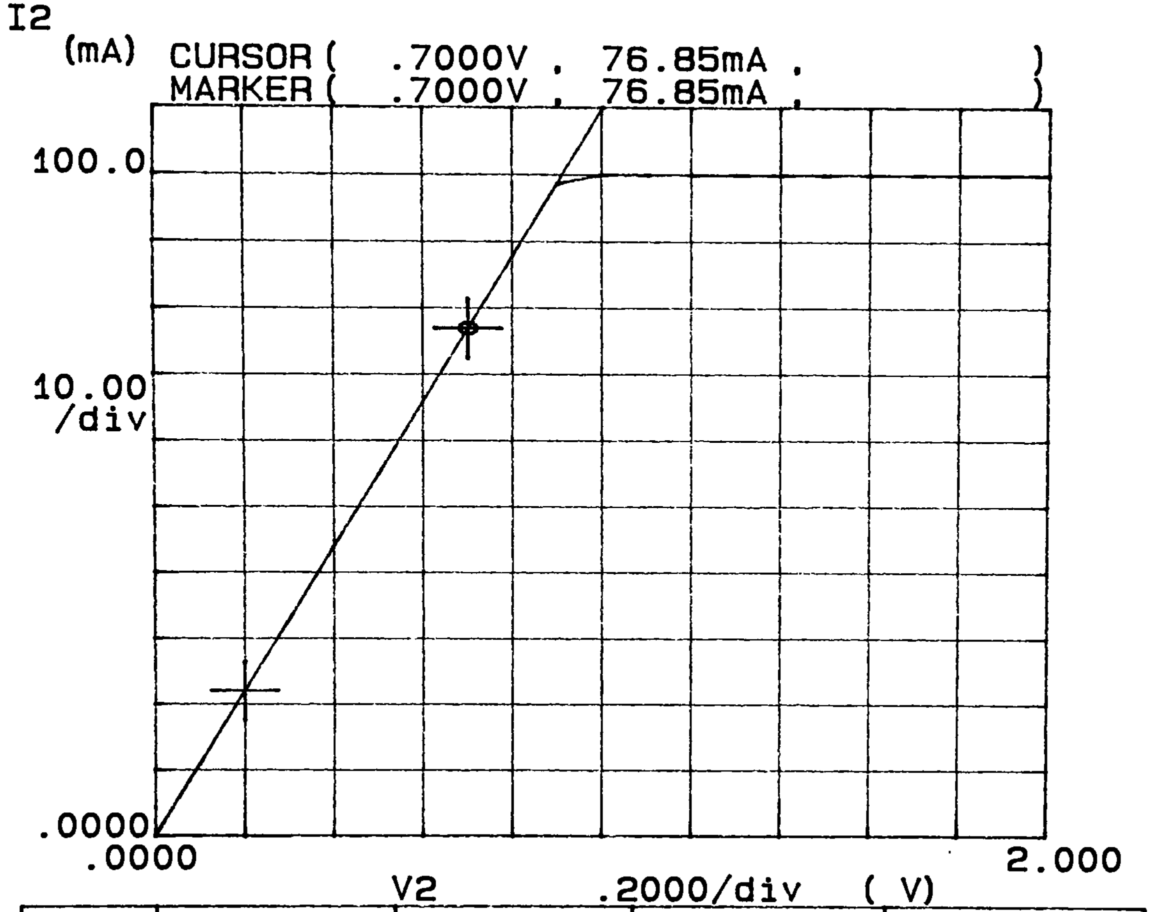

	GRAD	1/GRAD	Xintercept	Yintercept
LINE1	110E-03	9.12E+00	-534E-06	58.6E-06
LINE2				

Variable1:

V2	**-Ch2**	
Linear sweep		
Start		**.0000V**
Stop		**2.0000V**
Step		**.1000V**

Constants:

V1	**-Ch1**	**.0000V**

****** GRAPHICS PLOT ******
20X20 VIA CHAIN

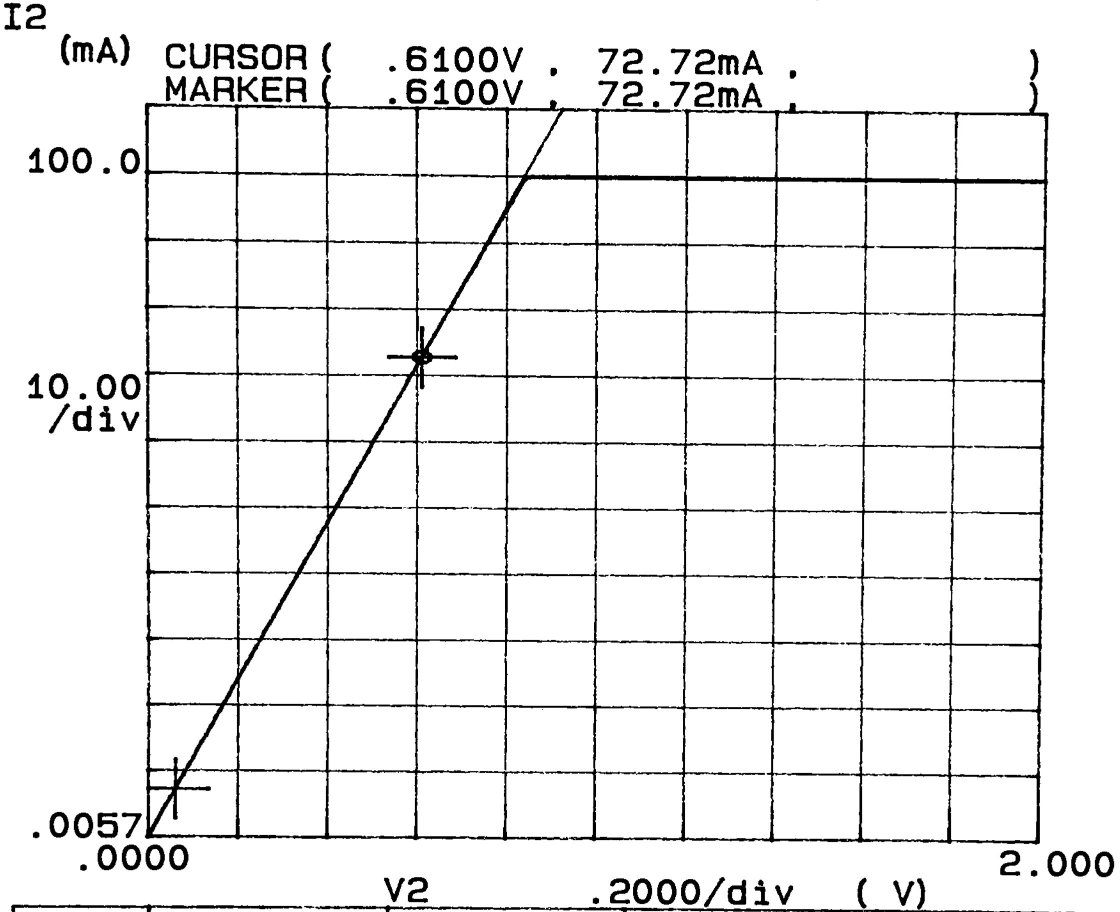

```
CURSOR (   .6100V ,  72.72mA ,                  )
MARKER (   .6100V ,  72.72mA ,                  )
```

```
Variable1:
 V2     -Ch2
 Linear sweep
 Start              .0000V
 Stop              2.0000V
 Step               .0100V

Constants:
 V1     -Ch1    .0000V
```

	GRAD	1/GRAD	Xintercept	Yintercept
LINE1	119E-03	8.39E+00	-398E-06	47.4E-06
LINE2				

****** GRAPHICS PLOT ******

10X10 VIA CHAIN

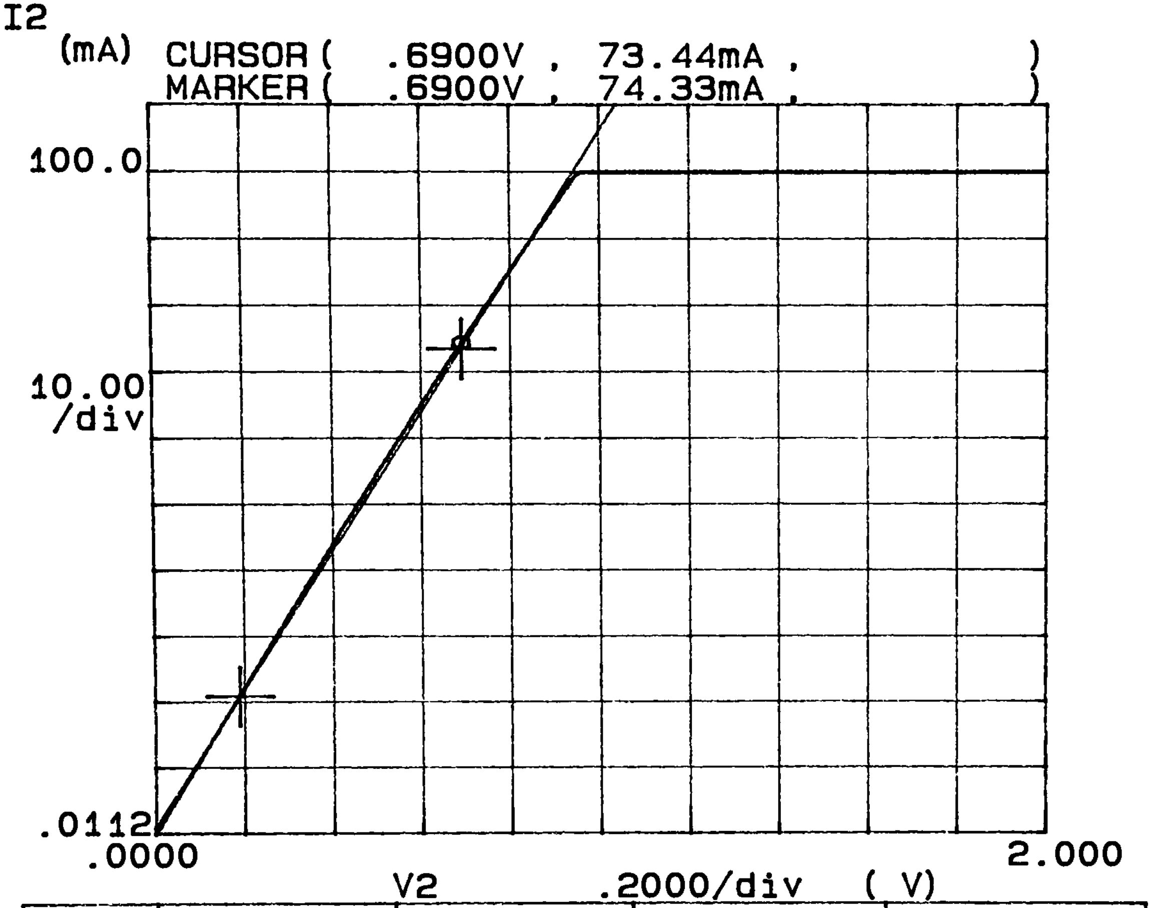

	GRAD	1/GRAD	Xintercept	Yintercept
LINE1	105E-03	9.50E+00	-7.95E-03	837E-06
LINE2				

Variable1:
V2 -Ch2
Linear sweep
Start .0000V
Stop 2.0000V
Step .0100V

Constants:
V1 -Ch1 .0000V

****** GRAPHICS PLOT ******

6X6 VIA CHAIN

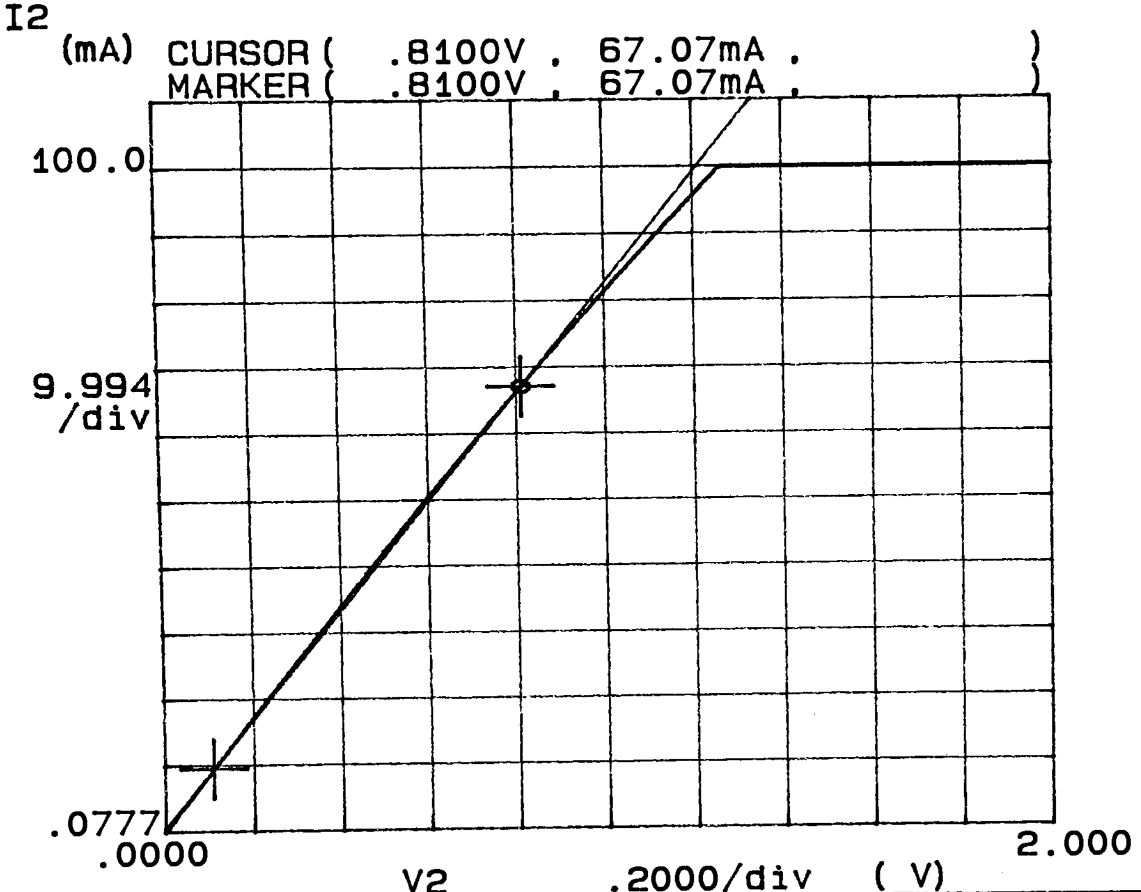

	GRAD	1/GRAD	Xintercept	Yintercept
LINE1	82.2E-03	12.2E+00	-5.66E-03	465E-06
LINE2				

Variable1:
V2 -Ch2
Linear sweep

Start	.0000V
Stop	2.0000V
Step	.0100V

Constants:
V1 -Ch1 .0000V

Section 9 : References

1. Arthur Sherman, *Chemical Vapor Deposition for Microelectronics.* Noyes Publications, New Jersey (1987).

2. Ludmila Eckertova, *Physics of Thin Films*, Second Edition. Plenum Press, New York and London (1986).

3. *SiO_2 and Its Interfaces*, Materials Research Society Symposium Proceedings Vol105. Editors: S.T. Pantelides and G. Lucovsky (1987).

4. *Polycrystalline and Amorphous Thin Films and Devices*, Materials Science Series, Academic Press, New York (1980).

5. *Preparation and Properties of Thin Films*, Treatise on Materials Science and Technology Vol24, Academic Press, New York (1982).

6. *Analytical Techniques for thin Films*, Treatise on Materials Science and Technology Vol27, Academic Press, New York (1988).

7. *Chemical Vapor Deposition*, Proceedings of The Ninth International Conference on CVD. The Electrochemical Society, Inc. Proceedings Vol84-6 (1984).

8. *Handbook of Thin-Film Deposition Processes and Techniques.* Noyes Publication, New Jersey. Edited by Klaus K. Schuegraf (1988).

9. *Structure Property Relations in Thin Films*, The Education Committee of American Vacuum Society, New York (1988).

10. Kazuo Nakamoto, *Infrared and Raman Spectra of Inorganic and Coordination Compounds*, Third Edition. John Wiley & Sons, New York (1978).

11. George E. P. Box and Norman R. Draper, *Empirical Model-Building and Response Surfaces.* John Wiley & Sons, New York (1987).

12. George E. P. Box, William G. Hunter and J. Stuart Hunter, *Statistics for Experimenters.* John Wiley & Sons, New York (1978).

13. Robert L. Mason, Richard F. Gunst and James L. Hess, *Statistical Design & Analysis of Experiments.* John Wiley & Sons, New York (1989).

14. William Mendenhall, *The Design and analysis of Experiments.* Wadsworth Publications, Belmont, California (1968).

15. Shyam P. Murarka and Martin C. Peckerar, *Chemical Vapor Deposition Nucleation and Growth of Thin Solid Films.* Electronic Materials Science and Technology (1989).

16. Takuji Goda, Hirotsugu Nagayama, Akihiro Hishinuma and Hideo Kawahara, *Physical and Chemical Properties of Silicon Dioxide Film Deposited by New Process.* Materials Research Society Symposium. Proc. Vol105 (1988).

17. W. A. Pliskin, *Comparison of Properties of Dielectric Films Deposited by Various Methods.* Journal of Vacuum Science and Technology Vol14, No.5 (Sep/Oct 1977).

18. Werner Kern and Richard S. Rosler, *Advances in Deposition Processes for Passivation Films.* Journal of Vacuum Science and Technology Vol14, No.5 (Sep/Oct 1977).

19. James C. Mitchener and Imad Mahawili, *LPCVD: Forced-Convection Flow and the Deposition of LTO, PSG and BPSG Dielectric Films.* Solid State Technology (August 1987).

20. B. Gorowitz, R.H. Wilson and T.B. Gorczyca, *Recent Trends in LPCVD and PECVD.* Solid State Technology (October 1987).

21. Jack Lee, Chris Hegarty and Chenming Hu, *Electrical Characteristics of MOSFET's Using Low-Pressure Chemical Vapor Deposited Oxide.* IEEE Electron Device Letters, Vol9, No.7 (July 1988).

22. Richard S. Rosler, *Low Pressure CVD Production Processes for Poly, Nitride and Oxide.* Solid State Technology (April 1977).

23. Rolf Sokoll, Hans Jurgen Tiller and Thomas Hoyer, *Thermal Desorption and Infrared Studies of Sol-Gel Derived SiO_2 Coatings on Si Wafers.* Journal of Electrochemical Society Vol138, No.7 (July 1991).

24. Chris Langdon and Al Sasaci, Advanced Crystal Sciences, Inc., San Jose, California, personal communications (1991).

25. *Advanced Crystal Sciences Model 500 LPCVD System Manual*, Rev.1 (1986).

26. Cathie Burke and Dan Roll, Xerox Corporation, Rochester, New York, personal communications (1991).

27. Stanley Wolf and Richard N. Tauber, *Silicon Processing for the VLSI Era*, Volume 1 and 2. Lattice Press, Sunset Beach, California (1986, 1990).

28. S. M. Sze, *VLSI Technology.* Second Edition, McGraw-Hill Press, New York (1988).

29. Sorab K. Ghandhi, *VLSI Fabrication Principles.* John Wiley & Sons, New York (1982).

30. John L. Vossen and Werner Kern, *Thin Film Processes.* Academic Press, New York (1978).

31. Rolf Sokoll, Hans-Jürgen Tiller and Tomas Hoyer, *Thermal Desorption and Infrared Studies of Sol-Gel Derived SiO_2 Coatings on Si Wafers.* Journal of Electrochemical Society, Vol. 138, No. 7 (July 1991).

32. G. Lucovsky, S. S. Kim, D. V. Tsu, G. G. Fountain and R. J. Markunas, *The Effects of Subcutaneous Oxidation at the Interfaces between Elemental and Compound Semiconductors and SiO_2 Thin Films Deposited by Remote Plasma Enhanced Chemical Vapor Deposition.* Journal of Vacuum Science and Technology, B7(4) (July/August 1989).

33. G. Lucovsky, P. D. Richard, D. V. Tsu, S. Y. Lin and R. J. Markunas, *Deposition of Silicon Dioxide and Silicon Nitride by Remote Plasma Enhanced Chemical Vapor Deposition.* Journal of Vacuum Science and Technology, A(3) (May/June 1986).

34. G. Lucovsky, P. G. Pai, S. S. Chao and Y. Takagi, *Infrared Spectroscopic Study of SiO_x Films Produces by Plasma Enhanced Chemical Vapor Deposition.* Journal of Vacuum Science and Technology, A(3) (May/June 1986).

35. Ian W. Boyd, *Deconvolution of the Infrared Absorption Peak of the Vibrational Stretching mode of Silicon Dioxide: Evidence for Structural Order?.* Applied Physics Letters, 51(6) (August 1987).

36. Ian W. Boyd and John B. Wilson, *Structure of Ultrathin Silicon Dioxide Films.* Applied Physics Letters, 50(6) (February 1987).

37. B. R. Bennett, J. P. Lorenze and K. Vaccaro, *Low-Temperature Chemical Vapor Deposition of SiO_2 at 2-10 Torr.* Applied Physics Letters, 50(4) (January 1987).

38. N. M. Ravindra and J. Narayan, *Optical Properties of Amorphous Silicon and Silicon Dioxide.* Journal of Applied Physics, 60(3) (August 1986).

39. T. E. Orlowski and H. Richter, *Ultrafast Laser-Induced Oxidation of Silicon: A New Approach Towards High Quality, Low Temperature, Patterned SiO_2 Formation.* Applied Physics Letters, 45(3) (August 1984).

40. T. E. Orlowski, H. Richter, M. Kelly and G. Margaritondo, *Ultrafast UV-Laser-Induced Oxidation of Silicon: Control and Characterization of the Si-SiO_2 Interface.* Journal of Applied Physics, 56(8) (October 1984).

41. T. E. Orlowski, Xerox Corporation, Rochester, New York, personal communications (1991).

42. Werner Kern, *Chemical Vapor Deposition.* Microelectronic Materials and Processes (1986).

43. STAT-EASE, Inc, *DESIGN-EASE and DESIGN-EXPERT version 2.* Personal computer experimental design software for IBM/PC compatible computers.

44. Wacker-Chemitronic GMBH, N-Type Silicon wafers, 2.96-3.00" diameter, 25-28 mils thickness, 50-100 ohms and <100> orientation.

45. MKS Corporation, Baratron Pressure Sensor, Model 222BA-00010AA.

46. Leybold Heraeus, D30AC two-stage, rotary vane mechanical vacuum pump. Pump speed 26.7 CFM / 760 LPM, oil type Inland TW.

47. Transene Company, Inc., Buffered HF (7% HF, 36% NH_4F) solution.

48. PLASMOS Automatic Ellipsometer, *Thin Film Measurement Systems SD2000 Operating Manual.* Edition May 16, 1990.

49. Frank L. McCrackin, *A FORTRAN Program for Analysis of Ellipsometer Measurements*, National Bureau of Standards # 479 (1969).

50. Pelkin Elmer Corporation, *Multiple Internal Reflection Accessory Instructions.* Perkin Elmer Publication 0186-0799 (November 1987).

51. G. Erikson, Acta Chem. Society 25, 2651 (1971).

52. Michael J. Bailey, *Multilevel Metallization.* Rochester Institute of Technology, Microelectronic Engineering Senior Project, unpublished.

53. Nanometric NanoSpec/AFT Reflectance Microspectrophotometer User Manual, Nanometric Corp., Santa Clara, California (1981).